2013-04-22

In-Plane Cyclic Testing of Reinforced Concrete Masonry Walls to Assess the Effect of Varying Reinforcement Anchorage and Boundary Conditions

Hoque, Nusrat

UNIVERSITY OF CALGARY

In-Plane Cyclic Testing of Reinforced Concrete Masonry Walls to Assess the Effect of Varying Reinforcement Anchorage and Boundary Conditions

by

Nusrat Hoque

A THESIS

SUBMITTED TO THE FACULTY OF GRADUATE STUDIES

IN PARTIAL FULFILLMENT OF THE REQUIREMENTS FOR THE

DEGREE OF MASTER OF SCIENCE.

DEPARTMENT OF CIVIL ENGINEERING

SCHULICH SCHOOL OF ENGINEERING

CALGARY, ALBERTA

APRIL, 2013

Abstract

The design of reinforced masonry walls for in-plane shear according to the current Canadian masonry standard CSA S304.1 is quite conservative. So an extensive experimental program was designed to observe the quasi-static performance of partially grouted reinforced masonry walls with variable parameters. The experimental program described in this dissertation is a portion of the larger experimental program and the focus here is on the anchorage conditions of the bond beam reinforcement, changes in boundary conditions and changes in the loading protocol for walls that have the same vertical reinforcement and grouting. The predominant mode of failure was diagonal shear for all walls. The crack pattern, stiffness reduction, strength, ductility and energy absorption are the properties that are discussed in the thesis. Some aspects of behaviour of the walls such as crack pattern, stiffness degradation, and energy dissipation are affected by the change in parameters.

Acknowledgements

I would like to express my sincere gratitude to Dr. Shelley Lissel for her patience, supervision and inspiration throughout my research as well as her support with the completion of my manuscript. I would also like to thank the examination committee: Dr. Nigel Shrive, Dr. Lynne Cowe Falls and Dr. Les Sudak for their precious time. Acknowledgement is also due to the University of Calgary, Department of Civil Engineering, NSERC and the Canada Masonry Design Center for the financial support that made it possible for me to complete my graduate studies. I would like to thank the lab technicians Don Anson, Dan Tilleman, Mirsad Berbic and Terry Quinn and the masons Ray and Kris for their help, without which my work would not have been possible. Thanks are also extended to Expocrete Ltd. for providing the masonry blocks, Brock and White company for providing the joint reinforcement and Target Products for their donation of regular and quick setting mortar and grout. My heart-felt thanks also go to summer student Ruth Laing for her rigorous and enthusiastic help in the lab work. Sincere thanks to Jocelyn Dickie, Rashid Popal and Monica Guzman for their advice and suggestions.

Finally I would like to thank my parents as well as my family for being by my side all the time. Special thanks to Mohon Ahmed for his continuous support.

To my Parents

Contents

List of Tables

List of Figures

List of Symbols

A_{hys} = Area enveloped under the hysteresis curve.

A_v = Area of vertical reinforcement (mm^2).

A_h = Area of horizontal reinforcement (mm^2).

A_{env} = Area under the experimental envelope curve.

C_k = Stiffness ratio.

d_v = Effective length of wall (mm).

d_{cr} = Deformation of the wall at first cracking (mm).

d_{max} = Maximum deformation experienced by the wall (mm).

d_{hmax} = Deformation corresponding to maximum lateral load (mm).

$d_{top\ pull}$/ d_{u1} = Maximum deformation at top of wall in pull direction (mm).

$d_{top\ push}$/ d_{u2} = Maximum deformation at top of wall in push direction (mm).

$D_{sliding}$ = Maximum sliding.(mm).

$D_{uplif\ t}$= Maximum uplift (mm).

d_{peak} = Deformation corresponding to maximum load same as d_{hmax} (mm).

d_{cr} = Lateral deformation corresponding to first crack (mm).

d_e = Deformation at the highest elastic limit (mm).

e = Eccentricity of axial load (mm)

e_1 = Eccentricity of actuator one from the centre of the wall (mm).

e_2 = Eccentricity of actuator two from the centre of the wall (mm).

E_{diss} = Energy dissipated.

E_{inp} = Input energy.

$f_m{}'$ = Masonry compressive strength (MPa).

f_y = Yield strength of vertical reinforcement (MPa).

$F_{flexure}$ = Shear force due to flexure (kN).

h_{wall} = Height of the wall (mm).

H_{max} = Maximum lateral load experienced by the wall (kN).

H_{Dmax} = Lateral load corresponding to the maximum displacement (kN).

H_u =Maximum lateral load for bilinear idealized curve (kN).

H_c = Lateral force corresponding to first cracking (kN).

H_m = Maximum lateral resistance of any wall (kN).

H_{cr} = Lateral load corresponding to first crack (kN).

K= Stiffness (kN/mm).

K_e = Effective or cracking stiffness (kN/mm).

L = Length of wall (m).

M_{cap} = Moment at the top of the wall (kN-m).

M_{bottom} = Moment at the bottom of the wall (kN-m)

M = Flexural moment (kN-m).

N = Axial load (kN).

N_1 = Axial load in actuator one (kN).

N_2 = Axial load in actuator two (kN).

$P_{sliding}$ = Sliding force (kN).

S = Stress applied on plate.

S_1,S_2,S_3 = Stress applied in three orthogonal directions of a solid body.

S_v = Spacing of vertical reinforcement (mm).

S_h = Spacing of horizontal reinforcement (mm).

v_c = Shear contribution from masonry compressive strength (MPa).

V_f = Flexural shear (kN).

V = Shear load (kN).

V_p = Shear contribution from axial load (kN).

V_{cr} = Shear load corresponding to first cracking (kN).

α = angle formed between the wall axis and the strut from the point of load application to the centre of the flexural compression zone at the wall plastic hinge critical section (Chapter 2 and 3)

α = Stiffness parameter (Chapter 5).

β = Stiffness parameter.

Δ_o = Minimum displacement recommended by FEMA (mm).

Δ_m = The desired maximum deformation amplitude by FEMA (mm).

Δd = Displacement increment (mm).

ΔE_{inp} = Energy input in the wall.

ρ_v = Vertical reinforcement ratio.

List of Abbreviations

ASTM: American Society for Testing and Materials

CSA: Canadian Standard Association

ESECMaSE: Enhanced Safety and Efficient Construction of Masonry Structures in Europe

FEMA: Federal Emergency Management Agency

LVDT: Linear Variable Differential Transformer

MTS: Materials Testing System

MPT: Multipurpose Testware

NEHRP: National Earthquake Hazards Reduction Program

UBC: Universal Building Code

Chapter 1: Introduction

1.1 Introduction

Masonry is one of the most important construction materials in the history of mankind. Masonry has been used as a basic construction material for public and residential buildings in the past several thousand years: from the great-wall of China to the pyramids of Egypt, from the ancient fortress of Machu Pichu to the beautiful Taj Mahal, all these masonry structures are standing as a witness of time. Although the use of reinforced concrete is much more prevalent in modern day construction, masonry is still a popular material choice for non-loadbearing walls and structural walls to resist lateral load induced in buildings by wind, seismic and other actions. Masonry is also one of the best options for low rise buildings and is often used in residential construction up to 4 storeys (Moroni, et al., 2002). Several advantages make masonry a popular construction material, including aesthetics, easy and speedy construction as no formwork is required and there is less waiting for curing required, fire and heat resistance, increased thermal resistance, and extended design life. There are also some disadvantages such as the requirement of skilled labour, poor tensile capacity of masonry and most importantly its heavy weight which can attract high lateral forces and thus make the structures vulnerable and less suitable in seismically active areas.

Masonry construction in North-America until the early 20th century mainly consisted of buildings constructed with solid, unreinforced, loadbearing walls. Poor seismic behaviour of unreinforced masonry walls led to the inclusion of reinforcement and the development of thinner, perforated walls that are reinforced and grouted. Inclusion of steel reinforcement in masonry can reduce the brittleness and increase ductility due to redistribution of lateral load, and provides better energy dissipation under seismic loading. During an earthquake, ground movement can occur in all directions; however, the vertical movements do not typically exceed the resistance of the structure in the vertical direction. The substantial damage or the catastrophic failure of buildings typically occurs due to the lateral movement, which compromises the stability of the structure causing it to fail; therefore the design of reinforced masonry walls for horizontal load is a major concern. While designing for horizontal load, in-plane shear strength of walls is critical in terms of its contribution to a lateral load resisting system. However,

predicting the in-plane shear capacity of masonry walls is still an issue where researchers have not yet reached any consensus. The lack of a standardized testing method to gain better understanding of the in-plane shear capacity under cyclic loading of masonry walls has led to the determination of design capacity based on empirical relations derived from different experimental results. Therefore, the research presented in this thesis concentrates on experimental investigation of the in-plane behaviour of concrete block masonry shear walls in order to address some of the gaps in this research area.

1.2 Aim and Objectives

The main aim of this thesis is to understand the in-plane response of concrete reinforced masonry shear walls subject to cyclic loading. This aim will be achieved through the following objectives:

- To gather information on existing knowledge of the response of masonry shear walls through a comprehensive literature review.
- To investigate the effectiveness of various existing in-plane shear prediction models based on the results of the research reviewed in the first objective.
- To carry out experiments on walls built with full scale blocks with a view to examining the effect of different anchorage conditions of bond beam reinforcement, boundary conditions of walls and different load histories to determine the effect of these changes. The most important aspects of behaviour to be considered in the analysis of the test results are crack pattern, strength, stiffness, energy absorption, ductility, and cracking tensile strength.

1.3 Scope and Limitations

The scope of the thesis is to examine the in-plane response of masonry shear walls.
The following is a list of limitations:

- The experimental work deals with single leaf shear walls made from concrete block.
- The shear walls with bond beams did not have any joint reinforcement.
- Walls with openings are not included in the experimental program.

1.4 Organization of the Thesis

The thesis consists of six chapters. This first chapter includes the introduction along with the objectives, scope and limitations of the thesis. A comprehensive literature review is presented in Chapter 2. Different analysis methods used in the data analysis in Chapter 5 are also discussed in this chapter. Different in-plane shear prediction models used for design of walls are described in Chapter 3 and they are compared by checking the theoretical results against the experimental shear values accumulated in a shear test database. Development of a modified equation and a look at the failure from the point-of-view of cohesive strength are also presented in this chapter. The fourth chapter describes the experimental arrangements. Chapter 5 contains the detailed results obtained from the testing and analysis of the experimental results using various theoretical methods as well as comparison of the results of different groups of walls. The last chapter presents the conclusions drawn from the research presented here and future recommendations for researchers on masonry shear behaviour under in-plane loading.

Chapter 2: Literature Review

2.1 Introduction

A general discussion of shear walls and previous research on masonry shear walls is briefly presented in this chapter. The current understanding with regard to the effect of various parameters on the shear strength of masonry walls is also discussed based on results of previous researchers. This chapter also provides the details of the various analysis methods adopted in the thesis.

2.2 Masonry Shear Walls

The key structural components in masonry buildings are structural walls which are provided to resist some or all of the load effects of axial compression due to vertical gravity loads, transverse wind, earthquake or blast loads and eccentric loads creating out of plane bending moments. Lateral wind and earthquake loads applied to a building system in a direction parallel to the plane of the wall create in-plane bending and shear.

Horizontal inertia forces develop in the walls and the floor and roof slabs of masonry buildings when they are subjected to earthquake loads. These inertia forces are proportional to the mass of these structural components and the acceleration at any given level. The lateral load is transferred to the lateral load resisting system through floor and roof slabs which are also called diaphragms. In Figure 2.1 the roof diaphragm acts like a horizontal beam spanning between walls A and B. The end reactions of this beam are transferred to walls A and B. The walls subjected to lateral load along their longitudinal axis are called shear walls. Shear walls transfer the lateral load to the foundation along with the floor and roof diaphragms (Anderson & Brzev, 2009).

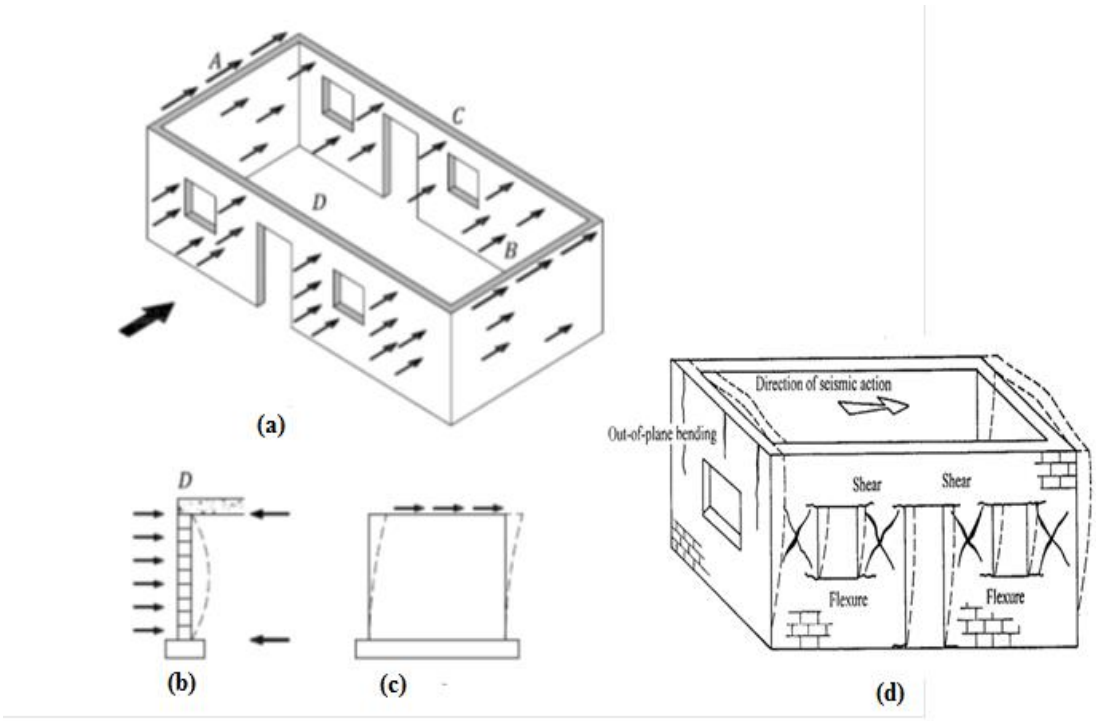

Figure 2.1 Simple Masonry Building a) Isometric View Showing Lateral Loads, b) Out -Of -Plane Loads, c) In-Plane Loads Resisted by Shear Walls (Anderson & Brzev, 2009)**, (d) Response of Masonry Building Under In-Plane Loading** (Tomazevic, 1999)**.**

Shear walls are one of the possible main lateral load resisting systems of a seismic force resisting system (SFRS) according to NBCC 2005 (NBCC, 2005).

Masonry shear walls can be described not only in terms of the type of masonry unit used (solid or hollow, brick or block and clay or concrete), but also as load bearing or non-load bearing, reinforced or unreinforced, single wythe or multi wythe, solid or perforated, rectangular or flanged, and cantilever or coupled (Hatzinikolas & Korany, 2005). The research presented in this thesis deals specifically with testing of single wythe reinforced concrete block masonry walls.

2.2.1 Reinforced Masonry

In areas of high seismicity, unreinforced masonry (URM) walls are not normally permitted since they have limited capacity to withstand the ground excitation. Therefore,

in seismic regions, reinforced masonry walls are required. Typically, reinforced masonry walls consist of hollow concrete block where vertical reinforcing bars are placed in the open cells of the masonry units as shown in Figure 2.2, to resist vertical loads, out-of-plane loads and the forces resulting from moments induced by vertical eccentricities. The reinforcement is usually uniformly distributed throughout the length of the wall. Two types of arrangements can be used for horizontal reinforcement: 1) ladder or truss type reinforcement placed in the mortared bed joint, 2) steel bars placed in grouted bond beams which are provided at specified locations over the wall height. Cells of masonry units which contain vertical and horizontal reinforcement are filled with grout which is similar to concrete but has small aggregate and high slump.

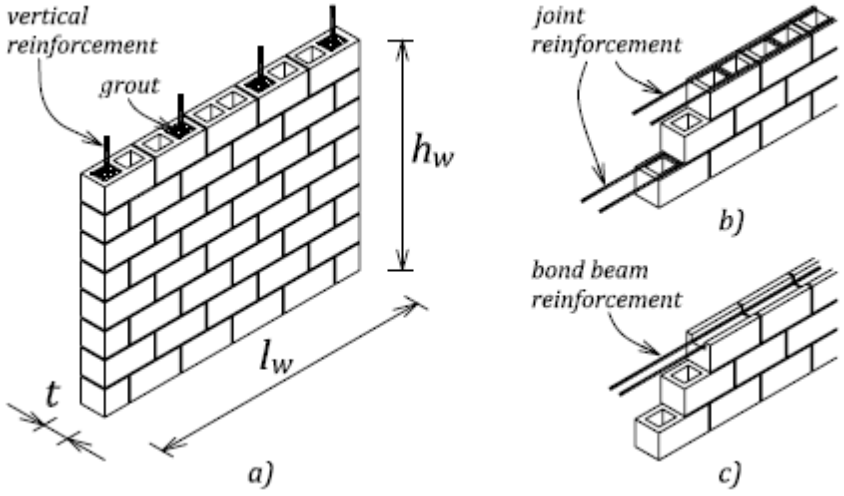

Figure 2.2 Typical Reinforced Concrete Masonry Block Walls a) Vertical Reinforcement b) Joint Reinforcement and c) Bond Beam Reinforcement (Anderson & Brzev, 2009)**.**

Grout serves two purposes: increasing the load bearing capacity of masonry by increasing its area, and bonding the reinforcement to the masonry units so that the reinforcement and the unit act together. If only the reinforced cells are grouted then the masonry is called partially grouted, whereas walls are termed as fully grouted if all cells are grouted.

2.2.2 Failure of Masonry Shear Walls

The critical regions for shear walls are the heel, toe, centre and point of application of load. The failure in these regions controls the overall behaviour of shear walls. Under combined in-plane and axial loading (Hatzinikolas & Korany, 2005) three typical modes of failure are recognized for shear walls which are: sliding shear, flexure, and diagonal shear. The typical failure modes of reinforced masonry shear walls are illustrated in Figure 2.3.

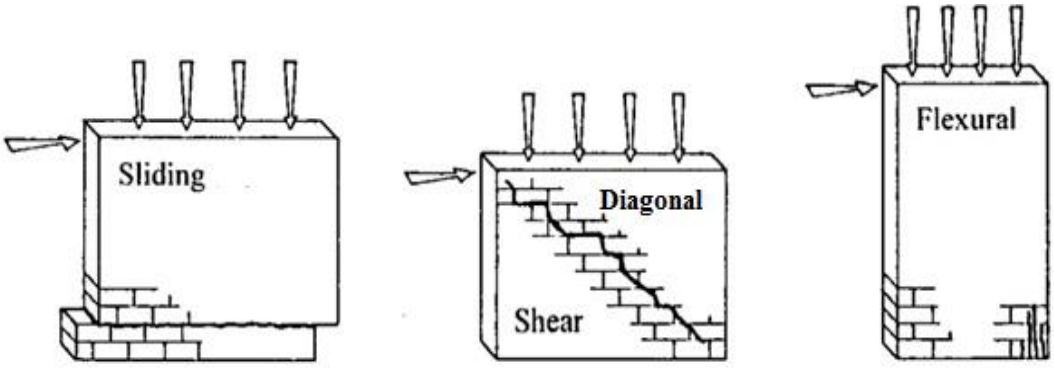

Figure 2.3 Typical Failure Modes of Masonry Shear Walls Subjected to In-Plane Load (Tomazevic, 1999)

Flexural failure may be of three types: ductile flexural failure, lap-splice slip, and flexural/out-of –plane stability. Ductile flexural failure typically occurs in walls with aspect ratio (ratio of height to length) greater than 1 and subject to moderate levels of axial load. The wall acts as a vertical cantilever causing the vertical reinforcement near the heel to yield or the masonry near the wall toe to crush; leading to flexural failure. Usually biaxial compressive stresses cause toe failure whereas failure at the heel occurs due to vertical tensile stresses. Effective energy dissipation and ductility can be achieved in this type of flexural failure as soon as the yielding of vertical reinforcement takes place, therefore this is considered as the most preferred mode of failure. According to Tomazevic (Tomazevic, 1999) vertical reinforcement is effective in resisting tensile stresses and experimental results have shown that it yields shortly after cracking of the masonry. Damage is characterized by both horizontal flexural cracks and small diagonal shear cracks concentrated in the region where plastic deformation takes place i.e. the hinge zone. Lap-splice slip failure occurs when reinforcing bars projecting from the

foundations have insufficient lap splice length or when the rebar size is large compared to the wall thickness causing bond degradation and eventually rocking of the wall at the foundation level. In the beginning, vertical cracks appear at the location of the lap splice followed by cracking and spalling at the wall toe. Though this mode is fairly ductile, it causes severe strength degradation and hence provides less energy dissipation. At levels of high ductility, flexural instability takes place. When large tensile strains develop in the tensile zone of the wall, that zone may become unstable when the load direction reverses in the following cycles causing compression. This type of failure is not too common in actual structures but has been seen in walls tested in the laboratory (Paulay & Priestley, 1993).

Sliding shear is assumed to occur along a horizontal plane when the shear stress along that plane exceeds the frictional resistance of the wall and typically occurs under low axial load and high lateral load. Dowel action of the reinforcement may also contribute in carrying shear but if the vertical steel is at yield then the bending resistance of the bar essentially vanishes and cannot support a shear force necessary for dowel action (Anderson & Priestley, 1992). When shear walls have low aspect ratios or are constructed using low strength mortar combined with low axial load they may fail in the sliding mode along one of the mortar bed joints (Hatzinikolas & Korany, 2005).

Diagonal shear failure is marked by the presence of diagonal cracks traversing across the shear wall and occurs when the principal tensile stress surpasses the tensile strength of the masonry under increasing imposed lateral load. When inadequate horizontal reinforcement is provided without proper anchorage, the diagonal cracks that appear at the very beginning cannot transfer the tensile forces. Therefore the cracks open up more and more and if load reversal occurs while testing then these cracks finally result in a pair of major X-shaped diagonal cracks, thus leading to a relatively abrupt and brittle failure. These diagonal cracks may develop either through blocks or along the mortar joints.

Failure often occurs by the combination of two or more modes. Failure of tall walls is usually in the form of a progressive flexural mechanism characterized by heel cracking followed by toe crushing whereas squat shear walls predominantly fail by diagonal shear cracking. Failure of squat reinforced walls involves several complicated mechanisms such as the compression strut mechanism, aggregate interlock forces and dowel action of

the vertical reinforcement (Haider, 2007). In squat walls, flexure and shear are intermingled and thus cannot be separated; so they are discussed together, whereas in tall walls, bending dominates the failure. Experimental studies have proved that walls failing in a combined flexural and shear mode of failure exhibit higher lateral load resistance than if they fail only due to flexure (Haider, 2007).

2.3 Masonry Shear Wall Studies Under In-Plane Loading

In-plane loading of masonry shear walls has been studied quite extensively however due to differing test arrangements, masonry typologies, loading regimes, and the number of variables involved, it is often difficult to compare the results of various researchers. A summary of several research works reported in the literature is found below in Table 2.1 and a discussion of what is understood from these studies follows in Section 2.4.

Table 2.1 Summary of Research Obtained From Various Sources

Name of Researcher	Aspect Ratio	Type of Grouting	Reinforcement			Material	Boundary Conditions	Type of Shear Load
			Vertical (%)	Horizontal (%)	Joint			
Schneider (Schneider, 1959)	1	Partial and full	0.2-0.3		Wall Mesh	Clay brick, concrete brick and shel brick.	Fixed	Racking
	Remarks: The type of mortar, amount of wall reinforcement and the location of opening discontinuities were the main concern of the research.							
Priestley (Priestley, 1976)	0.75	Full	0.34-0.66	0.45-0.6	-	Concrete Block	Fixed	Cyclic
	Remarks: 1. Walls were tested to find the effect of reinforcement ratio, vertical load, and confinement. 2. The cyclic loading was applied to a maximum value of 70% of the theoretical ultimate capacity with 2 cycles at each load for displacement ductility factors of 2, 4 etc. (According to the source displacement ductility of 2 means the maximum displacement would be two times the yield displacement.)							

Name of Researcher	Aspect Ratio	Type of Grouting	Reinforcement			Material	Boundary Conditions	Type of Shear Load
			Vertical (%)	Horizontal (%)	Joint			
Eikanas (Eikanas, 2003)	0.72, 0.93, 1.5,2.1	Full	0.242 and 0.484	0.156	-	Concrete Block	Fixed	Cyclic
	Remarks: Concrete masonry shear walls with various aspect ratios and flexural reinforcement were investigated to study the validity of the maximum reinforcement provisions found in the 2000 International Building Code (IBC)							
Matsumura (Matsumura, 1987)	0.83, 1.05, 1.13, 1.36, 1.51, 1.86, 1.96, 2.28	Partial and full	0.049-1.148	0.071-0.67	-	Clay Brick and Concrete Block	Cantilever	Cyclic
	Remarks: 1. The ends of vertical bars were anchored in RC beams or portions of walls. The ends of all horizontal reinforcing bars were bent in a semicircular shape (180̊ hook) and hooked with vertical bars at the ends of the walls. 2. Most specimens were subjected to 4-5 cycles of repeated loading before entire failure of the wall under constant axial load							

Name of researcher	Aspect Ratio	Type of Grouting	Reinforcement			Type of Materials	Boundary Conditions	Type of Shear Load
			Vertical (%)	Horizontal (%)	Joint			
Woodward and Rankine (Woodward & Rankine, 1985)	0.67, 0.8, 1.33	Ungrouted	-	-	-	Concrete Block	Fixed	Cyclic
	Remarks: Lateral in-plane displacements were applied at the top of the wall while maintaining a constant compressive axial load.							
Okamoto (Okamoto, et al., 1987)	0.9, 1,5, 2.25	Full	0.248	0.167, 0.67	-	Clay Brick and Concrete Block and R.C.C	Cantilever	Cyclic
	Remarks: Two computer controlled vertical actuators were used to prevent the rotation of the top end of the wall and to maintain constant vertical load. Displacement controlled cyclic loads were applied to the specimen using different cycles and drift angles.							

Name of researcher	Aspect Ratio	Type of Grouting	Reinforcement			Type of Materials	Boundary Conditions	Type of Shear Load
			Vertical (%)	Horizontal (%)	Joint			
Mayes et.al. (Mayes, et al., 1976), Hidalgo et.al. (Hidalgo, et al., 1978), Chen et.al. (Chen, et al., 1978), Sveinsson et al. (Sveinsson, et al., 1985)	1, 2	Full and partial	0.17-0.51	0.167-0.668	-	Clay Brick and Concrete Block	Fixed	Cyclic
	Remarks: 1. Piers were tested under cyclic lateral loads simulating the conditions of a lower story pier in a perforated wall subjected to earthquake excitation by imposing fixed end conditions and realistic bearing stresses. 2. Mayes (Mayes, et al., 1976) conducted tests on double piers by applying dynamic and pseudo static loads on the same type of specimen. Hidalgo (Hidalgo, et al., 1978) reported the results of tests on piers of height to width ratio of 2 and Chen et.al (Chen, et al., 1978) presented results of tests on piers having height to width ratio of 1. Three types of anchorage were used for horizontal reinforcement : 90 degree bend, 180 degree hook and welded end plate (Sveinsson, et al., 1985). 3. The action of rigid floor diaphragms in actual construction was simulated by the top and bottom beams which were connected to the vertical actuators. The vertical actuators served two purposes: first they provided vertical load equivalent to the gravity load experienced by the original structure and secondly they prevented rotation of the top beam by developing a reaction couple and thus providing fixed end conditions during the test.							

Name of researcher	Aspect Ratio	Type of Grouting	Reinforcement			Type of Materials	Boundary Conditions	Type of Shear Load
			Vertical (%)	Horizontal (%)	Joint			
Kaminsono et. al. (Kaminsono, et al., 1988)	0.9,1.6, 2.4	Not mentioned	0.262,0.349	0.167		Concrete block, Clay Brick and reinforced concrete.	Fixed	
	Remarks: Tested under constant axial stress in order to obtain the basic seismic behaviour of the walls and to evaluate the effect of axial stress, aspect ratio, amount of shear reinforcement, spiral reinforcement at the compressive toe of the wall and joint method of reinforcing bar.							
Brammer (Ingham, et al., 2001)	0.57, 0.92, 1.33, 3	Full and Partial	-	-	-	Concrete Block	Cantilever	Cyclic
	Remarks: 1. Walls were tested without axial stress to compare the results obtained with those predicted by the New Zealand standard. 2. Bond beam reinforcement was used sometimes with stirrups as used in beams. 3. Spacing of vertical reinforcement was 800 mm except for walls with aspect ratio 3 where the spacing was 600 mm.							

Name of researcher	Aspect Ratio	Type of Grouting	Reinforcement			Type of Materials	Boundary Conditions	Type of Shear Load
			Vertical (%)	Horizontal (%)	Joint			
Fujisawa and Kawashima (Fujisawa, et al., 1986)	0.9, 1.56, 2.28	Full	0.514-0.817	0.167	-	Clay Brick and Concrete Block	Fixed	Cyclic
	Remarks: The specimens were subjected to horizontal deformation under a constant axial load by three servo controlled actuators.							
Feng et. al. (Feng & Xia, 1986)	Not Provided.						Fixed/Cantilever	Cyclic
	Remarks: 1.Walls were unreinforced or reinforced with heights varying from 400-1800 mm and lengths varying from 1250-3500 mm with fixed thickness of 240 mm. 2. The reinforcement scheme was also changed such that walls had only horizontal or vertical reinforcement or a combination of both.							
Scrivener (Scrivener, 1967)	1.08	Partial	0-0.42		-	Concrete Block		Fixed	Static incremental
	Remarks: The geometry of the test setup was such that the ratio of horizontal to vertical load was kept at 0.9.							

Name of researcher	Aspect Ratio	Type of Grouting	Reinforcement			Type of Materials	Boundary Conditions	Type of Shear Load
			Vertical (%)	Horizontal (%)	Joint			
Shing et. al. (Shing, et al., 1990)	1.0	Full	0.38-0.74	0.14-0.24	-	Clay Brick and Concrete Block	Fixed	Cyclic
	Remarks:1. Tested under constant axial load. 2. One specimen had toe confinement in the form of wire mesh. 3. Horizontal reinforcement had 180 degree hooks around the vertical reinforcement. 4. A standard displacement history of increasing amplitude was applied to each specimen except for one specimen which was subjected to larger amplitudes at an earlier stage of loading.							
Minae et. al. (Minaie, et al., 2009) (Minaie, et al., 2010)	0.67 and 1.37	Full and Partial	0.15	0.12	-	Clay Brick and Concrete Block	Fixed/ Cantilever	Cyclic
	Remarks: 1. Partially grouted walls were subjected to reverse cyclic displacements with test variables of initial average vertical stress level, boundary condition (single versus double curvature) and mortar formulation. 2. The horizontal reinforcement of the test specimen was hooked around the vertical reinforcement according to MSJC (Masonry Standard Joints Committee, 2008)							

.

Name of researcher	Aspect Ratio	Type of Grouting	Reinforcement			Type of Materials	Boundary Conditions	Type of Shear Load
			Vertical (%)	Horizontal (%)	Joint			
Schultz (Schultz, 1996), (Schultz, et al., 1998)	0.5, 0.7 and 1	Partial	0.205-0,409	0.056 and 0.12	-	Concrete Block	Fixed	Cyclic
	Remarks: 1.The outermost cell of the wall contained all the vertical reinforcement and all the horizontal reinforcement was concentrated in a single bond beam placed at the mid-height of the wall. 2. 180º hooks were provided for the horizontal bars.							
Tomazevic and Lutman (Tomazevic, et al., 1996)	1.2 and 2.3	Partial	0.26 and 0.52	0, 0.14,0.28 and 0.5	-	Concrete Block	Cantilever	Cyclic
	Remarks: Tested under constant axial load and cyclic horizontal deformation repeated three times at each amplitude.							
Voon (Voon, 2007)	1.0	Full and partial	0.623-1.454	0, 0.05, 0.14	-	Concrete Block	Cantilever	Cyclic

2.4 Factors Affecting In-Plane Diagonal Shear Strength

While the factors affecting flexural and sliding shear failure are fairly clear, the factors affecting diagonal shear failure are still somewhat disputed. Several parameters that govern the failure of a shear wall are applied load, wall geometry, properties of materials and details of reinforcement. It is therefore necessary to examine the effects of these factors on the behaviour of the wall.

2.4.1 Effect of Horizontal Reinforcement on Shear Strength

Some researchers have observed that horizontal (shear) reinforcement has limited efficiency in masonry walls. According to Anderson and Priestley (Anderson & Priestley, 1992) the efficiency of shear reinforcement on masonry shear strength is approximately half of that assumed in a reinforced concrete member. This behaviour may be explained by considering that the masonry carries all the shear stress upon initial loading of a wall and the shear reinforcement remains essentially unstressed. Upon the formation of diagonal cracks the reinforcing steel at the crack must go into tension, but because of crack opening the shear carried by the masonry across the crack is reduced. Two phenomena occur at the same time; tension in the shear reinforcement increases and the shear carried by the masonry decreases as the cracks become much wider (Voon, 2007). Hence, with the increase in deformation the rate at which the reinforcement influences shear capacity may be less than the rate at which the masonry loses strength, and so a maximum capacity is reached. According to Okamoto et al. (1987), horizontal reinforcement as well as spiral reinforcement (used to tie multiple horizontal bars) had a positive influence in reducing the deformation capacity of a wall. For piers failing in a shear mode, a sufficient (minimum 0.24%) amount of horizontal reinforcement and an increase in bearing stresses was shown to increase the ductile behaviour of the pier significantly (Mayes, et al., 1976). For hollow clay brick walls, the ultimate shear strength increased as the horizontal reinforcement increased up to a certain point, however this trend was not observed for double wythe grouted core clay brick walls (Hidalgo, et al., 1978). On the other-hand Tomazevic and Lutman (Tomazevic & Lutman, 1988) had another theory for the behaviour of horizontal reinforcement under lateral load such that the horizontal reinforcement remains under tension. After the

formation of cracks, vertical load causes the wall to expand laterally. Although not yielded, strain in the horizontal reinforcement accumulates when preventing the separation of the wall's cracked parts at repeated lateral load reversals. Although they noted that the full tension capacity of horizontal reinforcement cannot be developed due to loss of bond between the mortar and the reinforcement or crushing of the concrete blocks, they also remarked that adequate horizontal reinforcement causes better ductility and shear capacity, which can also help yielding of the vertical reinforcement and development of full flexural capacity in a wall section (Tomazevic & Lutman, 1988).

The test results of Chen et al. indicated that the ultimate shear strength of fully grouted piers did not show any consistent increase or decrease with the change in the amount of horizontal reinforcement. In almost all cases, the piers with horizontal reinforcement had the same strength as the pier without any reinforcement (Chen, et al., 1978). In contrast, Schultz (Schultz, 1996) observed that horizontal reinforcement does have a modest beneficial influence on the ultimate shear strength of walls in that there is a decrease in ultimate shear stress with an increase in horizontal reinforcement for the same aspect ratio. Sveinsson et al. also reported that improved ductility could be achieved by distributing horizontal reinforcement up to a reinforcement ratio of 0.07%. Beyond that value, the horizontal reinforcement was not expected to improve ductility. Horizontal reinforcement was also effective in slowing the formation of shear cracks (Sveinsson, et al., 1985). Shing et.al also suggested that increasing the amount of horizontal reinforcement can increase the post cracking ductility of a shear dominated specimen (specimens that failed under shear) (Shing, et al., 1990).

2.4.2 Effect of Vertical Reinforcement on Shear Strength

Vertical reinforcement was found to contribute to shear strength of masonry by Shing (Shing, et al., 1990). Dowel action of the reinforcement occurs when a shear crack intersects longitudinal reinforcing steel activating flexural and kinking actions whereby shear forces can be transferred along a diagonal crack. The dowel action of the reinforcement introduces tension into the surrounding grout, which can cause the grout to split along the axis of the bar. The contribution of dowel action to shear resistance is dependent upon the amount of longitudinal reinforcement, and when horizontal

reinforcement is present, the ability of this transverse reinforcement to restrain the splitting of masonry cracks or the increase in crack width. In addition, by helping to control the diagonal cracks, the vertical reinforcement also enhances friction along these crack interfaces, therefore resulting in an increase in shear capacity. However, at the onset of yielding of the longitudinal reinforcement, the effectiveness of these vertical bars inside an unconfined masonry structure would be significantly affected. Consequently, a conservative approach is to consider the resistance provided by the longitudinal reinforcement to diminish at the onset of yielding of these bars. Various experimental results have been studied with no direct result found relating the amount of vertical reinforcement to the shear strength. Several results show the combined effect of changing vertical reinforcement along with other parameters. Shing (Shing, et al., 1990) plotted $v_c/\sqrt{f_m'}$ against $\rho_v f_y$ where ρ_v is the vertical reinforcement ratio and found by using least square fitting that the rate of increase of the normalized (divided by square root of masonry compressive strength) masonry shear strength with respect to $\rho_v f_y$ is 0.0015. Actually, Shing et al. are among the few that consider the effect of vertical reinforcement in the equation proposed to determine diagonal shear strength. Different conclusions have been made by different researchers regarding the contribution of vertical reinforcement. For example, according to Chen et al. (1978), a change in the amount of vertical reinforcement did not change the ultimate shear strength significantly. Feng and Xia showed that the effect of reinforcement is very small before diagonal cracking; and the effect of reinforcement was only remarkable at the peak and ultimate strength (Feng & Xia, 1986). They also concluded that placing vertical reinforcement in the centre is more effective than when placed in the ends of the wall. Eikanas concluded that higher amounts of vertical reinforcement reduced the drift capacity though the drift values were always greater than 1.5% before 20% load degradation was reached (Eikanas, 2003).

2.4.3 Effect of Aspect Ratio on the Shear Strength

Aspect ratio has been shown to be inversely proportional to the shear capacity of walls, i.e. as the ratio of height to length increases, the capacity of the wall will decrease with low aspect ratio walls showing greater shear capacity than slender walls (Voon, 2007). The same result was obtained by Fujisawa et.al. where increasing the aspect ratio resulted

in a decreasing maximum shearing force with this effect being more significant for brick walls than concrete block walls (Fujisawa, et al., 1986). Schultz observed increased deterioration of post-peak strength and pinching of hysteresis loops with increasing height to length aspect ratio. "Pinching" means reduction in unloading stiffness at low lateral load levels (Schultz, 1996). This decreasing strength with increasing aspect ratio may be due to the fact that squat shear walls (walls with a low aspect ratio) undergo significant deformation due to shear whereas slender walls are more prone to flexural deformation (Eikanas, 2003). This is generally accounted for in design standards by allowing greater limits for masonry shear capacity for squat walls. Some codes such as NEHRP (Voon & Ingham, 2007) and UBC (Davis, 2008) take the effect of wall aspect ratio directly into account, however the Canadian standard accounts for the effect in the term ($2\text{-}M/V_f d_v$) and through a higher limit for the shear strength of squat walls.

2.4.4 Shear Strength Provided by Axial Load

Woodward and Rankine concluded from their test results that the post cracking behaviour of walls was affected by both aspect ratio and axial compressive stress. This may be attributed to the contribution of these two parameters to the shear friction mechanism of load resistance along the crack. If the resistance by shear friction is sufficiently high, then the lateral load resistance of the wall is maintained even after diagonal cracking occurs and vice-versa. However, there are also limits to the positive effects since walls with higher vertical compression tended to suffer more crushing (Woodward & Rankine, 1985). An increase in axial stress generally has a positive influence on the shear strength capacity of the wall with walls subjected to moderate vertical load exhibiting better behaviour than walls without any vertical load (Priestley, 1976). The enhancement in shear strength of a wall may be due to an independent shear strength component resulting from the diagonal compression strut as shown in Figure 2.4**.** In the figure, α is the angle formed between the wall axis and the strut from the point of load application to the center of the flexural compression zone at the wall plastic hinge critical section (Voon, 2007). The mechanism of shear transfer through axial compression can be simply justified by the phenomenon of the formation of a compression strut at an angle to the wall axis so that stress can be transferred through the flexural compression zone. The applied shear force is resisted by the horizontal component of the strut force (Priestley, et al., 1994)

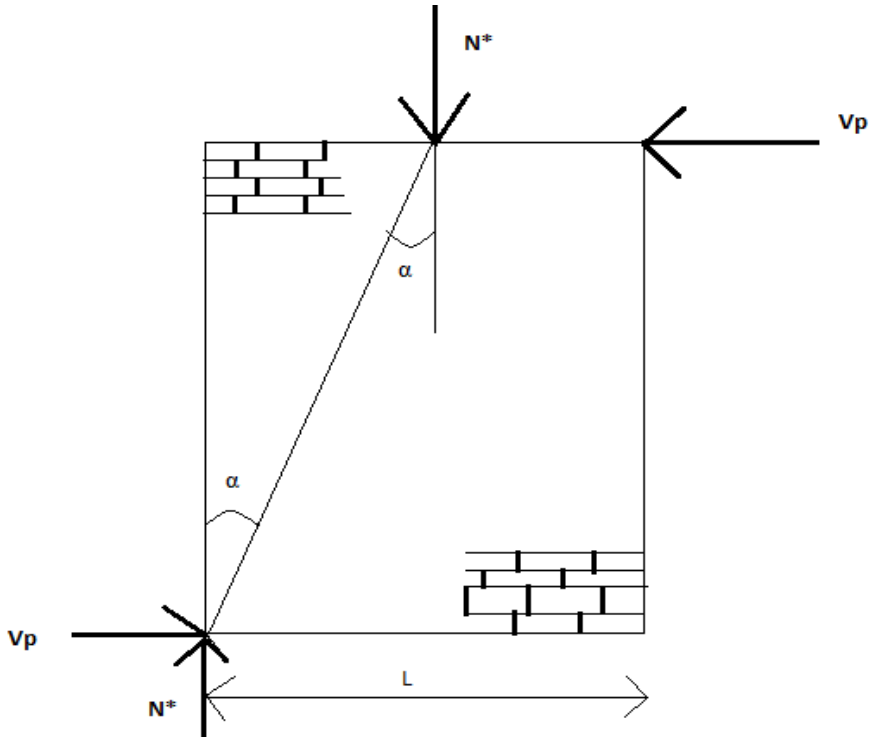

Figure 2.4 Contribution of Axial Stress to Masonry Shear Strength (Voon, 2007)

An increase in the shear strength due to the increase in the axial stress has also been proven with experimental results. According to Okamoto et al. (Okamoto, et al., 1987), axial stress was observed to increase the shear carrying capacity of walls, which may be attributed to the fact that masonry is weak in tension and the tensile stresses get suppressed under high axial stress (Voon, 2007). Sveinsson et al. concluded from their test results that vertical stress significantly affected the seismic behaviour of piers. Axial load can also change the mode of failure. Low vertical stress is associated with the flexural mode of failure whereas high vertical stress results in the diagonal shear mode of failure (Sveinsson, et al., 1985). Maximum shear strength increased and deformation capacity decreased as the axial load increased and the aspect ratio decreased for specimens failing in shear according to Kaminsono et al. (Kaminsono, et al., 1988). The experimental results also showed that the post cracking deformation capacity of a wall decreases as the axial stress increases. This was because the failure became more brittle with the increase in axial stress and the increased axial stress inhibits the formation of cracks as tensile stresses develop due to loads that have to exceed the compressive field generated by the axial load.

For higher compressive stress maximum lateral load resistance was also affected by aspect ratio where longer walls had more load resistance (Woodward & Rankine, 1985). It is clearly evident from the test results that the failure mode can be changed from a ductile flexure/shear mode to a brittle shear mode with increasing axial stress. As the axial stress increases, more rapid load degradation seems to occur due to more severe toe crushing. However, ductile flexural behaviour under high axial load may be achieved by using proper toe confinement (Shing, et al., 1990).

2.4.5 Effect of Horizontal Reinforcement Anchorage

As the maximum strength is reached in walls dominated by shear they tend to exhibit brittle behaviour and quick strength degradation. This type of failure is undesirable in seismic events, as failure or collapse of structures without adequate warning becomes much more likely. Enhanced ductility of shear dominant walls can be achieved by providing a sufficient amount of appropriately anchored horizontal reinforcement which can also help develop the full capacity of the bar (Sveinsson et al., 1985). As discussed in Section 2.4.2, the horizontal reinforcement remains ineffective until crack initiation and once the cracks develop, the reinforcement plays a significant role in carrying the shear. However, in order to ensure that the transverse reinforcement can contribute sufficiently to the overall shear strength (or post cracking ductility) of the wall, it must be properly anchored; which can be achieved by providing transverse reinforcement with 180° hooks around the extreme vertical reinforcement (Sveinsson, et al., 1985). Proper anchoring also causes more gradual failure of the wall. Investigation of post-earthquake damage over the past few years helps in understanding the importance of reinforcement detailing. In the case of severe earthquake loading, negligence in detailing may lead to major damage. Sveinsson et al. also reported results from tests including walls that had shear reinforcement with various end anchorage arrangements. Some of the test walls had 180 degree hooks on the ends of the horizontal shear reinforcement while others had 90 degree bends, and some of the walls had end plates welded onto the horizontal reinforcement. From Sveinsson's results it can be said that walls with hooks (180 degree) are most effective in carrying lateral load. In the shear mode of failure, strength and ductility can be improved by proper anchorage of horizontal reinforcement. Horizontal

reinforcement with insufficient bond area should be hooked 180˚ around vertical reinforcement (Sveinsson, et al., 1985).

2.4.6 Effect of Grouting

Grout is used to bond reinforcement to the block to make them act as a composite. Walls may be fully grouted or partially grouted. Experimental studies by various researchers prove that when strength is calculated with regard to net area of the section then the strength difference between the two types of walls becomes insignificant although apparently it seems that fully grouted walls can carry higher load because of the large load bearing area. Both partially and fully grouted walls showed the same maximum strength based on net area (Voon, 2007). However, some conflicting reports on the effect of grouting can also be found in the literature.

2.5 Experimental Testing of In-Plane Shear Behaviour of Masonry Walls

2.5.1 Existing Test Methods

Testing of walls is carried out in order to determine the factors affecting seismic shear resistance of masonry walls. Ideally, the test specimens should be subject to the same loading conditions and the same restraint as they experience in real buildings. In real structures the vertical compression changes during earthquakes depending on the distribution of stresses that occur due to the presence of the restraints which prevent the rotation of walls at higher horizontal displacement. As it is extremely challenging to replicate the real conditions while testing, walls are generally tested with controlled levels of vertical load. Full-size or reduced-scaled specimens constructed of various materials have been tested over the last few decades under different boundary conditions as described in Section 2.3. The applied load-history also varies with static, dynamic, cyclic and monotonic loading conditions being used.

To determine the capacity of masonry under diagonal tension two methods have been described by ASTM and are schematically shown in Figure 2.5. According to ASTM C1391 (Drysdale & Hamid, 2005) one type of testing involves loading a square panel through steel shoes on two diagonally opposite corners of the specimen as shown in

Figure 2.5. Failure occurs by the formation of cracks parallel to the line of action of the compression force. The disadvantage of this method is that the crack tends to form along the path of compression loading, though this may not be the path of least resistance for all boundary conditions (Drysdale & Hamid, 2005). Sometimes local compression failure can occur before actual shear failure.

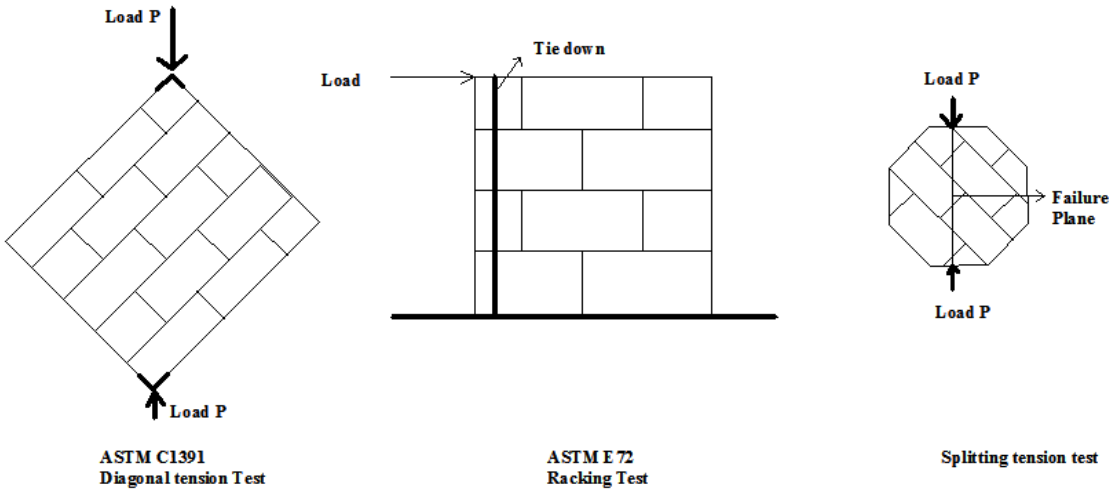

Figure 2.5 Typical Test Methods (Drysdale & Hamid, 2005)

In order to study the parameters affecting the in-plane tensile strength, the splitting tension test could be used on disks and square masonry assemblages although this test presents the same issue as in the ASTM C1391 where the failure follows the path of loading instead the path of least energy (Drysdale & Hamid, 2005). ASTM E72 describes a racking test method that has evolved due to the difficulty related to the diagonal tension test method. In this method, a horizontal force is applied along the top of a wall with or without an axial compression load. To prevent the specimen overturning, a tie down is required. Shear capacity provisions in codes for cases similar to the test environment can be confirmed by the results obtained from this test.

From the brief discussion in the preceding paragraph it can be concluded that racking tests are more favourable than diagonal tension tests. There are many variations of racking test methods as reported by Vliet (Vliet, 2004) such as the types of material tested, the presence or absence of an opening, how the load is distributed, the boundary conditions at the top and bottom, the presence or absence of vertical preloading and the

type of loading. In most cases, the horizontal force is applied at the upper edge of the wall with the lower edge fixed following any of the methods shown in Figure 2.6

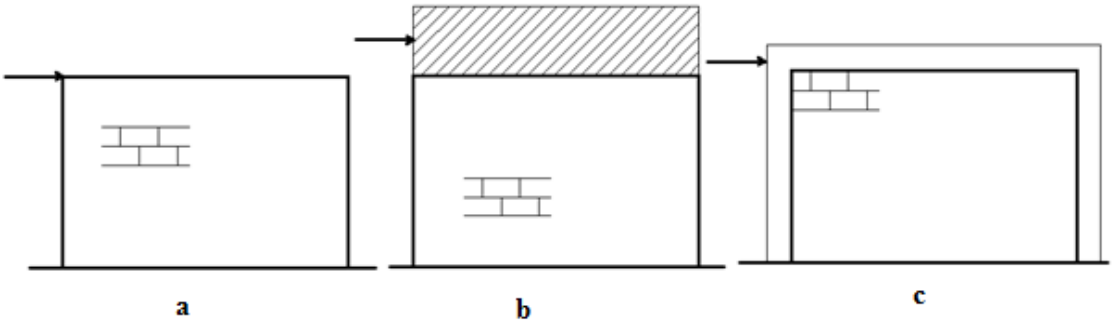

Figure 2.6 Different Ways of Introducing the Horizontal Load

The shear force can be applied at the side of the wall as a concentrated load as shown in (a), through a very stiff beam as in (b) so that the shear force is distributed along the upper edge of the wall, or through a frame surrounding the complete wall panel as shown in (c).

The application of horizontal load causes the wall panel to be loaded in shear, but this in turn can create an overturning moment as in cases (a) and (b) shown above (does not occur where load is applied as in (c) because the frame counteracts the developed moment). The overturning moment can cause compression failure at the toe or can cause failure of the wall in another mode before it achieves the desired shear failure. If the top is not fixed, another problem will be that the upper part of the wall will not be parallel to the base of the wall and the desired shear loading will not be introduced. Hence vertical load is very often applied at the top of the panel in racking tests to reduce the chance of tensile failure at the base of the walls. However, this type of loading introduces additional problems in that the compression can exceed the material compressive strength and thus can cause failure of the panel as shown in Figure 2.7. To prevent rotation of the upper edge of the wall, supports have sometimes been provided in the form of vertical rebar running from the top to the base although this does not ensure the desired shear loading mainly due to the relatively low stiffness of tension rebar. In some test arrangements, a steel or reinforced concrete frame is constructed around the wall. This type of arrangement can force the wall to deform in the manner as shown in Figure 2.8.

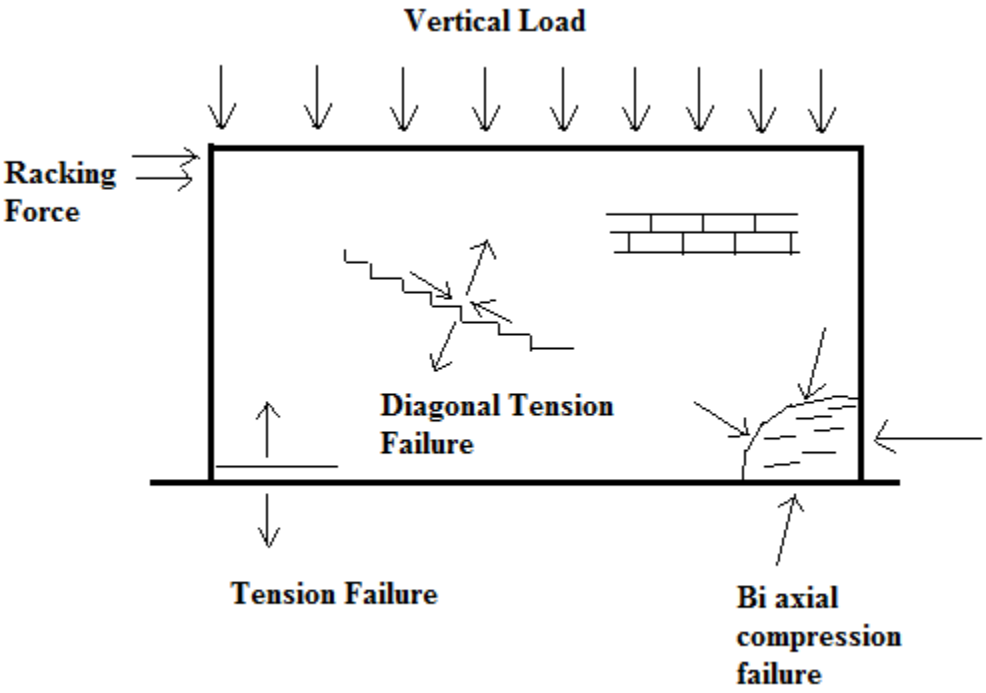

Figure 2.7 Possible Failure of Walls Under Load

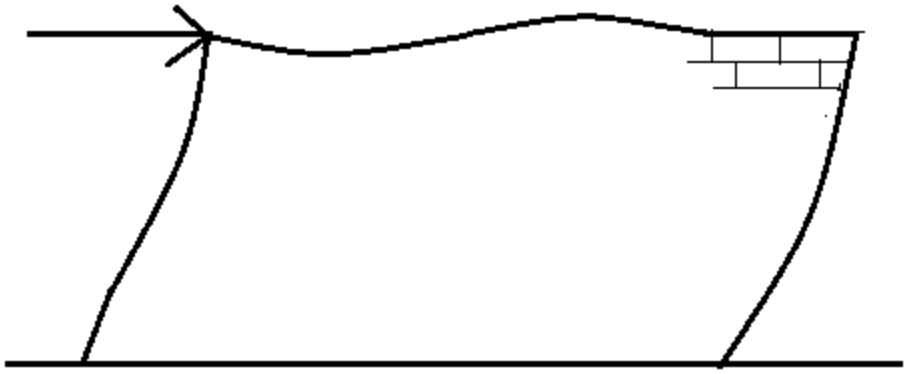

Figure 2.8 Deformation Due to Horizontal Load

2.5.2 Development of Test Method by ESECMASE

One test arrangement utilizing 2 vertical actuators to apply load to the top of the wall was developed within the European research initiative, ESECMaSE (Enhanced Safety and Efficient Construction of Masonry Structures in Europe) (ESECMaSE, 1995). Numerical

models were used to analyze the stress states in residential structures and the test arrangement was developed to try to duplicate the reality as closely as possible. In a structure, restraint from the floor slabs results in bending moments at the top and bottom of the wall as well as a distribution of the axial force so that the axial force should be considered eccentric producing an axial normal force, N, and a bending moment, M=N•e. Full scale masonry walls are tested under displacement controlled horizontal load to ensure observation of post peak resistance with the eccentricity, 'e', of the normal force applied such that the resultant moment at the centre of the wall due to the horizontal force, V, and the normal force is zero. The vertical load is both displacement as well as force controlled in order to keep the absolute value of the ratio

($\frac{M_{cap}}{M_{Bottom}}$) at 1 and to maintain the following relationship :

$$M_{cap} = N \cdot e = V \cdot \frac{h_{Wall}}{2} = -M_{bottom} \qquad \text{(Eq.2.1)}$$

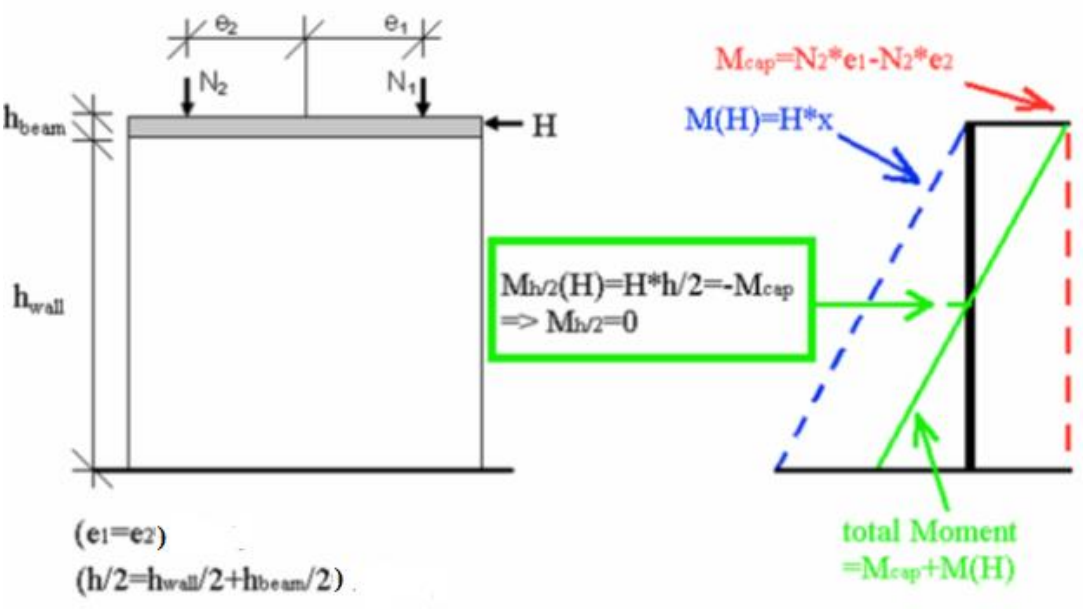

Figure 2.9 Schematic of Loading and Relation Between Loading and Moment in the ESECMaSE Test

The relationship between load and moment is shown schematically in Figure 2.9. In addition to the above mentioned conditions, in the ESECMaSE test method, the total vertical force also has to be constant throughout the test. Otherwise the mechanism for controlling the cap moment can lead to the introduction of other vertical forces which is not desirable.

2.5.3 Loading Protocol

The vertical compression at higher displacement varies in real structures due to the restraints preventing the rotation of wall. This cannot be reproduced accurately in the test condition so walls are typically tested under controlled vertical loading which is usually kept constant during the test within the tolerable limits of axial loading in the actual structure. The cyclic lateral displacement can be applied either statically or dynamically to understand the behaviour under seismic conditions as shown in Figure 2.10. The displacement pattern affects the behaviour significantly as shown by Tomazevic (Tomazevic, 1999) in Figure 2.11.

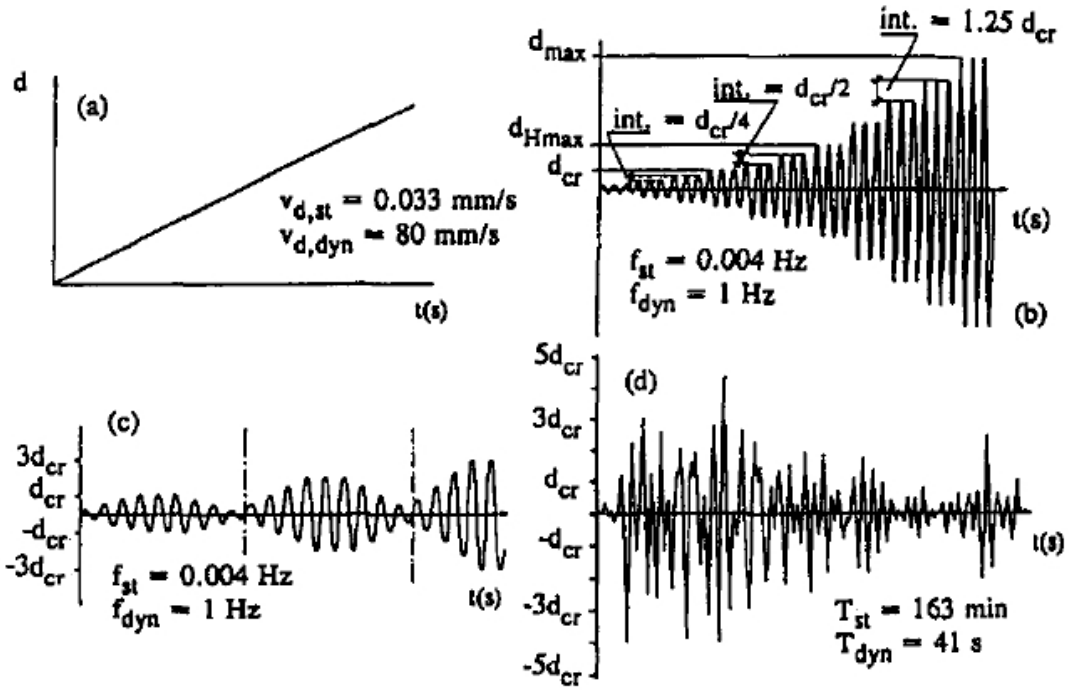

Figure 2.10 Loading Pattern Used for Simulating Earthquake Loading in Masonry Walls (Tomazevic, 1999)

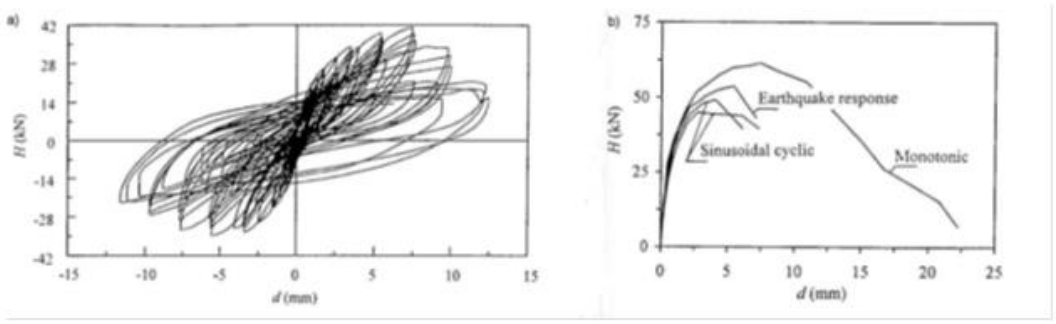

a b

Figure 2.11 a) Typical Load-Displacement Hysteresis Loops Used for Testing Walls b) Load-Deformation Envelopes Found From the Testing of Similar Walls Under Different Test Conditions (Tomazevic, 1999)

From Figure 2.11 it is obvious that the monotonic load pattern gives higher resistance than sinusoidal (cyclic) or earthquake loads. So it is indeed important to test walls under cyclic loading. Tomazevic et. al. (Tomazevic, et al., 1996) also reported that statically applied load gives lower resistance than dynamically applied load. So to be on conservative side it would be a good option to test walls using a quasi-static cyclic load pattern.

Quasi-static cyclic testing is also recommended by FEMA in interim protocol-1 to model the seismic behaviour. A slow cyclic load or deformation is applied to a wall according to a predetermined pattern. The recommended cyclic loading history by FEMA (FEMA461, 2007) is shown in Figure 2.12.

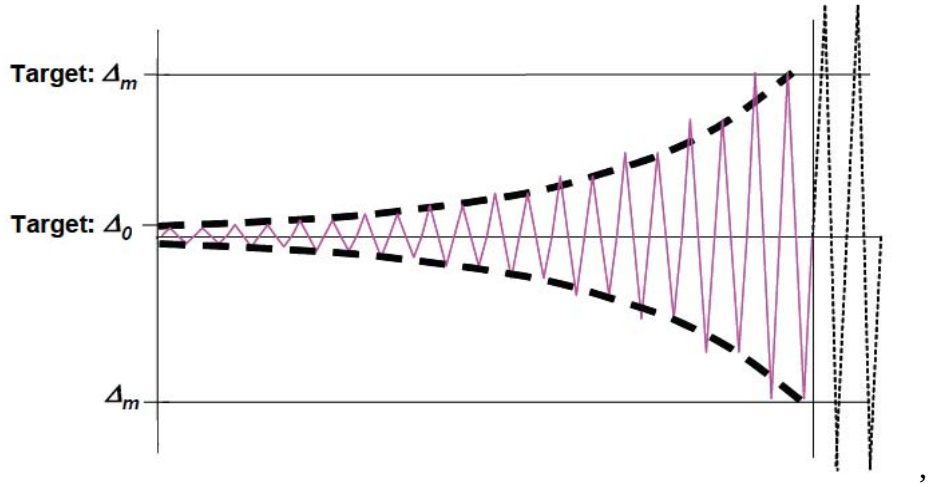

Figure 2.12 Recommended Loading History for Deformation Controlled Test, Consisting of Two Cycles of Step-Wise Increasing Deformation Amplitudes
(FEMA461, 2007)

The minimum displacement recommended by FEMA is Δ_o, which must be safely smaller than the amplitude at which the lowest damage state is first observed. The desired maximum deformation amplitude of the loading history, Δ_m, is an estimated value of the imposed deformation at which the most severe damage level is expected to initiate.
On the other-hand, the ESECMaSE test method also provides a recommendation for the load history based on the cracking displacement, d_{cr}, where the test execution is divided into three levels depending on the behaviour of the wall:

Level A: no relevant cracks are assumed to appear: $d < d_{cr}$ and $V < V_{cr}$
Level B: post-cracking: $d_{cr} < d < D_{V,max}$ and $V_{cr} < V < V_{max}$
Level C: post-peak: $D_{V,max} < d$ and $V_{max} < V$
where d and V are the actual displacement and horizontal shear force, respectively and $D_{V,max}$ is the displacement at the maximum horizontal shear force, V_{max}. Within each of these levels, the increments, Δd, by which the horizontal displacement should be increased, are as follows:

Level A: $\Delta d = 0.25 d_{cr}$
Level B: $\Delta d = 0.50 d_{cr}$
Level C: $\Delta d = 1.25 d_{cr}$

Finally, ESECMaSE also suggests that at each load step, three cycles of horizontal displacement ±d be applied in the form of a sinusoidal function. Based on this, the maximum velocity of the load application should be d_{cr} over 2 minutes (Fehling & Schermer, 2008).

According to FEMA, when deformation controlled testing is conducted, the deformation increment should be sufficiently small so that the dynamic effect remains negligible. At the same time, the deformation increment should be large enough so that the test duration remains reasonable (FEMA461, 2007).

2.6 Methods of Analysis

In Chapter 3, shear strength predictions are compared using equations from different researchers and for different modes of failure. The calculations for the various failure modes are explained below. In Chapter 5, various aspects of the experimental results presented in Chapter 4 are analysed and compared. The methods used in their comparison are also described below.

2.6.1 Shear Strength Prediction

2.6.1.1. Calculation of Flexural Shear Strength

Simple flexural theory can be used to calculate the flexural shear strength of masonry walls assuming that plane sections remain plane after bending. The use of a rectangular compressive stress block with a depth of 'a' and stress level of $0.85f_m'$ can be used for computing nominal flexural strength. The stress and strain profiles of the walls are shown in Figure 2.13.

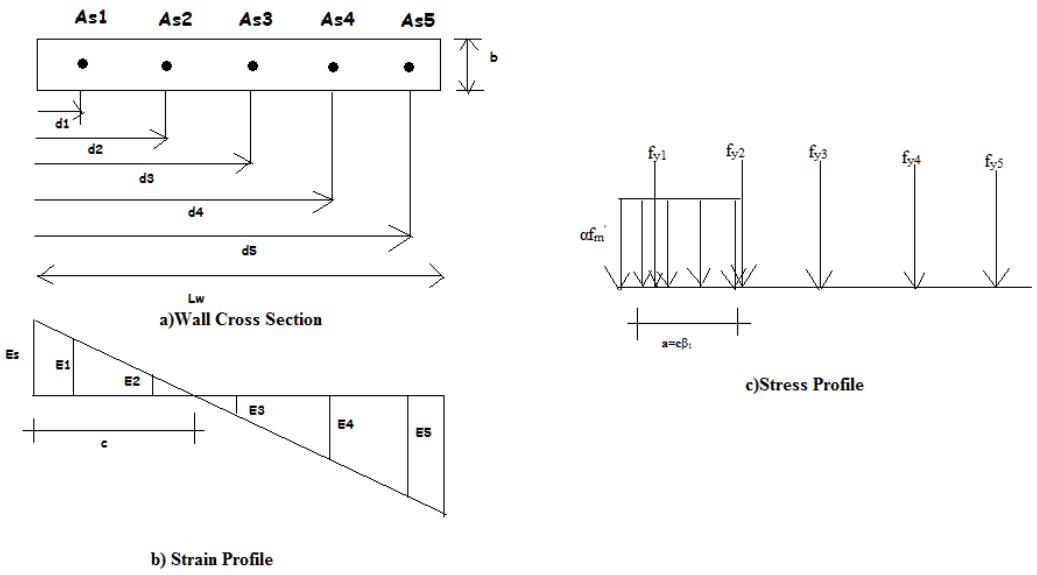

Figure 2.13 Strain and Stress Profile of Wall Cross-Section

The nominal capacity of a wall section can then be evaluated by:

$$M_n = C_m\left(c - \frac{a}{2}\right) + \sum_i^n C_{si}(c - d_i) + \sum_i^n T_i(d_i - \frac{l_w}{2}) \quad \text{(Eq.2.2)}$$

$$\text{And } P = C_m + C_{si} - T_{si} \quad \text{(Eq.2.3)}$$

Where $\sum_i^n C_{si}$ and $\sum_i^n T_i$ are the compressive and tensile strength of the vertical reinforcement obtained from:

$$\sum_i^n C_{si} \text{ or } \sum_i^n T_i = \sum_i^n A_{si} E_{si} \varepsilon_{si} \quad \text{(Eq.2.4)}$$

Where $E_{si}\varepsilon_{si} \leq f_y$

The depth of the equivalent rectangular compressive block can be found by solving the following:

$$a = \frac{C_m}{0.85 f'_m b} \quad \text{(Eq.2.5)}$$

So the nominal strength F_{flex} of a shear wall with an effective height h_e can be expressed as

$$F_{flex} = \frac{M_n}{h_e} \quad \text{(Eq.2.6)}$$

2.6.1.2 Diagonal Shear Resistance

In Clause 10.10.1.1 the Canadian Standard Association CSA S304.1-04 (CSA-Masonry-Standard, 2004) gives the equation for the diagonal shear resistance of a reinforced wall as follows:

$$V_n = \varphi_m(v_m\ b_w d_v + 0.25\ P_d)\gamma_g + 0.6\varphi_s A_v f_y \leq 0.4\sqrt{f'_m} b_w d_v \gamma_g \quad \text{(Eq.2.7)}$$

Where φ_m and $\varphi_s$are the material resistance factors for masonry and the reinforcement, respectively. γ_g is the grouting factor and :

$$v_m = 0.16\left(2 - \frac{M}{Vd_v}\right)\sqrt{f'_m} \text{ Where } 0.25 \leq \left(2 - \frac{M}{Vd_v}\right) \leq 1 \quad \text{(Eq.2.8)}$$

2.6.1.3 Sliding Shear Resistance

The resistance to sliding shear that occurs in reinforced masonry is given by the CSA S304.01-04 (CSA-Masonry-Standard, 2004):

$$V_r = \emptyset_m P_2 \quad \text{(Eq.2.9)}$$

Where, μ is a friction coefficient with a value of 1.0 for masonry to masonry. P_2 is a term that includes the compressive force in the masonry acting normal to the sliding plane, the dowel action of the vertical reinforcement, as well as the diagonal strut forces acting on the wall. In order to get the nominal resistance the material resistance factor, φ_m is eliminated, and the full axial and compression strut loads will be used. As this is not the primary failure mode, no further discussion is provided on this failure model.

2.6.2 Idealization of Experimental Results

The actual hysteretic behaviour of masonry walls subjected to combined vertical load and a sequence of lateral load reversals can be represented by an idealized bi- or tri-linear resistance envelope (Tomazevic, 1999). Three characteristic features in the observed behaviour of the tested walls have to be defined first in order to idealize the experimental envelope:

- The first major cracks in the wall that would change the stiffness i.e. the slope of the envelope.
- Maximum lateral resistance obtained during the test, $H_{max,}$ and the corresponding displacement, d_{Hmax}

- The maximum displacement achieved during the test and the corresponding resistance, H_{Dmax}.

The stiffness of the wall is the ability of the wall to resist lateral loading under elastic deformation. This can usually be evaluated as the slope of the load deformation curve.

Bilinear idealization is adopted in this thesis since it is not as complicated as tri-linear idealization. Therefore, some details of bilinear idealization are highlighted here. When the resistance envelope is idealized with a bilinear relationship, the final/ultimate resistance of the idealized envelope, $H_{u,}$ can be determined by taking the energy dissipation capacity of the actual and idealized curves as equal. So the area below the idealized and experimental curves must be the same.

It should be emphasized here that the ultimate resistance is $H_{u.}$ The maximum design value is not meant by this H_u rather it represents the idealized maximum experimental value. Tomazevic (Tomazevic, 1999) reported that the average value of the ratio of H_u/H_{max} was 0.90 based on the results of more than 60 walls. The value of ultimate displacement, $d_{u,}$ can be found where the line of $0.8H_{max}$ intersects the descending branch of the actual curve. Adopting a value of $0.8H_{max}$ means that although walls may be highly degraded before collapse, for practical calculation this is limited to not more than 20%.

2.6.3 Energy Dissipation Capacity

It is possible to calculate the cumulative energy input, E_{inp} and dissipated energy, E_{diss} from the experimental hysteresis curve. Input energy, E_{inp}, can be well-defined as the work done by the horizontal actuators while the walls deform. The actuator work is the work done pushing and pulling the wall to maximum displacement amplitude in any loading cycle. ΔE_{inp} can be calculated as the total of the areas under the positive and negative parts of the hysteresis loop (Tomazevic, et al., 1996). On the other-hand, the amount of dissipated energy in one cycle of loading can be calculated as the area of hysteresis loop between two successive displacement peaks as shown in Figure 2.14.

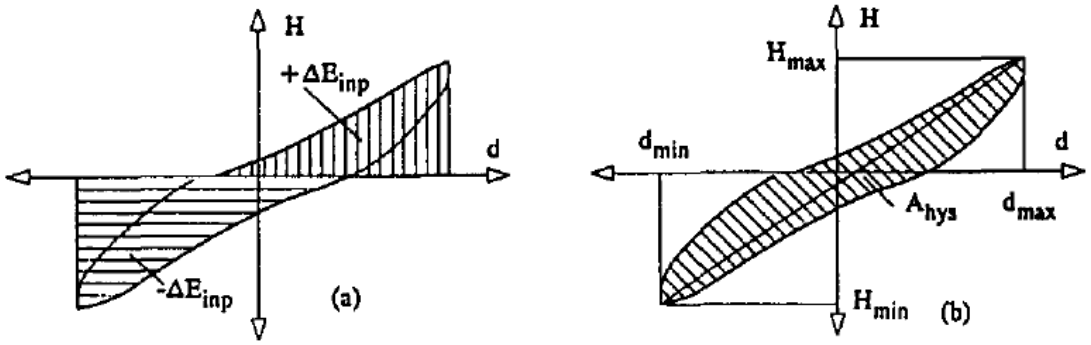

Figure 2.14 a) Evaluation of Input Energy in One Loading Cycle b) Evaluation Of Dissipated Energy In One Loading Cycle (Tomazevic, et al., 1996)**.**

2.6.4 Strength and Stiffness Degradation

When masonry walls are subjected to cyclic load reversals, they undergo strength and stiffness degradation and deterioration. This phenomenon leads to lower lateral load resistance for walls tested under cyclic loading than for monotonic loading with different vertical loading situations and irrespective of whether the load application is dynamic or static (Tomazevic, et al., 1996).

The shape of a non-dimensional stiffness degradation curve has been shown to be similar for all types of masonry walls such as plain, confined and reinforced, as shown in Figure 2.15.

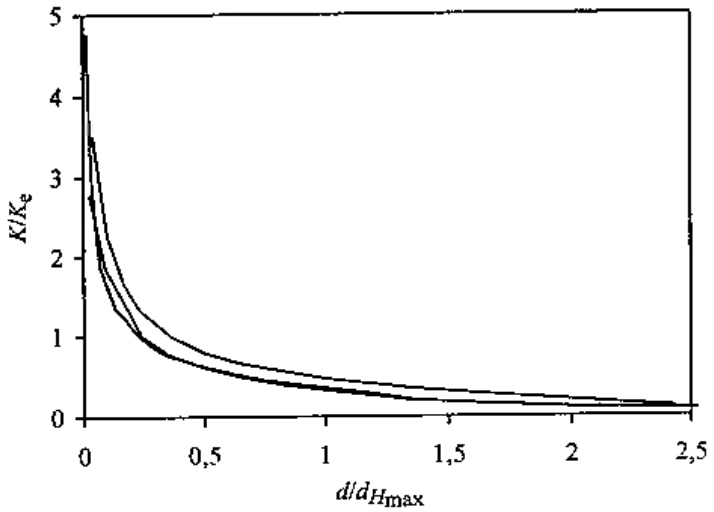

Figure 2.15 Stiffness Degradation of Reinforced Masonry Walls Depending on Normalized Lateral Displacement (Tomazevic, 1999)

2.7 General Concept of Fracture in Compression

In uniaxial compressive testing of brittle specimens, the failure is accompanied by numerous cracks parallel to the compression direction. The phenomena of multiple cracking and crack direction are in direct contrast with the tensile fracture. From the two basic criteria of fracture it is obvious that there must be tension to break the inter-atomic bonds and the release of a sufficient amount of energy should occur. There is a factor that is common to both tensile as well as compression fracture and that is the presence of a void or flaw. If a spherical particle in an infinite medium is an air void, tension develops parallel to the surface at the top of the void, which is perpendicular to the applied compression. That is the tension that is required for the crack to develop. Similar stress concentrating abilities can be observed for different shaped voids. Many voids seem to have similar effects in compression. As a result, cracks can be initiated at a number of voids rather than a particular one and that results in multiple cracking. It is generally recognized that flaws such as cracks, pores, voids and fissures exist in materials even before the application of load (Xiao, 2009). These flaws act as stress raisers and the crack can initiate in the compressive stress fields.

Many structural elements, such as shear walls, are subject to multi-axial stress states, rather than purely uniaxial. Therefore, the strength of concrete, masonry and stone, when subjected to stress states other than uniaxial, is of importance. In biaxial stress states, loads are applied in a single plane. The application of shear loads reduces the principal stresses which results in a pair of principal stresses and the principal stresses can be determined from Mohr's circle. The principal stress in the third principal direction becomes zero. The crack patterns for brittle materials under varying biaxial stress shown in Figure 2.16 and Figure 2.17 are of a general form where cracking is perpendicular to the principal tensile stress though this pattern can be changed due to the presence of a particular weak plane.

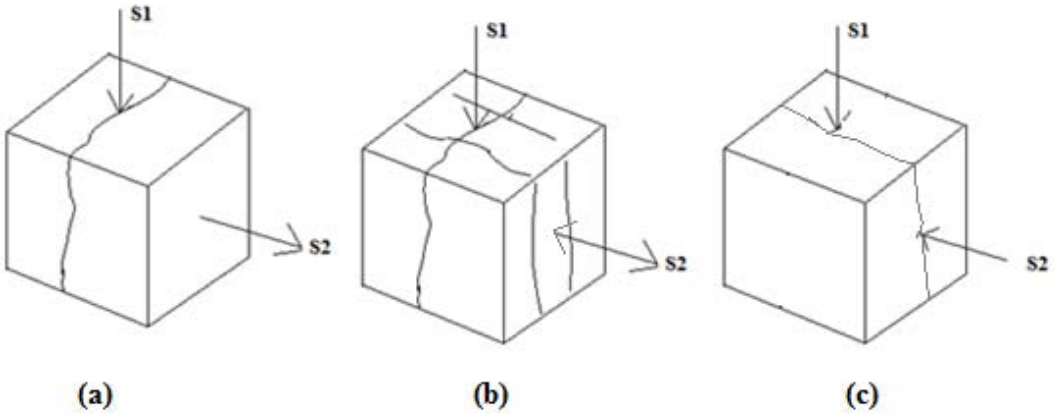

Figure 2.16 a) Biaxial Tension-Compression is Perpendicular to the Tension and Parallel to the Compression b) When the Second Stress is Small (Compared Withthe First) the Cracking is Parallel to the Main Compression. c) When Two Compressions are Applied the Cracking is Parallel to Both

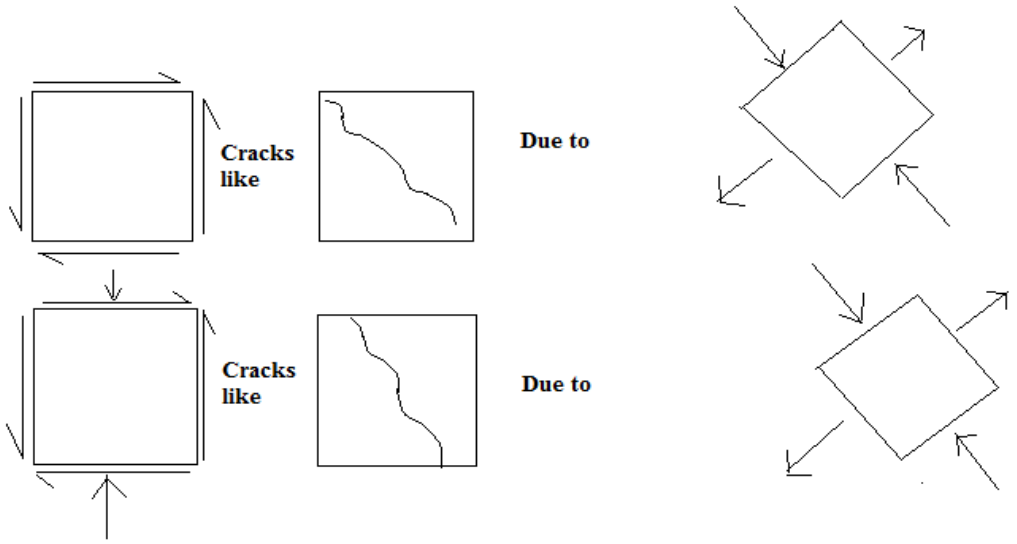

Figure 2.17 Pure Shear Results in a Diagonal Tension Crack Perpendicular to the Equivalent Principal Tension. For Compression and Shear, the Crack is More Steeply Angled but Still Parallel to the Principal Compression, and Perpendicular to the Principal Tension

Cylindrical and spheroidal shaped voids are two types of flaw that might be present in concrete. It remains unknown whether the flaws present in masonry are cylindrical or spheroidal in shape. The following paragraphs discuss the stress due to these two types of flaw and the computation of cracking stress will be carried out for both before comparing the results to see which one better fits the assumption.

2.7.1 Effect of Circular Holes on the Stress Distribution in a Plate

If a plate with a circular hole in the middle of it is subjected to uniform tension, S, as shown in Figure 2.18, the stress distribution in the neighborhood of the hole increases though it remains unchanged at a distance away which is large compared to the radius of the circle.

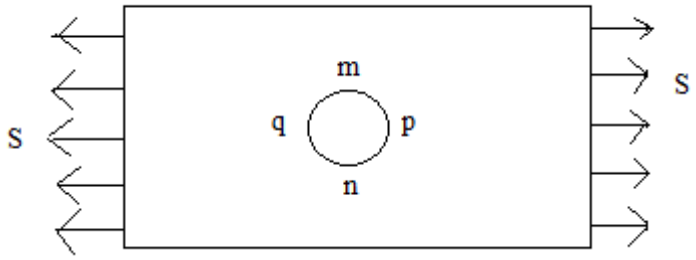

Figure 2.18 Effect of Circular Hole in a Plate (Timoshenko & Goodier, 1951)

The stress at the edge of the hole can be found from the solution given by Kirsch's equation as mentioned by Timoshenko and Goodier (Timoshenko & Goodier, 1951):

$$\sigma_r = \frac{S}{2}\left(1 - \frac{a^2}{r^2}\right) + \frac{S}{2}\left(1 + \frac{3a^2}{r^4} - \frac{4a^2}{r^2}\right)\cos^2\theta \qquad \text{(Eq.2.10)}$$

$$\sigma_\theta = \frac{S}{2}\left(1 + \frac{a^2}{r^2}\right) - \frac{S}{2}\left(1 + \frac{3a^4}{r^4}\right)\cos 2\theta \qquad \text{(Eq.2.11)}$$

$$\tau_{r\theta} = -\frac{S}{2}\left(1 - \frac{3a^4}{r^4} + \frac{2a^2}{r^2}\right)\sin 2\theta \qquad \text{(Eq.2.12)}$$

Where '*a*' is the radius of the hole. Therefore, $\sigma_\theta = 3S$ at the boundary at m and n, and $\sigma_\theta = -S$ at the boundary at p and q.

The maximum tensile stress at points m and n is three times the stress applied S, while at points p and q the stress, –S, is a compressive stress of the same magnitude as that developed around the hole in the direction parallel to the applied stress. So if compressive stress of value S_1 is applied in the direction perpendicular to the tensile stress then a tensile stress of magnitude S_1 would develop at points 'm' and 'n'. So the maximum tensile stress in the plate would then be at points m and n and be equal to S_1 +3S. When this circular hole is present in a solid body the flaw becomes cylindrical.

2.7.2 Effect of Spheroidal Holes on Stress Distribution

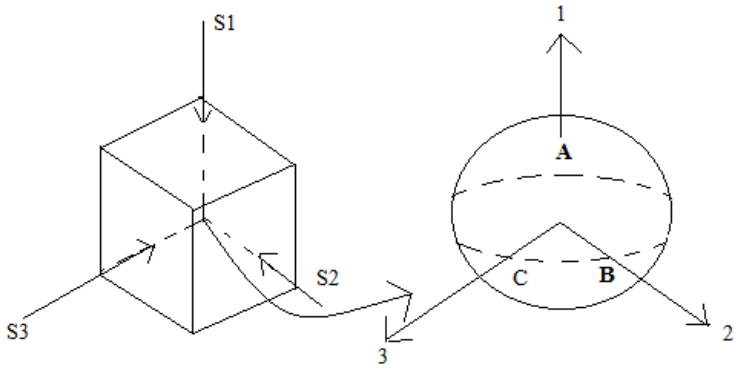

Figure 2.19 Spheroidal Hole in a Solid Body.

If a spheroidal flaw is present in a solid body as shown in Figure 2.19, under the externally applied stresses S_1, S_2 and S_3, the resulting stress at the surface of the flaw due to the presence of the flaw can be estimated by the formula given by Goodier (Shrive, 1983). The stress σ_{22} at point A is then given by:

$$\sigma_{22} \text{ (in dir'n of B)} = S_2 + \frac{1}{14-10\upsilon}[S_1(-3-15\nu) + S_2(13-5\nu) + S_3(-3+15\nu)] \quad \text{(Eq.2.13)}$$

So the stress is found to be dependent on Poisson's ratio but not on the modulus of elasticity where Poisson's ratio, υ=0.15 for masonry.

2.8 Summary

Having considered the previous test configurations and experimental results reported in the literature, several gaps were identified for further study. Results regarding the effect of different parameters are only comparable to a limited extent, due to varying test arrangements and limits to the range of certain parameters. The research project described in this thesis attempts to fill some of the holes that exist in concrete block masonry wall research under cyclic loading in order to bring the state of the art in masonry shear wall research to a new height. Therefore, walls with different types of horizontal reinforcement anchorage will be tested using the ESECMaSE test method. The effect of applying constant vertical load and different boundary conditions will also be investigated. The application of monotonic load versus cyclic load will also be investigated for this test arrangement.

Chapter 3: Analysis of Different Experimental Data

3.1 Introduction

Masonry structures exist and continue to be built all over the world in areas prone to seismic activity. Therefore, predicting the strength of masonry shear walls is of particular importance. Quite a lot of research has been carried out on reinforced masonry shear walls made of concrete block or clay brick in the United States, Canada, New Zealand, and Japan. Based on this research, various equations have been developed to predict the in-plane shear strength of masonry walls, mainly by regression analysis of the test data. This chapter aims to compare five of the most well-known equations for predicting in-plane shear strength of masonry walls using results from various sources and thus evaluate the accuracy of each equation. Finally, a modified equation is formulated and evaluated.

3.2 Shear Strength and Different Equations

The shear mechanism in masonry is quite a complex phenomenon as discussed in Chapter 2. As a result, for diagonal shear alone, there have been numerous models developed by various masonry researchers. For simplicity when calculating the nominal shear strength, commonly the contribution from masonry, reinforcement and axial stress are calculated separately and then added ignoring the fact that these factors might be dependent on each other. This chapter deals with five equations selected from the literature for determining in-plane diagonal shear strength of masonry walls to determine how effective they are in estimating strength by comparing the predicted strengths to test data reported by various researchers. The selection of these equations is based on the criteria that two of these, namely the Anderson and Priestley (Anderson & Priestley, 1992) equation and the NEHRP (NEHRP, 1997) equation are the basis of the Canadian and U.S design equations respectively. The Shing equation is one of the most cited equations and one of the few which accounts for the contribution of vertical reinforcement. The Matsumura equation is another popular equation because it takes into account the effect of all the parameters that are believed to affect the shear strength. In

addition, Voon's equation was the basis for the in-plane shear equation provided in the New Zealand design standard (Voon & Ingham, 2007).

3.2.1 Shing Equation (Shing, et al., 1990)

Shing proposed an equation for predicting shear based on the test results from 22 walls. The proposed formula was also checked for its accuracy using the test results obtained by Sveinsson et al. (1985). In the formulation of this equation, the shear strength depends mainly on the residual masonry strength and the amount of horizontal reinforcement. The residual masonry strength depends on the amount of vertical or axial stress which helps resist crack opening and thus increases the aggregate interlock force which in turn increases the residual strength of the masonry. In evaluating the strength contribution of the horizontal reinforcement, Shing (1990) proposed that since diagonal cracks occur at approximately 45 degree angles, only the bars spread over the height of the wall will be activated whereas the reinforcing bars in the top and bottom courses would not have adequate development length beyond where they intersect the crack to develop tensile resistance. With these considerations, the equation takes on the following form:

$$V_s = \left(0.166 + 0.0217\rho_v f_y\right)\sqrt{f'_m} + 0.0217\sqrt{f'_m}\sigma + \frac{\left(\frac{L-2d'}{s}-1\right)(A_h\, f_{yh})}{Lt} \qquad \text{(Eq. 3.1)}$$

Where

d' = depth to vertical reinforcement from the end of the wall in the cross-section (mm).

ρ_v = vertical reinforcement ratio.

f_y = yield strength of vertical reinforcement (MPa).

f_m' = compressive strength of masonry (MPa).

σ = vertical stress (MPa).

A_h = area of horizontal reinforcement (mm^2).

L= length of the wall (mm).

f_{yh} = yield strength of horizontal reinforcement (MPa).

t = thickness of wall (mm).

3.2.2 Anderson and Priestley (Anderson & Priestley, 1992) Equation

Anderson and Priestley (1992) outlined formulae for each mode of failure containing various coefficients for various parameters. These coefficients were then evaluated by

fitting them to test data obtained from three sources: Sveinsson et al. (1985) Shing et al. (1990) and Matsumura (1987). According to their results, in the equation for diagonal shear, the contribution from horizontal reinforcement in masonry is half that for reinforced concrete and surprisingly the vertical reinforcement had no effect on strength. Their explanation as to why the contribution of the horizontal reinforcement is so low is that the shear reinforcement remains unstressed when the loading begins, as all the shear is carried by masonry. As the diagonal cracks start to form, the reinforcing steel crossing the cracks must go into tension, but because of the crack opening, the shear carried by the masonry across the crack is reduced. This phenomenon intensifies as the crack widens. As a result, with increased deformation, the rate at which the reinforcement influences shear capacity may be less than the rate of loss of masonry strength itself and so an optimum capacity is achieved. They also concluded that since the predictive equation did not seem to fit one set of data better than the other, it is possible that wall shear strength is not dependent on aspect ratio. So this equation does not contain any term to account for the effect of aspect ratio.

$$V = C_{ap} k \sqrt{f'_m} + 0.25\sigma + 0.5 A_s f_{ys} \frac{d}{sA_n} \qquad \text{(Eq.3. 2)}$$

Where

C_{ap} = factor used to account for the type of masonry used in construction

= 0.24 for concrete block

= 0.12 for clay brick

k = ductility coefficient factor

= 1 for a flexural ductility ratio of up to 2 and then decreases linearly to zero at a ductility ratio of 4.

s = spacing of horizontal reinforcement (mm).

A_n = net cross-sectional area (mm^2).

A_s = area of shear (horizontal) reinforcement (mm^2).

d = distance from extreme compression fiber to centroid of longitudinal tension reinforcement or 0.8L for walls

3.2.3 NEHRP (NEHRP, 1997)

The National Earthquake Hazard Reduction Program (NEHRP) encourages U.S design and building practices that address earthquake hazards so that the resulting damage may be minimized. NEHRP proposed a masonry shear equation similar to the Anderson and Priestley equation with the exception of a modification to account for the aspect ratio and then the equation becomes:

$$V = 0.083\left[4 - 1.75\frac{M}{VL}\right]\sqrt{f'_m} + 0.25\sigma + 0.5A_s f_{ys}\frac{d}{sA_n} \qquad \text{(Eq.3.3)}$$

Where the ratio M/VL should not be greater than unity. Depending on this value of M/VL there is a limitation on the maximum total shear strength as follows:

$$V_{n(max)} = \begin{cases} 0.5A_n\sqrt{f'_m} & \text{for } \frac{M}{VL} \le 0.25 \text{ or} \\ 0.33\,A_n\sqrt{f'_m} & \text{for } M/VL \ge 1 \end{cases} \qquad \text{(Eq.3. 4)}$$

With straight line interpolation to be used for M/VL values between 0.25 and 1.

3.2.4 Matsumura Equation (Matsumura, 1987)

Matsumura developed his equation based on the results of his own research as well as the results of others researchers in Japan. Regression analysis of the test results was used to fit the equation for different parameters such as horizontal reinforcement, vertical reinforcement, axial stress, aspect ratio, loading condition, grouting and masonry contribution.

$$V_n = [K_u K_p\left(\frac{0.76}{\left(\frac{h}{d}\right)+0.7} + 0.012\right)\sqrt{f'_m} + 0.2\sigma_n + 0.18\gamma\delta\sqrt{\rho_h f_{yh} f'_m}](0.875td) \qquad \text{(Eq. 3.5)}$$

Where

K_u = a reduction factor for respective difference in the kind of masonry or method of loading

= 1 for fully grouted masonry.

= 0.64 partially grouted masonry.

K_p= coefficient taking into account the effect of flexural reinforcement=$1.16\rho_{ve}^{3}$

$\rho_{ve} =$ flexural reinforcement ratio, $a_t/td(\%)$.

$a_t =$ cross sectional area of flexural reinforcing bar (one side) (mm^2)

γ = factor concerning the extent of grouting

= 1 for fully grouted

= 0.6 for partially grouted

δ = factor concerning loading method.

= 1 for double bending

= 0.6 for cantilever.

3.2.5 Voon's Equation (Voon, 2007)

Voon developed a new equation based on his research which closely resembles the NEHRP equation but introduced the effect of vertical reinforcement and displacement ductility on masonry shear strength:

$$V_n = 0.8k(C_a + C_b)A_n\sqrt{f'_m} + 0.9N^*\tan\alpha + A_h f_{yh}\frac{D_{eff}}{s_h} \leq 0.33A_n\sqrt{f'_m} \qquad \text{(Eq 3.6)}$$

Where

C_a = coefficient to account for vertical reinforcement as in Shing's equation

$= 0.022\rho_v f_{yv}$

C_b = factor to account for the effect of wall aspect ratio

$= 0.083[4 - 1.75\frac{M}{VL}]$

D_{eff}= L-2d´-l_{dh}

Where l_{dh} is taken as $20d_b$ and $35d_b$ for reinforcement strengths of 300 MPa and 500 MPa, respectively.

α = angle formed between the wall axis and the strut from the point of load application to the centre of flexural compression zone at the wall plastic hinge critical section for cantilever walls, For walls in double bending condition, this is the angle between the wall axis and the line joining the centre of flexural compression at the top and bottom of the wall as shown in Chapter 2.

N^*= axial load

The displacement ductility factor used in this equation is more conservative than that adopted in the Anderson and Priestley equation as the latter uses a 'k' value of 1 up to a ductility ratio of 2 assuming that no strength degradation occurs up to that point, whereas Voon takes the limiting ductility ratio as 1.25 for k = 1. Above this limit, 'k' decreases

linearly to zero at the ductility ratio of 4 for both cases. The shear stress contribution from axial stress was considered as a result of the diagonal compression strut.

Voon (2007) also proposed a different factor to Anderson and Priestley for the contribution of horizontal reinforcement explaining that the low factor obtained by Anderson and Priestley could have been due to different anchorage conditions at the ends of the reinforcement which could have resulted in insufficient development length. Therefore, Voon defined a dead zone at the end of the wall where the reinforcement cannot develop the full yield strength and thus excludes this dead zone in the definition of D_{eff} in the equation as shown above.

3.3 Test Results Used For Comparison

Experimental results of reinforced masonry walls that failed in shear were gathered from different sources and the details of the test specimens and results were collected in a database. The database is used here for analysis and comparison of the equations discussed in the previous section. The research projects that have been included in the database are shown in Table 3.1.

Table 3.1 Database Resources

Name of Researcher	Location/ Project Name	Number of specimens
Shing et al. (1990).	US Japan Joint technical Committee on Masonry Research (TCCMAR) Program. University of Colorado	22
Matsumura (1987)	Kanagawa University	56
Voon (2007)	University of Auckland	10
Kaminosono et al. (1988)	US-Japan Co-ordinated Earthquake Research Program	19
Sveinsson et al.(1985) Chen et.al. (1978) and Hidalgo et al (1978)	University of California Berkeley.	60

Name of Researcher	Location/ Project Name	Number of specimens
Okamoto et al. (1987)	Japan's building research institute, Ministry of construction in connection with TCCMAR program.	26
Fujisawa (1986)	US-Japan Research Program.	6
Khattab and Drysdale (1993)	University of McMaster, Ontario.	5
Tomazevic and Lutman (1988)	Institute for testing in Research in material and Structures (ZRMK) Ljubljana, Yugoslavia.	16
Schultz et al. (Schultz, 1996) (Schultz, et al., 1998)	Building and Fire Research Laboratory of The National Institute of Standards and Technology.	12
Yancey and Scribner (Yancey & Scribner, 1989)	National Institute of Standards and Technology (NIST), USA.	10
Kesperik (Kasperik, 2009)	McMaster University, Canada	5
Dickie (Dickie & Lissel, 2010)	University of Calgary, Canada	20
Priestley (Priestley, 1976)	University of Canterbury.	6
Shedid et. al (Shedid, et al., 2008), (Shedid, et al., 2010)	McMaster University, Canada	13
Woodward and Rankin (1985)	National bureau of Standards, USA	7

The test results accumulated in the database above vary in different aspects. Variables include difference in support conditions, grouting, reinforcement ratios, aspect ratio, and axial stress. Some necessary information was not reported in the literature, for example

the ductility ratio which is needed to calculate strength in the Anderson and Priestley and Voon equations. In those cases a reasonable value is assumed for calculation purposes.

3.4 Comparison of Different Equations

Initially, theoretical values of shear resistance for each of the different test specimens were calculated using the equations discussed in Section 3.2. Subsequently, the theoretical results were compared against the actual experimental results to determine if, and by how much, the theoretical values deviate from the actual experimental ones. An analysis was carried out to determine how many theoretical values were below the actual experimental values (i.e. on the conservative side) and also how often the results were predicted within a given range. This may help to have an idea how the equations behave for a large set of data. While comparing the test results, only specimens that were reported to have failed in diagonal shear were considered. The summary of this analysis is shown in Table 3.2.

Table 3.2 Comparison of Experimental vs. Theoretical Results

Name of Equation	% of data that are lower than actual	% of data that are within ±10% of actual ones	% of data that are within ±15% of actual ones	% of data that are within ±20% of actual ones	% of data that are 0-20% lower than actual	% of data that are 0-10% lower than actual
Shing	55.4	26	32	39.0	25.6	16.4
Matsumura	55.8	22.5	32.5	39.0	23.8	13.4
Anderson and Priestley	62.8	16.0	23.8	35.1	19.1	6.5
NEHRP	43.7	16.9	29.9	41.1	22.9	10.4
Voon	34.6	13.0	21.6	27.6	19.9	13.0

It is evident from the table that the Voon equation more consistently overestimates the in-plane shear strength than any other equation where only 34.6% of the calculated values are less than the actual experimental values. Only 13% of the calculated values fall within

±10% of the actual values and only 27.6% of values falls within ±20% of the actual values. The other equations all had higher percentages of calculated values that are less than the actual shear values; 55%, 56%, 62.8% and 43.7% for the Shing, Matsumura, Anderson and Priestley and NEHRP equations, respectively. The Anderson and Priestley equation seems to give the highest number of dataset values that fall below the actual results. The Shing and Matsumura equations give the highest number of calculated values that are closest to the actual ones with around 25% within ±10% and 39% within ±20% of the actual experimental values. Another comparison was made to find out what proportion of the data are lower than the actual values but fall within a certain percentage i.e those values that give an experimental to predicted strength ratio between 1-1.1 or 1-1.25. These values are shown in the last two columns of Table 3.2 and show that the Shing equation is best at predicting values closer to the actual values. Although Shing's equation and Matsumura's equation are the best in terms of the comparison presented above, there is still room for improvement.

3.5 Effectiveness of Different Equations for Predicting In-Plane Shear

The in-plane shear of reinforced masonry walls can be computed by the following simple formulation:

$$V_n = V_m + V_p + V_s + V_f \qquad \text{(Eq.3.7)}$$

Where V_n = nominal shear strength

V_m = shear contribution from masonry, should also include the contribution due to aspect ratio.

V_p = shear contribution from axial stress

V_s = shear contribution from shear (horizontal) reinforcement.

V_f = shear contribution from flexural (vertical) reinforcement.

While the experimental results from different sources show varying degrees of dependency on the various factors, some of the equations discussed in section 3.2 consider all the factors, while others don't. Therefore, a modified equation should be developed that not only includes the effect of all the related parameters as shown in Eq. 3.7 but also yields predicted values closer to the actual ones. Each of the factors assumed

to affect shear capacity are examined in the following discussion in order to determine the modifications necessary.

3.5.1 Effect of Axial Stress

A comparison was carried out using selected data where the only variable was axial stress, while aspect ratio, vertical reinforcement and horizontal reinforcement were kept constant. The experimental results from various wall sets with varying axial stress were chosen and the predicted shear strength values obtained from the above five equations are presented below. In the following discussions, the stresses are calculated based on the net area of the walls and are normalized by dividing them by the square root of the compressive strength ($\sqrt{f_m'}$) in order to eliminate the effect of masonry compressive strength. It should be mentioned here that the square root of masonry compressive strength is used to normalize because in all equations the contribution from the masonry strength is in the form of the square root of f_m'.

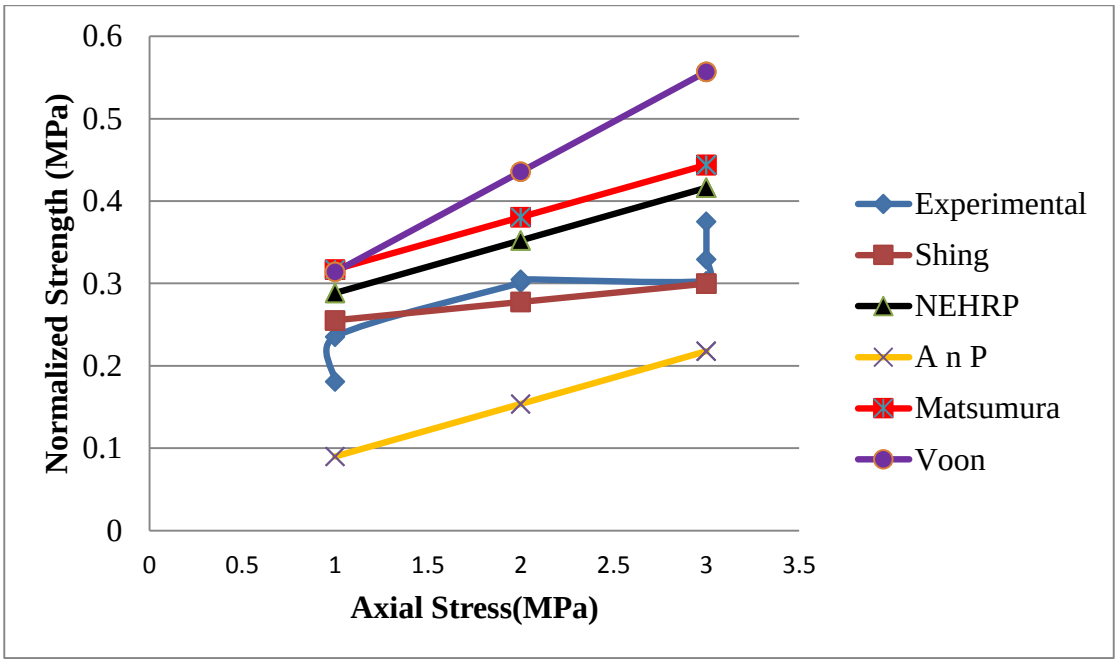

Figure 3.1 Comparison of Experimental vs. Theoretical Results for Dickie's Dataset

One of the datasets originates from testing at the University of Calgary (Dickie & Lissel, 2010). Figure 3.1 shows that the predicted values are less than the experimental values for Shing's equation and the Anderson and Priestley equation, whereas the values

predicted by the NEHRP equation, and Matsumura give slightly higher values but Voon's equation gives significantly higher values than the experimental results. Though the factor applied to axial stress is the same for both the NEHRP and Anderson and Priestley equations, they predict very different values which must be attributed to the term containing the aspect ratio since this is the only real difference between the two equations. When compared to Okamoto's dataset (Okamoto, et al., 1987) as shown in Figure 3.2, all of the equations underestimate the strength. In order to assess the shear strength contribution from axial stress, the slopes of the lines in Figure 3.2 were calculated to be 0.069, 0.022, 0.063, 0.064, 0.064 and 0.122 for the experimental results, Shing, Matsumura, Anderson and Priestley, NEHRP and Voon equations, respectively. Therefore, the influence of axial stress on shear strength seems to be best captured in the Matsumura equation or by the Anderson &Priestley/NEHRP (both have the same term) equations.

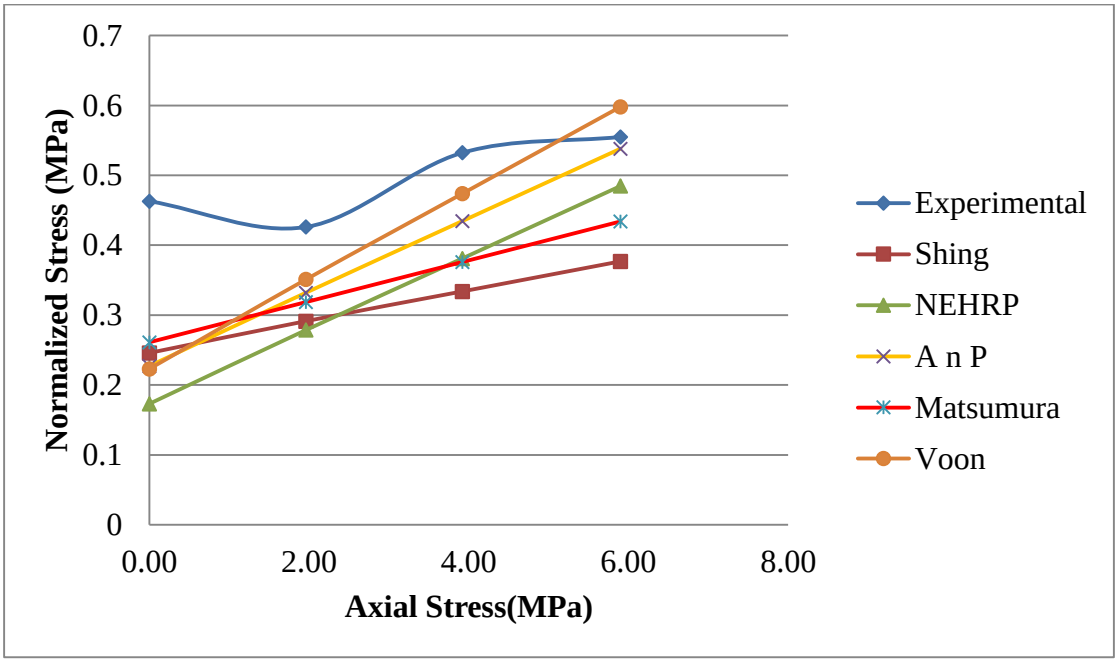

Figure 3.2 Comparison of Experimental vs. Theoretical Values for Okamoto's Dataset

3.5.2 Effect of Aspect Ratio and Masonry Compressive Strength

Aspect ratio refers to the ratio between the height and length of the wall. It has been shown through different experimental results that as the aspect ratio decreases, and the

walls become less slender, the shear strength capacity increases. Among the five equations that are being used for comparison here in this thesis, only the Matsumura and NEHRP equations consider the contribution of aspect ratio, while Voon adopted the NEHRP term for aspect ratio in his equation. As above, various experimental results were compared with calculated results in order to evaluate the contribution of aspect ratio together with the masonry compressive strength to shear strength.

Initially, a few test results from Hiraishi's dataset (Hiraishi, 1985) were chosen where the main variable is the aspect ratio while the configuration, reinforcement, and axial stress are constant. The masonry compressive strength also changed between test results therefore the results are normalized by dividing the predicted and experimental shear stress values by the square root of masonry compressive strength to circumvent the effect of masonry compressive strength as much as possible. Graphical comparisons of the experimental and theoretical results are shown in Figure 3.3 and Figure 3.4.

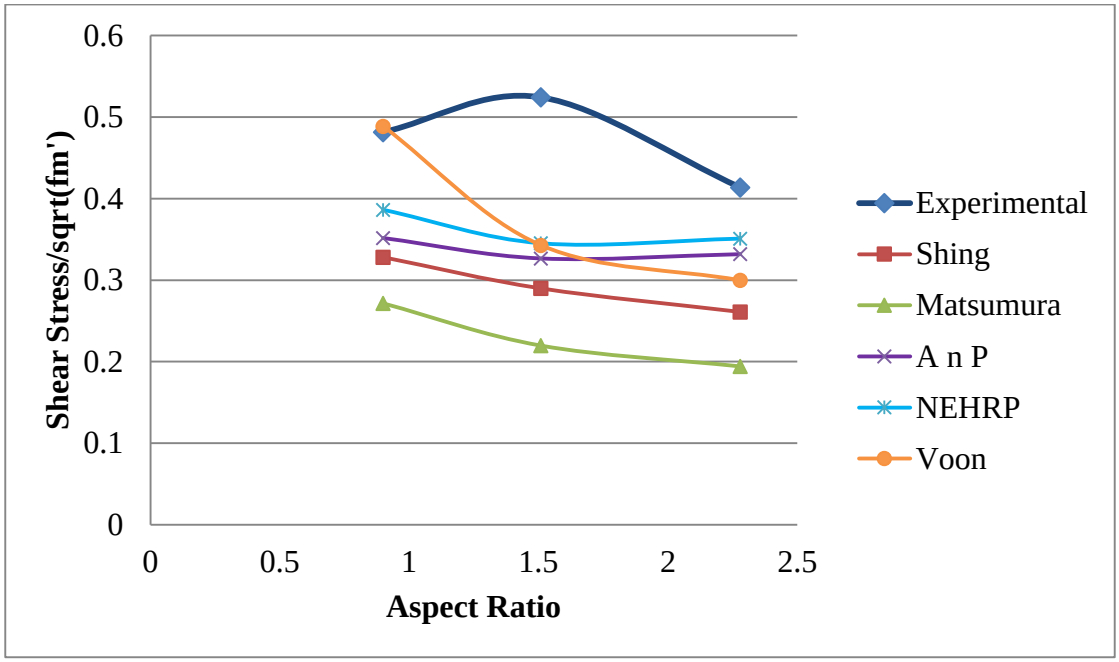

Figure 3.3 Comparison of Test Results and Theoretical Results With Changing Aspect Ratio (Hiraishi, Block Results)

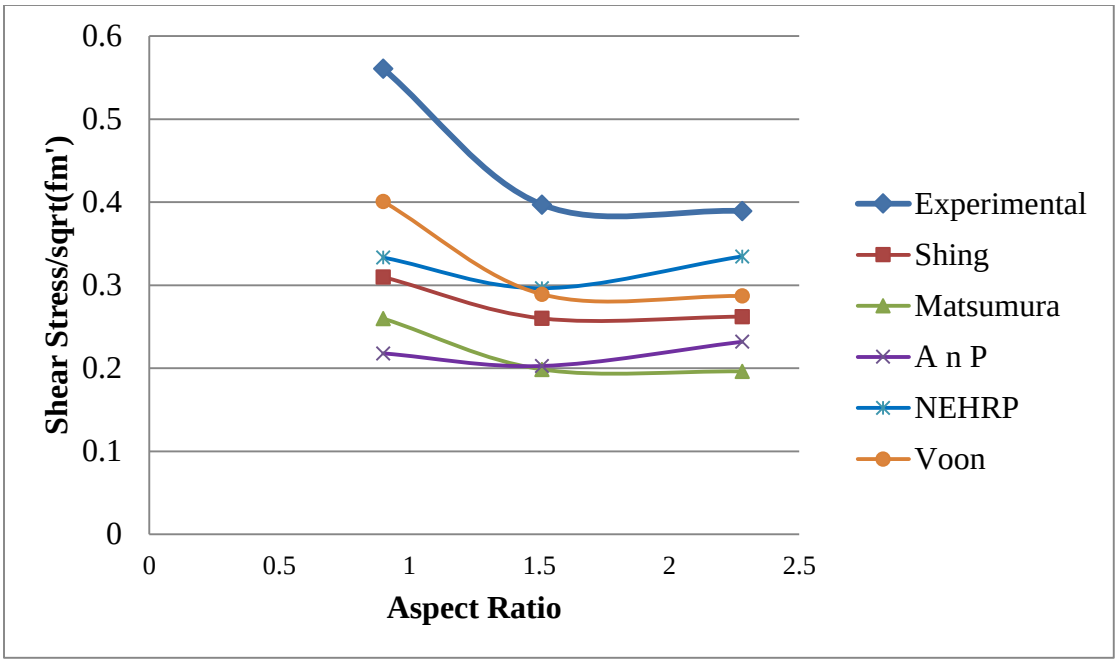

Figure 3.4 Comparison of Test Results and Theoretical Results With Changing Aspect Ratio (Hiraishi, Brick Results)

In both cases, all the equations underestimate the experimental values. The results of Okamoto (Okamoto, et al., 1987) and Voon (Voon, 2007) were also compared with the theoretical results as shown in Figure 3.5 and Figure 3.6 where the tendency to underestimate the shear strength is confirmed.

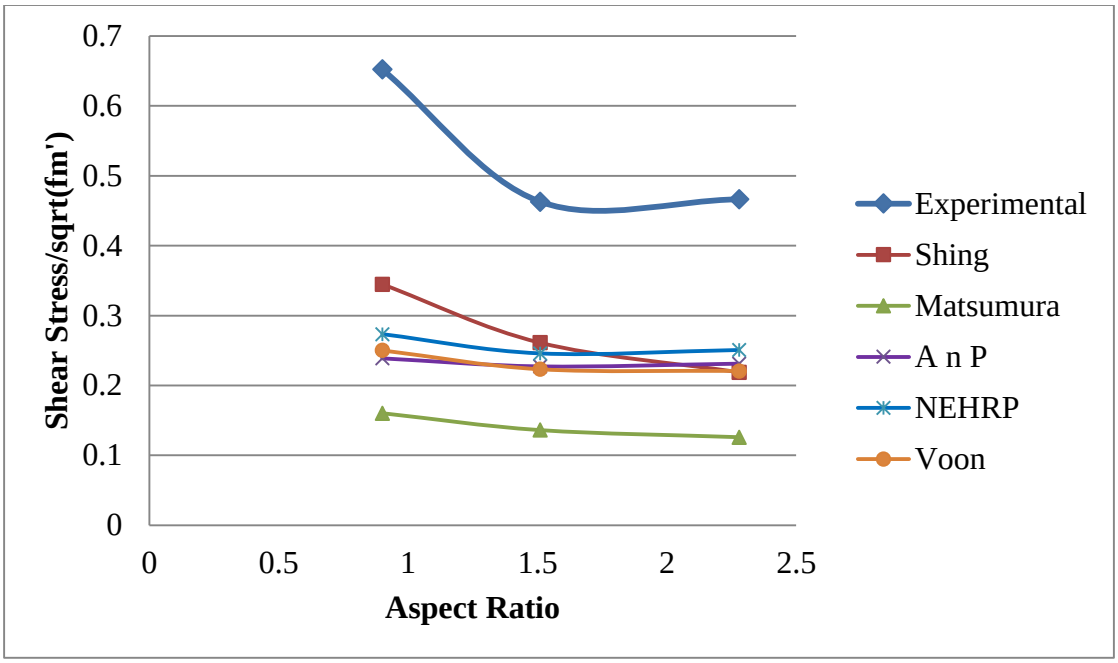

Figure 3.5 Comparison of Test Results and Theoretical Results With Changing Aspect Ratio (Okamoto)

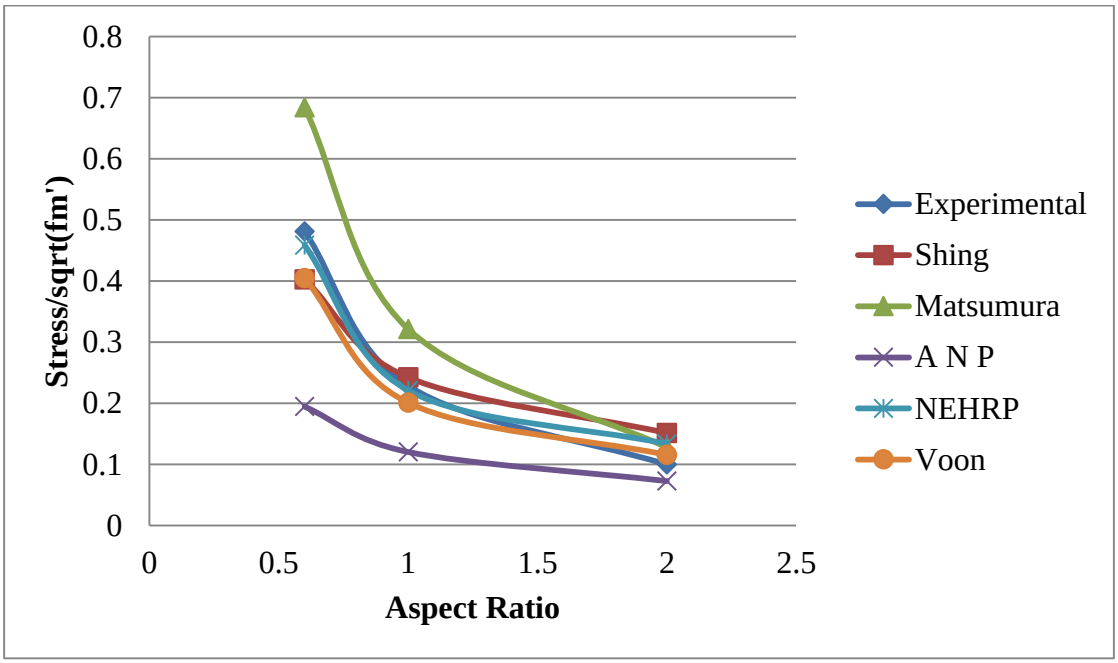

Figure 3.6 Comparison of Test Results and Theoretical Results With Changing Aspect Ratio (Voon)

As mentioned earlier, only Matsumura, NEHRP and Voon consider the effect of aspect ratio in their equation, where Voon actually reproduces the NEHRP term in his equation. The Anderson and Priestley equation does not account for the aspect ratio, therefore the

variation seen in the above figures is because of the varying compressive strength affecting the first term of Eq. (3.2).

From the figures above, it can be said that among the three equations that include effects of aspect ratio (Matsumura, Voon and NEHRP), all of them actually resemble the shape of the actual curve but they are not close to the actual values. Therefore, although the calculated values were much lower than the actual ones for some cases, the NEHRP equation still gives results that are the closest to the actual ones. To better evaluate how well the equations capture the effect of aspect ratio, the shape/slope of the curves between consecutive points was calculated for comparison as shown in Table 3.3. The comparison shows that the NEHRP and Voon equations (both have the same term for aspect ratio) match the experimental results the best for Voon's dataset. In this case, the equation that gives values that are lower than the actual results and are also consistently closest is chosen to be on the conservative side. Since it is assumed that the variation is only due to the change in aspect ratio then it seems that the term used in the NEHRP equation for aspect ratio should be included in shear prediction models. The values obtained for other datasets show no clear trend and no conclusion can be drawn from those results as shown in Table 3.3.

Table 3.3 Calculation of Change Due to Aspect Ratio at Two Consecutive Points for Theoretical and Experimental Results

Heading	Dataset	Experimental	Shing	Matsumura	Anderson and Priestley	NEHRP	Voon
Slope between first two points	Voon	0.253	0.160	0.345	0.074	0.237	0.204
	Okomoto	-0.18	-0.08	-0.02	-0.01	-0.03	-0.03
	Hiraishi (Block)	0.04	-0.04	-0.05	-0.03	-0.04	-0.14
	Hiraishi (Brick)	-0.16	-0.05	-0.06	-0.02	-0.04	-0.11

Heading	Dataset	Experimental	Shing	Matsumura	Anderson and Priestley	NEHRP	Voon
Slope between last two points	Voon	0.129	0.091	0.184	0.048	0.087	0.138
	Okomoto	0.003	-0.04	-0.01	0.004	0.004	-0.002
	Hiraishi (Block)	-0.11	-0.03	-0.03	0.005	0.006	-0.04
	Hiraishi (Brick)	-0.007	0.002	-0.002	0.03	0.04	-0.002

Note that the aspect ratios used by the researchers for the datasets discussed above are not the same in most cases. Observation of Table 3.3 indicates that the effect of aspect ratio is perhaps not an independent term but rather it may be correlated to other parameters such as masonry compressive strength or axial stress.

3.5.3 Effect of Vertical Reinforcement

Neither the Anderson and Priestley equation nor the NEHRP equation contain a term that accounts for the vertical reinforcement, however the vertical reinforcement might have an influence on the strength as can be seen by the test results of Dickie (Dickie & Lissel, 2010) shown in Figure 3.7 where the only variable is the amount of vertical reinforcement. It is also noted in the figure that there is a decrease in strength at the highest amount of reinforcement. Increasing shear strength with increasing vertical reinforcement has, however, been observed by other researchers, including Shing and Matsumura. The test results of Matsumura and Shing along with the theoretical results from the different equations are shown in Figure 3.8 and Figure 3.9. According to these comparisons it is obvious that Shing's equation gives the closest value to the experimental results not only for Shing's test data but also for other cases. Although the Matsumura equation is the only one to show the same decrease for the last data point of Dickie's results, in general, Shing's equation gave results closest to the actual results in

all other cases. Therefore, the vertical reinforcement term given in Shing's equation will be adopted in the modified formula.

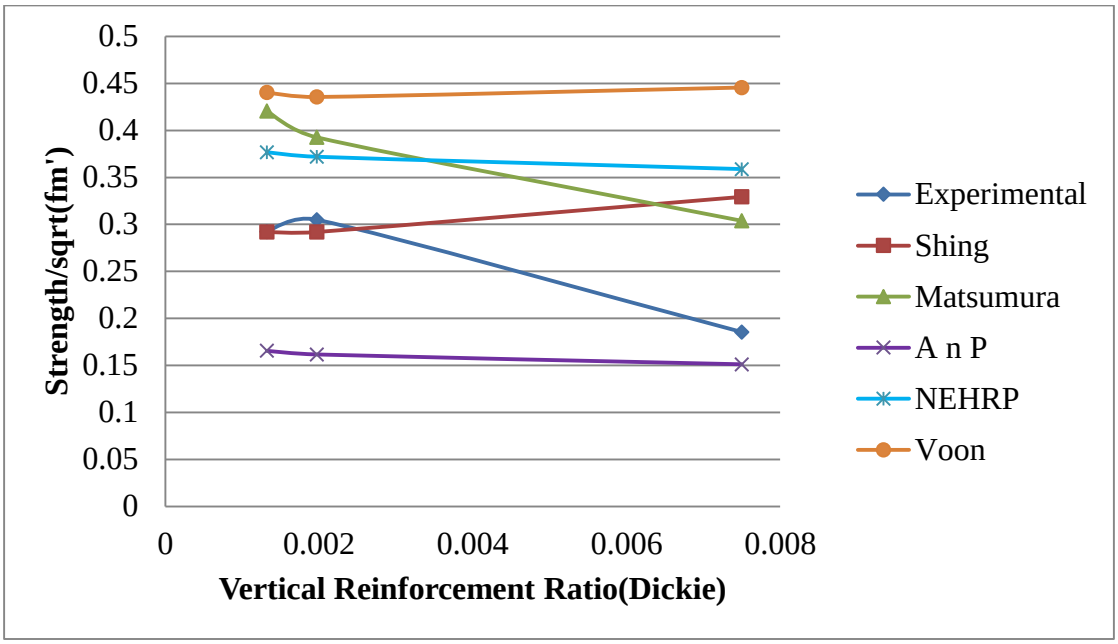

Figure 3.7 Comparisons of Test Results and Theoretical Results With Changing Vertical Reinforcement Ratio (Dickie Dataset)

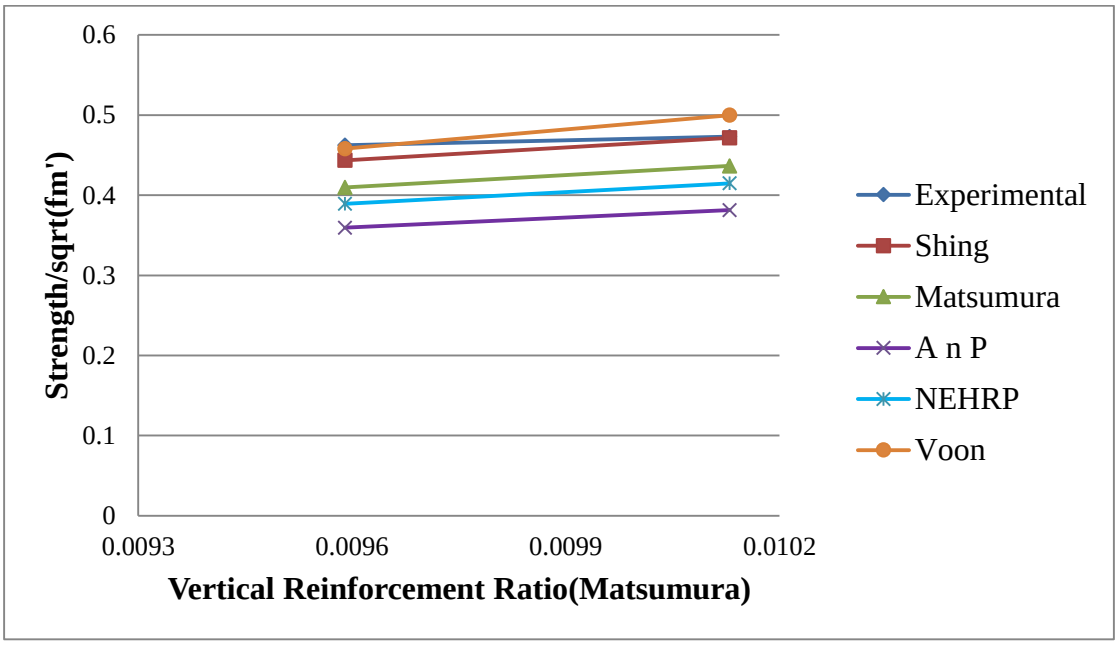

Figure 3.8 Comparisons of Test Results and Theoretical Results With Changing Vertical Reinforcement Ratio (Matsumura Dataset)

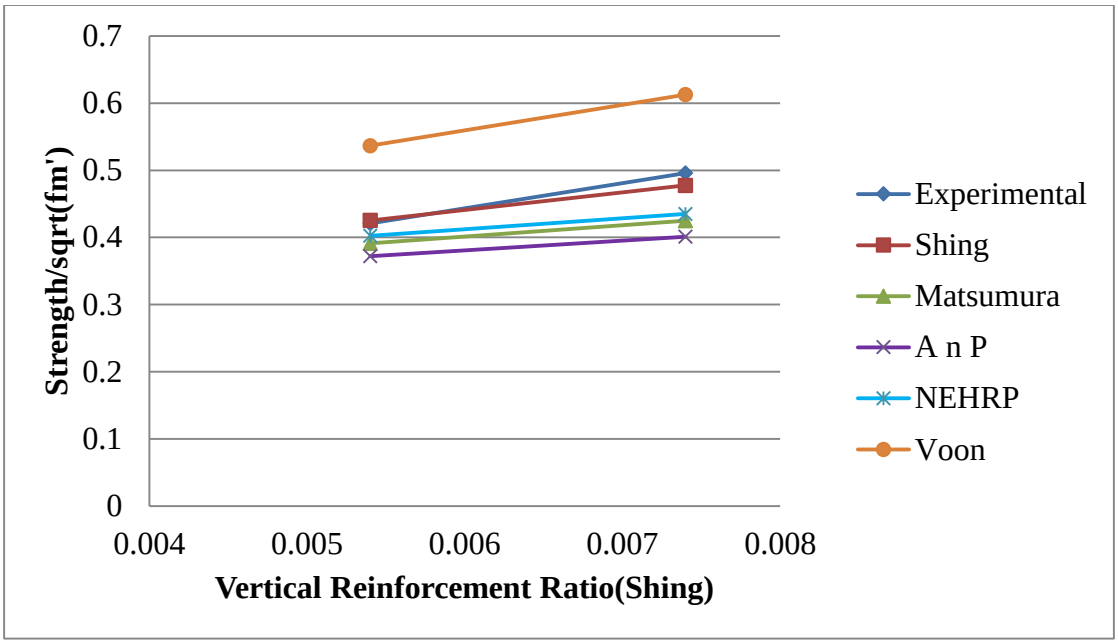

Figure 3.9 Comparisons of Test Results and Theoretical Results With Changing Vertical Reinforcement Ratio (Shing Dataset)

3.5.4 Effect of Horizontal Reinforcement

Location and percentage of horizontal reinforcement play a significant role in the behaviour of reinforced masonry walls. According to Alcocer and Meli (Alcocer & Meli, 1995), horizontally reinforced walls have higher resistance than unreinforced walls but the reinforcement does not actually affect the initial stiffness of walls. In terms of increasing the ultimate load carrying capacity under static racking load, early tests on masonry shear walls performed by Schneider (Schneider, 1959) and Scrivener (Scrivener, 1967) showed optimum shear reinforcement ratios of 0.2% and 0.3%, respectively. The results of Tomazevic et al. (1996) also showed a similar trend and it was observed that, in most cases, the shear strength decreases for a horizontal reinforcement ratio beyond approximately 0.25%. On the contrary, Hidalgo et al. (1978) showed no significant change in strength though the change in horizontal reinforcement ratio was quite notable. Test data were chosen from Tomazevic et al. (1996), Hidalgo et al. (1978), Matsumura (1987), Sveinsson et al. (1985) and Dickie (Dickie & Lissel, 2010) to examine the effect of horizontal reinforcement on shear strength of walls and determine how well different equations capture the effect of changing reinforcement ratio. These comparisons are

shown in Figure 3.10(a) through (h). The reinforcement ratio here refers to the actual reinforcement ratio not as a percentage.

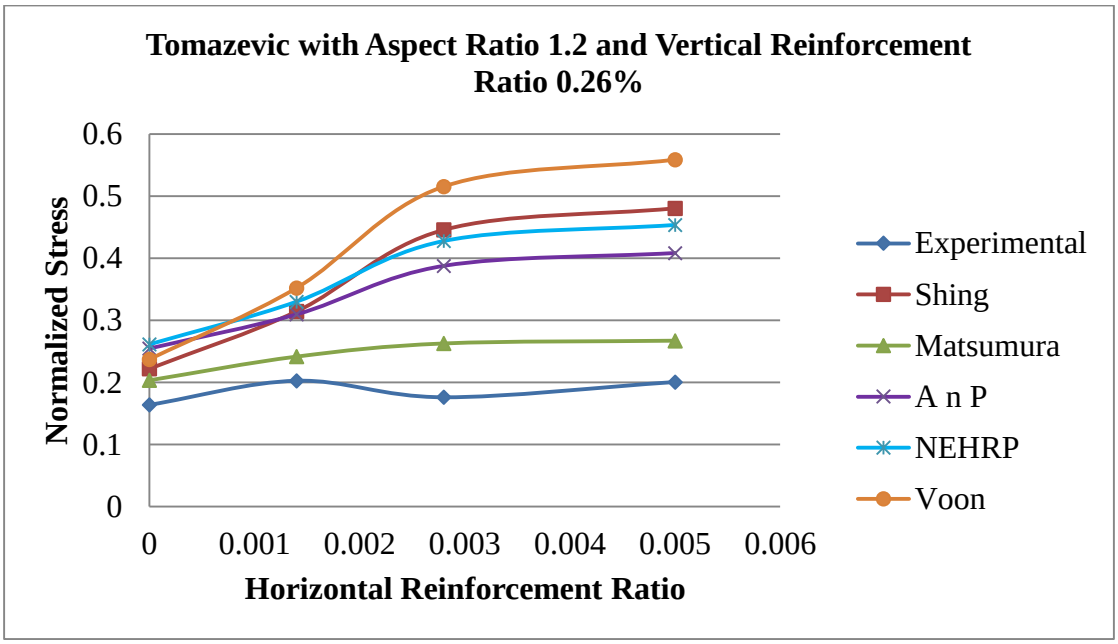

(a)

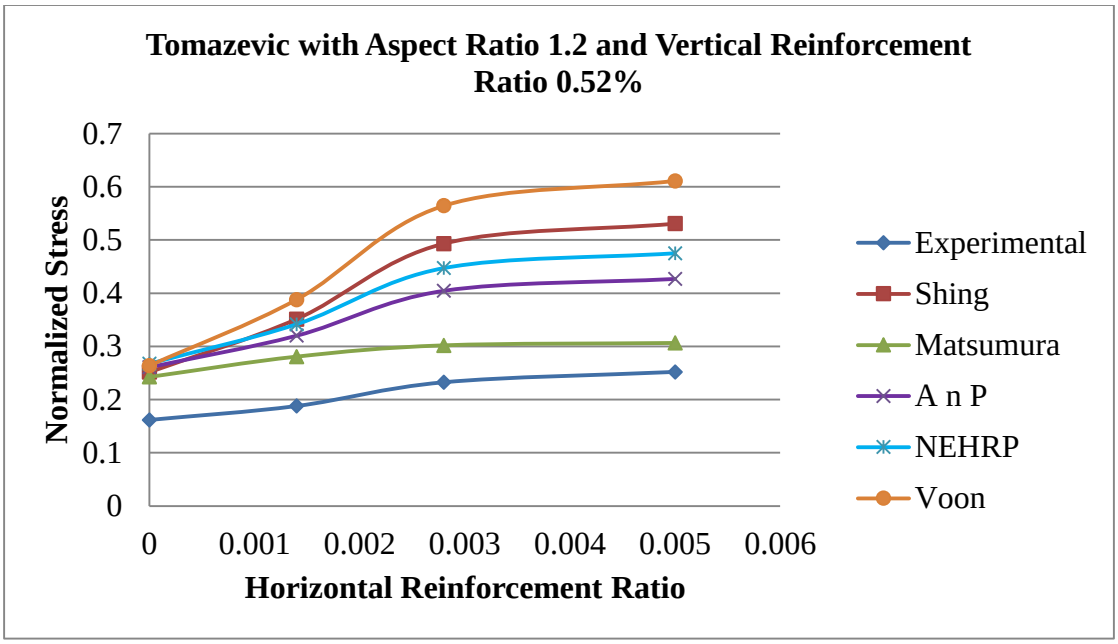

(b)

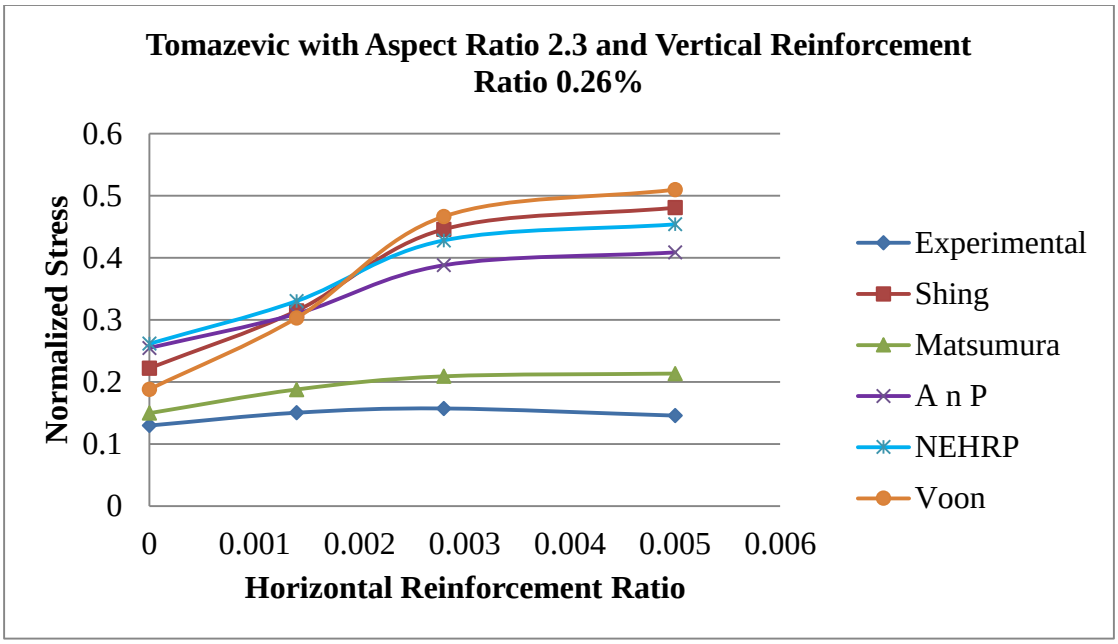
Tomazevic with Aspect Ratio 2.3 and Vertical Reinforcement Ratio 0.26%
Normalized Stress
0.6
0.5
0.4
0.3
0.2
0.1
0
0
0.001
0.002
0.003
0.004
0.005
0.006
Horizontal Reinforcement Ratio
Experimental
Shing
Matsumura
A n P
NEHRP
Voon

(c)

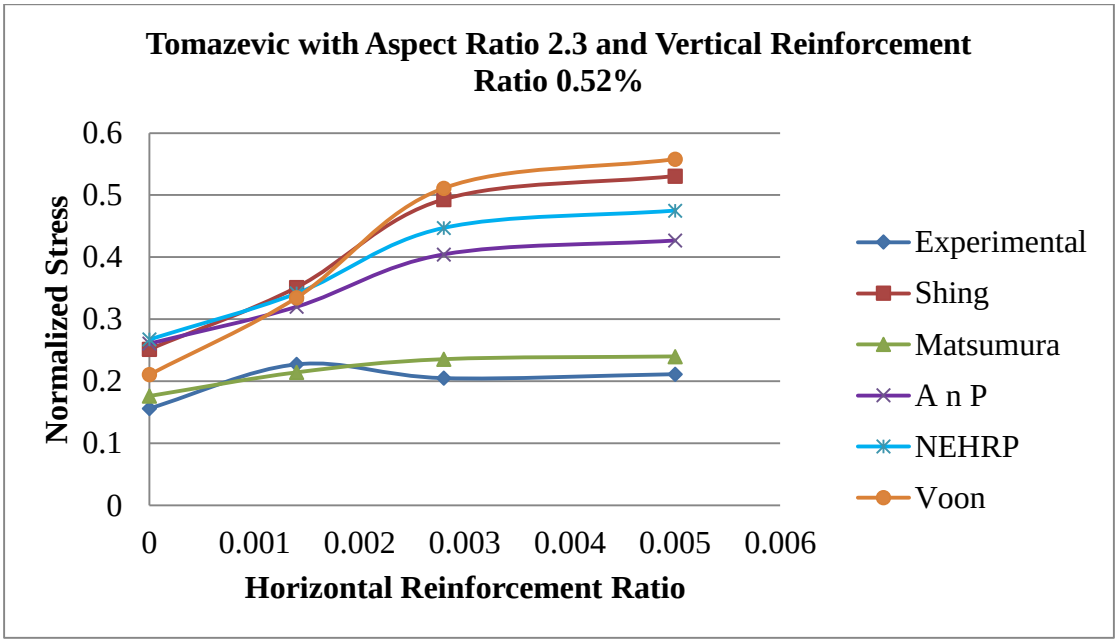
Tomazevic with Aspect Ratio 2.3 and Vertical Reinforcement Ratio 0.52%
Normalized Stress
0.6
0.5
0.4
0.3
0.2
0.1
0
0
0.001
0.002
0.003
0.004
0.005
0.006
Horizontal Reinforcement Ratio
Experimental
Shing
Matsumura
A n P
NEHRP
Voon

(d)

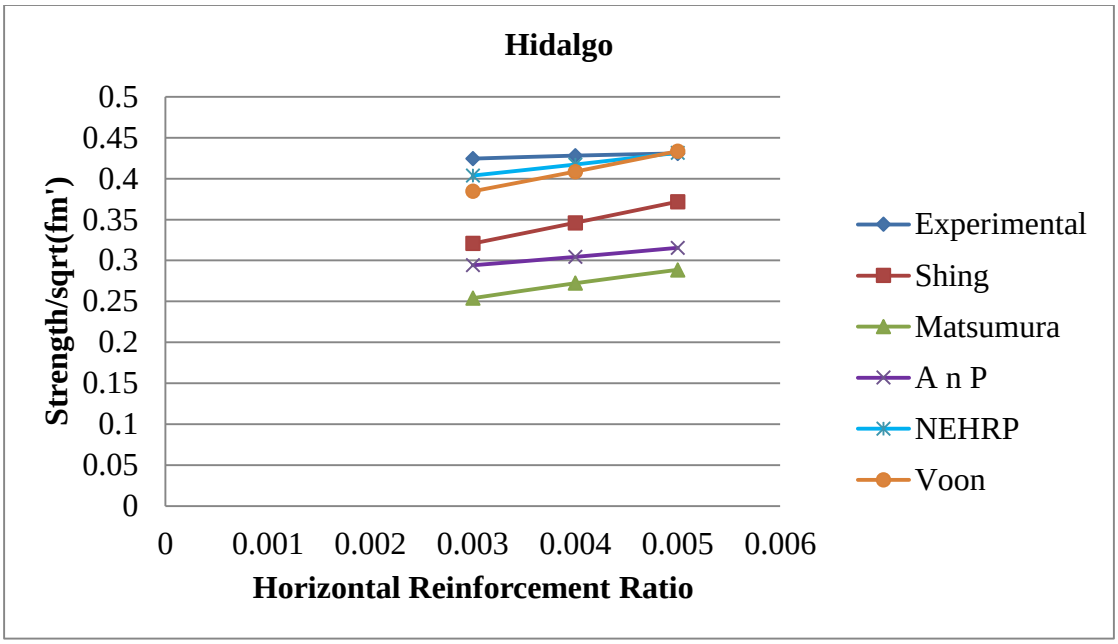
Hidalgo
Strength/sqrt(fm')
0.5
0.45
0.4
0.35
0.3
0.25
0.2
0.15
0.1
0.05
0
0
0.001
0.002
0.003
0.004
0.005
0.006
Horizontal Reinforcement Ratio
Experimental
Shing
Matsumura
A n P
NEHRP
Voon

(e)

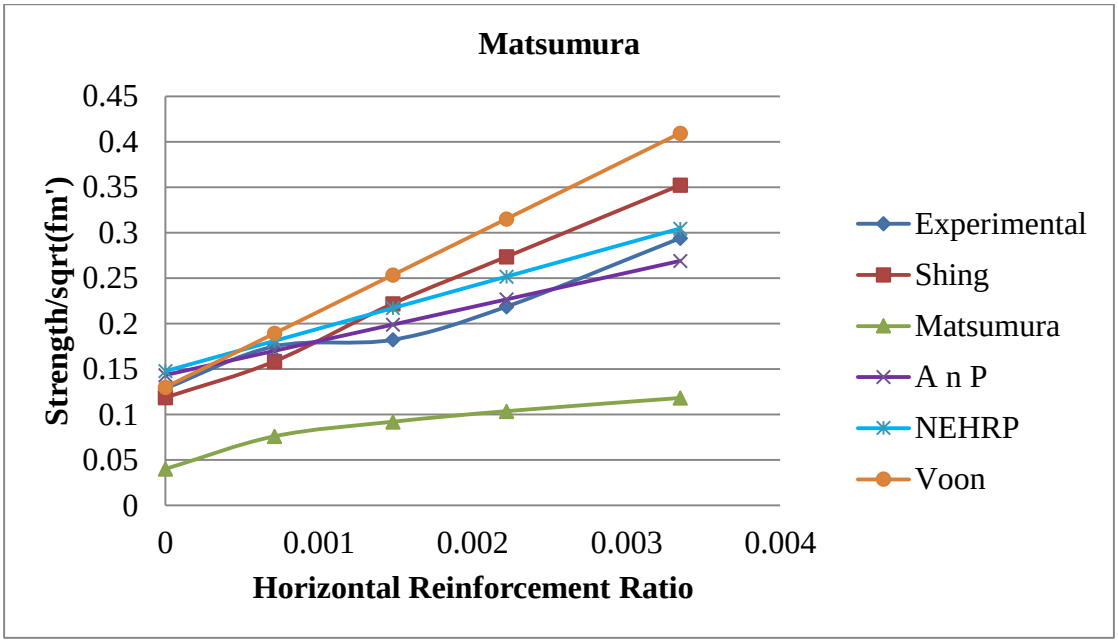
Matsumura
Strength/sqrt(fm')
0.45
0.4
0.35
0.3
0.25
0.2
0.15
0.1
0.05
0
0
0.001
0.002
0.003
0.004
Horizontal Reinforcement Ratio
Experimental
Shing
Matsumura
A n P
NEHRP
Voon

(f)

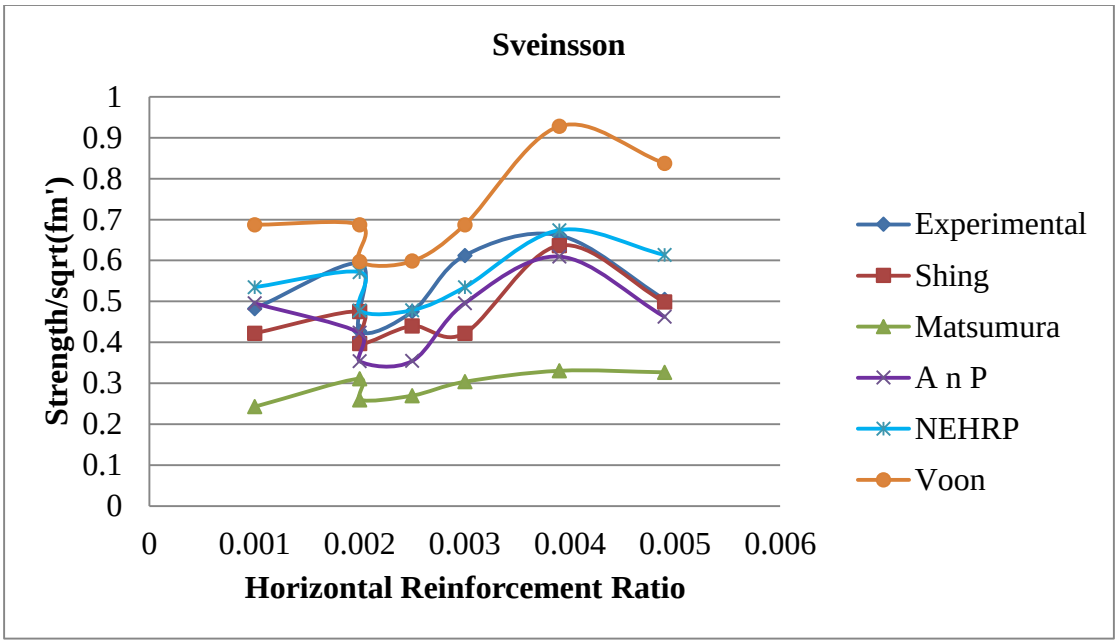

(g)

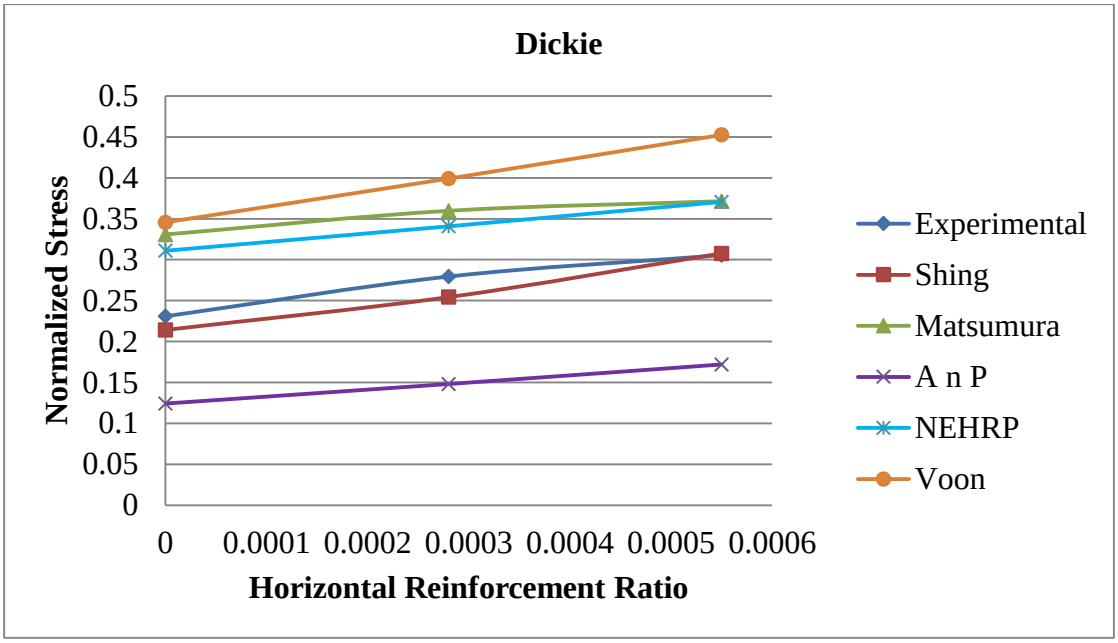

(h)

Figure 3.10 Comparison of Test Results and Theoretical Results With Changing Horizontal Reinforcement Ratio for Tomazevic (a,b,c,d), Hidalgo (e), Matasumara (f) , Sveinsson (f) and Dickie (h)

Quite strange behaviour is observed for Sveinsson's test results which may be due to the varying masonry compressive strength in these walls. In addition, Sveinsson's results do not show any optimum value or trend, but rather there are fluctuations in the results.

Matsumura's equation produces results very close to the actual results for Tomazevic's data sets however, for his own data, it is not one of the better equations. It cannot be concluded from the figures shown above as to which equation gives better results than the others. Therefore, another set of data from Voon was selected where the axial stress is zero, the vertical reinforcement ratio and aspect ratio were constant and only the horizontal reinforcement ratio changed. The comparisons of this data set with the theoretical results are plotted in Figure 3.11.

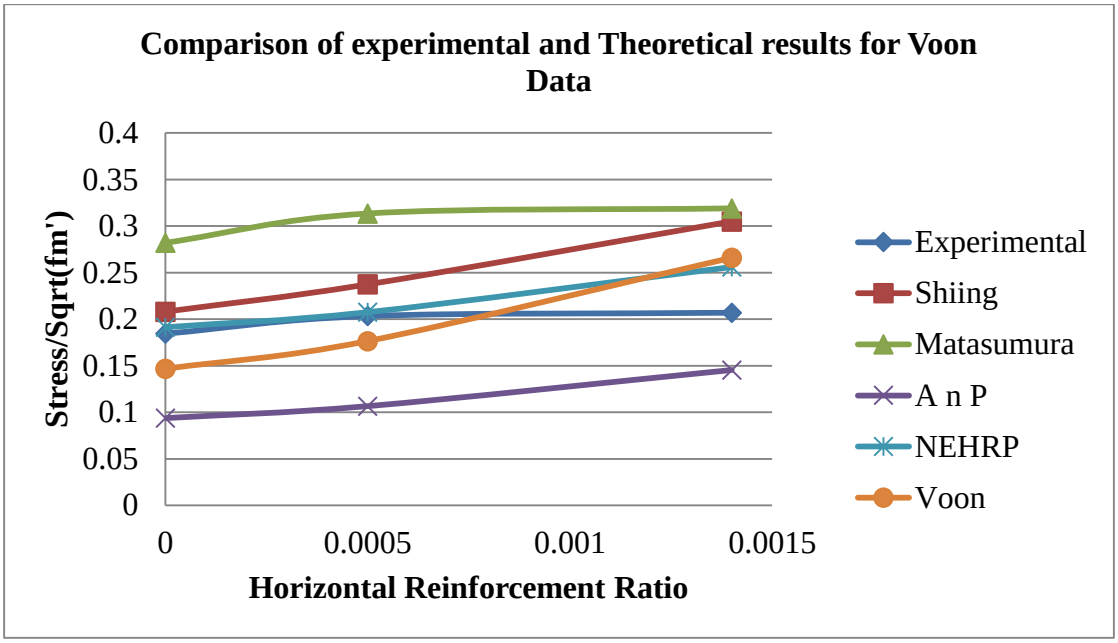

Figure 3.11 Comparison of Test Results and Theoretical Results With Changing Horizontal Reinforcement Ratio for Voon

Both the NEHRP and Anderson and Priestley equations show the same general relationship between shear strength and amount of horizontal reinforcement, the only difference being the term that takes into account the contribution of the masonry strength that makes the difference. In order to minimize the effect of other parameters, the difference in normalized stress for three subsequent values (for Voon's case) was compared to determine which equation best matched the experimental results in terms of the rate of change in strength with increasing reinforcement ratio. This comparison revealed that Matsumura's equation was closest to the experimental results for Voon's data set. This kind of comparison was applied to the other data sets as well revealing that the other equations usually overestimated the influence of increasing horizontal

reinforcement. Therefore, it was concluded that the horizontal reinforcement ratio term from Matsumura's equation would be used in the modified equation.

3.6 Modification to In-Plane Shear Equation

From Section 3.4 it appeared that the Shing equation was the best one amongst the equations described herein. For Shing's equation, 26% of the data maintain a certain ratio (1-0.8) between experimental and theoretical results, whereas the other equations either give very high or very low values compared to the experimental results. As a result, these equations could result in overdesign and therefore expensive heavy structures. Therefore, the equation needs to be modified further. In order to develop a more optimum equation, the Shing equation was selected as a starting point because it was generally the best one, and then modifications were made to incorporate the parts of the other equations which best captured the effects of certain factors such as aspect ratio, reinforcement ratio, etc. Taking into consideration all the comparisons discussed in Section 3.4, the modified equation takes the form of:

$$V_n = \left[0.083\left(3.5 - 1.75\frac{M}{VL}\right) + 0.0217\rho_v f_y + 0.0217\,\sigma\right]\sqrt{f_m'}A_n + \left(\frac{L - 2d'}{s_h} - 1\right)A_h f_{yh} \quad \text{(Eq.3.8)}$$

Where V_n is the ultimate load resistance of the wall.

Here, only the aspect ratio term is new but is slightly changed from the NEHRP equation, since it was shown earlier in Section 3.5.2 that the NEHRP equation captured the effect of aspect ratio extremely well compared to the experimental results. The term has been slightly modified to be on the conservative side. On the other-hand, modification to include the horizontal reinforcement term from Matsumura's equation in Shing's equation did not prove to be effective in improving the theoretical results. Therefore this term remains unchanged in Shing's equation. The modified equation shows that only the contribution from horizontal reinforcement is independent of the masonry compressive strength. The dependency of axial stress and vertical reinforcement contribution on masonry compressive strength can be explained by the concept of aggregate interlock force. The shear strength of a reinforced masonry wall is dependent not only on the diagonal tensile strength but also on other mechanisms like aggregate interlock, and dowel action of vertical reinforcement, similar to reinforced concrete members (Shing, et

al., 1990). Since the applied axial stress and the percentage of vertical reinforcement both prevent crack widening, they also affect the aggregate interlock force and hence the in-plane shear strength as well. Vertical reinforcement can also transfer shear by the dowel action along the crack. Experiments have also proven the dependency of shear strength on aspect ratio. Therefore, the fact that the modified equation contains these contributions is quite reasonable.

Now, if this modified equation is used for calculating strength of walls and compared with the experimental results, it is found that around 62% of the data fall below the experimental results and 28.6% are lower than the original results for ratios of experimental to theoretical values of 1.1-1.25. Therefore, the general results did not actually change significantly compared to Shing's results. However, when the coefficient of variation of the experimental to theoretical ratio is compared for the different equations, only a slight improvement is observed for the modified formula in some cases as shown in Table 3.4 and Table 3.5. The mean, standard deviation, and coefficient of variation for the experimental to theoretical ratios are presented in Table 3.4 and Table 3.5 for different grouting and support conditions. All the values calculated here are for the actual strengths which were not normalized with respect to masonry compressive strength.

Table 3.4 Comparison of the Ratio of Predicted Strength to Test Strength Using Different Equations for Different Grouting Conditions

Equation	$V_{exp}/V_{theoretical}$ (Full grouting)	$V_{exp}/V_{theoretical}$ (Partial grouting)
Shing	1.26±0.49 39%	0.84±0.32 38%
Matsumura	1.37±0.91 66.4%	1.01±0.49 48.5%
Anderson and Priestley	1.56±0.75 48%	0.99±0.56 57%
NEHRP	1.19±0.43 36%	0.71±0.23 32%
Voon	1.11±0.7 63%	0.61±0.32 52.5%
Modified	1.35±0.53 39.3%	0.88±0.34 38%

Table 3.5 Comparison of the Ratio of Predicted Strength to Test Strength Using Different Equations for Different Support Conditions

Equation	$V_{exp}/V_{theoretical}$ (Single curvature)	$V_{exp}/V_{theoretical}$ (Double curvature)
Shing	0.79±0.30 38%	1.11±0.48 43%
Matsumura	0.85±0.17 20%	1.26±0.81 64%
Anderson and Priestley	1.23±0.84 68%	1.29±0.70 54%
NEHRP	0.86±0.38 44%	0.97±0.43 44%
Voon	0.94±0.45 47.9%	0.85±0.62 72.94%
Modified	0.84±0.31 37%	1.17±0.52 44.5%

It appears that no better result is obtained for the modified equation. However, it should be noted that the approach used for the development of the new equation is quite simple. The correlation of each influencing parameter cannot be determined using regression analysis on multiple sets of data. The data were treated separately because there was much dissimilarity between the datasets with respect to loading protocol, test arrangement, anchorage of reinforcement. Additionally, the approach of simply adding the contributions from the various parameters (aspect ratio, vertical reinforcement, horizontal reinforcement, axial stress) was not changed. Actually, one of the future directions in development of a better shear prediction model should be in using a different approach to this simple additive approach. For example, in the development of the Anderson and Priestley equation, it was discussed that the reinforcement does not come into effect until cracks form and once cracks initiate, the contribution of the masonry is reduced. Anderson and Priestley included this effect in their equation by reducing the reinforcement contribution by a factor of 0.5. However, no experimental results have been reported that examine the reduction in strength and the resulting contribution of reinforcement once a wall is cracked. This is one example of the gaps that still exist and which need to be addressed in further research. Another gap that could be mentioned here is investigation of the bend diameter adopted for the 180 degree hooked bond beam reinforcement. In the research project described in the following chapters of this thesis, the bend diameter was 129 mm whereas Sveinsson et al. (1985) used a diameter of only 50.8 mm. No work has been reported that determines which will give

the optimum contribution of horizontal reinforcement. Finally it can be said that modification of the formula or proposing a new formula is a difficult task using data reported by various researchers. Hence, an ongoing test program is being conducted at the University of Calgary covering all the varying parameters and thus will allow regression analysis of those test results which will eventually lead to a new equation.

3.7 Summary

From the discussion presented in this chapter it can be concluded that the already existing equations for in-plane shear prediction are not adequate enough to capture the actual behaviour of walls. Again, it is also not possible to formulate a new and effective equation from the database created by accumulating data of various researchers due to differences in test boundary conditions and loading protocols. Therefore, a comprehensive test program should be conducted which focusses on all parameters with ranges that might possibly affect the strength. Regression analysis could then be applied to the data to formulate a new equation. The following chapters describe the setup and results of some testing carried out as part of a larger project of wall testing ongoing at the University of Calgary.

Chapter 4: Experimental Program

4.1 Introduction

Sixteen walls were tested in the structural high bay laboratory at the University of Calgary. The experimental program was run with the purpose of determining the in-plane shear strength of masonry walls constructed from locally available materials following the usual construction practice and to contribute to the currently available data on masonry research throughout the world. Parameters varied included reinforcement anchorage conditions and boundary conditions in the test arrangement used. This chapter contains a detailed description of the test specimens, the construction procedure for the walls and prisms, grouting, and other testing related details such as instrumentation, description of the test frame, and data acquisition.

There were eight varied sets of parameters; with two identical walls tested for each set of parameters having the same configuration. The walls in same set are designated as 'A' and 'B' for identification with the set name before 'A' and 'B'.

The main variables considered in the test series were:

1) Position of the bond beam;
2) Reinforcement anchorage type in the bond beam;
3) Dowel and splice position;
4) Variation in load history.

4.2 Construction Details

4.2.1 Description of Base and Top Beam

All specimens were built on C-section steel beams. There are a few reasons for building walls on a steel footing. First, they provide a rigid support for the walls to facilitate anchoring of the base to the laboratory strong floor through eight bolts. Most of the specimen sets also required splicing of the flexural reinforcement at the bottom of the wall with a 600 mm (greater than the minimum splice length as per clause 12.16.1 of CSA A23.3-04 (CSA-Concrete-Standard-A23.3-04, 2004) rebar dowel of the same size as the flexural reinforcement. The dowels were welded to the steel base beam which could easily be replaced if they or the welded connection were heavily damaged in a

previous test. Each footing also had four lifting hooks which facilitated transport of the walls within the laboratory using the overhead crane. A typical footing is shown in Figure 4.1.

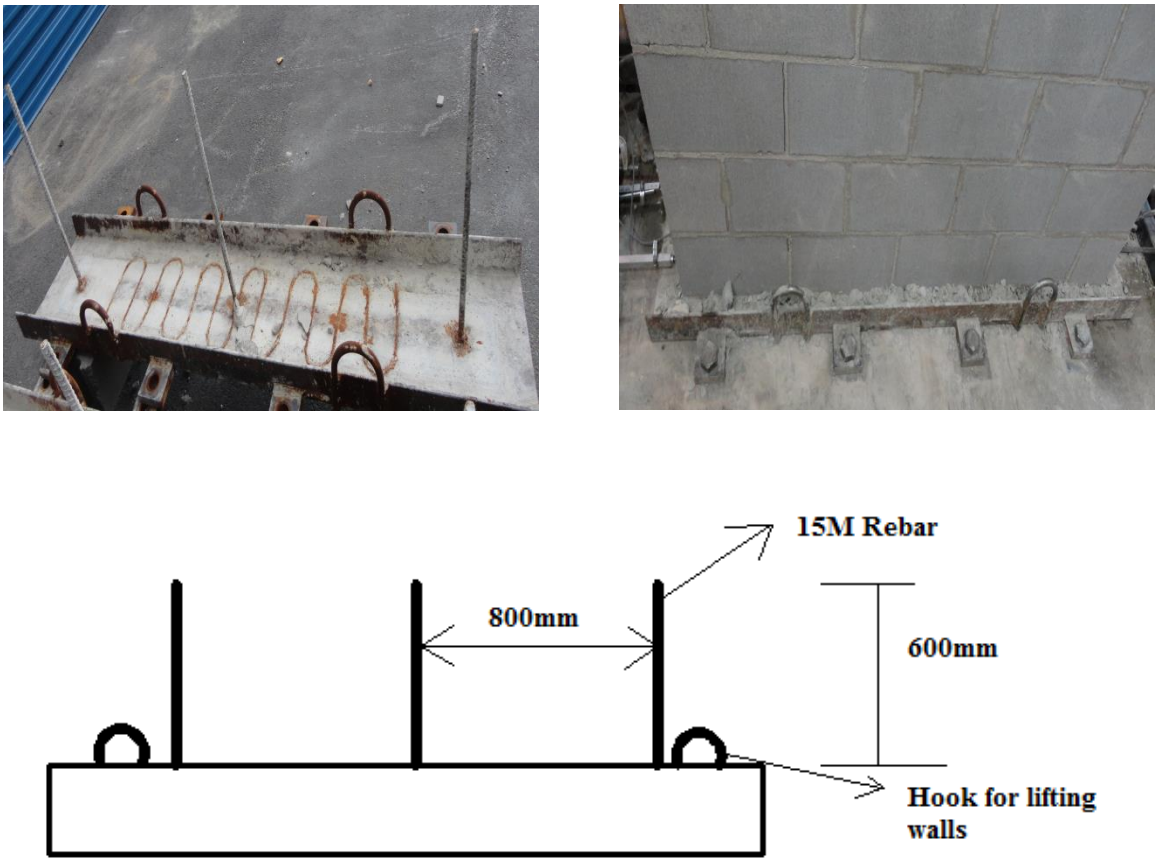

Figure 4.1 Footing Details

4.2.2 Wall Construction

All walls were designed such that the predominant mode of failure would be shear not flexure. The dimensions of the walls were 1800 mm x 1800 mm x 190 mm (height x length x thickness) resulting in an aspect ratio of 1. This required nine courses of blocks over the height and four and a half units along the length. All walls were built in running bond with face shell bedding. No mortar was placed on the webs except adjacent to grouted cells since in running bond, the cells do not align perfectly vertically. In the case of grouted cells, mortar was placed on the webs in order to prevent grout from flowing out. Mortar joints were compacted using a cylindrical jointer. Eight parameters were

selected for testing however, the amount and spacing of vertical reinforcement was not varied. All the walls were partially grouted with 3 single 15M vertical reinforcing bars placed at 800 mm o.c. (on centre) and only the reinforced cores were grout filled. Each wall was constructed over two days by an experienced mason under constant supervision. On day one the wall was built up to the 5^{th} course (level of the bond beam) and then grouted. The mason then continued to build the wall to full height and on day two the remainder of the wall was grouted. This type of grouting is called low-lift grouting. After pouring the grout it was compacted using a rod. When grouting bond beams, grout was placed up to half height of the course, then the reinforcement was placed and grout was cast on top of the reinforcement. This is the practice in the field and ensures proper bonding between the reinforcement and the wall. The reinforcement with 180° hooks required special consideration for grouting because the width of the hooked reinforcement exceeds the inside dimension of the block, therefore the hook had to be inclined in order to accommodate placement in the walls.

The parameters varied include the anchorage detail of the reinforcement in the bond beams, spacing of the bond beams, and the presence of dowels/splices at the top and bottom of the walls. These parameters made up six wall pairs while two additional sets involved changes in the load history of the testing program. The parameters that remained constant during testing are tabulated in Table 4.1 while the various wall sets are outlined in Table 4.2.

Table 4.1 Constant Parameters

Height (mm)	Length (mm)	Thickness (mm)	Axial Load (MPa)	Grout	Area of Vertical Reinforcement A_v (mm^2)	Vertical Reinforcement Spacing, s_v (mm)
1800	1800	190	2	Partial	200	800

Table 4.2 Variable Parameters

Wall group	Area Of Horizontal reinforcement A_h (mm^2)	Spacing of Horizontal Reinforcement S_h (mm)	Anchorage	Remarks
1	200	800	No hook	Only Two Bond Beams Were Placed
2	200	800	180 ° hooks	
3	200	800	Shear Stud	
4	200	600	90 ° hook	
5	21.5	400	No bottom splice	Joint Reinforcements Were Equally Spaced
6	21.5	400	Top splice	
7	21.5	400	Horizontal load constant	
8	21.5	400	Monotonic Loading	

The first three sets (set 1, 2, 3) of walls contain bond beams at the 5th (mid-height) and 9th (top) courses with 15M reinforcement in the bond beam. One set of walls tested in a previous study (Dickie & Lissel, 2011) was of similar construction and will be compared to these three sets in Chapter 4. For more clarity the schematics of the walls are shown in Figure 4.2 and Figure 4.3. The set tested by Dickie had bond beam reinforcement with 90 degree hooks provided for anchorage. The three sets tested in the current study have bond beam reinforcement with varying anchorage conditions: 1) no anchorage provided (straight ends), 2) 180˚ hooks as per clause A12.2.3 of CSA A23.3-04 (CSA-Concrete-Standard-A23.3-04, 2004) and 3) circular discs welded to the bar ends. The latter condition is essentially the same as the concept of shear studs and has been adopted from that used in reinforced concrete slabs for providing punching shear resistance. Previous tests have confirmed that the full yield strength of the stud will be developed without appreciable slip if the anchorage head has an area equal to 9-10 times the area of the stud (Subramanian, 2005). Therefore the disc (head) diameter was chosen as 50 mm with a thickness equal to half the diameter of the reinforcement (7.5 mm) and had a centre hole (diameter 18 mm) to allow protrusion of and facilitate welding the reinforcement as shown in Figure 4.4.

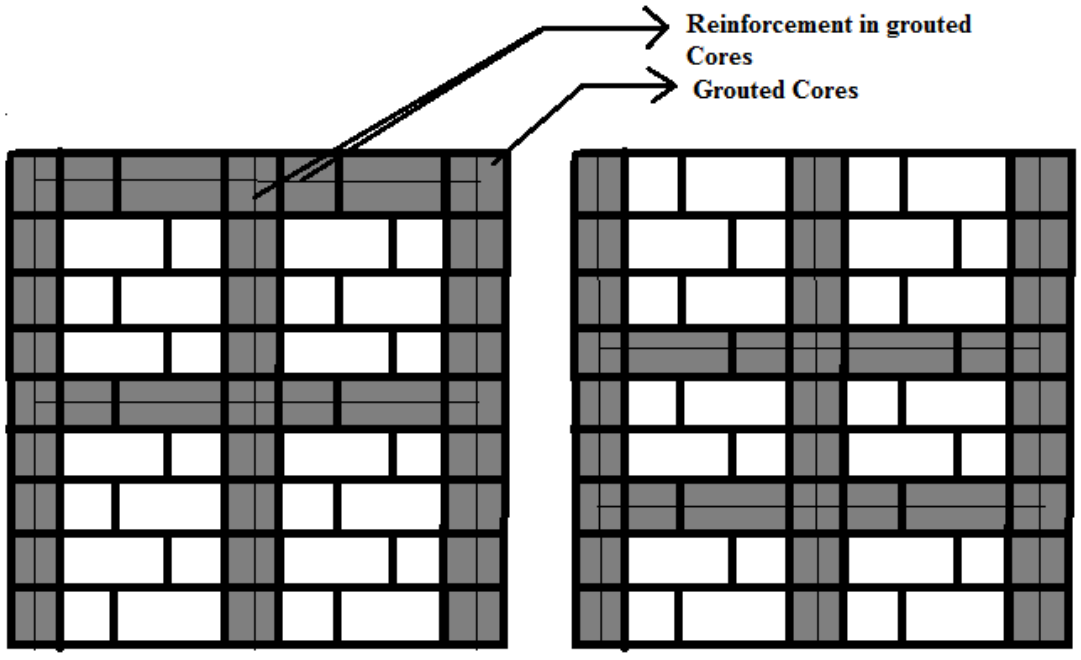

Figure 4.2 Position of Grouted Cores and Bond Beams a) For Set 1-3 b) For Set 4

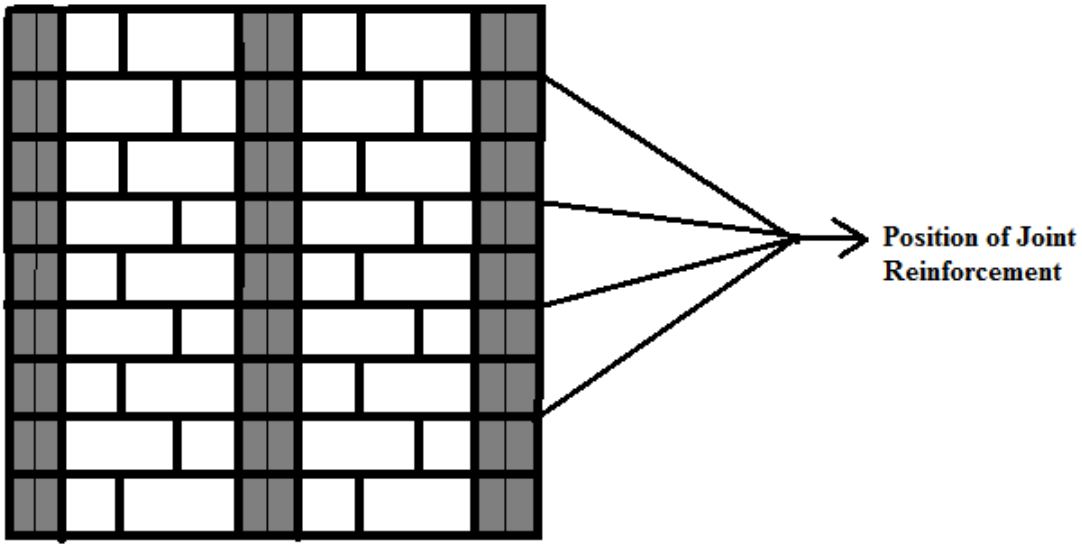

Figure 4.3 Grouted Cores and Position of Joint Reinforcement for Wall Sets 5-6

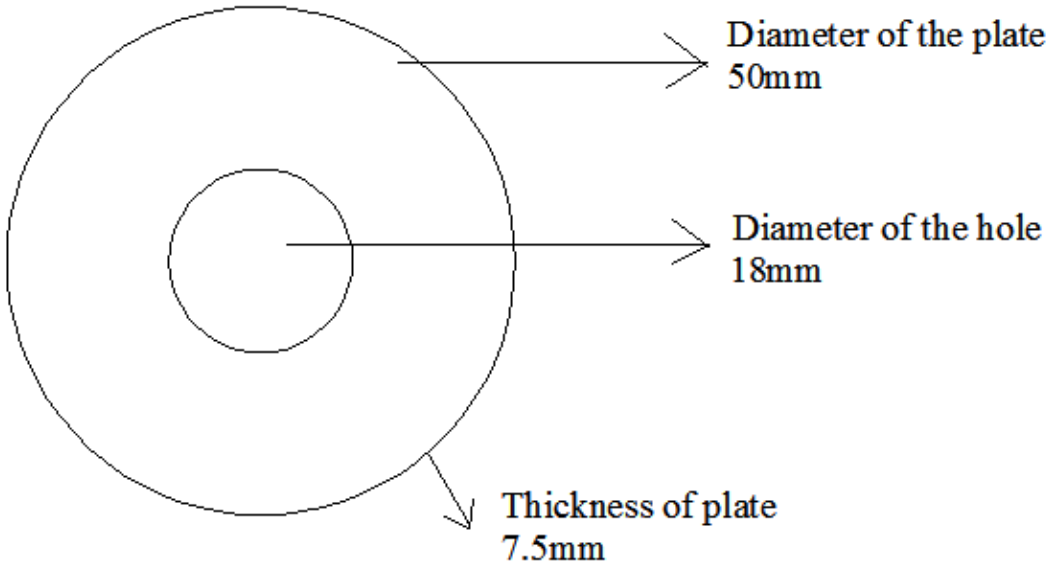

Figure 4.4 Details of Stud Head

The fourth set has bond beams at the third and sixth courses with 90 degree hooks provided for the horizontal reinforcement. The remaining four sets were all provided with bed joint reinforcement at every second course (400 mm) rather than bond beams. The 5th set was constructed without any dowels welded to the steel base beam so there is actually no mechanical connection between the wall and the base beam.

The sixth set not only has bottom dowels but was also provided with additional dowels at the top, by protruding reinforcement from the top of the wall which was subsequently welded to a steel plate of the same width as the capping beam lower flange. The steel plate was additionally welded to the capping beam lower flange. Pictures of the construction of the walls are provided in Appendix 1. The conditions in the fifth and sixth sets are supposed to change boundary conditions at the bottom and top. Therefore, these two parameters will be referred to as change in boundary conditions in further discussion. The final two sets had the usual vertical reinforcement, bottom dowels, and joint reinforcement as mentioned earlier, however, the loading conditions were varied. The last set was subject to monotonic load rather than cyclic load and for the seventh set the load in both vertical actuators was held constant rather than being variable to maintain zero moment at the middle of the wall.

4.2.3 Construction Materials

The materials required for construction of the walls are block, mortar, grout, and reinforcement. The specification and the properties of the materials are described in the following sections.

4.2.3.1 Blocks

The masonry blocks used in the research were standard 200 mm hollow concrete masonry units as shown in Figure 4.5 with the dimensions being 190 x 190 x 390 mm (height x thickness x length). For walls with bond beams, knock-out units were used at the desired course to facilitate placement of horizontal reinforcement. Regular half blocks and bond beam half blocks were used as required. The compressive strength of the blocks was 15 MPa as specified by the supplier and the compressive strength was also determined from tests on half blocks cut from the regular full block and manufactured half block as shown in Table 4.3.

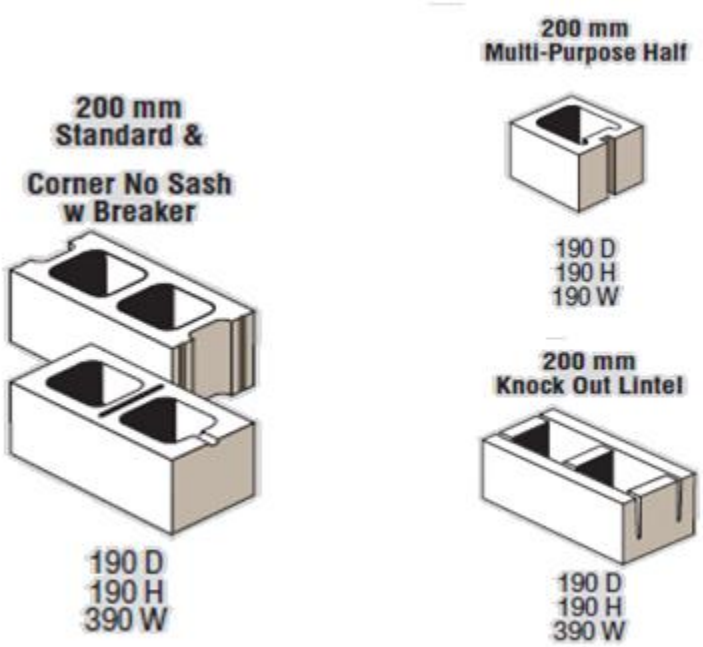

Figure 4.5 Standard Masonry Units Courtesy Expocrete Concrete Website (Expocrete-Concrete, 2013)

Table 4.3 Compressive Strength of Units from Tests on Half Blocks

Types of block	Sample no.	Strength (MPa)	Average (MPa)	Standard deviation (MPa)	COV(=St. Deviation /Average) (%)
Regular Block	1	15.7	16.5	0.7	4.3
	2	17.0			
	3	16.9			
Half block cut from full block	1	15.9	16.5	1.4	8.5
	2	18.0			
	3	15.4			

4.2.3.2 Mortar

The material properties of the mortar that influence the structural performance of masonry are compressive strength, bond strength and elasticity. The compressive strength of mortar is less important than the bond strength, workability and water retentivity, therefore the latter three properties should be given consideration in mortar selection.

Specmix Type S mortar (Portland cement, lime and sand) was mixed with water onsite and used in the construction of the walls in this research project. Specmix Type S mortar conforms to ASTM C 270 (Spec-Mix, 2009) (standard specification for mortar for unit masonry). Test cubes of mortar with side length of 50 mm conforming to CSA A 179-04 (CSA-Masonry-Standard, 2004) were cast during construction of the walls. The results of the mortar compressive strength tests are provided in Table 4.4. Since most of the walls were tested at an age of around 28 days or at an age of 42 days, the mortar samples were tested for these two ages.

Table 4.4 Mortar Compressive Strength

Age of test	Sample no.	Strength (MPa)	Average (MPa)	Standard Deviation (MPa)	COV (%)
28 Days	1	4.9	5.7	0.7	12.1
	2	6.2			
	3	5.9			
42 days	1	6.3	6.2	0.1	2.2
	2	6.3			
	3	6.1			

4.2.3.3 Grout

Specmix corefill coarse grout was employed to fill the reinforced cores and bond beams in the walls. This grout contains Portland cement, pozzolans and aggregates meeting the requirement of ASTM C 476 (Spec-Mix, 2009). The grout was mixed onsite by adding water to the ready mix product. The volume of water added had to be sufficient to ensure fluidity of the grout within the wall and proper quality was ensured by mixing a certain volume of water to a certain volume of grout mix all the time. The compressive strength of the grout is reported in Table 4.5. Samples of grout were also tested at the age where wall groups were tested. The designation batch 1 and batch 2 refers to grout from two different shipments of grout that were available for construction. Though they are

supposed to have the same properties, the compressive strength was significantly different.

Table 4.5 Compressive Strength of Grout Sample

Age of test	Sample no.	Strength (MPa)	Average (MPa)	Standard deviation (MPa)	COV
28 Days (Batch 1)	1	29.2	30.1	0.9	2.9
	2	30.9			
	3	30.2			
42 days (Batch 1)	1	34.4	30.1	4.4	14.6
	2	30.3			
	3	25.7			
42 Days (Batch 2)	1	16.1	18.3	2.2	12.1
	2	18.5			
	3	20.5			

4.2.3.4 Reinforcing Steel

All vertical and bond beam reinforcing used in the walls were 15M bars with tensile strength of 450 MPa as tested in the laboratory with a coefficient of variation of 1%. The reinforcement was cut to length and bent as required according to clause 12.5.2 of CSA A23.3-04. For walls with bed joint reinforcement, hot dipped galvanized wire reinforcement in ladder configuration was used. This is prefabricated reinforcement especially designed for embedment in horizontal mortar joints of masonry for 200 mm units. The ladder configuration consists of two parallel longitudinal rods weld connected to perpendicular cross rods spaced at 381mm (15 inch) o.c. to form a ladder design as shown in Figure 4.6. The cross rods are electronically butt welded to deformed side rods in a single plane. The cross sectional area of the ladder reinforcement (two longitudinal wires with diameter of 3.665 mm) is 21.5 mm^2. The yield strength of bed joint reinforcement was determined to be 520.8 MPa with a coefficient of variation of 1.1% (Saiedi, 2011). A typical stress-strain curve for the reinforcing steel is provided in Figure 4.7.

Figure 4.6 Ladder Reinforcement (Courtesy Brock White Construction Materials (Brock-White, 2013)

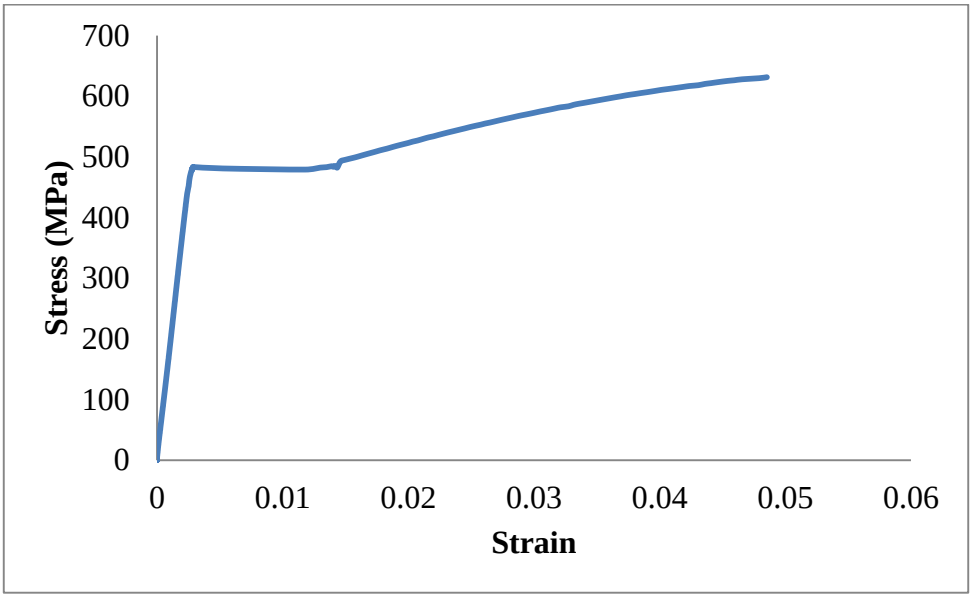

Figure 4.7 Stress-Strain Curve for Reinforcing Steel

4.2.4 Material Properties

Masonry prisms were constructed according to CSA S304.1-04 clause number 5.1.2.1 using the same materials used for wall construction. Both grouted and ungrouted prisms were constructed. Theoretically, a full set of prisms should be tested for each wall, however, each set of prisms consists of 5 prisms of each type (grouted and ungrouted) requiring a lot of space and handling and transporting them from the structural high bay to the concrete lab for testing is another difficult issue. Therefore, in this project, prism sets were tested at three ages (4 weeks, 5 weeks and 6 weeks) as all the walls were tested within the time span of 4-6 weeks. There was one additional set which consists of grouted

prisms that were grouted several days after building the hollow prisms. This is what occurred during construction of set 6 where a delay occurred due to the preparation of the top plate used in those walls. The size of the prisms was one unit length and two courses in height for ungrouted prisms and three courses in height for grouted prisms. Grouted prisms were constructed with alternating courses of whole units and two half units cut from whole units with a concrete saw. The cut ends of the half units face outwards. The prisms were tested using a controlled loading rate so that the prism did not fail abruptly. For the ungrouted prisms, fibre board was placed on the face shells both at the top and bottom of the prisms whereas for the fully grouted prisms, fibre board was placed covering the whole area of the top and bottom surfaces. The compressive strengths of the masonry prisms are tabulated in Table 4.6.

Table 4.6 Compressive Strength of Masonry Prisms

Age of test	Sample no.	Strength (MPa)	Average (MPa)	Standard Deviation (MPa)	Coefficient of variation (%)
28 days Ungrouted	1	22.0	19.9	2.0	10.2
	2	18.5			
	3	21.3			
	4	20.5			
	5	17.2			
28 days Grouted (Batch 1)	1	8.8	8.8	0.6	6.5
	2	9.2			
	3	9.0			
	4	7.8			
	5	9.1			
35 days Ungrouted	1	20.4	23.1	1.6	7.1
	2	22.7			
	3	24.4			
	4	24.3			
	5	23.6			

Age of test	Sample no.	Strength (MPa)	Average (MPa)	Standard Deviation (MPa)	Coefficient of variation (%)
35 days Grouted (Batch 1) (immediately)	1	10.5	10.0	0.7	6.8
	2	9.3			
	3	9.3			
	4	10.4			
	5	10.7			
35 days Grouted (after 30 days)	1	8.7	9.8	1.5	15.5
	2	8.0			
	3	11.2			
	4	11.5			
	5	9.5			
42 days Ungrouted	1	17.7	18.1	1.0	5.6
	2	17.7			
	3	18.1			
	4	19.9			
	5	17.5			
42 days Grouted (Batch 2)	1	8.9	8.5	1.0	11.9
	2	6.9			
	3	7.6			
	4	7.3			
	5	8.0			
	6	8.6			
	7	9.1			
	8	9.4			
	9	10.2			
	10	8.6			

Photos of the prisms are provided in Appendix 1. To determine the compressive strength of mortar and grout used for construction, samples were taken and tested according to the standard CSA A179. Wall compressive strength is calculated from the prism strength. The sample calculation for calculating wall strength is given in Appendix 3 and the results obtained from those calculations are mentioned in Table 5.1 of the following chapter.

4.3 Testing Frame

As discussed in Chapter 2, the ESECMaSE test method was adopted for this test program. Different aspects of the test frame and the loading scheme are described in the following sections.

4.3.1 Vertical Load Application

The vertical load was applied in force control through two hydraulic actuators of 1.5 MN maximum capacity placed on roller bearings to allow free horizontal movement of the capping beam while the vertical actuators remain still. Care was taken to ensure that the wall remained plumb and aligned with the actuators. The test frame is shown in Figure 4.8. Loads applied at the top of the wall were varied in such a way as to ensure zero bending moment at the mid-height centre of the wall. The total applied vertical load remains constant at $N = N_1 + N_2$ with N_1 and N_2 varying dependent on the specimen being tested and the applied horizontal load. The determination of N_1 and N_2 is done in real time during the test in order to counter the moment due to the horizontal load according to the equation below.

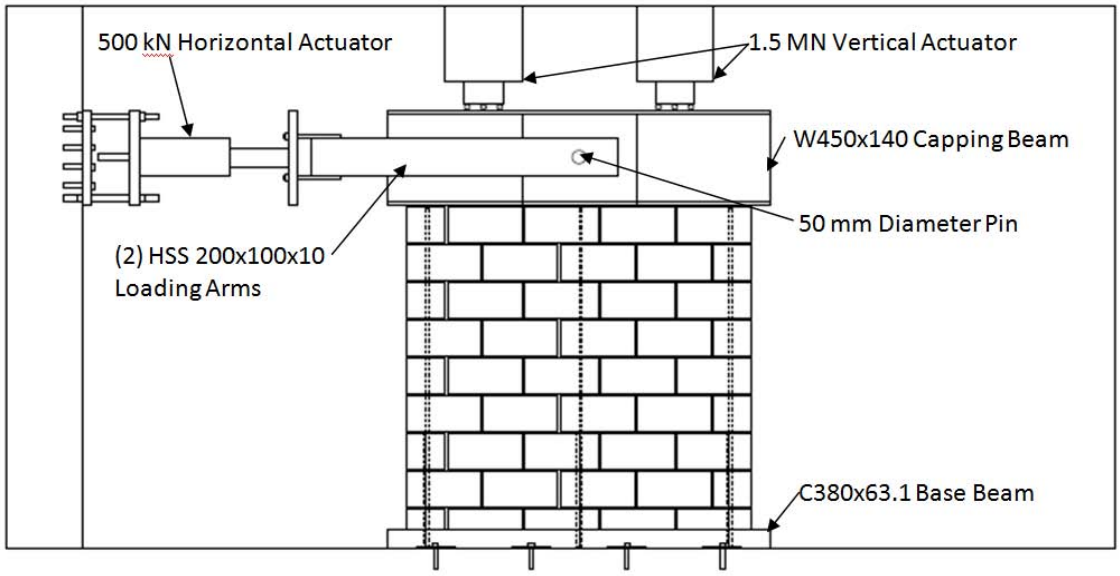

Figure 4.8 Schematic Diagram of the Wall Under Test Frame (Dickie & Lissel, 2010)

$$M = N_1 e_1 - N_2 e_2 = \frac{VH_{wall}}{2} \qquad \text{(Eq.4.1)}$$

Where e_1 and e_2 are 0.5 m in this case, V is the horizontal load, and H_{wall} is the height of the wall.

4.3.2 Horizontal Load

Horizontal load in this case was applied through an I-beam of high stiffness which was placed on a cement-mortar bed at the top of the wall. This beam had a welded bead pattern on the bottom flange so that sliding failure at the interface between the capping beam and the top of the wall could be prevented. Horizontal displacement was applied by the actuator through a pair of HSS load arms connected to the capping beam at the mid-length of the wall by a steel pin running through the beam as shown in Figure 4.9.

Figure 4.9 Loading Beam Showing the Point of Horizontal Load Application

Preliminary test results (Dickie & Lissel, 2011) showed the occurrence of the first visible cracks at 1 mm top-of-wall displacement. It was safe to assume that the maximum horizontal load for each wall specimen would vary, however the loading protocol was determined assuming a maximum load of 200 kN for a displacement equal to 10 mm. Therefore, the horizontal displacement was applied in 0.25 mm increments up to 1 mm (Level A), then in 0.5 mm increments up to 10 mm (Level B), and finally 1.0 mm increments until failure (Level C) as mentioned in Chapter 2. This load application is shown below in Figure 4.10. Instead of applying three cycles at each displacement step as mentioned in ESECMaSE, only two cycles were applied at a slightly accelerated rate in order to reduce the required testing time as recommended by FEMA 461 – Interim Protocols for Determining Seismic Performance Characteristics of Structural and Non-

structural Components through Laboratory Testing. The test duration would have exceeded 21 hours if the recommended loading rate of $d_{cr}/2$ minutes (0.0083 mm/s) was used and the wall attained a 15 mm displacement. Therefore, the loading rate was adjusted to 0.1 mm/s for level A and 0.25 mm/s for Levels B and C. The load was held at each peak for two seconds to allow sufficient time for the data acquisition system to record load and displacement.

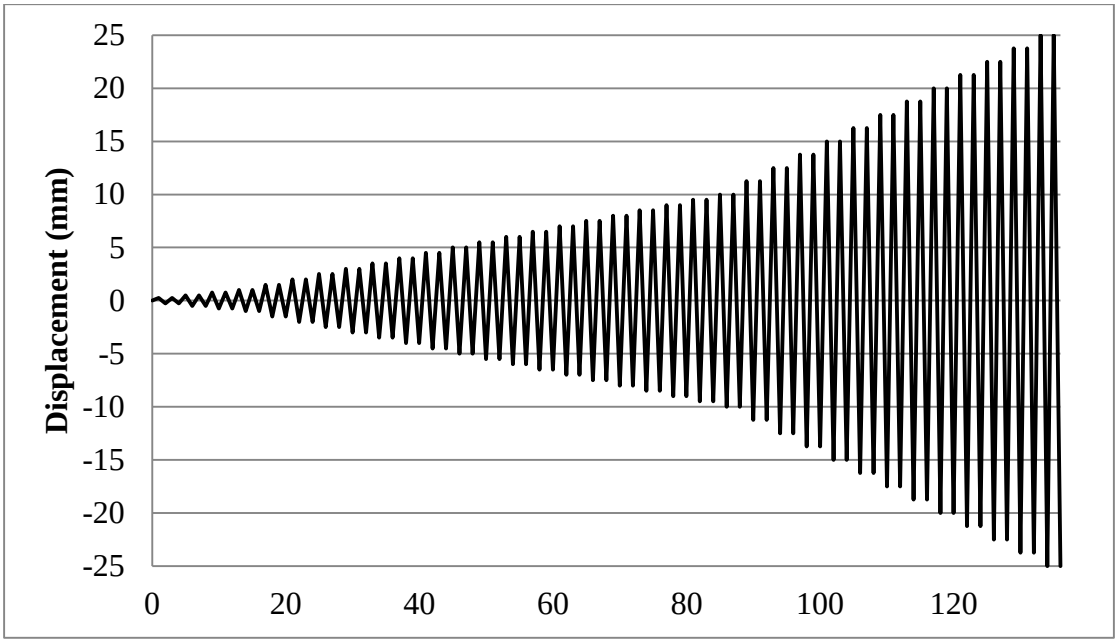

Figure 4.10 Displacement Step History

4.3.3 Data Acquisition System and Instrumentation of Walls

The instrumentation used for gathering data from the wall tests combined with the software are referred to as the data acquisition system. The instrumentation used here includes only displacement transducers. A brief description of the data acquisition system is provided below.

Load cells and linear variable differential transducers (LVDT) are incorporated within the MTS actuators. The MTS system controller with the 793.10 MPT (Multipurpose testware) was also used. Therefore, force and displacement could be measured while testing and saved in the connected PC as an electronic file.

The walls were instrumented with several displacement transducers (Linear Strain Converters). Displacement transducers 1- 6 measured the lateral displacement at the top,

middle and bottom of the wall at each end for each cycle of push and pull. The uplift of the base was measured at each end of the wall by transducers 7 and 8. Sliding displacements between the wall top and the top beam and between the wall bottom and the base beam were monitored by transducers 9 and 10, respectively. Transducer 1 was used to control the horizontal load application. A schematic of the instrumentation is shown in Figure 4.11.

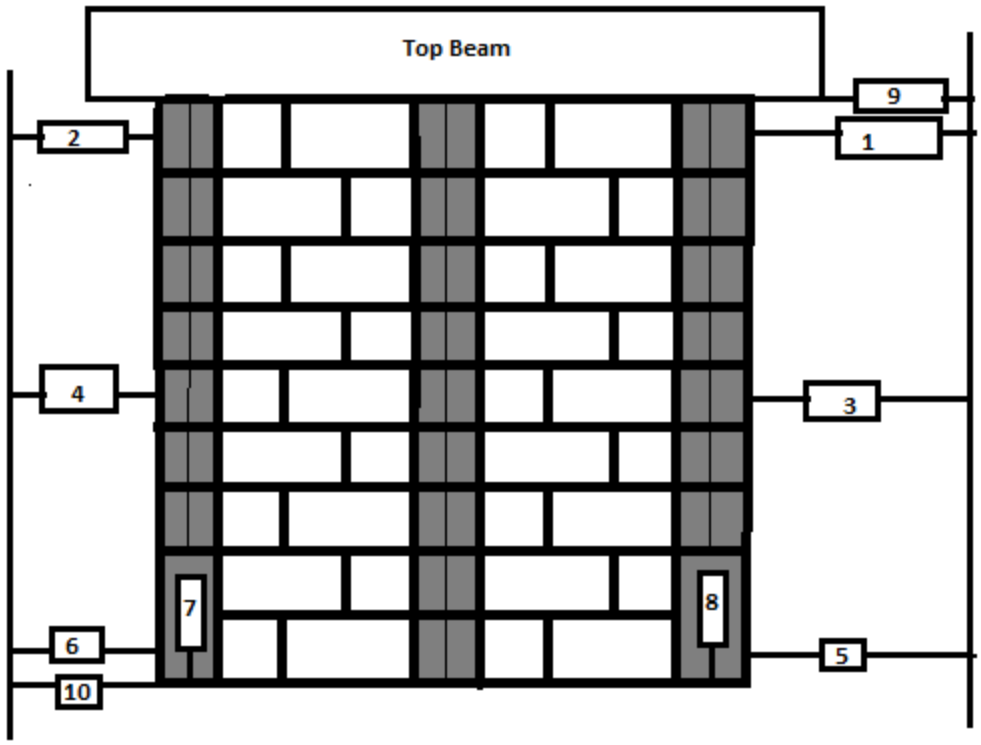

Figure 4.11 Instrumentation of Test Walls

4.4 Summary

In this chapter the material properties, test arrangement, loading frame, load application and data acquisition system were described in detail. The description of the test specimens was also provided in detail with illustrations and a description of the construction. The procedure used for construction and the parameters selected for investigations were also discussed.

Chapter 5: Experimental Results

5.1 Introduction

The results and observations obtained from the tests on 16 walls are the primary foci of this chapter. The results are analyzed and comparisons are made between the characteristics of different walls from the viewpoint of strength, stiffness, energy absorption, and strength predicted using different shear models

5.2 Summary of the Results

All the walls were tested using the test setup described in Chapter 4. A summary of the results is provided in Table 5.1 where the horizontal force at the first visible diagonal crack and the maximum forces for both the positive (pull) and negative (push) cycles are shown. Here positive refers to the pull cycle (load applied to the left) and negative refers to the push cycle (load applied to the right). In this thesis the south and north sides are, from the reader's perspective, the left and right ends of the wall, respectively. Furthermore the maximum deformation measured at the top of the walls for each direction of loading [d_{u1} and d_{u2}] are also given where d_{u1} refers to maximum pull and d_{u2} refers to maximum push. The values of d_{u1} and d_{u2} reported here are obtained from the transducer placed at the top of the north (right) side of the walls that was used for controlling the test. The values for maximum base sliding and maximum uplift are also noted. Sliding here refers to sliding at the bottom which is the difference in reading of the transducer placed at the bottom of the south (left) side of the wall and that at the base beam on the same side. In general, all the walls exhibited shear dominant behaviour characterized by the development of early mortar joint cracks and subsequently, diagonal cracks extending throughout the masonry panels.

Table 5.1 Summary Table

Wall	First cracking force H_c (kN)	Maximum lateral force-pull H_M (kN)	Maximum lateral force-push H_M (kN)	Ratio=H_c/H_M	Ratio= $H_{m(max)}/V$	$d_{top\ pull}$ d_{u1} (mm)	$d_{top\ push}$ d_{u2} (mm)	$D_{sliding\ bottom}$ (mm)	$D_{sliding\ top}$ (mm)	D_{uplift} (mm)	Parameter of the wall
1-A	133.8	229.6	189.0	0.7	0.56	8.0	8.1	2.5	1.9	0.9	Straight bar
1-B	157.3	227.1	225.6	0.7	0.55	6.5	6.5	4.2	2.5	1.6	Straight bar
2-A	200.2	250.7	254.1	0.79	0.62	6.6	6.5	0.6	1.4	1.5	180˚hooked bar
2-B	174.7	224.7	232.4	0.78	0.57	6.5	6.5	2.1	2.6	0.8	
3-A	214.3	251.4	233.5	0.85	0.62	7.1	7.0	1.5	1.1	0.9	Studded bar
3-B	196.7	225.6	246.3	0.87	0.60	7.5	7.5	1.2	1.8	1.4	
3-C	160.1	160.1	168.6	0.95	0.83	4.1	4.0	0.8	4.6	0.2	
4-A	180.7	236.8	195.0	0.76	0.58	4.9	5.0	0.7	0.5	1.1	Relocated bond beam with 90 degree hooked bar
4-B	213.1	230.8	250.5	0.92	0.61	7.1	7.0	1.2	2.7	1.2	
4-C	138.5	186.7	194.6	0.71	0.48	4.5	4.5	0.9	0.4	0.7	
5-A	165.6	208.1	204.9	0.79	0.51	9.1	9.0	1.9	0.8	1.9	w/o bottom splice
5-B	179.6	208.0	218.5	0.82	0.53	8.1	8.0	2.5	0.7	0.7	

Wall	First cracking force H_c (kN)	Maximum force-pull H_M (kN)	Maximum force-push H_M (kN)	Ratio=H_c/H_M	Ratio= $H_{m(max)}/V$	$d_{top\ pull}$ d_{u1} (mm)	$d_{top\ push}$ d_{u2} (mm)	$D_{sliding\ bottom}$ (mm)	$D_{sliding\ top}$ (mm)	D_{uplift} (mm)	Parameter of the wall
6A	77.5	202.0	204.9	0.38	0.50	10.1	10.0	1.5	1.1	0.9	With top splice
6-B	161.6	213.3	209.5	0.75	0.52	9.1	9.0	1.2	0.9	0.5	
7-A	134.2	175.7	177.7	0.76	0.44	12.1	12.5	1.0	5.4	2.1	Constant vertical load
7-B	124.1	190.0	180.7	0.70	0.47	13.0	13.1	1.0	1.4	2.7	
8-A	127.0	-	230.3	0.55	0.56	-	13.0	0.1	0.8	0.5	Monotonic load
8-B	175.1	-	235.8	0.74	0.58	-	15.0	0.1	0.5	0.8	

The top transducer placed at the top of the north side of the wall was checked frequently as this was the controlling one. All the transducers were checked for funtionality at the beginning of testing for each wall by inserting an object with a known thickness in between the transducer and the wall and then the values read by the computer were checked. The uplift, displacement of base beam, sliding of the wall with respect to the base beam, sliding of the top capping beam with respect to the wall were also analyzed and some of the results are reported here, however, no significant uplift or undesired displacement was measured in any case except for wall set 7 where uplift was measured higher than any other wall. All the values were checked and it was confirmed that the movements of the walls horizontally at the base and along the top were nearly zero except at the end of the test. For some walls it is seen that the values reported in Table 5.1 are quite high. However, in all cases this displacement actually occurred at the late stage of testing. The difference between the readings for transducers placed at the same height on two opposite sides of the wall gave values within ±0.5 mm of each other in most cases. The highest sliding at the bottom of wall was measured for wall 1-B whereas wall set-8 gives the lowest values. The top sliding was measured as high as 5.42 mm for wall 7-A but this may be attributed to failure rather than actual slip.

Table 5.2 gives the strength prediction for the walls in flexure, shear, and sliding according to CSA S304.1-04 on the basis of the wall properties and vertically applied loading. The sample calculations of the values in this table are included in Appendix 3.

Table 5.2 Prediction of Wall Strength Based on Measured Material Properties

Wall	f_m' (MPa)	$F_{flexure}$ (kN)	V_n (kN) CSA S304.1-04	$P_{sliding}$ (kN)	V_{max} (kN) from test
1-A	12.6	270.5	193.5	639.9	229.6
1-B	12.6	270.5	193.5	637.1	227.1
2-A	12.6	270.5	193.5	660.0	236.8
2-B	12.6	270.5	193.5	641.8	250.9
3-A	13.6	274.5	195.8	657.9	254.5
3-B	12.6	270.5	193.5	653.1	234.4
4-A	13.6	274.5	228.2	645.6	250.4
4-B	12.6	270.5	225.9	657.3	247.0
4-C	12.6	270.5	225.9	611.6	194.6
5-A	12.6	270.5	120.5	622.6	208.1
5-B	12.6	270.5	120.5	630.2	218.5
6-A	15.5	281.4	127.2	642.9	233.9
6-B	15.5	281.4	127.2	626.6	212.4
7-A	15.6	281.8	127.5	471.2	177.5
7-B	15.6	281.8	127.5	474.9	190.0
8-A	15.6	281.8	127.5	641.2	229.4
8-B	15.6	281.8	127.5	650.3	234.9

5.3 General Behaviour of Walls in Testing

This section comprises the failure pattern of the walls, details of crack formation in the different walls, and the load-deformation behaviour. The load-deformation behaviour is presented in the form of the hysteresis loops as well as the cyclic envelope for each set of walls along with the control walls for the corresponding set. It should be noted that the displacement controlled loading applied to the walls consists of two full cycles of displacement for each displacement value and each full cycle consists of one pull and one push cycle respectively. The control walls are those walls used as baseline to compare the results for each set and were tested in a previous study (Dickie & Lissel, 2010) using the same test arrangement and test procedure. Two different control sets are used in the comparisons with the results described in this chapter. The first control set (control set 1 denoted as CB in short) is comprised of two walls with bond beams in the 5^{th} and 9^{th} courses of the wall with 90° hooked bars in the bond beams. This control set is used to compare the results of set 1 to set 4 in Table 5.1. The second control set (control set 2 denoted as C in short) is comprised of walls having only horizontal bed joint reinforcement at 400 mm o.c., three vertical reinforcement bars at 800 mm o.c. and bottom splices. This control set will be used to compare the results of sets 5 through 8 in this study. Each set of walls are described separately below and at the end of the section general observations are provided.

5.3.1 Wall Set 1

This wall set had the same horizontal bond beam reinforcement as control set 1, however without any anchorage. Both walls of this set started to crack along the mortar joints (bed and head joints) at a displacement of 2 mm. For wall 1-A, first cracking occurred in the pull cycle whereas for wall 1-B, it occurred in the push cycle.

Figure 5.1 shows the hysteresis loops for wall set 1. Both the walls showed predominantly shear mode of failure along with some flexure which is characterized by long diagonal cracks along with heavy toe crushing and vertical cracks. Toe failure occurred in wall 1-B as a result of the failure of a compression strut assumed to form in the wall to transfer shear. This failure can also be referred to as shear-compression failure as the combination of vertical and horizontal load was significantly higher when that failure took place.

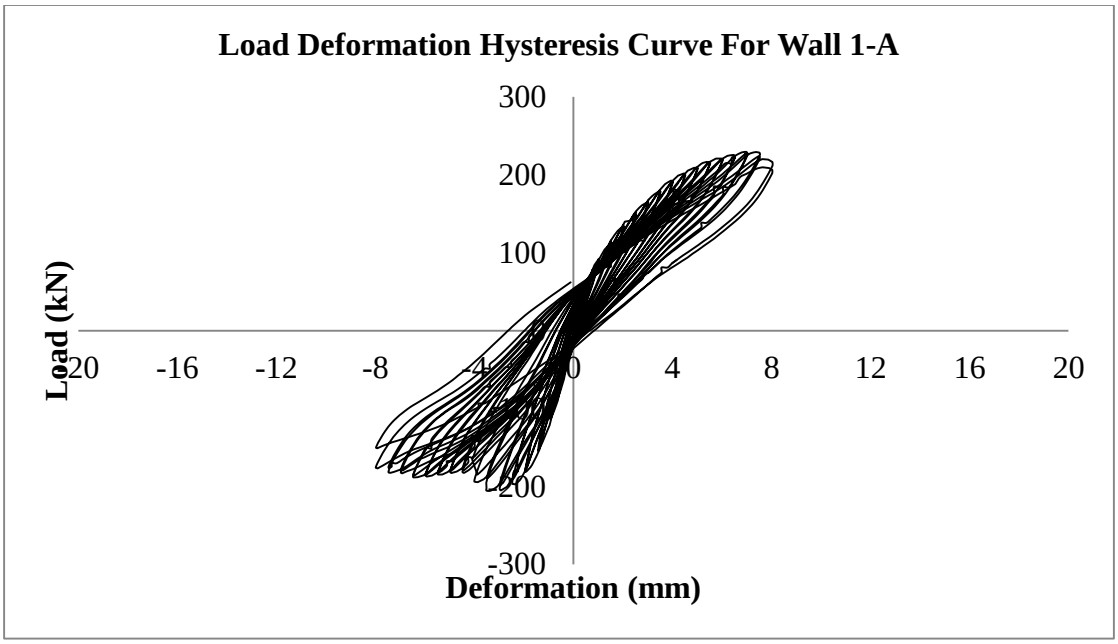

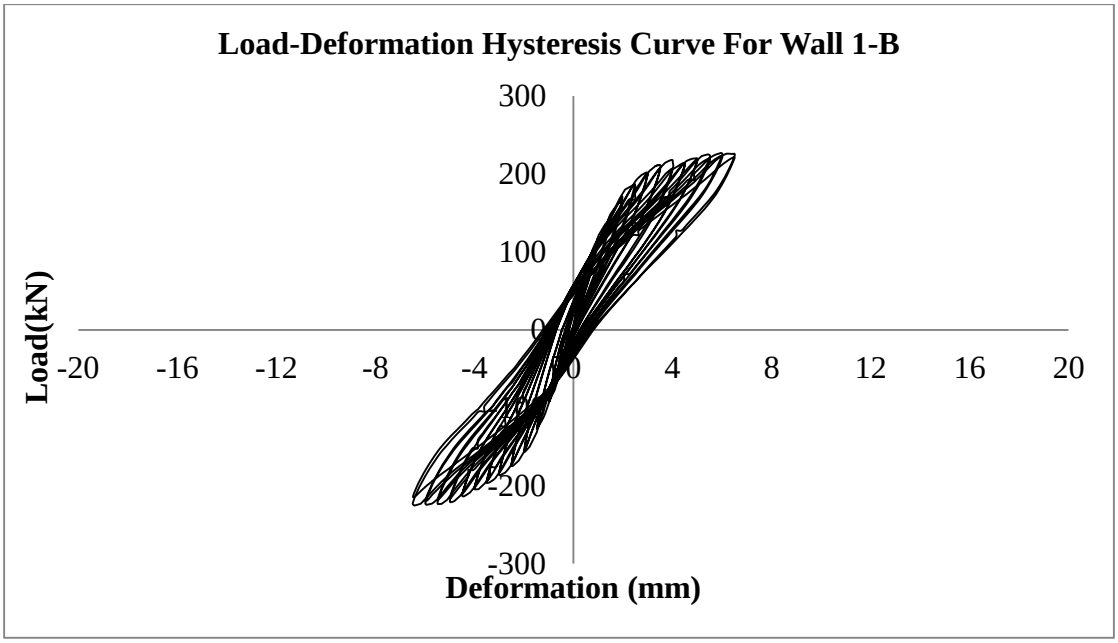

Figure 5.1 Hysteresis Loops for Wall Set 1

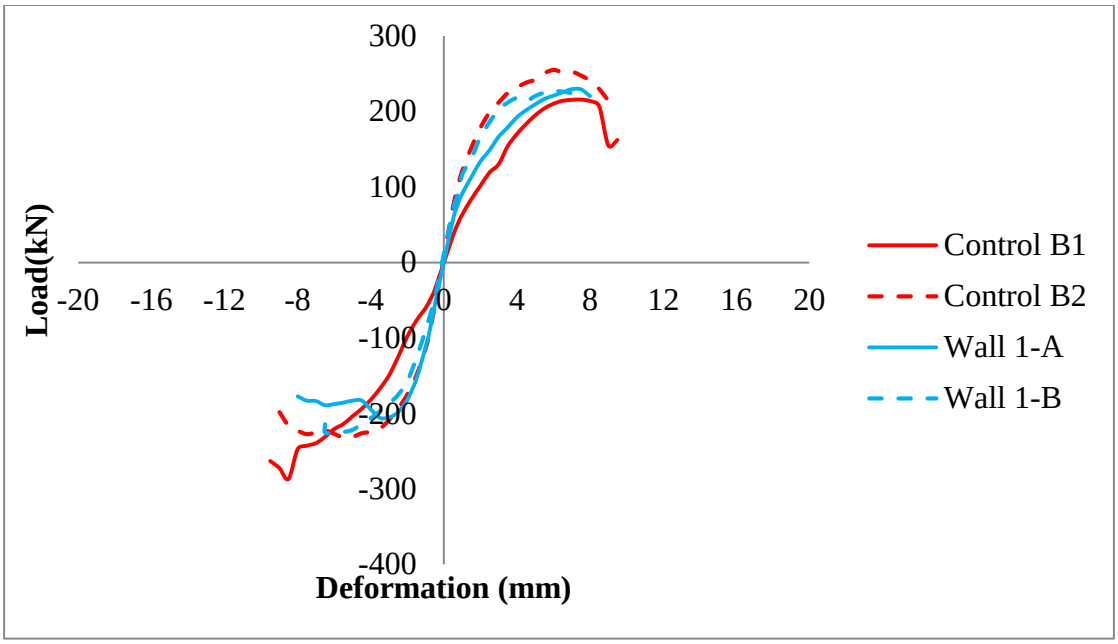

Figure 5.2 Load-Displacement Envelopes for Wall Set 1 and Control Walls

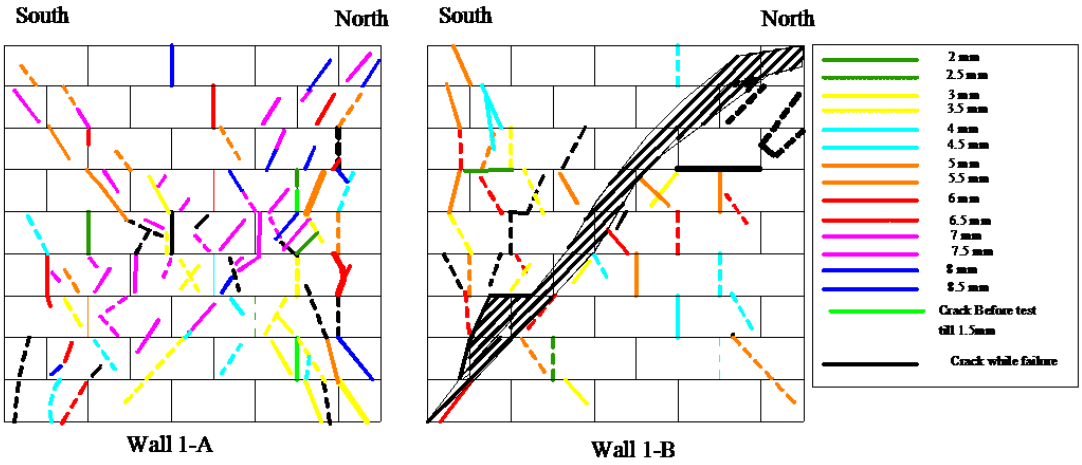

Figure 5.3 Cracks in Wall Set 1

From visual observation of the load-displacement envelope in Figure 5.2 it can be said that there is a significant difference in the initial stiffness between the push and pull cycles for wall 1-A all through the test except at the very early stage of loading. Wall 1-B was around 20% stiffer in the pull cycle than wall 1-A at early stages of loading whereas wall 1-A was 15% stiffer than wall 1-B in the push direction at the very beginning of testing. However, the stiffness of the two walls became the same in the pull cycle but in the push cycle the stiffness degradation of wall 1-A was higher than wall 1-B by around 15%. Control wall B1 (CB1) had much lower stiffness (around 50%) than control wall

B2 (CB2) which had similar stiffness to both walls 1-A and 1-B, especially at the early stages of testing.

For wall 1-A the first diagonal crack through the units occurred in the north toe at 3 mm and then over multiple courses at 3.5 mm displacement in the pull cycle as shown in Figure 5.3. The first crack in the south toe occurred at a displacement of 4.5 mm. The north side seemed to be more distressed than the south side given that the cracks that appeared at low displacements in the north side got as wide as 5 mm or greater at post-peak displacements. Most of the cracks in the walls were diagonal rather than in the mortar joints. Approximately 70% of the total diagonal cracks in the bottom three courses appeared before d_{peak} (displacement at which peak load occurs) whereas this percentage was less than 50% for the top three courses. It should be mentioned here that these percentages are the fraction of the cracks in those courses not in the total wall. The percentage of cracks present at or after the peak is around 60% for the courses around the mid-height bond beam (bond beam course and courses just above and below the bond beam course). Therefore, it can be said that most of the cracks before peak were concentrated in the bottom courses and the top courses contained mainly post- peak cracks. A crack in the end of the wall (crack occurring along the thickness of the wall out-of load plane) was seen at a displacement of 4.5 mm in the north pier. Peak loads of 229.6 kN and 189.0 kN were obtained in the pull and push cycles at displacements of 7 mm and 6.5 mm, respectively. The test was stopped after the first push cycle of 8 mm when the average load drop was approximately 5% in both directions although it had been intended to stop loading after at least 10% drop from peak loading. More toe cracking started to occur at the north end at the point where the test was stopped.

For the second wall of this set, the first diagonal crack appeared at a displacement of 3 mm. The first toe cracking started in the south side at a displacement of 3.5 mm and in the north side at 5.5 mm displacement. There was significantly less cracking in the north side of this wall compared to wall 1-A. This also explains the observation made from the load-deformation curve that wall 1-A was much softer in the push direction than wall 1-B. More than 50% of the cracks in this wall occurred before the peak load. As the displacement increased, the crack widths increased in the south side so that they no longer remained as hairline cracks. No new cracks appeared in the bottom courses after

d_{peak}. End cracking occurred in the south end at a displacement of 6.5 mm and in the north end at the time of failure. Long continuous vertical cracks occurred adjacent to the southernmost grouted core, mainly through the blocks and a few through the mortar joints; whereas wall 1-A had vertical mortar joint cracks next to the north grouted core as shown in Figure 5.3. The lack of anchorage of the bond beam reinforcement may be what led to this type of vertical cracking in or around the grouted cores. The wall reached peak loads of 227.1 kN and 225.9 kN at displacements of 6 mm and 6.5 mm in the pull and push directions, respectively. Although the post-peak capacity did drop in the push direction, there was a much more abrupt drop in the pull direction. The wall failed quite suddenly in the first pull cycle of 7 mm when crushing occurred along a large diagonal as shown in Figure 5.3. It appeared that all the cracks that had formed along the diagonal in the pull cycles came together and resulted in sudden failure of the diagonal strut. Both walls showed pinching behaviour as observed from the hysteresis loops. Pinching indicates a reduction in unloading stiffness at low lateral load level.

5.3.2 Wall Set 2

Wall set 2 had the same vertical and horizontal reinforcement as control set 1 (CB1), however the reinforcement in the bond beams were anchored with 180˚ hooks. Based on the values in Table 5.2 the mode of failure is expected to be shear. The crack pattern also showed mainly shear failure with diagonal cracks in the walls but long vertical flexural cracks at the end of the test indicated that flexural cracks developed in both the walls. Pictures of this end cracking are provided in Appendix 1. Figure 5.4 and Figure 5.5 show the hysteresis curves and load-deformation envelope for the wall set.

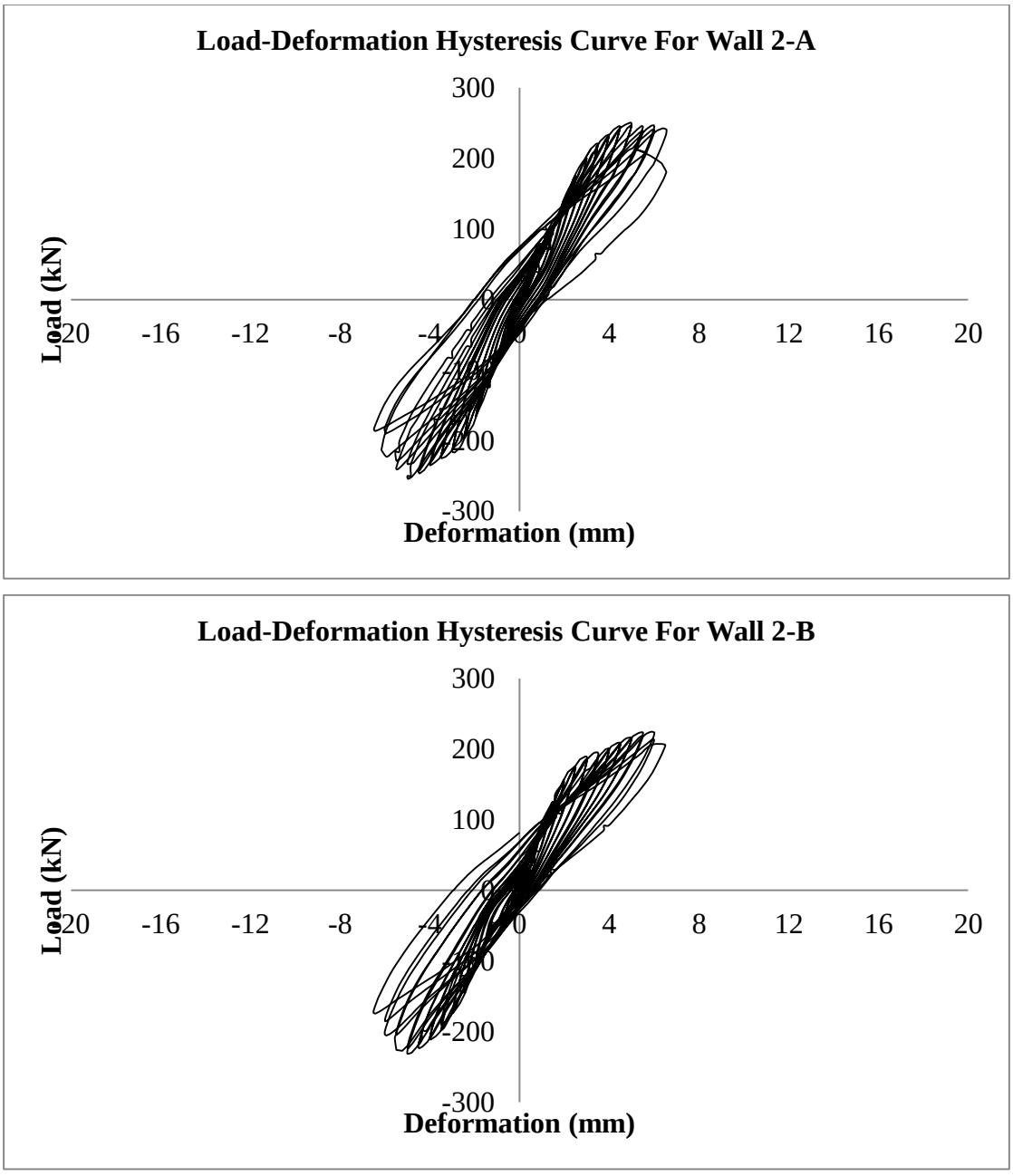

Figure 5.4 Hysteresis Loops for Wall Set 2

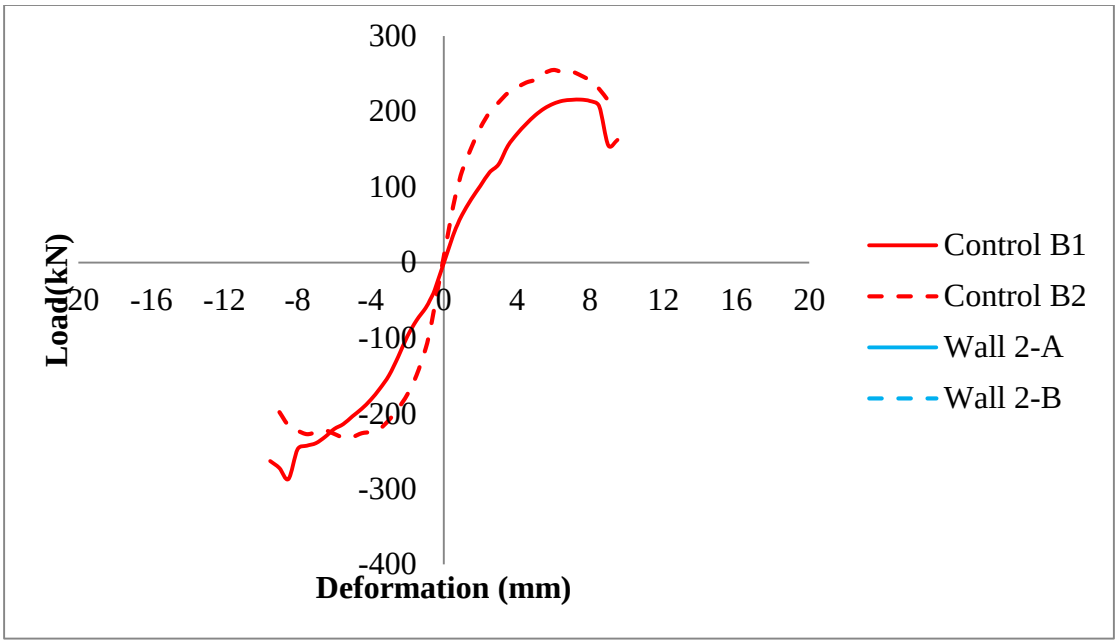

Figure 5.5 Load-Deformation Envelopes for Wall Set 2 and Control Walls

The stiffness of both tested walls was quite similar though control wall CB-1 was stiffer than wall CB-2 as is evident from Figure 5.5. Both walls in this set have nearly the same stiffness as control wall CB2. The stiffness in both directions of loading is not exactly same, they are extremely close in pull cycle (only 5% difference in stiffness) but had around 20% difference in stiffness in the push cycle. The first diagonal crack occurred in the 3 mm pull cycle for wall 2-A. Cracks through the blocks as well as through the mortar joints opened up as wide as 5 mm in the top of the north side.

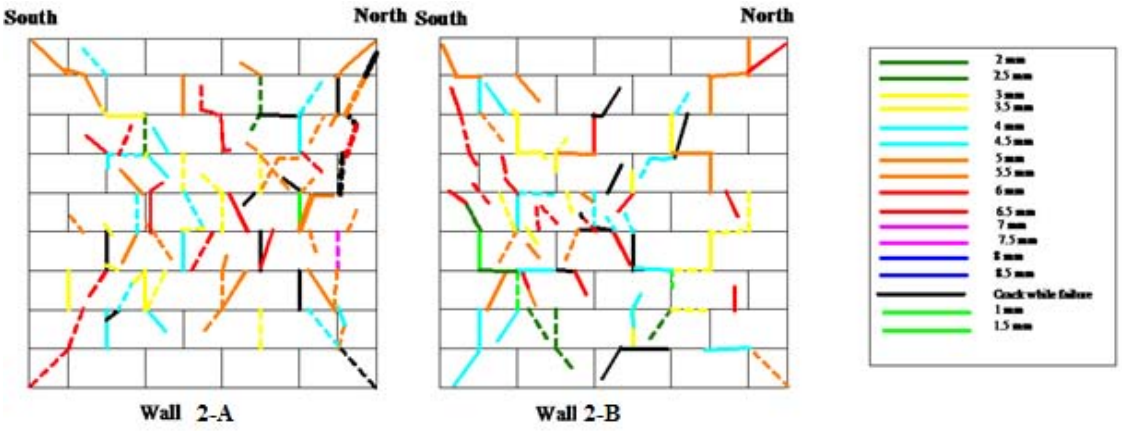

Figure 5.6 Cracks in Wall Set 2

Figure 5.6 shows the final crack patterns for both walls whereas Figure 5.7 shows a few of the very wide cracks that formed in wall 2-A at different locations. Generally, the cracks that widened during the push cycle would nearly close during the pull cycle and vice versa. More than 65% of the cracks formed at or after d_{peak} (d_{peak}=5 mm for both push and pull). When observing parts of the wall, then it can be said that of the total cracks present in the bottom three courses, 50% were post-peak and that percentage is around 65% in the top three courses. The mid-height bond beam contained around 85% post-peak cracks of the total cracks present there whereas the course below this bond beam had all the cracks at or after d_{peak} except one crack through a head joint. Around 70% of the cracks in the course above the bond beam were post-peak cracks. The wall reached maximum horizontal loads of 250.7 kN and 254.5 kN in the pull and push directions, respectively, at a displacement of 5 mm in both cases. Both end cracking and toe cracking in the wall occurred at failure. For wall 2-A loading was stopped after the second pull cycle of 6.5 mm.

(a) (b)

Figure 5.7 a) Cracks in the Top Corner of the North Side of Wall 2-A b) Crack At Bottom of North Toe

In wall 2-B, the first diagonal crack started at a displacement of 2.5 mm for both the pull and push cycles. Toe cracking started at displacements of 4 mm and 5.5 mm in the south and north toes, respectively. The top three courses contained around 55% post peak

cracks whereas only 40% of the cracks in the bottom three courses were post-peak cracks. The cracks in the mid-height bond beam were 60% post-peak and in the courses immediately below and above the bond beam were 50% and 70% post-peak, respectively. All the percentages are the fraction of the total on that particular part of the wall. More than half the cracks in the wall as a whole were post peak cracks. The maximum loads reached in the pull and push cycles were 224.9 kN and 232.4 kN at displacements of 6 mm and 5 mm respectively. End cracking occurred in wall 2-B at 6.5 mm displacement in both the north and south ends of the wall. Loading was stopped after completing one full cycle of 6.5 mm for this second wall of the set.

5.3.3 Wall Set 3

This wall set was similar in all respects to sets 1 and 2 and control set 1 except that the bond beam reinforcement was anchored with circular discs, or "heads", at the ends. According to Table 5.2 for these walls the mode of failure should be shear. Though there were three walls in this set the results of wall 3-C are not discussed here because it showed a completely different behaviour than the other two as is also evident from the hysteresis curve in Figure 5.8. The crack patterns also confirm this, which is included in Appendix 1. The reason behind this different behaviour was traced to the transducer which controls the loading of the wall and was not working properly while testing. So further discussion of this wall's behaviour wall 3-C) is discarded and hence a third wall was tested, namely wall 3-B. No significant flexural cracks were observed for wall 3-A. Though wall 3-B failed under shear which is obvious by the presence of a huge number of diagonal cracks, a few long vertical end cracks were seen at the end of test which may be due to flexural failure of wall. Hysteresis loops obtained from the two walls are presented in Figure 5.8 and the envelopes are shown in Figure 5.9. It can be said generally from the envelope that wall 3-A was around 50% stiffer initially than wall 3-B (though as the test went on the difference in stiffness reduced) and stiffer than both control walls while wall 3-B was stiffer than the first control wall (CB1) but not the second one (CB2).

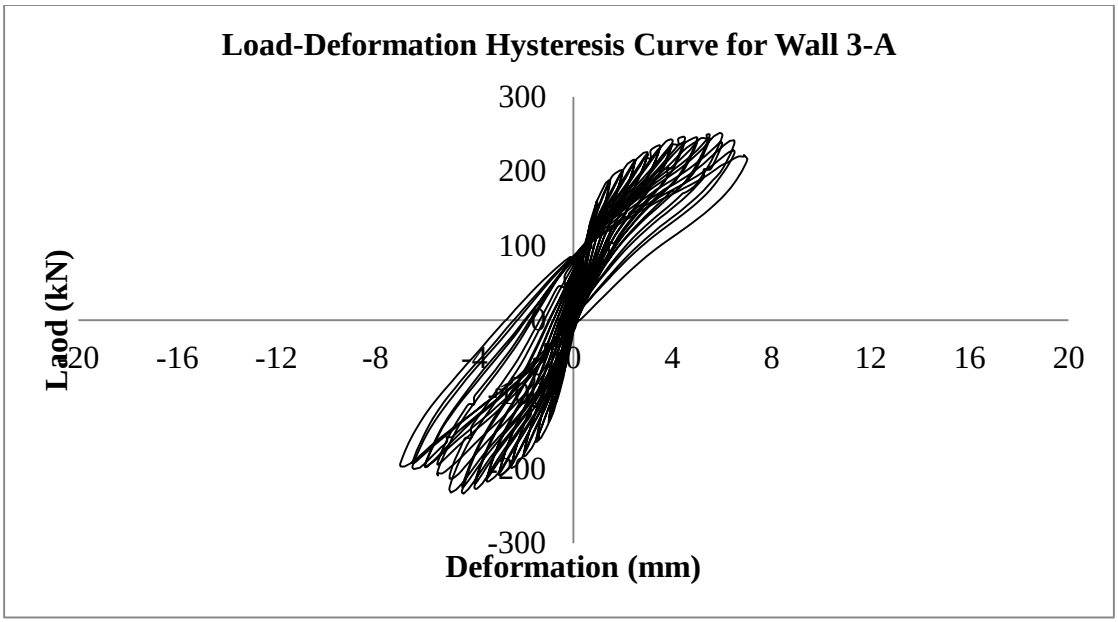
Load-Deformation Hysteresis Curve for Wall 3-A
300
200
100
0
-200
-300
-20
-16
-12
-8
4
8
12
16
20
Laod (kN)
Deformation (mm)

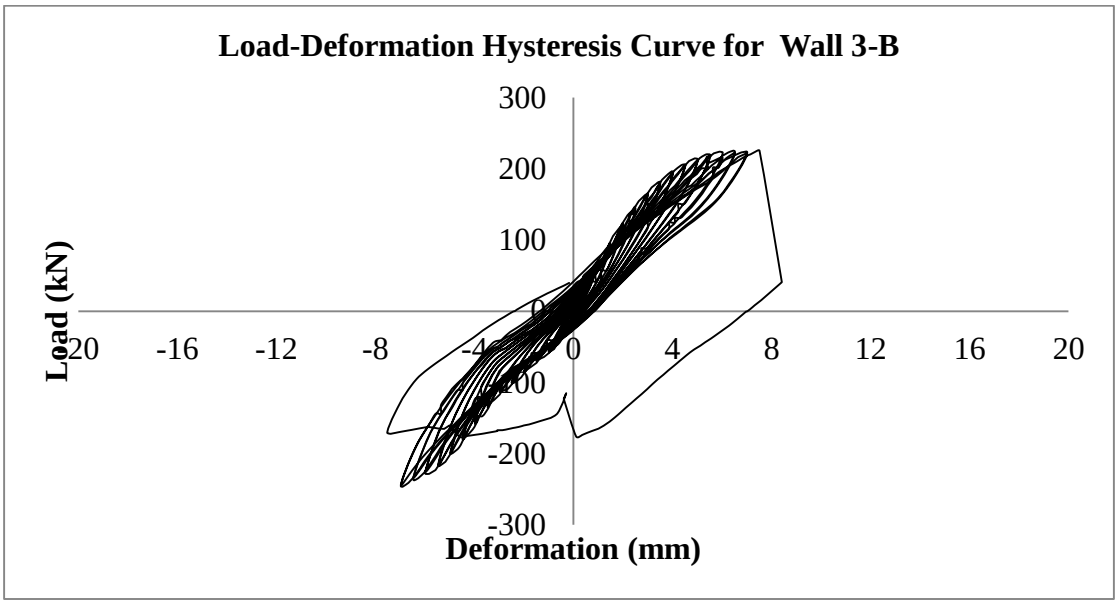
Load-Deformation Hysteresis Curve for Wall 3-B
300
200
100
0
-200
-300
-20
-16
-12
-8
0
4
8
12
16
20
Load (kN)
Deformation (mm)

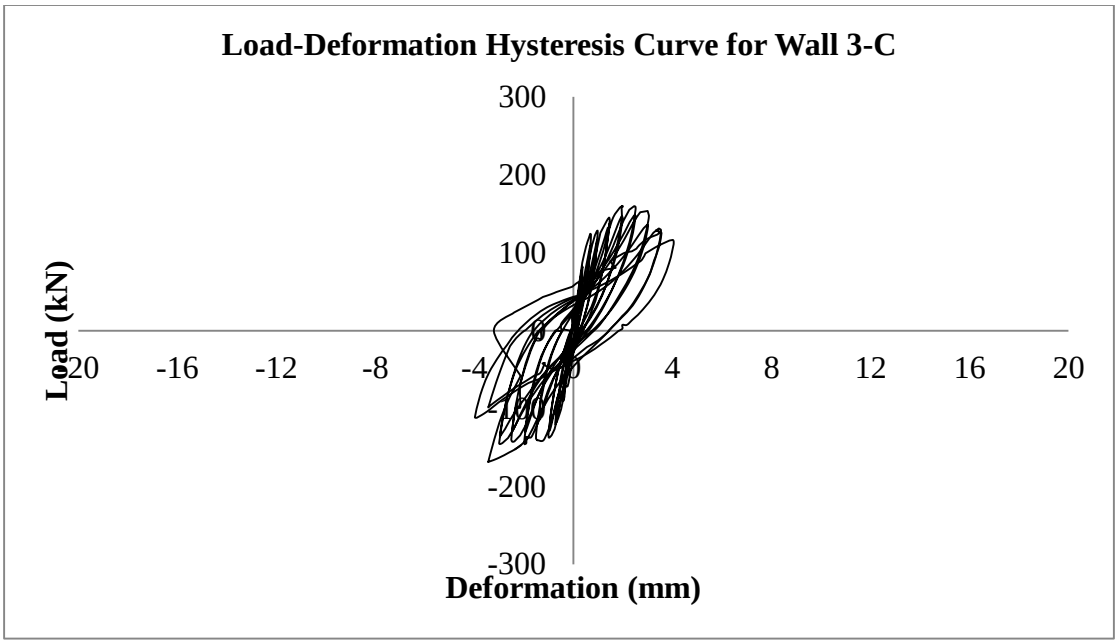

Figure 5.8 Hysteresis Loops for Wall Set 3

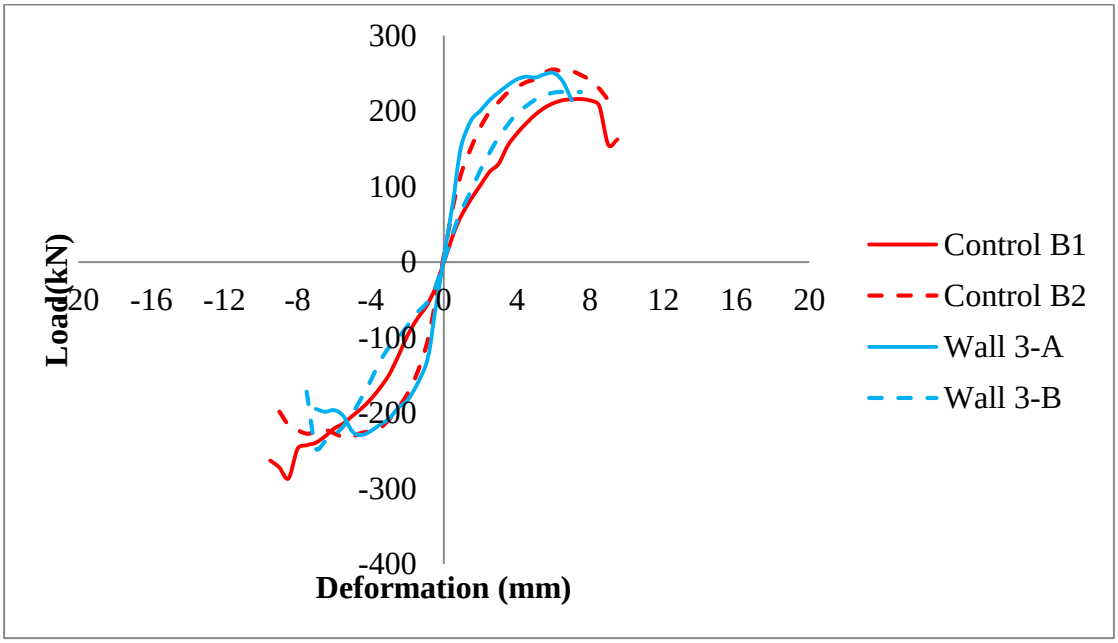

Figure 5.9 Load-Deformation Envelopes for Wall Set 3 and Control Walls

Figure 5.10 shows the final crack pattern of the walls. The first diagonal cracks in wall 3-A took place in the pull cycle of 2.5 mm displacement. Toe cracking in the north side occurred at a displacement of 3.5 mm whereas in the south side it took place at a displacement of 4.5 mm. This wall had cracks along the south grouted core. In the bottom

three courses, around 50% of the cracks occurred at or after d_{peak}. In the mid-height bond beam, more than 25% of the cracks occurred at or near d_{peak}. The proportion of post-peak cracks is as high as 50% in the course below the bond beam and around 35% in the course above the bond beam. Around 60% of the cracks in the top three courses occurred at or after d_{peak} and about 50% of all cracks in the wall were post-peak cracks. The peak loads occurred at displacements of 6 mm and 4.5 mm for the pull and push cycles respectively, and correspond to peak loads of 250.4 kN and 229.3 kN. End cracking at both ends was seen at the last cycle that was applied. Loading was stopped after the first full cycle of 7 mm.

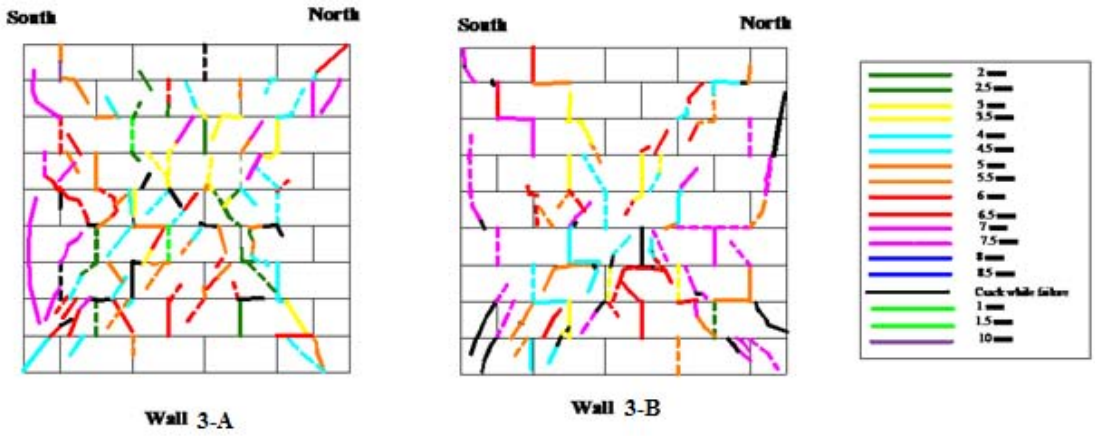

Figure 5.10 Cracks in Wall Set 3

For wall 3-B, the first diagonal cracks started at a displacement of 4 mm and toe cracking started at displacements of 5.5 mm and 7.5 mm in the south and north toes respectively. End cracking started both in the north as well as in the south end at a displacement of 7.5 mm. The wall had cracks through both the south and north grouted end cores. From observation of the cracks in the wall it was noted that about 40% of the cracks in the bottom three courses appeared at or after peak load whereas the proportion is only around 25% for the top three courses. The courses at and near the mid-height bond beam were observed with much interest as well. In the bond beam itself, about 50% of the cracks occurred at or after d_{peak}, while around 35% of the cracks were post-peak in the courses above and below the bond beam. The wall reached maximum capacity of 225.5 kN and 247 kN in the pull and push cycles at displacements of 6.5 mm and 7 mm respectively. Loading was stopped after the first full cycle of 7.5mm.

5.3.4 Wall Set 4

Wall set 4 had the same amounts of vertical and horizontal reinforcement as the previous 3 sets and control set 1 (CB1 and CB2), however the two bond beams were located at the third and sixth courses from the bottom and the bond beam reinforcement was anchored with a 90˚ hook as in control set 1. There were three walls in this set. Firstly, two walls were tested as usual but significantly different strength and behaviour was observed, therefore another wall was tested. According to Table 5.2 the mode of failure should be shear for all wall**s**. However, from observation of the cracks in the walls while testing, it appears that wall 4-A failed under shear with a few vertical cracks at the end of the wall test. Wall 4-B showed some out-of-plane instability and the final failure may be due to this flexure failure. Wall 4-C failed under shear with quite heavy toe crushing at the end. However, the crack pattern in wall 4-C was significantly different than wall 4-A as shown in Figure 5.13.

Generally speaking, Wall 4-A was much stiffer than wall 4-B (40 % and 65% respectively in pull and push direction) as is evident from the hysteresis loops in Figure 5.11 or the load deformation envelope in Figure 5.12. With two reinforced bond beams crossing the potential crack compared to only one in the control walls (assuming the top bond beam does not contribute) it was expected that this set of walls would have higher strength compared to the control walls. This was oddly not the case and also contrary to expectations, however may be because the applied shear load was transferred from the steel beam to a hollow top course similarly to the walls with joint reinforcement and this consequently did not increase the resistance of the walls. Very little post-peak strength was exhibited by these walls. There was a sudden and significant drop in load for wall 4-A, whereas wall 4-B exhibited a more gradual degradation in strength as shown in Figure 5.12. The most interesting feature of all the walls tested with this configuration is that there was no pinching observed in the hysteresis curves.

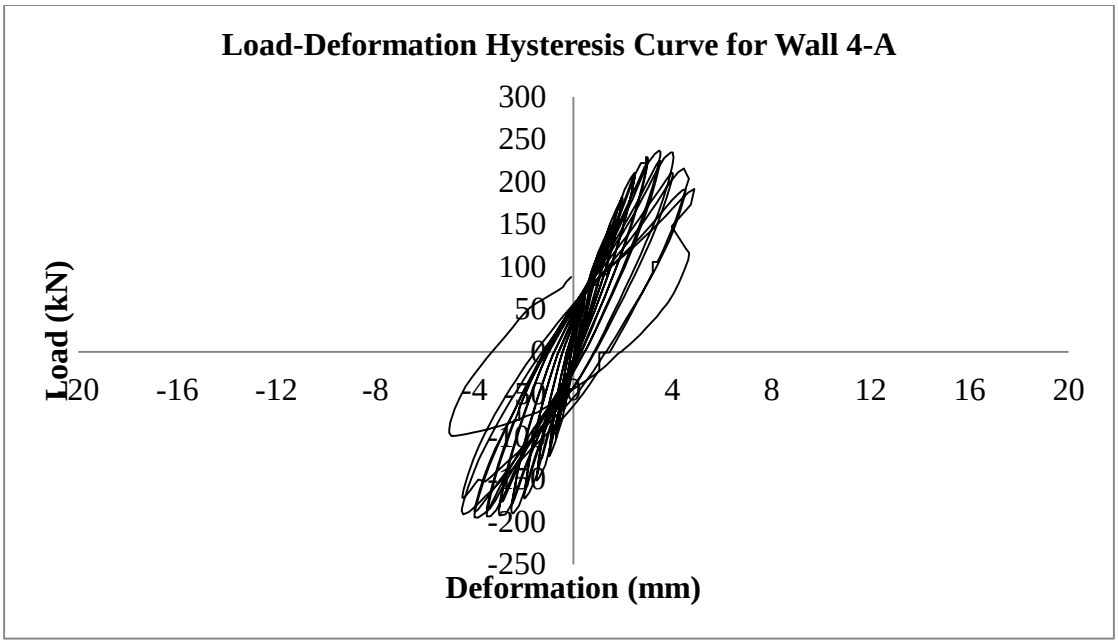
Load-Deformation Hysteresis Curve for Wall 4-A
300
250
200
150
100
50
0
-200
-250
-20
-16
-12
-8
-4
4
8
12
16
20
Load (kN)
Deformation (mm)

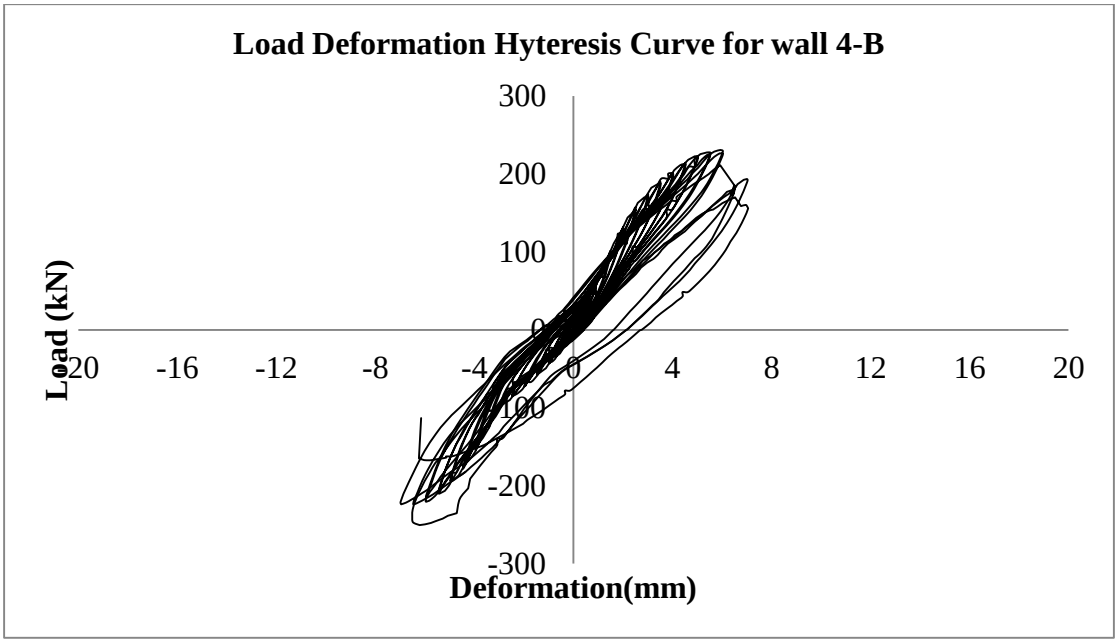
Load Deformation Hyteresis Curve for wall 4-B
300
200
100
0
-100
-200
-300
-20
-16
-12
-8
-4
0
4
8
12
16
20
Load (kN)
Deformation(mm)

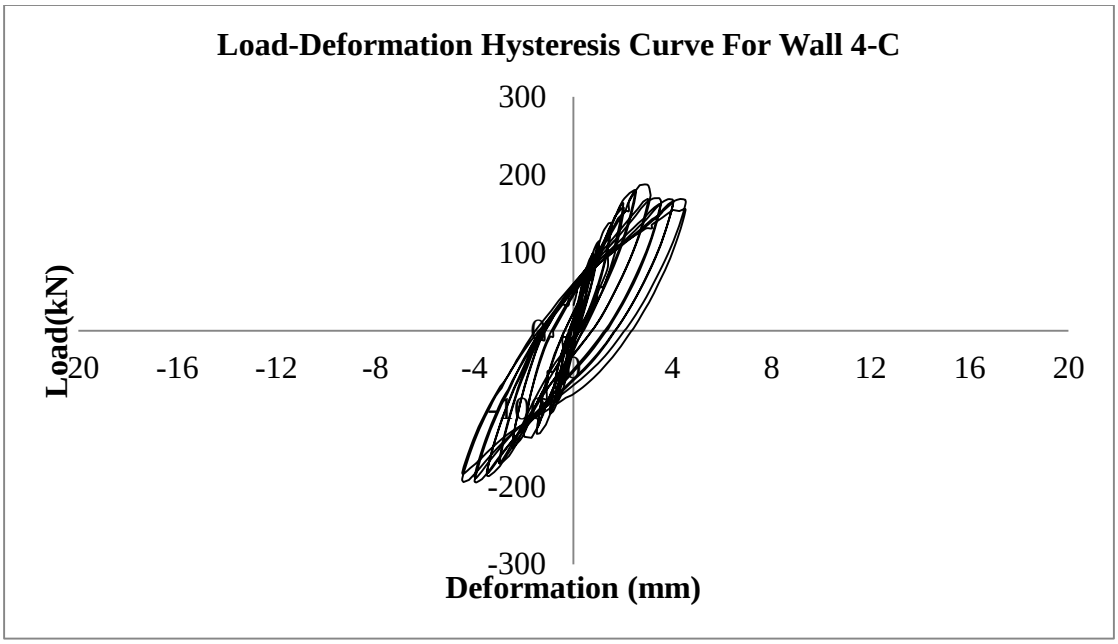

Figure 5.11 Hysteresis Loops for Wall Set 4

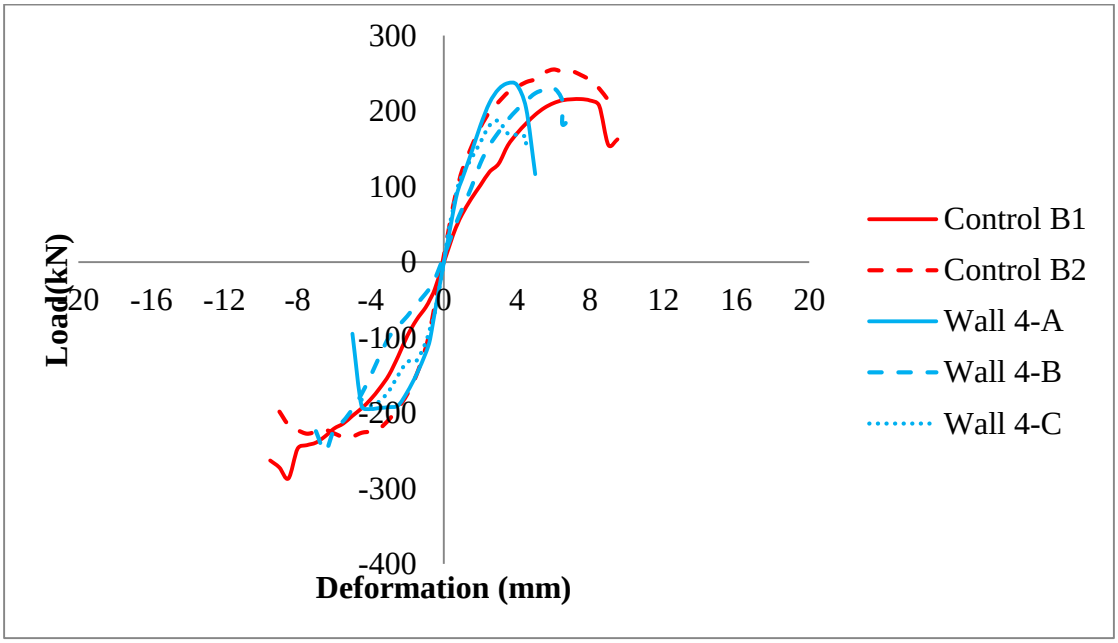

Figure 5.12 Load-Deformation Envelopes for Wall Set 4 and Control Walls

When the hysteresis curves for the walls are examined as shown in Figure 5.11 it can be said that according to the stiffness, wall 4-A and 4-C showed similar behaviour and were stiffer than wall 4-B. However, from the point of view of strength, wall 4-A and 4-B had higher resistance than wall 4-C.

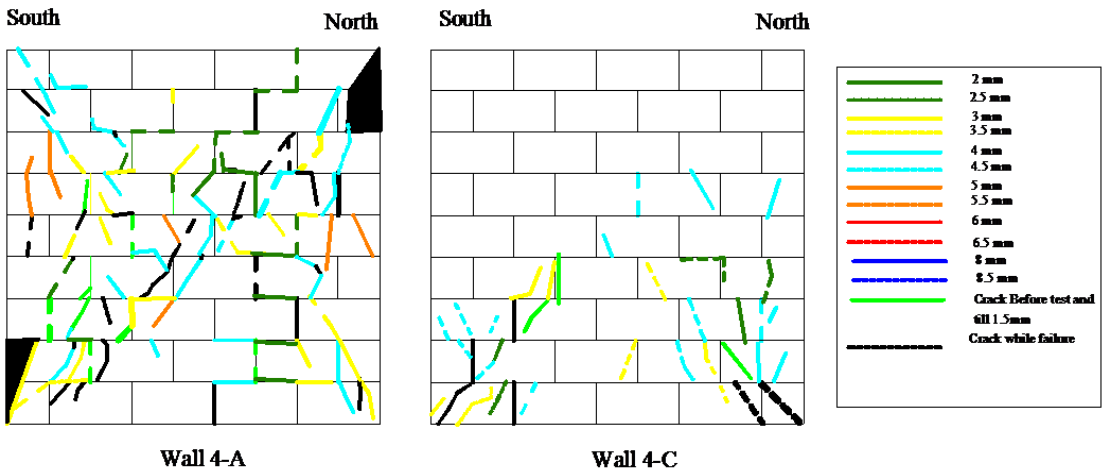

Figure 5.13 Cracks in Walls 4-A and 4-C

The final crack pattern is shown in Figure 5.13. For wall 4-A, the first diagonal crack occurred in the pull cycle at 2 mm displacement. Toe cracking started at the displacement of 3.5 mm in both the north and south toes. Cracks from the top north corner merged and formed a huge diagonal crack which ended in the bottom south corner as shown in Figure 5.13. The face shell of the blocks spalled off at these corners and the grout came into view. The three courses at the middle of the wall, bounded by the two bond beams, had 40% of the total cracks in the wall and of these 65% occurred at or after $d_{peak.}$ In the top three courses, more than 70% of the cracks occurred at or after d_{peak}. Among the two bond beams, the top one (at the sixth course) contained around 60% cracks that occurred at or after d_{peak} whereas this proportion was as low as 35% for the bottom bond beam at the third course from the base of the wall. The bottom two courses of the wall contained around 50% cracks at or after d_{peak}. Overall, nearly 65% of the cracks in the wall were post peak cracks. A few cracks in the wall widened ≥5 mm. Some of the head joint cracks also got wider; however the bed joint cracks remained thin regular cracks all through the wall. Cracks were also seen through the grouted end cores of the wall. End cracks in both the north and south ends appeared in the final cycle. Loading was stopped after the first full cycle of 5 mm. The peak loads 194.7 kN and 236.8 kN occurred at displacements of 4 mm and 3.5 mm respectively for the push and pull cycles.

The first diagonal crack in wall 4-B appeared in the pull cycle of 4.5 mm. Very few cracks formed in the push cycle of loading and no crack was seen in the push cycle until 5.5 mm. Toe cracking occurred first at the south toe at a displacement of 5.5 mm. Before

failure, peak loads of 230.9 kN and 250.9 kN were reached at displacements of 6 mm and 6.5 mm in the pull and push directions, respectively. End cracking occurred at the south end at a displacement of 7 mm. The wall was rotated at the top which was clearly visible and the north toe was fully crushed. The wall failed before completion of the second push cycle of 7 mm. The load bearing capacity degraded by almost 10% immediately after the d_{peak} in both the push and pull cycles. The wall mainly failed in the mortar joints. The final crack pattern of the wall is not presented since it collapsed at failure so no picture of the final crack pattern could be taken. As can be seen in Figure 5.13, wall 4-C had all the cracks concentrated at the bottom courses. The wall also started exhibiting toe cracking at a displacement of only 1.5 mm which was pretty unusal. Some end cracking occurred just before the cycle where loading was stopped.

5.3.5 Wall Set 5

Wall set 5 is the same as control set 2 (C) except for the absence of splice reinforcement at the bottom. The hysteresis curves for the two walls and the envelopes are shown in Figure 5.14 and Figure 5.15. The stiffness of both walls are nearly the same in the pull cycle (except at the beginning of loading) but there is a significant difference between the stiffness of the two in the push cycle where wall 5-B is observed to be 30% stiffer than wall 5-A. The stiffness of wall 5-A was pretty close (within 5%) to the control walls. The control walls displaced more than the walls of set 5.

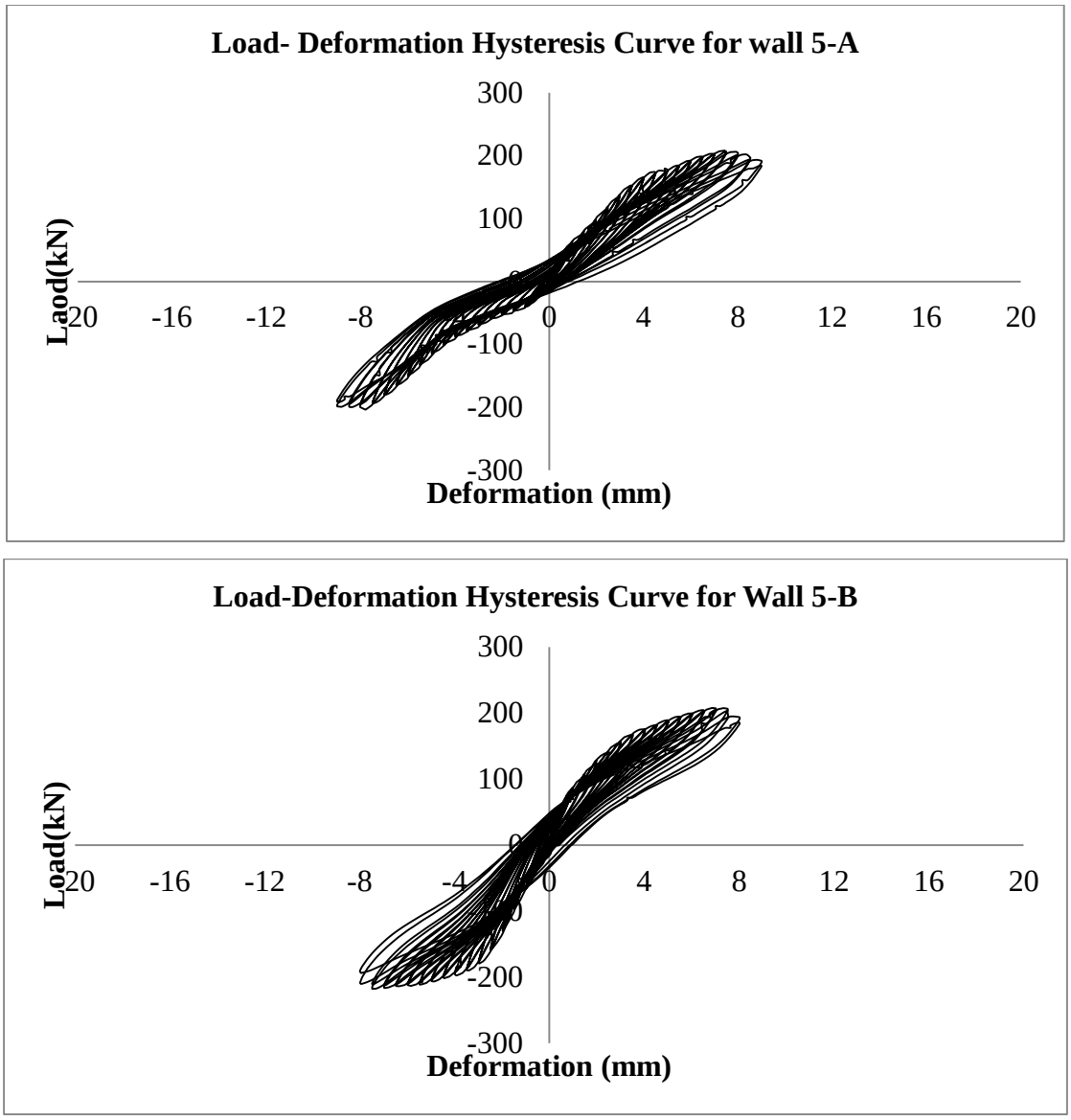

Figure 5.14 Hysteresis Loops for Wall Set 5

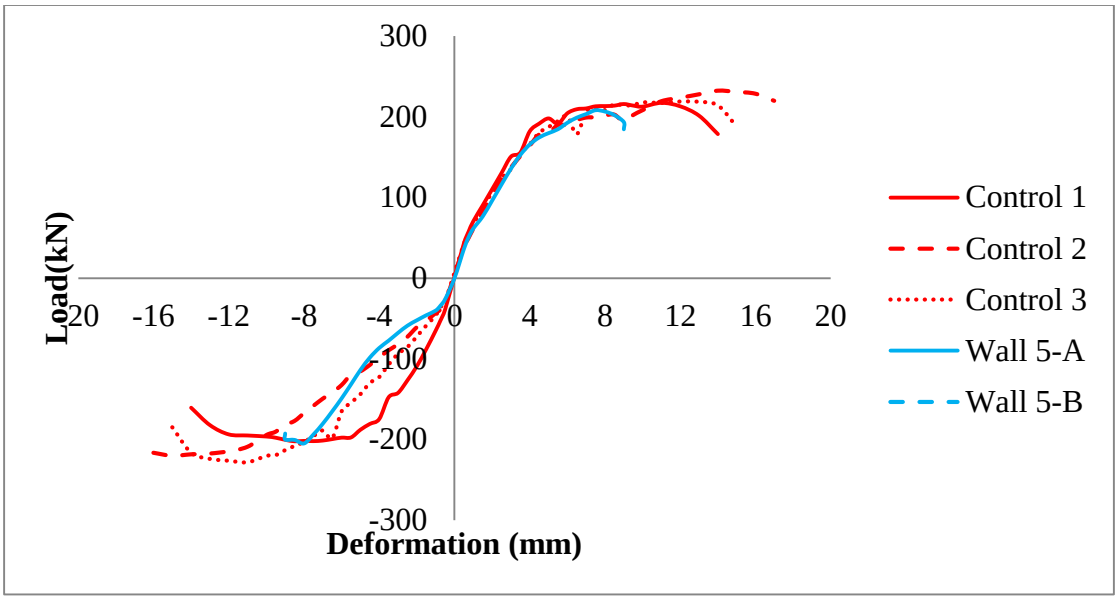

Figure 5.15 Load- Displacement Envelopes for Wall Set 5 and Control Walls.

For wall 5-A the first diagonal crack started at the pull cycle of 4 mm displacement. Toe cracking started at displacements of 8 mm and 9 mm in the south and north toes respectively. In the bottom three courses as well as in the middle three courses around 40% of the cracks appeared at or before d_{peak}. In contrast, in the top three courses around 70% of the cracks occurred before peak displacement d_{peak}. Overall, nearly 50% of the cracks in the wall occurred post peak. The mode of failure was purely shear as only diagonal tension cracks were observed. End cracking occurred at a displacement of 8.5 mm at the top of the north end. Most of the cracks were diagonal with a few stepped cracks in the joints as depicted in Figure 5.16. The peak loads of 204.9 kN and 208.1 kN occurred at displacements of 7.5 mm and 8 mm for the pull and push cycles respectively. Loading was stopped at the second push cycle of 9 mm. Small vertical flexural cracking took place at the end of testing in the bottom of the south end.

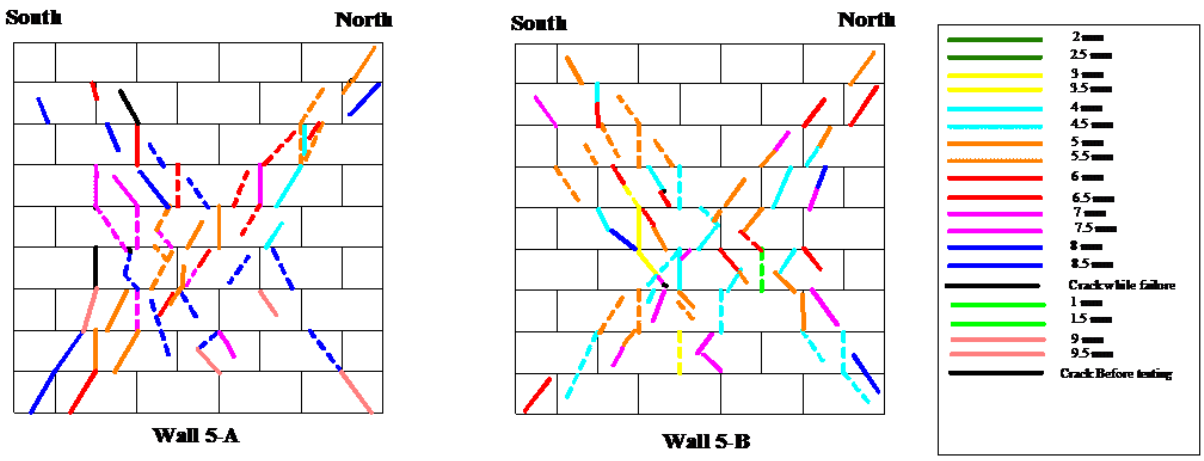

Figure 5.16 Cracks in Wall Set 5

For the second wall designated as 5-B the first diagonal crack started in the push cycle of 3 mm. Toe cracking started at displacements of 6 mm and 4.5 mm for the south and north toes respectively. In the bottom three courses more than 70% of the cracks took place before peak displacement. The number of cracks at or after peak was about 10% in the middle three courses. Around 15% of the cracks in the top three courses occurred at or after d_{peak}. The mode of failure was purely shear with numerous diagonal cracks. There were around 20% post peak cracks in the wall. End cracking occurred at a displacement of 8 mm at the top of the north end. This wall experienced peak loads of 208.0 kN and 218.5 kN in the pull and push cycles at displacements of 7 mm and 7.5 mm respectively. Loading was stopped at the second push cycle of 8 mm.

For these two walls the behaviour in the top three courses is nearly the same in that most of the cracks occurred before d_{peak}. On the other-hand, the behaviour of the walls in the bottom 6 courses is completely different. For wall 5-A most cracks occurred at or after d_{peak} and for wall 5-B, the opposite is true. The crack pattern is probably independent of the fact that there is no welded rebar or splicing in the bottom of the wall. Though sliding of the wall base was comparatively higher than for the other wall sets with the same type of loading, uplift for these walls was similar to that observed for other wall sets. For both walls, mortar joint failure was not as dominant as the block failure. There were no cracks through the grouted cores at the end of the walls for both walls.

5.3.6 Wall Set 6

This set has two walls with the same configuration as control set 2 (C1 , C2 and C3) except there was a plate inserted at the top of the wall having three rods which provide splicing at the top of wall in addition to the splicing at the bottom. From the load displacement envelope as illustrated in Figure 5.18 it can be said that the initial stiffness of the second wall in the pull cycle was more than 50% higher than the first wall and the difference in stiffness between the two walls decreases as the test progresses. The stiffness in the push and pull cycles for wall 6-B are very similar in contrast to wall 6-A. The stiffness of wall 6-A in the pull direction is more than 15% higher than the stiffness in the push direction. Figure 5.17 shows the hysteresis curves for the wall set. Wall 6-B exhibits cyclic strength degradation where it is observed that, unlike the other walls, the strength in the push direction sometimes decreases rather than constantly increasing up to the peak resistance.

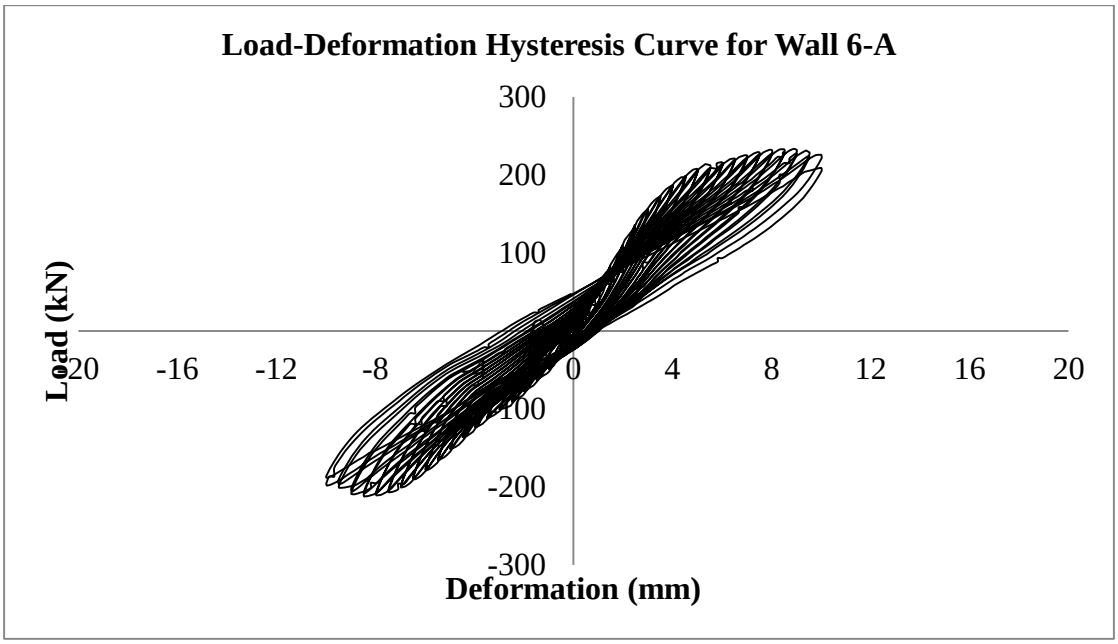

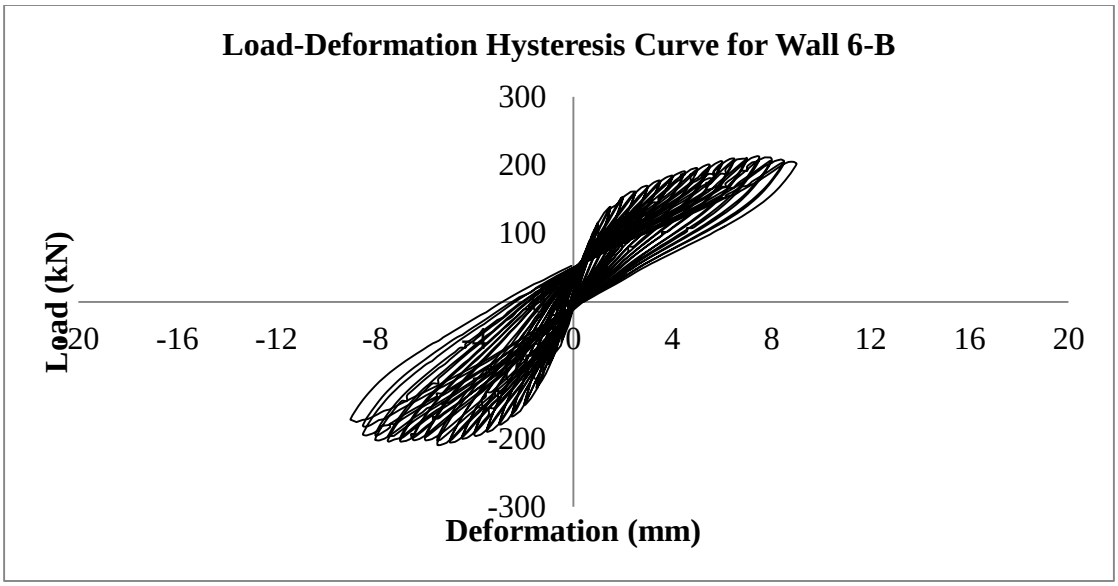

Figure 5.17 Hysteresis Loops for Wall Set 6

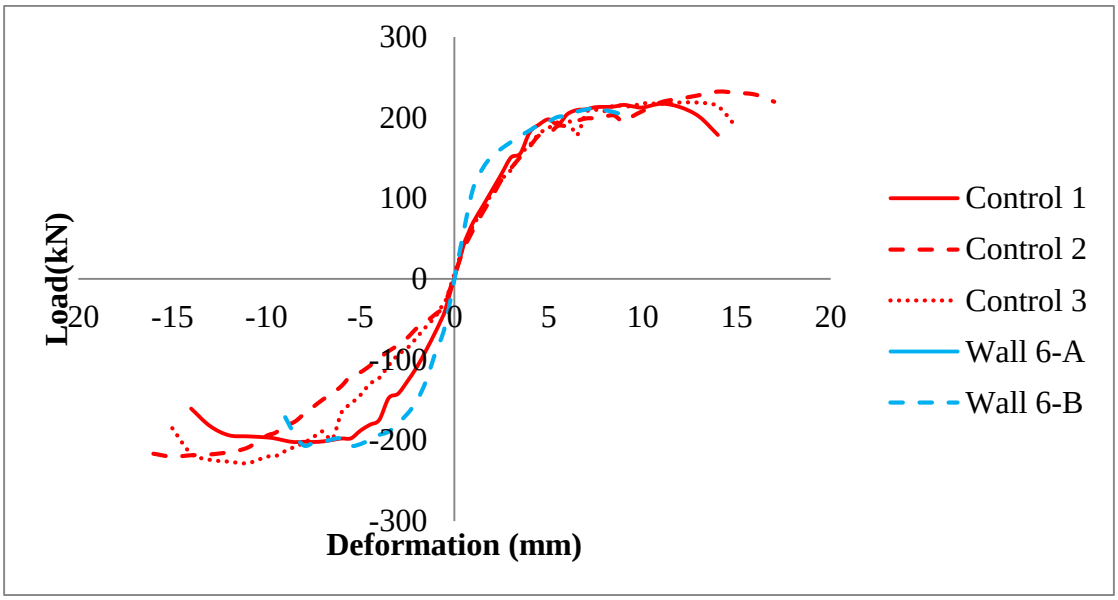

Figure 5.18 Load-Displacement Envelopes for Wall Set 6 and Control Walls

Toe cracking started for wall 6-A at displacements of 6 mm and 7.5 mm in the south and north toes and the cracks became quite wide. There were no cracks in the end grouted cores as shown in Figure 5.19. The first diagonal crack was seen at the push cycle of 3.5 mm. Around 50 % of the cracks in middle three courses occurred at or after peak resistance. Only 20% of the cracks in the bottom three courses and the top three courses occurred at or after d_{peak}. So as a whole, the wall contained around 30% post peak cracks.

All the cracks formed the usual diagonal pattern indicative of a shear failure. A few cracks in the top south corner became quite wide (~ 5 mm). A mortar joint failure also took place in the top south corner. No vertical flexural cracks occurred at the end of the wall. There were very few mortar joint cracks in the wall. The peak loads of 233.9 kN and 231.2 kN in the pull and push cycles occurred for wall 6-A at a displacement of 8.5 mm in both directions. The loading was stopped after the completion of the second push cycle of 10 mm.

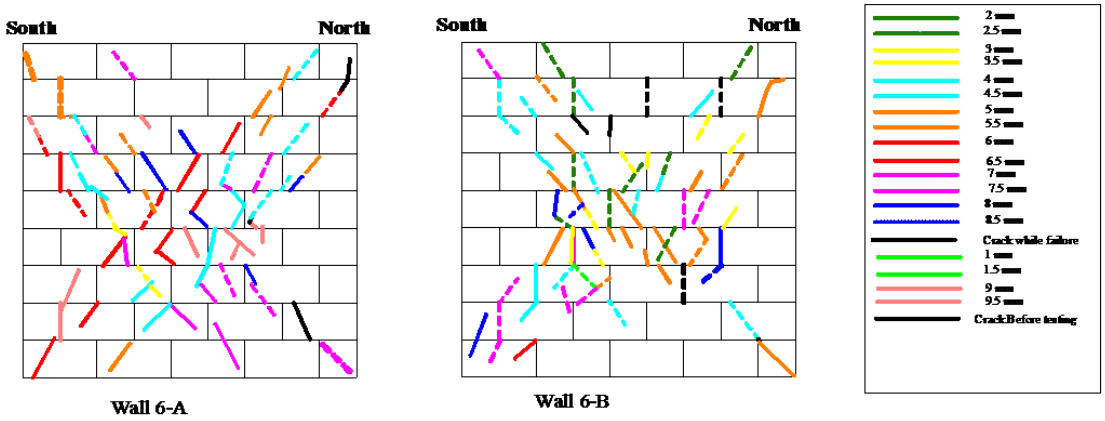

Figure 5.19 Cracks in Wall Set 6

For wall 6-B the first diagonal crack appeared in the pull cycle of 2.5 mm. Toe cracking started at displacements of 6 and 5 mm for the south and north toes. In the bottom three courses 50% of the cracks occurred at or after the peak displacement. Around 15% of the cracks in the three courses at the middle of the wall occurred at or after the peak. No cracks formed in the top three courses after the peak load. There were not more than 20% post peak cracks in the wall. Cracks in the end of the wall occurred at 7.5 mm. Peak loads of 212.4 kN and 206.7 kN were reached at displacements of 7.5 mm and 8 mm for the pull and push cycles, respectively. Loading was stopped after finishing the second push cycle of 9 mm.

5.3.7 Wall Set 7

Walls in this set were of the same construction as control set 2 (C1, C2 and C3), however they were tested under the condition that constant vertical loads were applied through the

two vertical actuators before the test started and this load was held constant in force control throughout the test.

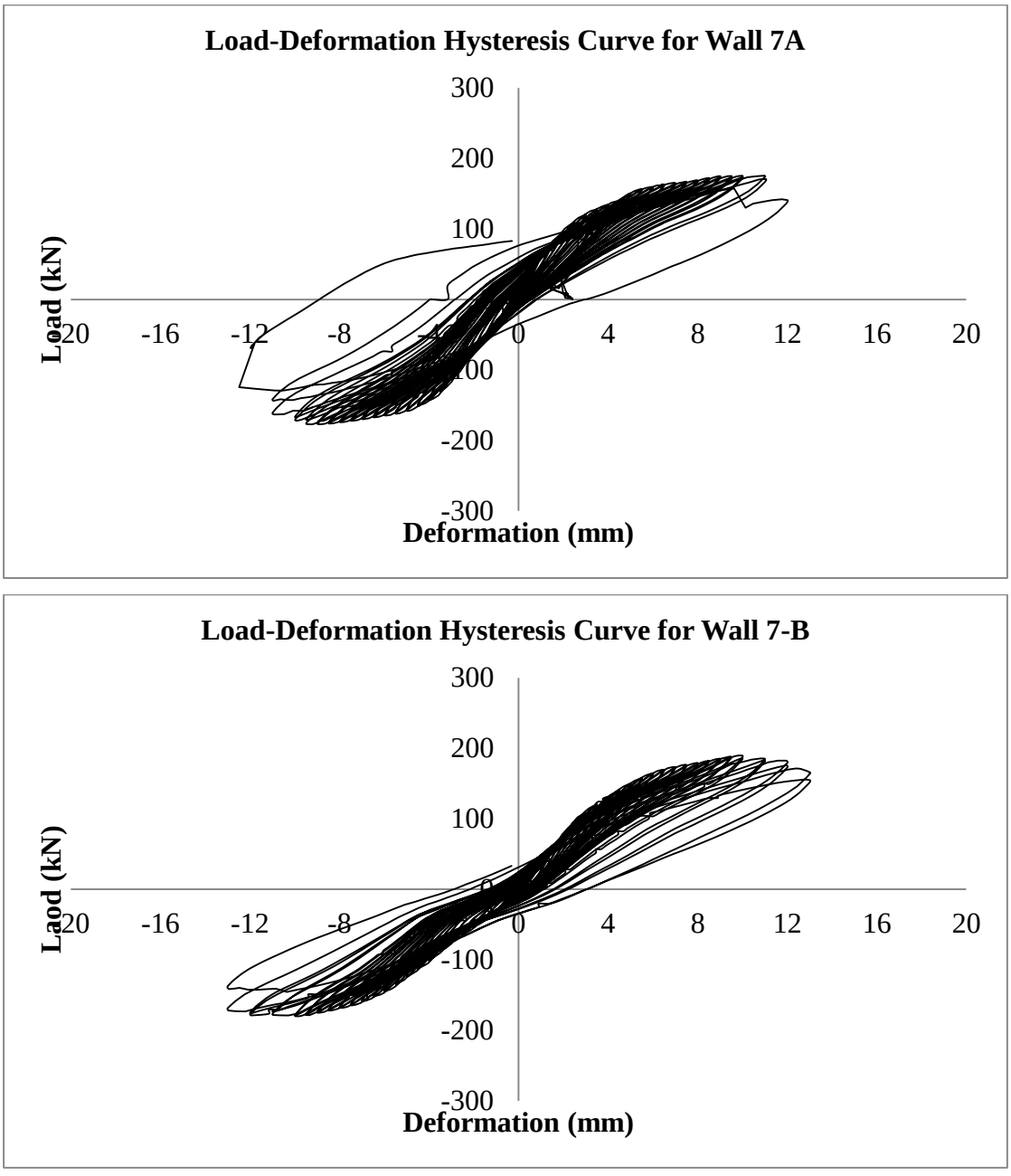

Figure 5.20 Hysteresis Loops for Wall Set 7

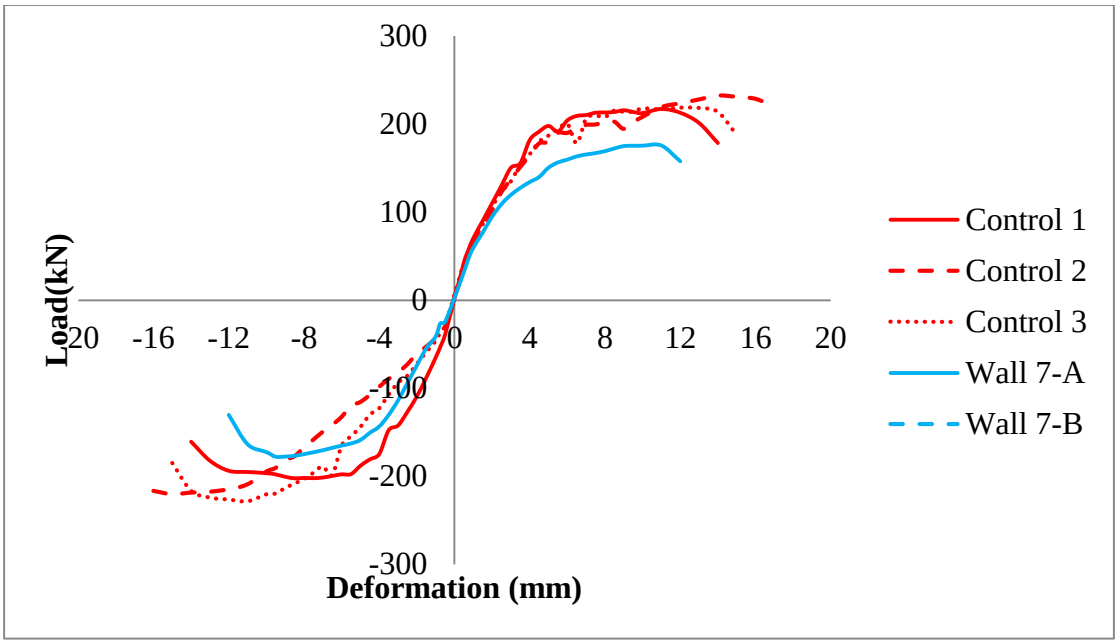

Figure 5.21 Load-Deformation Envelopes for Wall Set 7 and Control Walls

The hysteresis loops for the walls and load-deformation envelopes are shown in Figure 5.20 and Figure 5.21. As seen from the envelopes it seems that the initial stiffness of wall 7-A was about 30% higher than wall 7-B in the pull direction whereas in the push direction it was only 5% higher than the second wall. Both of these walls took longer to fail than the time taken for the other wall sets, on average 71 minutes. The crack patterns for the walls are shown in Figure 5.22.

For wall 7-A the first diagonal crack occurred in the pull cycle of 4 mm. Around 20% of the cracks in the bottom three courses occurred at or after peak displacement, whereas the proportion of post peak cracks was around 30-35% for the middle three courses and the top three courses. Overall, 45% of the cracks in the wall occurred in the middle three courses, around 20% occurred in the top three courses, and the remainder were distributed in the bottom part of the wall. Approximately 25% of the cracks in the wall were post-peak cracks. Toe cracking in the south toe began at early stages of loading and continued until failure while cracking in the north toe occurred during failure. Figure 5.23 shows the south toe of wall 7-A. End cracking also occurred at failure of the wall. The peak loads of 175.7 kN and 177.7 kN occurred at displacements of 11 and 9.5 mm respectively for the pull and push cycles. Loading was stopped after the first pull cycle of 12 mm.

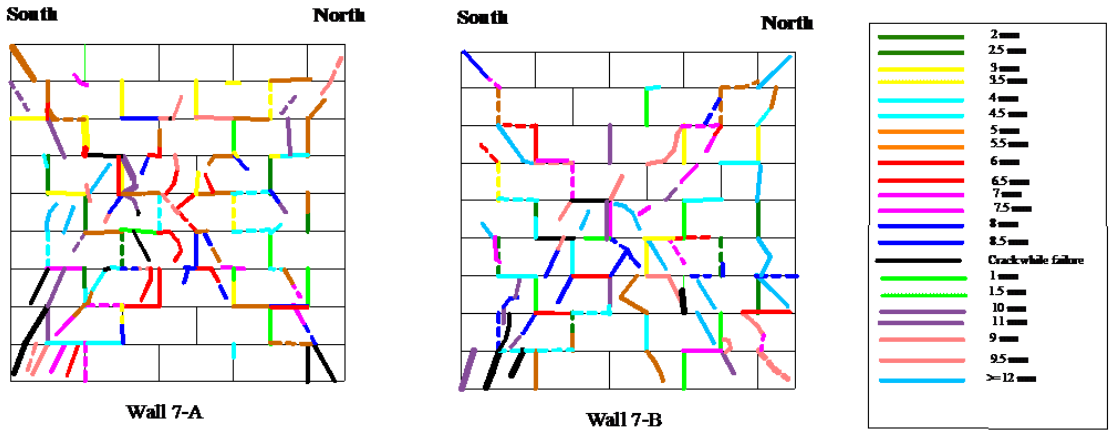

Figure 5.22 Cracks in Wall Set 7

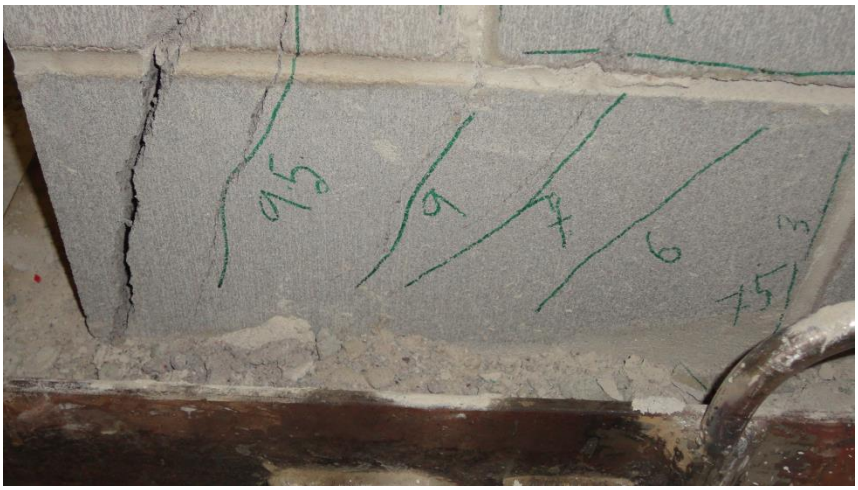

Figure 5.23 Cracking in the South Toe of Wall 7-A

For wall 7-B the first diagonal cracks appeared at a displacement of 5 mm in both the push and pull cycles. The peak loads were 190 kN and 180.7 kN at a displacement of 10 mm in both cycles. The peak displacement was 10 mm for both the push and pull cycles. In both the bottom three courses as well as the middle three courses, approximately 40% of the cracks occurred at or after d_{peak}. The top three courses contained less than 30% post peak cracks. Overall, the cracks in the wall were distributed as follows: 42%, 35% and 23% in the bottom, middle and top third respectively. Approximately 35% of the cracks that occurred in the wall were post-peak. Toe cracking started at a displacement of 9.5 mm in the north toe while severe distress occurred in the south toe as shown in Figure

5.24. End cracking occurred in the south end at a displacement of 11 mm whereas end cracking in the north end occurred during failure. Loading was stopped after the second push cycle of 13 mm.

Figure 5.24 Cracking in the South Toe of Wall 7-B

5.3.8 Wall Set 8

Wall set 8 was tested under monotonic push loading so that it could be compared with control set 2 (C1, C2 and C3) to examine the differences in wall behaviour under cyclic and monotonic loading. It was decided prior to the tests that the test span would not be longer than 30 minutes and the rate was determined based on this test length; however both tests lasted almost 40 minutes at the rate of 0.0075 mm/s or 0.45 mm/min. Figure 5.25 and Figure 5.26 show the load-displacement behaviour of the walls and the final crack patterns.

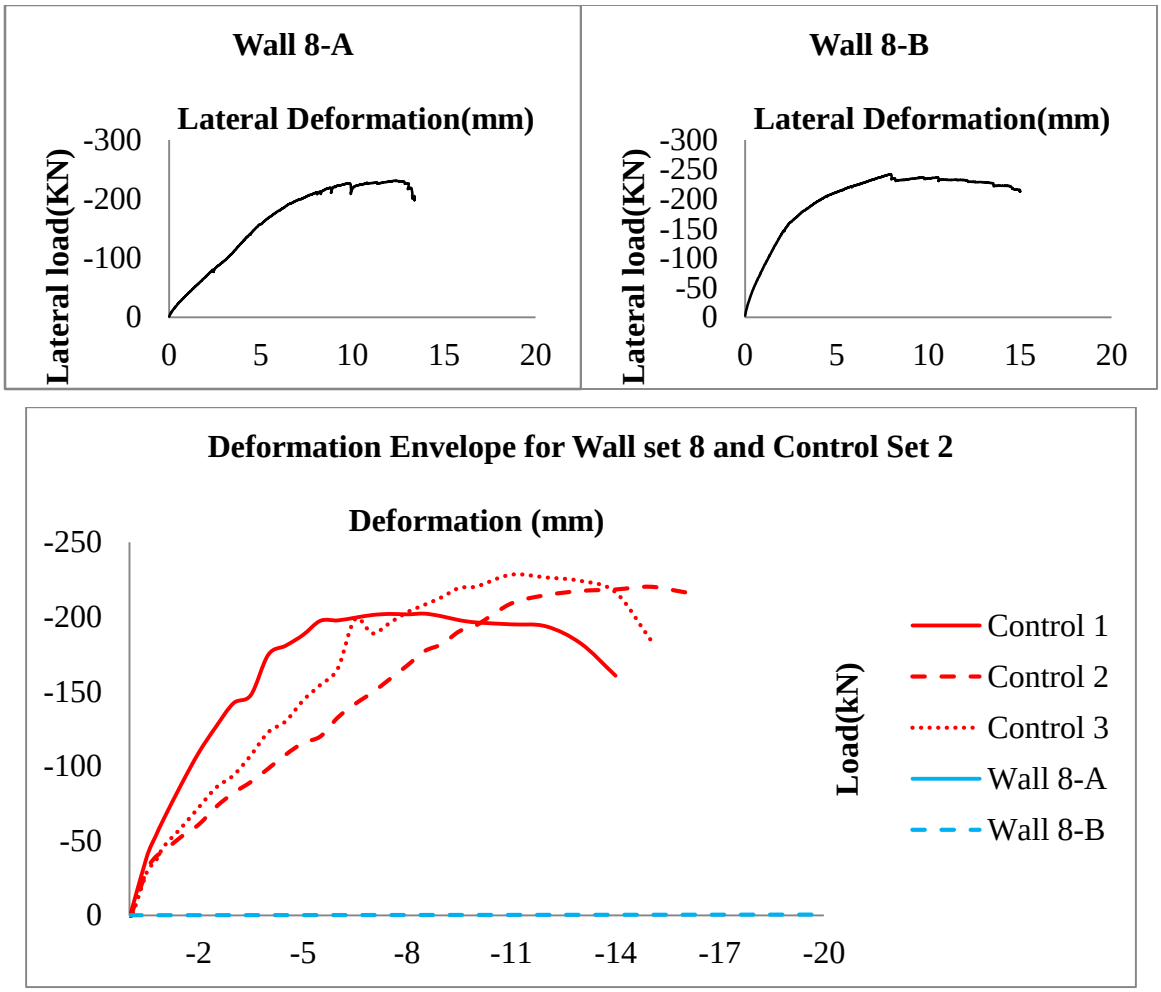

Figure 5.25 Load-Deformation Curves for Wall Set 8 and Control Walls

Comparison of the wall behaviour under monotonic loading to cyclic loading can be made from observation of the curves shown in Figure 5.25. Wall 8-B was stiffer than any of the control walls and initially it was stiffer than wall 8-A by more than 30%. In general, lateral deformation of the walls under monotonic loading was higher than for the walls under cyclic loading which is quite obvious.

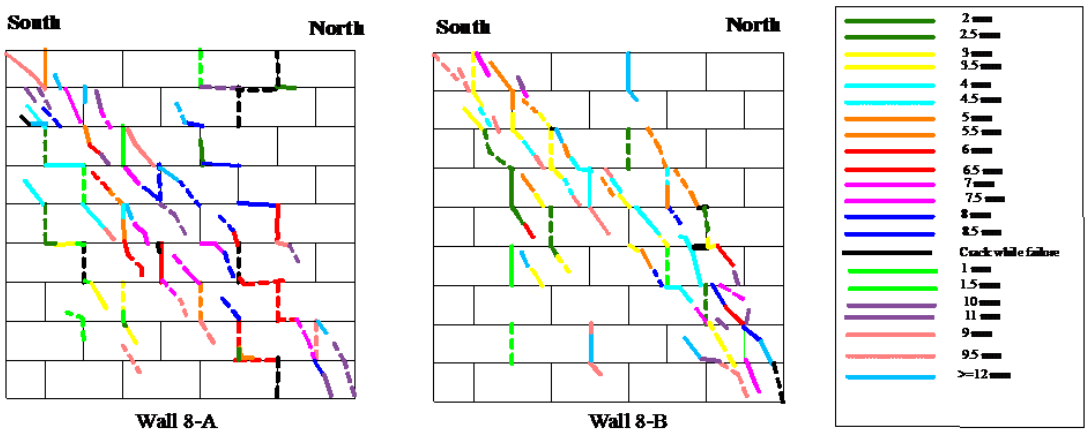

Figure 5.26 Cracks in Wall Set 8

At lower displacements, stepped cracks in the mortar joints were visible, but as the load increased, diagonal cracks through the blocks started to form in the walls. For wall 8-A the first diagonal crack occurred at a displacement of 4 mm. Toe cracking started at a displacement of 8 mm in the north toe and vertical end cracking occurred at failure. For wall 8-B, the first diagonal cracks occurred at a displacement of 3 mm and end cracking started at a displacement of 13 mm. In both walls the cracks took on a pure diagonal pattern joining the top south corner and the north toe as was expected. The two walls reached maximum loads of 230.8 kN and 242.0 kN at displacements of 12.3 mm and 7.9 mm respectively. The maximum displacements were 13.4 mm and 15.1 mm respectively. For wall 8-A, the load dropped to as low as 183.1 kN before termination of the test. In the case of wall 8-B, the load decreased to 213.0 kN, more than a 10% reduction from the peak load, before the test was stopped.

5.3.9 Summary

From the observations as discussed above, the following conclusions can be made:

- Walls with bond beam reinforcement have fewer cracks forming before the peak load compared to walls with joint reinforcement, with more cracks forming after peak resistance.
- Vertical cracks through the blocks in the grouted end cores tend to occur in walls with unanchored bond beam reinforcement. The reason behind this type of cracks

may be that when the wall is horizontally loaded at higher level of loads, the wall deforms in the direction of loading but the unanchored reinforcement does not move and this creates a tensile stress which might cause that sort of vertical cracking.

- In walls with bond beams, the cracks are more scattered throughout the walls; whereas for walls with joint reinforcement the cracks seem to form a clear X-shape pattern. This may be due to the reason that the presence of bond beams creates a relatively stiff region where the bond beam is located which forces the cracks to occur all over in the less stiff regions in contrast to the walls with joint reinforcement.
- When the percentages of post-peak cracks were compared, it was seen that the walls which had bond beam reinforcement with 90° hooks and 180° hooks had less cracking up to the peak strength than the walls with straight bars or shear studs.
- The mode of failure was mainly shear with some significant flexural cracks for walls with bond beams whereas for walls with joint reinforcement the failure mode was almost always pure shear.
- The walls with bond beams experienced less deformation than walls with joint reinforcement. The underlying fact behind this may be the non-uniform spacing of reinforcement in walls with bond beams in comparison to walls with joint reinforcement. The bond beams may also increase the stiffness of the walls.

5.4 Bilinear Idealization

The process of converting the load-deflection envelope into the bilinear idealized form was briefly discussed in Chapter 2. This methodology is applied to the envelopes presented in this chapter. The key values and points of interest that were calculated in determining the idealized curves are presented in Table 5.3 and Table 5.4.

The graphical representation of the typical bilinear idealized curve is shown in Figure 5.27 for wall 1-A. Plots for the remaining walls are included in Appendix 2. Normally, the initial cracking deformation d_{cr} is taken at the load $0.7H_{max}$ for the calculations. The values in Table 5.1 confirm that in most of cases, the ratio between the cracking force to maximum force is 0.7 with a few exceptions such as wall 6-A. However, in general the

value of H_{cr} is taken as $0.7H_{max}$. The other two points of interest are $d_{e,}$ the displacement at the idealized elastic limit, and $d_{u.}$. d_u is determined as the point of intersection of the line of $0.8H_{max}$ and the experimental envelope after the occurrence of peak load. If the experimental envelope does not drop enough to reach the line of $0.8H_{max}$ the maximum displacement d_{max} was taken as d_u. The area under the envelope, $A_{env,}$ is evaluated by dividing the experimental envelope into small strips (as trapezoid) using the same interval of displacement that was applied to the walls while testing and then applying the trapezoidal rule of area calculation. H_u for the bilinear idealized curve is then determined from the following equation:

$$H_u = K_e \left(d_{max} - \sqrt{d_{max}^2 - \frac{2\,A_{env}}{K_e}} \right) \qquad \text{(Eq. 5.1)}$$

Where $$K_e = \frac{H_{cr}}{d_{cr}} \qquad \text{(Eq.5.2)}$$

The ultimate ductility factor is determined by the ratio:

$$\mu_u = \frac{d_u}{d_e} \qquad \text{(Eq.5.3)}$$

And the displacement at the idealized elastic limit d_e is evaluated from:

$$d_e = \frac{H_u}{K_e} \qquad \text{(Eq.5.4)}$$

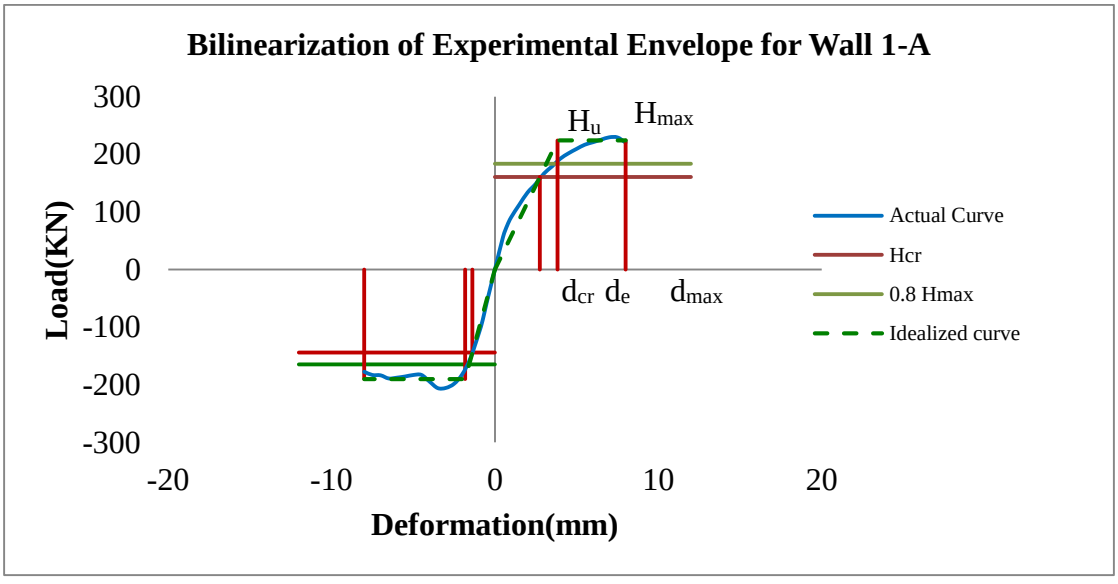

Figure 5.27 Typical Load Deformation Envelope and Bilinear Idealized Curve for Wall 1-A

Table 5.3 Calculated Values for Bilinear Idealization in the Pull Direction

Wall	H_{max} (kN)	H_{cr} (kN)	d_{cr} (mm)	K_e (kN/mm)	$0.8H_{max}$ (kN)	d_e (mm)	d_u (mm)	d_{max} (mm)	A_{env} (kN-mm)	H_u (kN)	H_u/H_{max}	Ductility d_e/d_u
1-A	229.6	160.7	2.8	58.4	183.7	3.8	8.0	8.0	1363.1	224.1	0.98	2.1
1-B	227.1	158.9	1.9	85.1	181.8	2.7	7.0	7.0	1265.1	222.1	0.98	2.6
2-A	250.7	175.5	2.6	68.7	200.6	3.5	7.0	7.0	1146.6	241.8	0.96	2.0
2-B	224.9	157.4	2.1	75.7	179.9	2.8	6.5	6.5	1077.8	211.1	0.94	2.3
3-A	250.4	175.3	1.3	136.1	200.3	1.7	7.0	7.0	1439.6	234.5	0.94	4.1
3-B	225.5	157.8	2.8	55.9	180.4	3.95	7.5	7.5	1222.4	221.3	0.98	1.9
4-A	236.8	165.8	1.8	92.6	189.5	2.4	4.6	5.0	837.8	219.6	0.93	1.9
4-B	230.9	161.6	2.7	59.6	184.7	3.7	6.5	7.0	1128.8	218.4	0.95	1.8
4-C	186.7	130.7	1.4	96.1	149.4	1.8	4.5	4.5	636.1	177.4	0.95	2.5
5-A	208.1	145.7	3.3	44.3	166.5	4.5	9.0	9.0	1343.7	198.9	0.96	2.0
5-B	208.0	145.6	2.7	54.7	166.4	3.7	8.0	8.0	1245.9	202.6	0.97	2.1
6-A	233.9	163.7	3.2	50.5	187.1	4.4	10.0	10.0	1746.6	224.5	0.99	2.3
6-B	212.4	146.9	1.8	80.7	167.9	2.46	9.0	9.0	1545.7	199.0	0.95	3.7
7-A	175.7	122.9	3.2	38.4	140.6	4.4	12.0	12.0	1661.4	169.7	0.97	2.7
7-B	190.0	133.0	4.1	32.4	152.0	5.6	13.0	13.0	1845.7	180.7	0.95	2.3

Table 5.4 Calculated Values for Bilinear Idealization in the Push Direction

Wall	H_{max} (kN)	H_{cr} (kN)	d_{cr} (mm)	K_e (kN/mm)	$0.8H_{max}$ (kN)	d_e (mm)	d_u (mm)	d_{max} (mm)	A_{env} (kN-mm)	H_u (kN)	H_u/H_{max}	Ductility d_e/d_u
1-A	205.7	143.9	1.4	104.3	164.6	1.8	8.0	8.0	1346.9	189.9	0.92	4.4
1-B	225.9	137.9	1.7	82.1	157.8	2.5	6.5	6.5	1093.1	209.1	0.93	2.6
2-A	254.5	178.2	2.2	81.4	203.6	2.8	6.3	7.0	1269.3	226.3	0.89	2.3
2-B	232.4	162.7	2.8	58.1	185.9	3.6	6.3	6.5	979.5	207.9	0.89	1.8
3-A	229.3	160.5	1.4	112.2	183.4	1.9	7.0	7.0	1274.4	210.2	0.92	3.7
3-B	247.0	172.9	4.3	39.8	197.6	6.0	7.3	7.5	1075.7	239.1	0.97	1.2
4-A	194.7	136.3	1.3	104.9	155.8	1.8	4.5	5.0	761.6	184.9	0.95	2.5
4-B	250.9	175.6	4.5	38.9	200.7	5.5	7.0	7.0	909.5	214.5	0.86	1.3
4-C	192.2	134.6	1.4	96.1	153.8	1.6	4.5	4.5	614.8	170.1	0.89	2.8
5-A	204.9	143.4	5.3	26.9	163.9	6.4	9.0	9.0	996.9	171.5	0.84	1.4
5-B	218.5	152.95	2.4	63.7	174.8	2.7	8.0	8.0	1321.7	206.2	0.94	3.3
6-A	213.2	77.5	2.0	38.8	170.6	4.8	10.0	10.0	1407.1	184.7	0.87	2.1
6-B	206.7	144.7	1.4	105.6	165.4	1.9	8.5	8.5	1523.9	202.0	0.97	4.5
7-A	177.7	124.4	3.3	37.7	142.2	4.4	11.6	12.0	1620.9	165.6	0.93	2.6
7-B	180.7	126.5	5.1	24.8	144.6	7.0	13.0	13.0	1652.9	174.1	0.96	1.9

Tomazevic reported a mean value for H_u/H_{max} of 0.9 (Tomazevic, 1999) whereas for the results presented here an average of 0.96 was found for walls in the pull cycle and 0.92 for the push cycle. Values of this order for the ratio between the peak experimental and idealized curve strengths indicate that the idealized envelope captures the experimental behaviour well and can be used with confidence for design and analysis purposes.

To avoid excessive damage to shear walls, the ultimate ductility factor has to be limited from the seismic resistance point of view. Tomazevic (Tomazevic, 1999) reported that the values of ultimate ductility factor of individual walls should be limited to 2 - 3 for plain masonry, 3 - 4 for confined masonry and 4 - 5 for reinforced masonry walls though larger values could also be acceptable if experimental results allow more. In Table 5.3 and Table 5.4 the ductility for all walls was also determined and it can be seen that none of them exceed the ranges defined above though in some cases the ductility was lower than the value defined for plain masonry. The ductility ratio was found to be in the range of 1.9- 4.1 in the pull cycle and in the range of 1.8- 4.5 for the push cycle. In general, a similar level of ductility was obtained for all sets of walls. The average ductility for control set 1 (with bond beams) is 2.8 in the pull cycle and 3.1 in the push cycle. For control set 2 (without bond beams) the average ductility is 3.1 and 2.8 for the pull and push cycles respectively. The ductility of all walls is shown in Figure 5.28.

When the results are compared with the control walls, as shown in Table 5.5, it is evident that nearly all wall sets had a decrease in ductility compared to the control walls with few exceptions.

For the walls with bond beams, the biggest reduction in ductility occurred for the walls where the bond beams were relocated i.e. for set 4. When the vertical actuator loading was kept constant (set 7), the ductility decreased by 20%. The ductility is lower for all the walls with bond beams regardless of the anchorage condition which may indicate that the bond stress developed in the reinforcement did not exceed the capacity of the rebar and the reinforcement anchorage did not come into action. All the walls with bond beams reached the level of peak lateral load at nearly the same level of displacement.

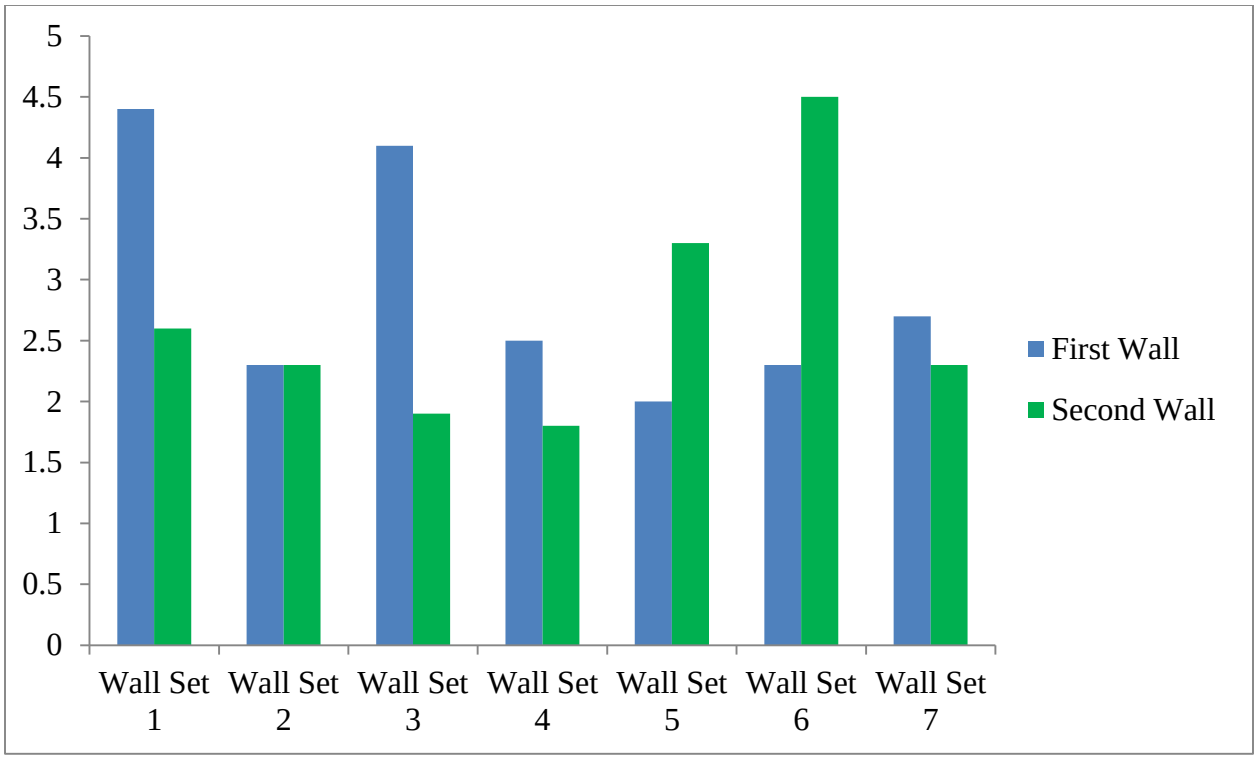

Figure 5.28 Ductility of Tested Walls Obtained from Bilinear Idealized Curves

Table 5.5 Ratio of Mean Ductility for Tested Walls and Control Walls

Wall Set	Ratio of Mean Ductilities (Exp./control in pull)	Ratio of Mean Ductilities (Exp./control in push)
1	0.80	1.10
2	0.80	0.70
3	1.10	0.80
4	0.70	0.70
5	0.70	0.80
6	1.00	1.20
7	0.80	0.80

5.5 Stiffness Degradation of the Walls

Structural stiffness is an important parameter due to its influence on final results. Stiffness drops as the inelastic deformation in structures increases. Lateral strength reduces as a function of both peak displacement demand as well as the hysteretic energy demand on the systems. Stiffness degradation is an indication of the damage occurring in the walls tested under cyclic loading in the study presented in this thesis. Stiffness degradation of structural elements can be defined as the rate of reduction in stiffness after occurrence of the yield stiffness. It usually results from cracking, loss of bond or the interaction of masonry with high shear or axial stresses. The level of stiffness degradation depends on the characteristics of the structure as well as on the loading history.

Mathematically, the stiffness ratio can be expressed as the ratio of the secant modulus at any particular loading stage to the secant modulus at the yield load of the load-displacement curve (Haider & Dhanasekar, 2011):

$$C_k = \frac{K}{K_e} \qquad \text{(Eq. 5.5)}$$

'K_e' is the slope of the line passing through the origin to the yield point and 'K' is the slope of a line passing through the origin to any other point on the load-displacement curve where the stiffness degradation curve needs to be determined.

The initial stiffness for each wall is calculated from the early cycles of the load-displacement histories, i.e. from the secant stiffness calculated at the point of occurrence of the first crack, K_e (Tomazevic, 1999). The slope can also be calculated from the early cycles of the load- displacement histories for which the peak lateral force did not exceed twice the force of first cracking (Schultz, et al., 1998). In that case the lateral stiffness can be calculated from the slope of the line connecting the positive and negative peaks of the force displacement cycles. The initial stiffnesses of the walls were calculated using both methods and are listed in Table 5.6. From these values, it can be said the initial stiffnesses calculated according to Schultz et al. (1998) are not always in the range of 5-20% of that calculated by Tomazevic (1999). Cases where there is a large difference between the two, for example wall 1-A, may be due to the large difference in the stiffness for the push and pull cycles which made it difficult to select the points for calculating the stiffness according to the definition described by Schultz et al. (1998). For the same

loading arrangement, higher initial stiffness is obtained for walls with bond beams than for walls with joint reinforcement. On the other hand, changing the loading protocol from cyclic to monotonic did not seem to affect the initial stiffness significantly. The softest initial behaviour was obtained for the walls with constant vertical load where moment is introduced at the mid-point of mid-height of wall (set 7). The initial stiffness using the Tomazevic definition was adopted for further calculation and comparison of stiffness degradation as shown in Table 5.6 and discussed in the following sections.

Stiffness degradation is determined from the load displacement curve. The stiffness reduction from the first major event d_{cr} to the point of peak loading is determined as a percentage of stiffness at d_{cr} which is also tabulated in Table 5.6. The mean stiffness degradation was in the range of roughly 30-50% for all wall sets except for sets 4 and 5. The relocation of the bond beams (set 4) can be said to be most effective in preventing reduction in stiffness compared to any other walls with or without bond beam. This may be attributed to the fact that in case of set 4 there is more grouted area in the central area of the wall where the cracks initiate. The highest stiffness reduction was observed for wall sets 1 and 6. Set 5 did not show too much reduction though the base splice was missing in this case implying that absence of the splice may not affect the stiffness reduction.

Table 5.6 Comparison of Stiffness Degradation

Wall ID	Initial stiffness (kN/mm)		Stiffness reduction at d_{hmax} as percentage of stiffness at d_{cr} (%)	Avg.	d_{cr} (mm)	d_{max} (mm)
	Schultz	Tomazevic				
Wall 1-A	114.2	67.4	51.0	52.6	2.0	7.0
Wall 1-B	118.0	103.6	54.3		2.0	8.0
Wall 2-A	74.80	66.7	24.9	28.9	3.0	7.0
Wall 2-B	71.0	69.9	33.0		2.5	6.5
Wall 3-A	148.5	111.4	51.3	40.4	2.5	7.0
Wall 3-B	54.5	60.1	29.5		4.0	7.5
Wall 4-A	84.7	90.3	25.1	25.2	2.0	5.0
Wall 4-B	51.5	47.4	18.8		4.5	7.5
Wall 4-C	137.0	91.0	31.6		1.5	4.5
Wall 5-A	50.8	41.4	33.0	37.8	4.0	9.0
Wall 5-B	81.9	59.9	42.7		3.0	9.0
Wall 6-A	58.0	38.8	49.1	52.7	2.0	10.0
Wall 6-B	118.6	66.8	56.2		2.5	9.0
Wall 7-A	50.5	33.6	52.4	44.5	4.0	12.0
Wall 7-B	32.4	24.8	36.5		5.0	13.0

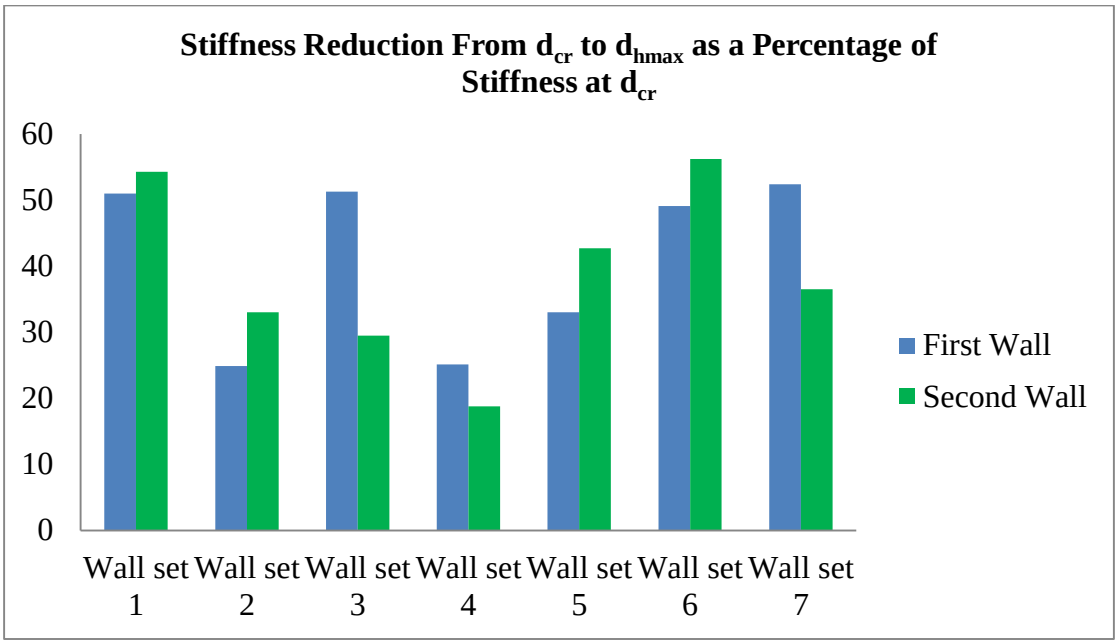

(a)

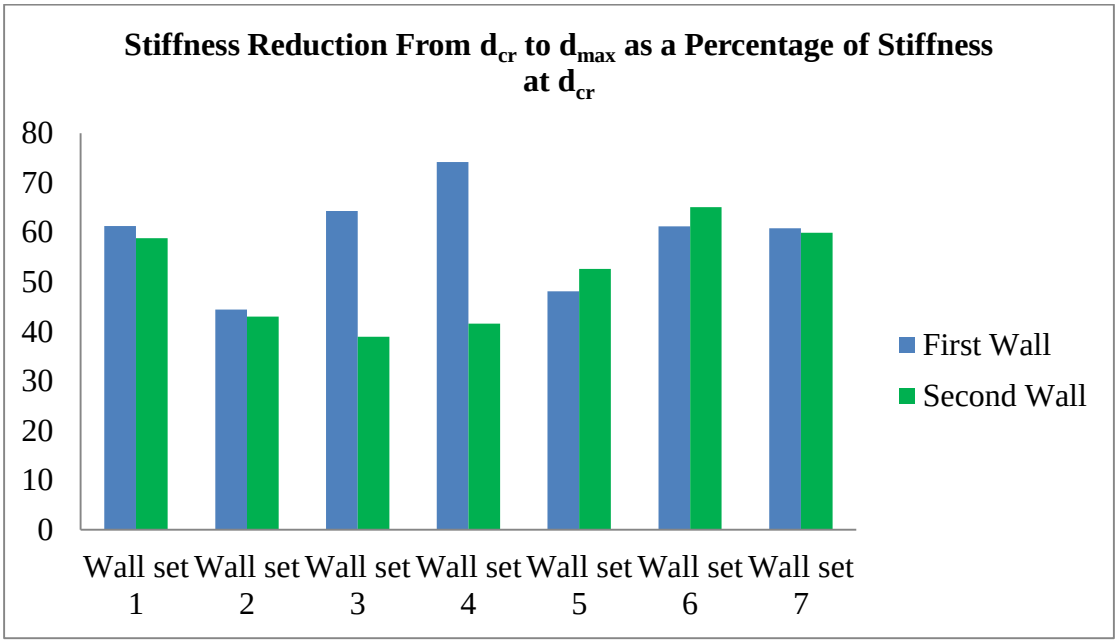

(b)

Figure 5.29 (a) Stiffness Reduction From d_{cr} to d_{hmax} (b) Stiffness Reduction From d_{cr} to d_{max} as a percentage of Stiffness at d_{cr}

Figure 5.29 shows the stiffness reduction from the point of first visible crack to the point of maximum resistance and to the point of maximum deformation. It is obvious from the graphs that stiffness reduction was generally lower for walls with bond beams than walls with joint reinforcement. Among the walls with bond beams, stiffness degradation is higher for walls with straight bars (set 1) than for any other walls. Wall sets 2 and 4 showed less reduction than any other walls to the point of maximum resistance. However, after the peak is achieved, the rate of stiffness reduction becomes quite high for those two sets. The envelope curves for the cyclically loaded walls are used for evaluating the stiffness degradation at different values of lateral displacement. Figure 5.30 and Figure 5.31 show the stiffness degradation ratio for the wall sets with different bond beam reinforcement anchorage and the log curves fitted to the original curves, respectively. In these figures the stiffness ratio (stiffness normalized with respect to elastic stiffness K_e) is plotted versus the normalized displacement (with respect to the displacement at which the peak load occurs). The secant stiffness was calculated at the same intervals of displacement which were used while testing: intervals of 0.25 mm for displacement up to 1 mm, intervals of 0.5 mm up to displacement of 10 mm, and intervals of 1 mm for displacement exceeding 10 mm. The shape of the stiffness degradation function i.e. the relationship between the stiffness ratio and the normalized lateral displacement of the walls, is similar in all cases. The following equation was proposed by Tomazevic et al. (Tomazevic, et al., 1996) to correlate the stiffness and deformation of shear walls under cyclic loading:

$$K = \alpha K_e \left(\frac{d}{d_{max}}\right)^{\beta} \qquad \text{(Eq. 5.6)}$$

The stiffness parameters, α and β, depend on the lateral load history and the compression stresses due to vertical loading acting on the wall (Tomazevic, 1999). These values should be determined using experimental data if available. Table 5.7 shows the experimental values of these parameters for the walls tested which were determined using log-fitted regression in MS Excel on the stiffness degradation curves for each wall.

Table 5.7 Values of α and β for Stiffness Degradation

Wall designation	Alpha(α)	Beta (β)
Wall 1-A	1.1	-0.5
Wall 1-B	1.0	-0.5
Wall 2-A	1.3	-0.5
Wall 2-B	1.1	-0.6
Wall 3-A	1.2	-0.7
Wall 3-B	1.2	-0.5
Wall 4-A	1.4	-0.6
Wall 4-B	1.4	-0.6
Wall 5-A	1.2	-0.4
Wall 5-B	1.0	-0.5
Wall 6-A	1.3	-0.5
Wall 6-B	0.9	-0.7
Wall 7-A	0.9	-0.6
Wall 7-B	1.3	-0.6
Wall 8-A	1.3	-0.4
Wall 8-B	1.1	-0.6

Tomazevic (Tomazevic, 1999) recommends values of α and β to be 0.3 and -0.85 in the absence of experimental data for normal compression stresses not exceeding 20% of the masonry compressive strength and cyclic lateral loads. However, from the experimental data, much higher α values and lower β values are obtained for the same conditions as assumed by Tomazevic. This may be due to the fact that the boundary conditions such as

load application, actuator position, splicing at the top and bottom of wall in this testing were actually different from Tomazevic's work. The average values of α and β are 1.12 and -0.54, respectively, for wall sets 1-6, while for the walls with constant vertical load (set 7), the average α and β values were 1.1 and -0.61. Therefore, if experimental data are not available, for wall types similar to those tested in this project and if the initial stiffness of the wall can be inferred then the values found here could be used to derive the stiffness degradation curve for any wall.

From observation of Figure 5.30 a common trend was noted that the stiffness decreases gradually from the start of loading until the end of the test except for wall 3-A which had a rise in stiffness just after loading began and then a significant drop. It can also be said that set 3 showed the highest resistance to stiffness degradation, whereas set 1 experienced the highest amount of degradation among all the sets. When compared with the control set, sets 2 and 3 experience less stiffness degradation, but the degradation of set 1 is almost the same.

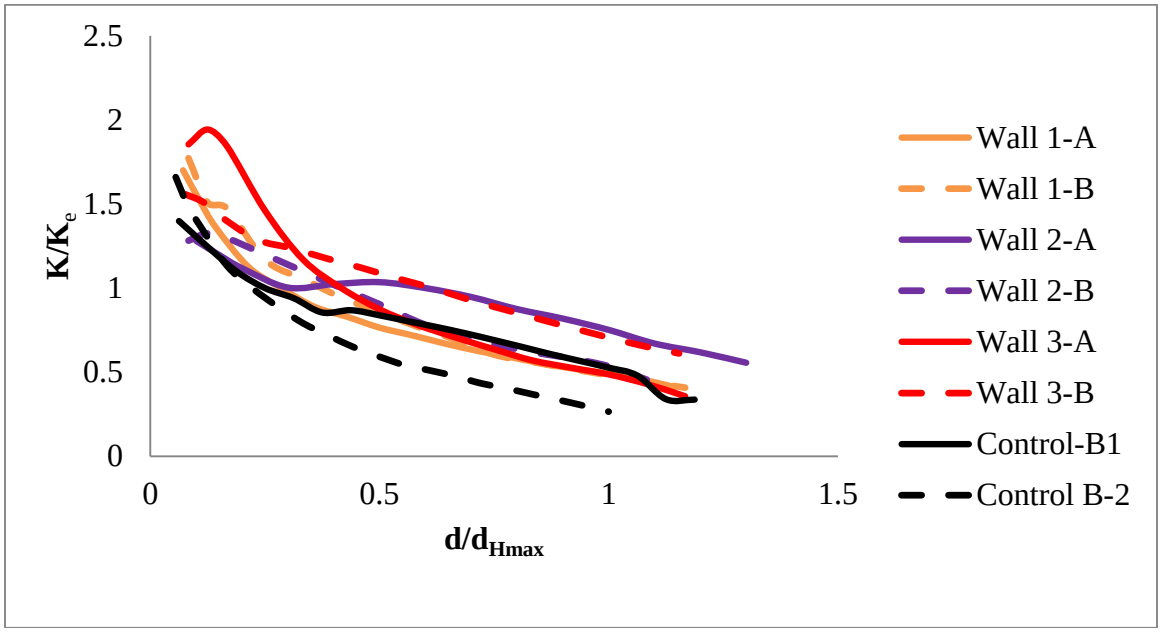

Figure 5.30 Stiffness Degradation versus Normalized Lateral Displacement of Walls with Bond Beams and Different Reinforcement Anchorage Conditions

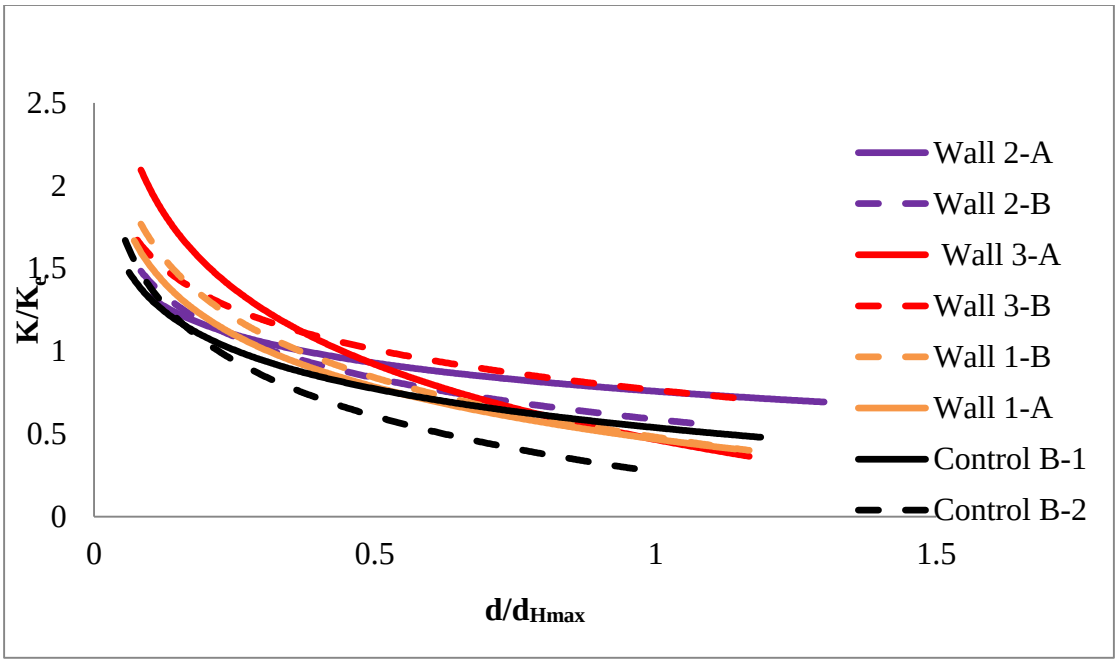

Figure 5.31 Log Curves Fit to Stiffness Degradation Curves of Figure 5.30

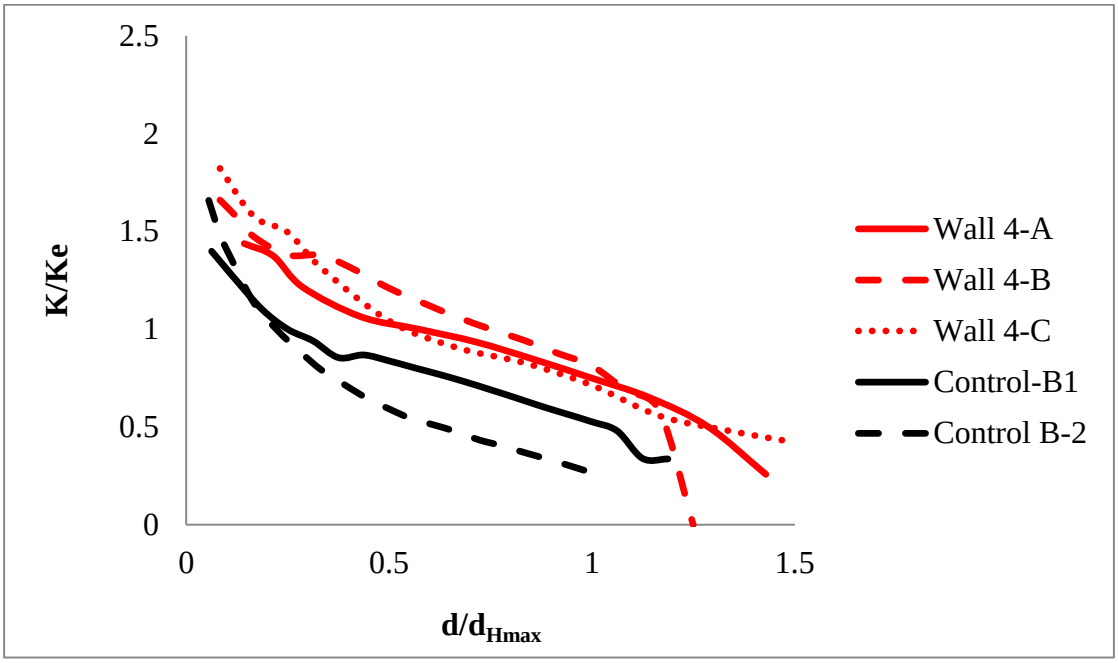

Figure 5.32 Stiffness Degradation versus Normalized Lateral Displacement of Walls with Relocated Bond Beams

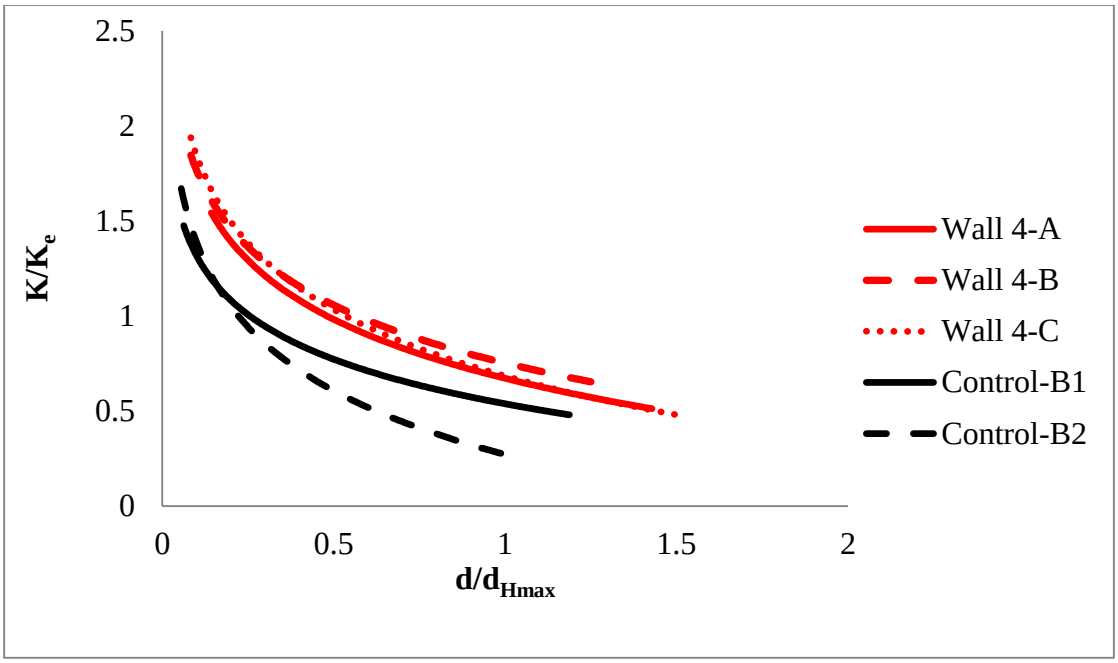

Figure 5.33 Log Curves Fit to Stiffness Degradation Curves of Figure 5.32

From Figure 5.32 and Figure 5.33 it is obvious that relocating the bond beams reduces the stiffness degradation of the walls from the beginning to the end of testing. The stiffness reduction was low from the beginning until the peak resistance.

The walls with different boundary conditions also exhibited stiffness degradation under the reversible cyclic loading as shown in Figure 5.34. The initial stiffnesses of the tested walls were higher than the control walls however, two of the tested walls (from two different sets) reach the same level of stiffness as the control walls whereas the others did not degrade as much as the control walls. From this observation it can be concluded that stiffness reduction is independent of the boundary conditions. Figure 5.35 shows the log curves fitted to the actual stiffness degradation curves and were used to determine the α and β values in Table 5.7.

Figure 5.36 and Figure 5.37 show the original stiffness degradation curves and the log fitted stiffness degradation curves for wall set 7. It is observed from Figure 5.36 that although both the control set and wall 7-B start at nearly the same initial stiffness, wall 7-B suffers less degradation than the control walls. On the other hand, wall 7-A has higher degradation than the control set, therefore, no definite conclusion about the effect of vertical load on the stiffness degradation can be drawn from the graphs.

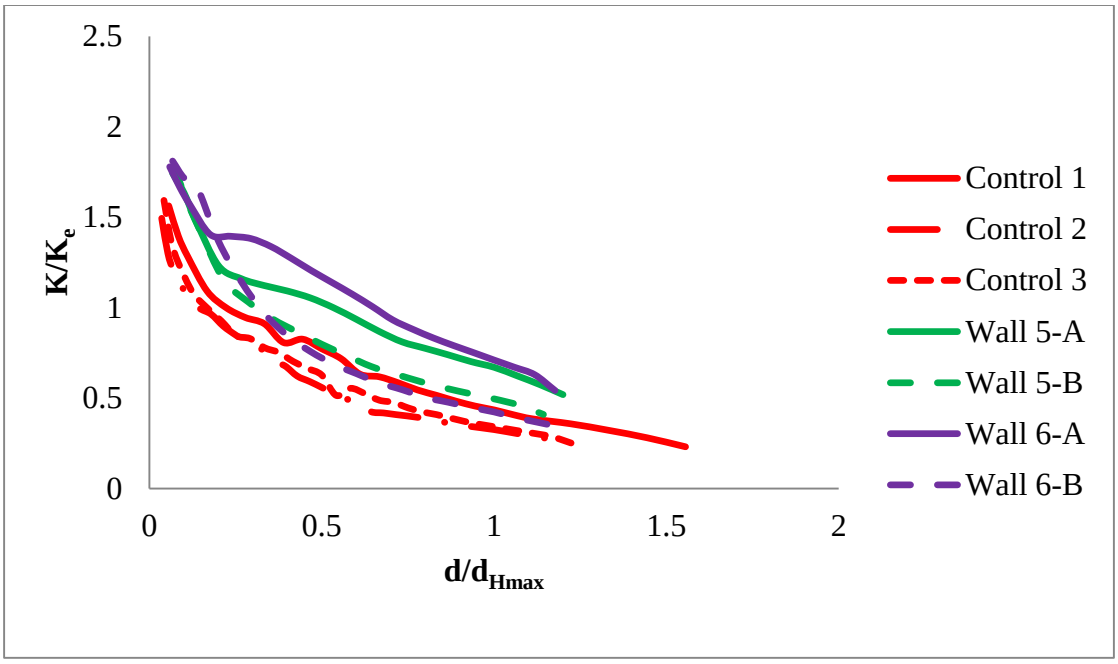

Figure 5.34 Stiffness Degradation versus Normalized Lateral Displacement of Walls Having Different Boundary Conditions

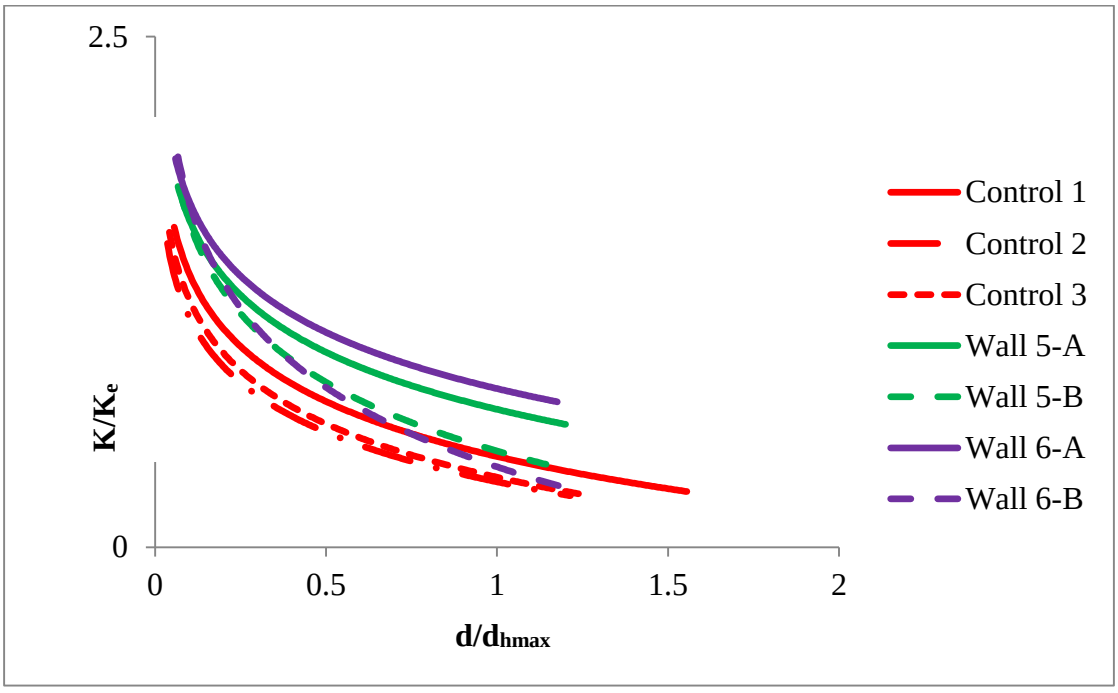

Figure 5.35 Log Curves Fit to Stiffness Degradation Curves of Figure 5.34

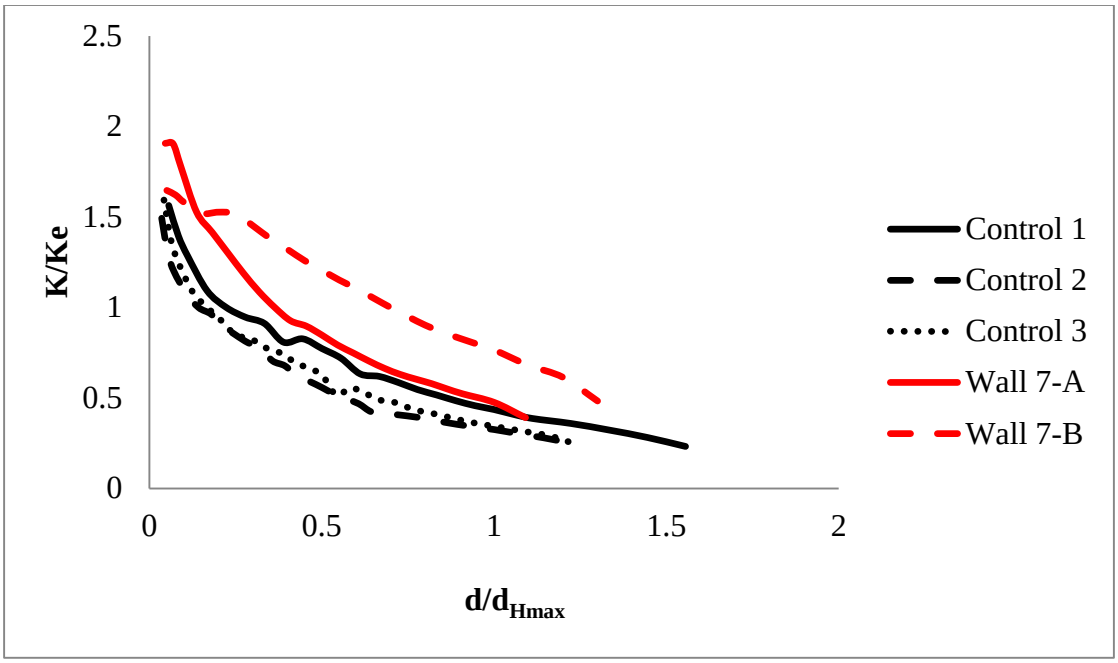

Figure 5.36 Stiffness Degradation versus Normalized Lateral Displacement for Walls Tested Under Constant Vertical Loading

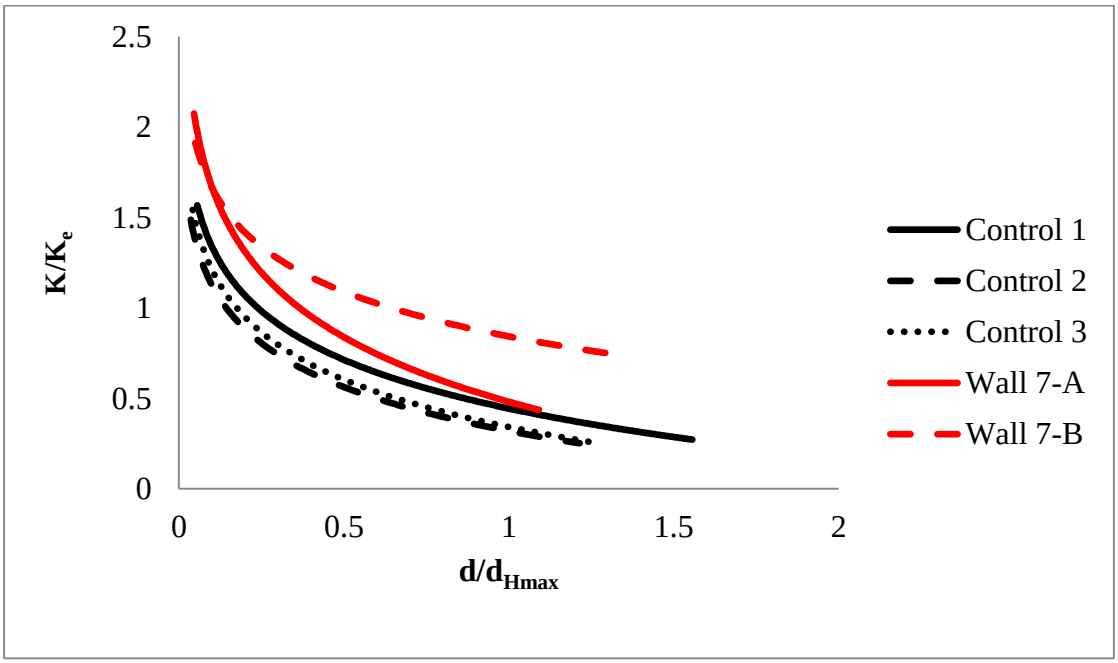

Figure 5.37 Log Curves Fit to Stiffness Degradation Curves of Figure 5.36

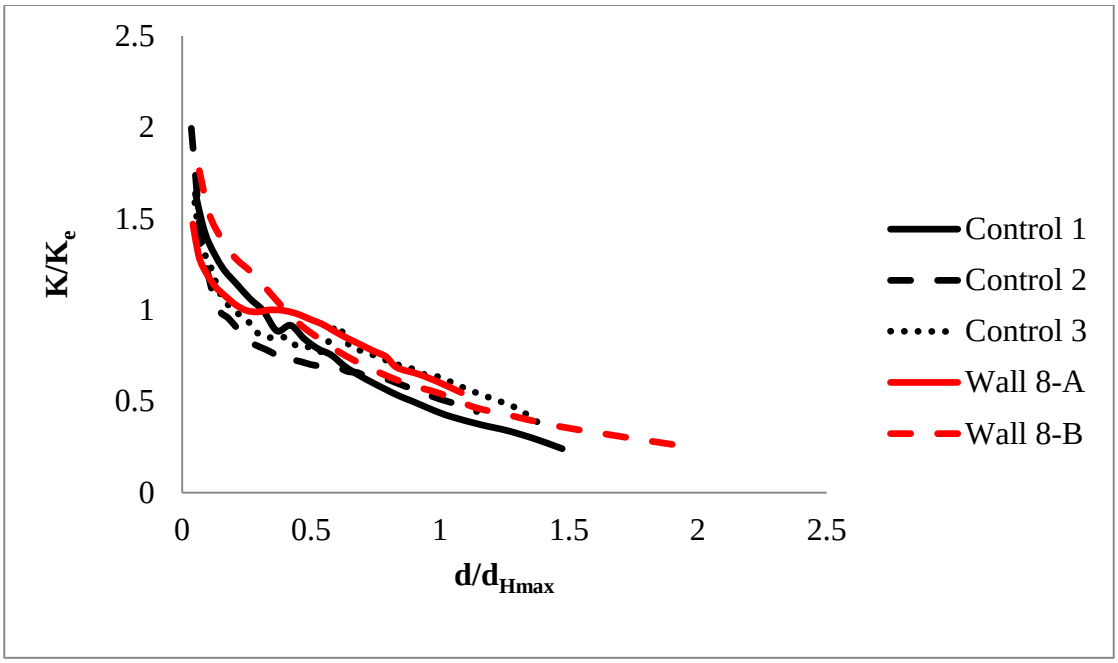

Figure 5.38 Stiffness Degradation versus Normalized Lateral Displacement for Walls Tested Under Monotonic Loading

Figure 5.38 and Figure 5.39 show the actual and log fit curves for stiffness degradation of wall set 8. Both walls had lower initial stiffness than the control set but the degradation was not as high as for the control walls.

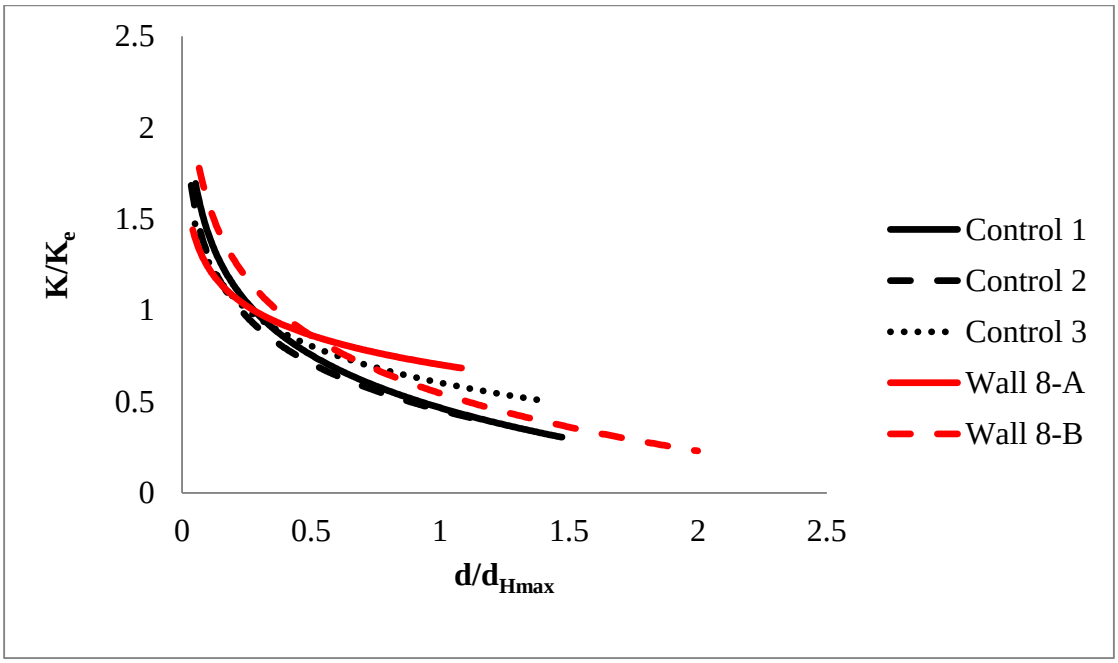

Figure 5.39 Log Curves Fit to Stiffness Degradation Curves of Figure 5.38

When the above stiffness degradation figures are compared with Figure 2.15, it can be said that the stiffness of walls mentioned in the literature deteriorates to half of the initial value at a displacement ratio of 0.15-0.25, whereas for the walls tested in this study, the stiffness degrades to half of the initial stiffness at a displacement ratio in the range of 0.40-0.60, except for set 2, where this ratio is higher at almost 0.8. The displacement ratio values for set 7 and set 8 are nearly in the same range as those reported in literature.

Figure 5.40 shows that the general trend in the stiffness reduction curves is similar for walls with and without bond beams. Therefore, the stiffness degradation is similar irrespective of the type of reinforcement.

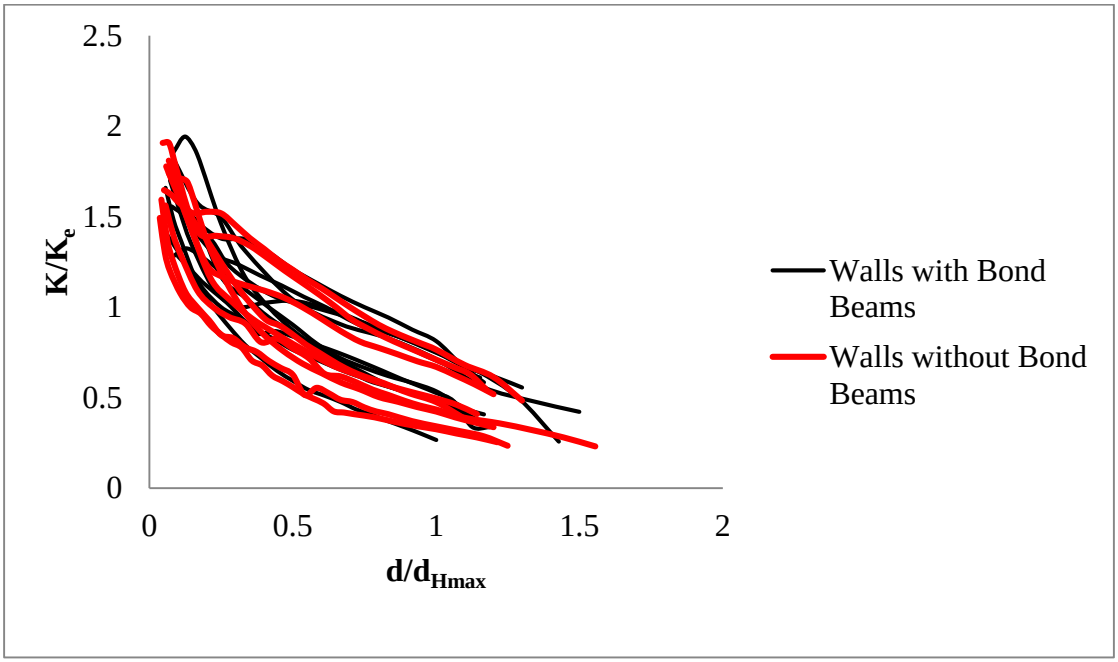

Figure 5.40 Combined Stiffness Degradation Curves for All Walls

5.6 Energy Dissipation

The hysteresis loops for the experimental walls were used to determine the energy dissipated by each wall. The dissipated energy for each cycle is obtained by calculating the area encompassed by the loops in one displacement cycle, i.e. between two consecutive peaks. A simple Matlab program was used to calculate the area under each hysteresis loop. The program is included in Appendix 3. The cumulative area for all the cycles in each test gives the total dissipated energy for each wall. The input energy is computed at the first cycle of each characteristic displacement point (i.e. d_{cr}, d_{Hmax} etc.)

and the ratio of the dissipated and input energy are shown in Table 5.8 only for these points.

Table 5.8 Ratio of Dissipated and Input Energy (Computed at First Cycle Only)

Wall ID	E_{diss}/E_{inp} (at d_{cr})	E_{diss}/E_{inp} (at d_{Hmax})	E_{diss}/E_{inp} (at d_{max})
Wall 1-A	0.4	0.5	0.5
Wall 1-B	0.5	0.4	0.5
Wall 2-A	0.3	0.5	0.7
Wall 2-B	0.4	0.6	0.7
Wall 3-A	0.4	0.5	0.5
Wall 3-B	0.4	0.4	0.9
Wall 4-A	0.4	0.6	0.6
Wall 4-B	0.3	0.4	0.6
Wall 4-C	0.6	0.8	0.7
Wall 5-A	0.4	0.4	0.4
Wall 5-B	0.3	0.4	0.5
Wall 6-A	0.4	0.4	0.4
Wall 6-B	0.5	0.4	0.5
Wall 7-A	0.3	0.4	0.8
Wall 7-B	0.3	0.4	0.7

According to Table 5.8 the dissipated energy was much lower than input energy and in most cases it was less than 50% of the input energy except in some cases of the last loading cycle. The walls with bond beams had more energy absorption capacity than the other walls, whereas changing the vertical loading in set 7 seemed to decrease the energy dissipation capacity.

Table 5.9 presents the cyclic energy dissipated at different states of damage, such as d_{cr}, d_{Hmax}, d_{max}, as the percentage of total energy dissipated by the wall. Comparing the

average values, it can be said that for the same damage level, walls in set 4 consistently dissipated more energy than any other set. Although the average energy dissipation for sets 2 and 3 was greater than set 4 at d_{Hmax} and d_{max}, the standard deviation was also much higher for sets 2 and 3 than for set 4.

On average, the percentage of energy dissipated at d_{cr}, d_{Hmax}, and d_{max} was around 2, 6 and 11% of total energy dissipated.

Table 5.9 Energy Dissipation as a Percentage of Total Dissipated Energy at Different Damage States

Wall ID	% of Energy dissipated at the cycle of d_{cr}	Avg.	% of Energy dissipated at the cycle of d_{Hmax}	Avg.	% of Energy dissipated at the cycle of d_{max}	Avg.
Wall1-A	1.1	1.5	5.8	6.4	7.4	7.8
Wall 1-B	1.9		7.0		8.3	
Wall2-A	2.8	2.4	6.1	8.0	10.	10.4
Wall 2-B	2.0		9.9		10.8	
Wall3-A	2.3	2.4	6.7	6.3	7.7	17.1
Wall 3-B	2.6		6.0		26.4	
Wall4-A	2.9	2.8	6.9	6.8	15.8	12.9
Wall 4-B	3.3		6.3		10.0	
Wall 4-C	2.2		7.2		12.9	
Wall5-A	2.0	2.0	0.4	5.2	7.2	7.8
Wall 5-B	2.0		0.4		8.4	
Wall6-A	0.5	0.9	4.9	4.9	6.7	6.8
Wall 6-B	1.4		4.9		7.0	
Wall7-A	1.2	1.2	5.9	4.8	14.4	11.4
Wall 7-B	1.3		3.8		8.4	

Further analysis was performed to calculate the in-cycle degradation of energy dissipation for a given level of displacement. The same damage states are selected for comparison as in the preceding paragraph and the energy absorbed in the second cycle of each displacement level is compared to that in the first cycle. The results are shown in Table 5.10. It can be seen from the table that there is less in-cycle degradation in energy dissipation at higher displacements irrespective of the change in parameter with very few exceptions. In some cases, at higher loading cycles, the in-cycle energy dissipation increases in the second cycle of loading rather than decreasing.

Table 5.10 In-Cycle Reduction in Energy Absorption

Wall Id	**Change in Energy Dissipation in second cycle from the first cycle of d_{cr}**	**Change in Energy Dissipation in second from the first cycle of d_{Hmax}**	**Change in Energy Dissipation in second cycle from the first cycle of d_{max}**
Wall 1-A	20.4	5.4	1.5
Wall 1-B	12.5	0.9	4.5
Wall 2-A	23.8	1.0	40.5
Wall 2-B	12.3	0.2	-[*1]
Wall 3-A	15.6	4.2	-0.7[*2]
Wall 3-B	7.4	6.7	2.9
Wall 4-A	17.9	11.4	8.7
Wall 4-B	1.2	-0.5	-28.5
Wall 4-C	26.9	11.7	-4.1
Wall 5-A	7.1	3.2	-11.2
Wall 5-B	17.4	4.3	0.7
Wall 6-A	22.2	4.5	-3.9
Wall 6-B	18.5	2.3	4.5
Wall 7-A	5.4	-18.7	-
Wall 7-B	7.8	0.6	-7.9

[*1] : The cycle of d_{Hmax} was the last cycle

[*2] Negative means increase instead of reduction.

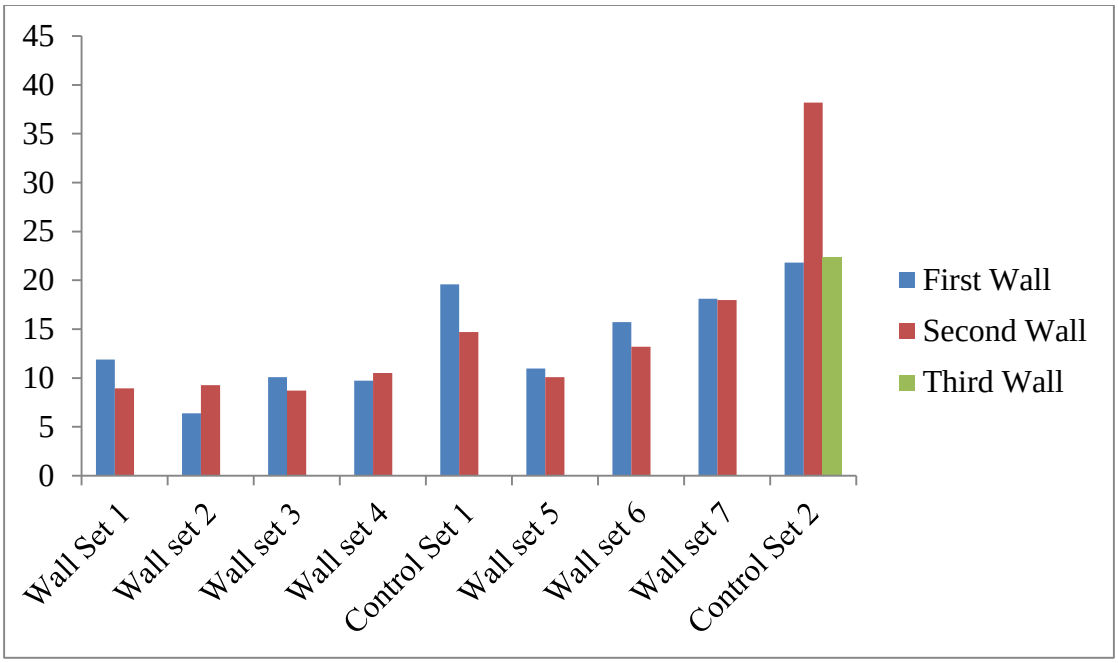

Figure 5.41 Total Energy Dissipated (kN-m) for All Tested Walls

The total energy dissipated for all the tested walls and the control walls are presented in Figure 5.41. From the figure it can be said that walls with bond beams dissipate less energy than walls with joint reinforcement. Again all the tested walls showed less energy dissipation capacity than the control set. It indicates that the change in the parameter from the control walls is not beneficial to the energy dissipation capacity.

When the normalized energy dissipation capacity (normalized with respect to the total energy dissipated) was analyzed as shown in Figure 5.42 and Figure 5.43, it can be inferred that energy dissipation capacity was higher for walls with anchored bond beam reinforcement (set 2 and set 4) than the other walls with bond reinforcement. On the other hand, for the walls without bond beams, dissipation capacity is lower for wall set 7 than the other walls. When the combined normalized curves are analyzed as shown in Figure 5.44 it shows that the dissipation capacity of walls with bond beams is higher than walls without bond beams. Since the deformation capacity of the walls without bond beams was generally higher, the total dissipated energy was also higher for those walls.

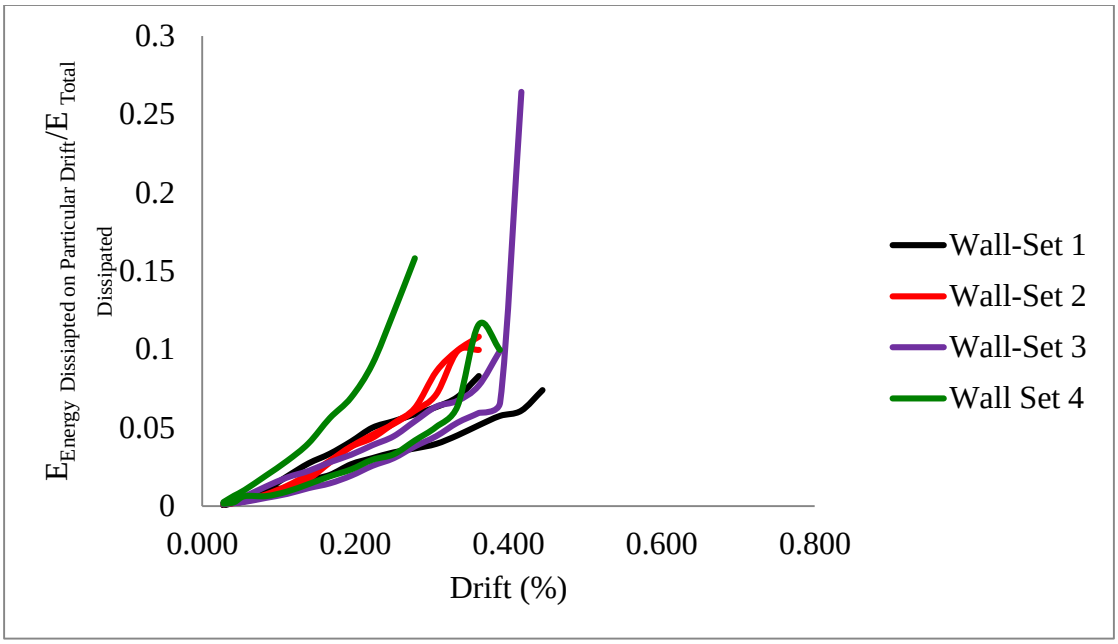

Figure 5.42 Normalized Energy Dissipation vs. Drift for Walls with Bond Beams

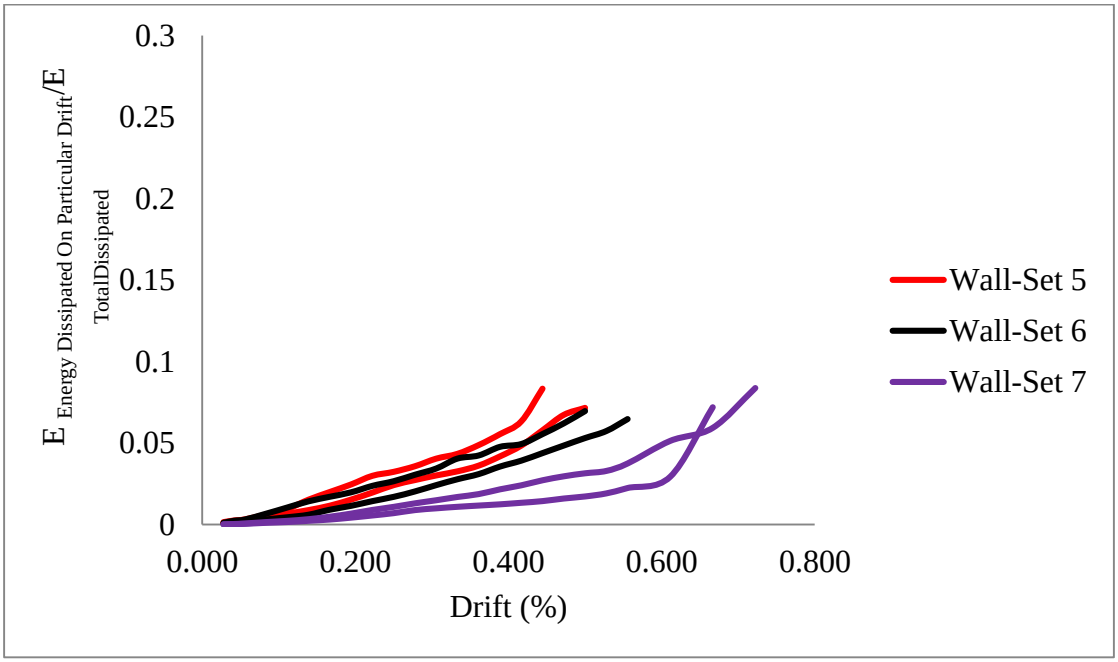

Figure 5.43 Normalized Energy Dissipation vs. Drift for Walls without Bond Beams

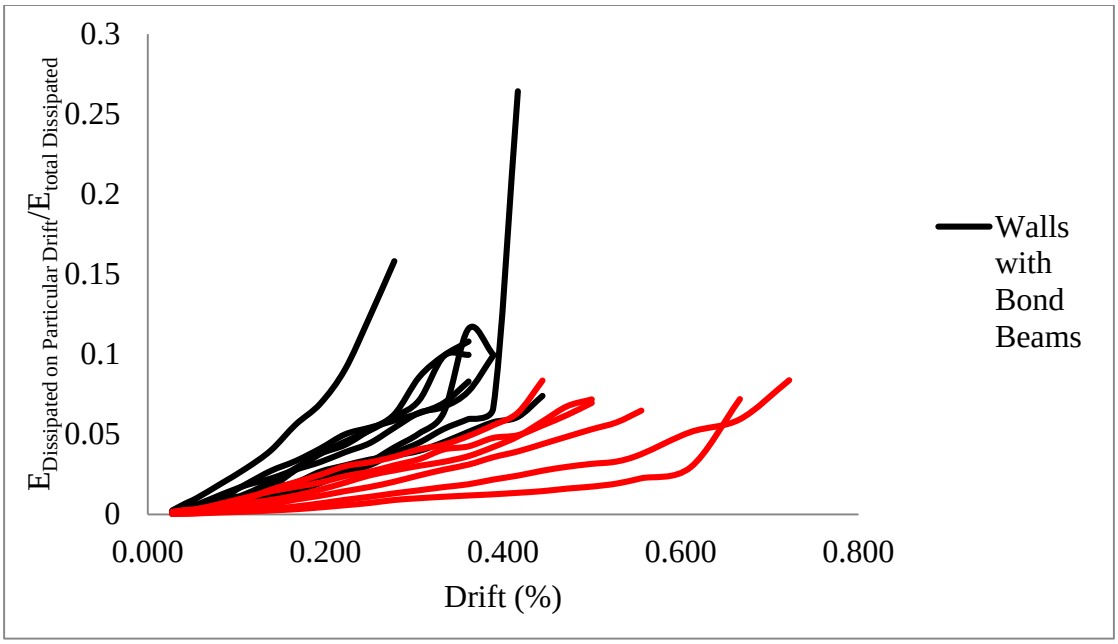

Figure 5.44 Normalized Energy Dissipation vs. Drift for All Walls

5.7 Strength

Comparison of the strengths for the walls with bond beams and control set 1 are summarized below in Table 5.11 and Table 5.12, including the mean of the results for the pull and push cycles.

Table 5.11 Shear Strength of Walls with Bond Beams & Different Anchorage (Pull Cycle)

Wall ID	End anchorage condition	Shear Strength (kN)	Mean (kN)	% change in Strength
Control Set 1	90 degree hooks	216.5	235.8	-
		255.0		
Set 1	No end anchorage	229.4	228.3	-3.2*[1]
		227.1		
Set 2	180 degree hooks	250.7	237.7	+0.8
		224.7		
Set 3	Headed studs	225.6	238.5	+1.1
		251.4		

*[1] Negative sign means reduction and vice-versa.

Table 5.12 Shear Strength of Walls with Bond Beams & Different Anchorage (Push Cycle)

Wall ID	End anchorage condition	Shear Strength (kN)	Mean (kN)	% change in Strength
Control Set 1	90° hooks in bond beam	292.2	262.9	-
		233.7		
Set 1	No End Anchorage	205.2	215.4	-18.1*[1]
		225.5		
Set 2	180° hooks	254.1	242.9	-7.6
		231.7		
Set 3	Headed Stud	233.5	239.9	-8.8
		246.3		

*[1] Negative sign means reduction and vice-versa.

Only the change in the resistance in the push direction for set 1 was significant relative to the variation in the masonry materials themselves. When the results are compared with the control walls it can be seen that the change in strength resistance in the pull direction is very trivial and the resistance decreases for wall set 1 whereas the resistance increases a little for sets 2 and 3. There is, however, a significant decrease in strength in the push cycle for set 1 compared to the strength of the control wall.

Comparison of control set 1 and set 4 allows evaluation of whether location of the bond beams affects the strength or not. The analysis shown in Table 5.13 and Table 5.14 revealed that relocating the bond beams had no appreciable effect in the pull cycle, however there is a decrease in the strength in the push cycle. From the tabulated results it can be said that the change in position of the bond beams had no positive effect on the strength.

Table 5.13 Shear Strength of Walls with Relocated Bond Beams (Pull Cycle)

Wall ID	Bond Beam Location	Shear Strength (kN)	Mean (kN)	% change in Strength
Control Set 1	5th and 9th course from bottom	216.5	235.8	-
		255.0		
Set 4	3rd and 6th course from bottom	230.8	233.8	-0.1
		236.8		

Table 5.14 Shear Strength of Walls with Relocated Bond Beams (Push Cycle)

Wall ID	Bond Beam Location	Shear Strength (kN)	Mean (kN)	% change in Strength
Control Set 1	5th and 9th course from bottom	292.2	262.9	-
		233.7		
Set 4	3rd and 6th course from bottom	250.5	222.8	-15.3
		195.0		

Results from wall set 5 (walls without bottom welded reinforcement) and 6 (walls that have welded rebar fixed at top) are compared to control set 2 as shown in Table 5.15 and Table 5.16.

Table 5.15 Strength Comparisons for Wall Sets 5 and 6 (Pull Cycle)

Wall ID	Boundary Condition	Shear Strength (kN)	Mean (kN)	% change in Strength
Control Set 2	Splice at bottom	219.2	224.9	-
		232.4		
		223.0		
Set 5	No splice at bottom	208.2	207.9	-7.6
		207.7		
Set 6	Splice at top and bottom	233.6	223.5	+0.6
		213.3		

Table 5.16 Strength Comparisons for Wall Sets 5 and 6 (Push Cycle)

Wall ID	Boundary Condition	Shear Strength (kN)	Mean (kN)	% change in Strength
Control Set 2	Splice at bottom	204.0	221.0	-
		222.0		
		237.0		
Set 5	No splice at bottom	203.7	210.6	-4.7
		217.4		
Set 6	Splice at top and bottom	212.4	210.9	-4.6
		209.5		

Strength comparison of these walls reveals that the change in boundary condition did not have a positive effect on the strength of the walls although the differences are not very significant relative to the variation expected in masonry materials. In the push direction, the strength decrement for both sets of walls (set 5 and 6) compared to the control set is almost the same. As was shown earlier in Table 5.1, changing the boundary conditions for set 5 and set 6 did not have any adverse or beneficial effect as there was no significant difference in either the sliding, or uplift compared to the control set.

Wall sets 7 and 8 were also compared to control set 2 to see if the change in vertical load application or the application of monotonic load versus cyclic load had any effect on the ultimate strength. Table 5.17 and Table 5.18 show this comparison.

Table 5.17 Strength Comparison for Wall Sets 7 and 8 (Pull Cycle)

Wall ID	Loading protocol	Shear Strength (kN)	Mean (kN)	% change in Strength
Control Set 2	Cyclic with changing vertical load in two actuators	219.2	224.9	-
		232.4		
		223.0		
Set 7	Cyclic with constant vertical load in two actuators	175.6	182.7	-18.8
		189.8		

Table 5.18 Strength Comparison for Wall Sets 7 and 8 (Push Cycle)

Wall ID	Loading protocol	Shear Strength (kN)	Mean (kN)	% change in Strength
Control Set 2	Cyclic with changing vertical load in two actuators	204.0	221.0	-
		222.0		
		237.0		
Set 7	Cyclic with constant vertical load in two actuators	177.1	178.6	-19.2
		180.1		
Set 8	Monotonic Loading	230.8	236.5	+7.0

For set 7, there appears to be a decrease in strength both in the pull and push cycles of loading. This may be due to the fact that the vertical load was maintained at a constant 204.5 kN, whereas when the vertical load varies to maintain zero moment at the wall centre, vertical load in a given actuator sometimes reached values of nearly 400 kN. It is well accepted that higher vertical load leads to higher lateral resistance. The strength of walls under monotonic loading was about 7% higher than the control walls. Tomazevic et al. (Tomazevic, et al., 1996) also showed that if other conditions remain the same, monotonic loading increases the lateral resistance. When the other test results such as sliding and uplift, were compared against the control walls, no significant difference was found in any of the walls at the early stages of loading. The peak load capacities of all walls are shown in the form of bar charts in Figure 5.45. The figure shows generally higher capacity of walls with bond beams by around 5-10% than walls without bond beams. Although the amount of horizontal reinforcement was much higher in the walls with bond beams, it does not appear to contribute significantly to load capacity.

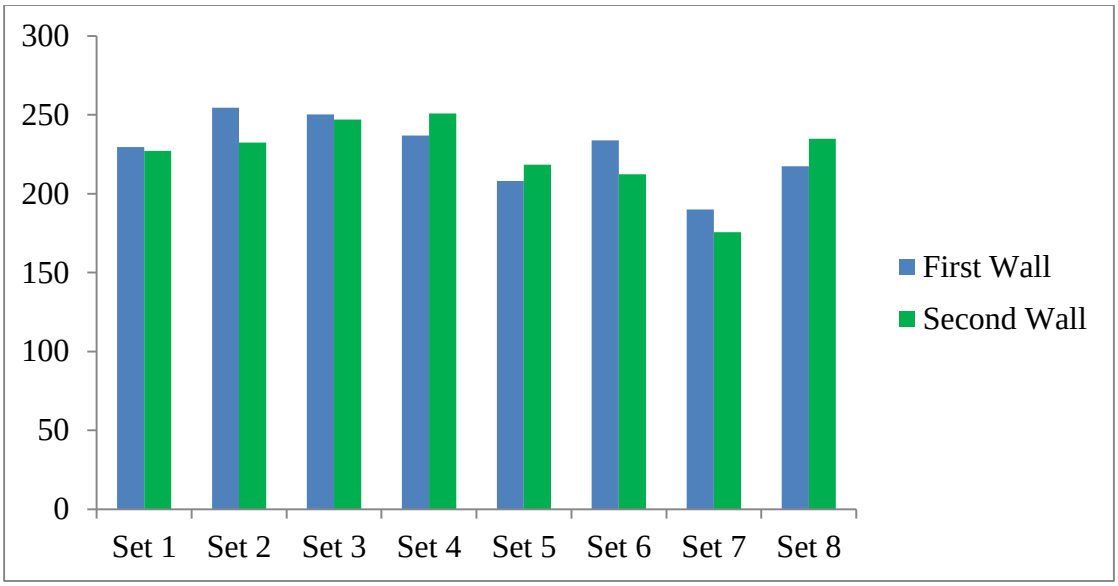

Figure 5.45 Comparison of Peak Load Resistance (kN)

5.8 Statistical Analysis

It is not known, nor can it be determined with any certainty, whether the test results are normally distributed. Hence, some statistical tests for both normally and non-normally distributed data were applied to the test results to determine whether the effects on wall behaviour discussed above due to changes in certain parameters are statistically significant or not. The well-known one-way ANOVA test was applied assuming that the results are normally distributed. This test was applied to several (minimum 4) sets of data simultaneously with the null hypothesis that the sets are part of one population. The parameter that is determined in the ANOVA test is called 'F' and the tabulated F-values are determined from the F-table as shown in Appendix 3, for the appropriate degrees of freedom. Different F-values are tabulated depending on the value of alpha. Alpha represents the confidence in the results. Lower values of alpha mean there is a higher possibility that there is a significant difference. As a general rule the alpha value is taken in the range of 0.1-0.001 (corresponding to confidence levels of 90% - 99.9%) in order to have confidence in whether the difference between the sets compared can be considered to be significant. For example, if alpha is 0.1, there is a 90% chance that the data compared are statistically different from each other with a 10 % chance that the data are from the same population. If the value obtained from the F-table (in Appendix 3) is

greater than the calculated value it can be concluded that there is no statistical difference between the sets being compared (the null hypothesis is correct). Two levels of confidence (5% and 10%) were used in applying the ANOVA test. In application of the ANOVA test, the test results from sets 1 to 4 and control set 1 were combined for the analysis of walls with bond beams, while for walls without bond beams, it is sets 5 to 8 and control set 2 that were combined. The results of the ANOVA test for various aspects of the wall behaviour are summarized in Table 5.19. From this table it is obvious that the change in bond beam reinforcement anchorage had no effect on the strength but changes are significant to a certain degree for the walls without bond beams. Significant change is also apparent for all walls when energy is considered. No significant effect is observed for ductility and stiffness of walls except for the ductility of walls without bond beams in the pull cycle.

Table 5.19 Results of ANOVA Test

Aspect of Behaviour Compared	F value (Calculated)	F value (Tabulated)		Result
		α=0.1	α=0.05	
Strength of walls with bond beam in pull cycle	0.1	3.5	5.2	Not significant
Strength of walls with bond beam in push cycle	0.9	3.5	5.2	Not significant
Strength of walls without bond beam in pull cycle	9.4	4.2	6.6	Significant
Strength of walls without bond beam in push cycle	17.8	3.5	5.2	Significant
Energy absorption of walls with bond beam	5.9	3.5	5.2	Significant for α=0.1
Energy absorption of Walls without bond beam	4.5	4.2	6.6	Significant for α=0.1
Ductility for walls with bond beam in pull cycle	0.7	3.5	5.2	Not significant
Ductility for Walls with Bond Beam in Push Cycle	0.6	3.5	5.2	Not significant
Ductility for Walls without Bond Beam in Pull Cycle	1.0	4.2	6.6	Significant up-to α=0.05
Ductility for Walls without Bond Beam in Push Cycle	0.2	4.2	6.6	Not significant
Stiffness for Walls with Bond Beam	0.3	3.5	5.2	Not significant
Stiffness for Walls without Bond Beam	0.5	4.2	6.6	Not significant

The Kruskal-Wallis test method is similar to the ANOVA test, but is applicable for non-normally distributed data. The same set combinations used for the ANOVA test were used in the application of the non-parametric Kruskal-Wallis test. The results of the Kruskal- Wallis test are provided in Table 5.20. The value of α has the same meaning as described for the ANOVA test and comparison of the H values for this test is similar to the comparison of F values in the ANOVA test to determine significance. The application of the Kruskal-Wallis method shows that no change in parameter gives a significant difference in the strength, ductility, stiffness, or energy absorption of the walls compared to the control sets with one exception being the energy absorption of walls without bond beams.

Table 5.20 Results of Kruskal - Wallis Test

Aspect of Behaviour Compared	H value (Calculated)	H value (Tabulated)		Result
		α=0.05	α=0.01	
Strength of walls with bond beam in pull cycle	0.55	9.5	13.3	Not significant
Strength of walls with bond beam in push cycle	4.9	9.5	13.3	Not significant
Strength of walls without bond beam in pull cycle	6.0	7.8	11.4	Not Significant
Strength of walls without bond beam in push cycle	8.1	9.5	13.3	Not Significant
Energy absorption of walls with bond beam	6.0	9.5	13.3	Not Significant
Energy absorption of walls without bond beam	9.7	7.8	11.4	Significant
Ductility of walls with bond beam in pull cycle	4.3	9.5	13.3	Not Significant
Ductility of walls with bond beam in push cycle	3.4	9.5	13.3	Not Significant
Ductility of walls without bond beam in pull cycle	5.4	7.8	11.4	Not Significant
Ductility of walls without bond beam in push cycle	1.2	7.8	11.4	Not Significant
Stiffness of walls with bond beam	1.1	9.5	13.3	Not Significant
Stiffness of walls without bond beam	1.5	9.5	13.3	Not Significant

The results of the ANOVA and Kruskal-Wallis tests do not give the same results. The ANOVA test indicates significance in a few cases whereas the Kruskal-Wallis test indicates significance only in one case. If the ANOVA or Kruskal-Wallis tests indicated significance, the t-test was performed to compare individual sets of data from within the combined sets. Once again, comparison of the calculated to tabulated t-values indicates significance with similar confidence values (alpha values) applied. The results of the t-test are shown in Table 5.21.

.

Table 5.21 Results of t-Test

Compared Wall Sets	t-Value	Alpha Value
Control Set 2 and Set-5 for Strength in pull cycle	4.30	0.03
Control Set 2 and Set-6 for Strength in pull cycle	0.10	Value Not Tabulated
Control Set 2 and Set-5 for Strength in push cycle	1.30	0.30
Control Set 2 and Set-6 for Strength in push cycle	2.4	0.09
Control Set 2 and Set-7 for Strength in pull cycle	5.2	0.02
Control Set 2 and Set-7 for Strength in push cycle	10.1	0.002
Control Set 2 and Set-8 for Strength in push cycle	2.2	0.10
Control Set 1 and Set-1 for Energy	2.4	0.20
Control Set 1 and Set-2 for Energy	3.3	0.09
Control Set 1 and Set-3 for Energy	3.1	0.09
Control Set 1 and Set-4 for Energy	2.8	0.10
Control Set 2 and Set-5 for Energy	3.1	0.09
Control Set 2 and Set-6 for Energy	2.4	0.10
Control Set 2 and Set-7 for Energy	1.7	0.20
Control Set 2 and Set-5 for Ductility in pull cycle	15.1	0.007
Control Set 2 and Set-6 for Ductility in pull cycle	0.30	Value Not Tabulated
Control Set 2 and Set-7 for Ductility in pull cycle	3.3	0.09

5.8.1 Summary of Statistical Results

The change in the bond beam reinforcement anchorage (sets 1 through 3 compared to control set 1) does not affect the ultimate strength significantly according to the ANOVA and Kruskal-Wallis tests. This may be due to the fact that the horizontal reinforcement does not come into action till the walls crack and the bar anchorage can only have an effect if the bar reaches its yield strength. There is also little or no significant difference in the strength indicated by any of the tests due to the presence of a splice at the top or absence of a splice at the bottom. This may be due to the fact that the load applied at the top is transferred from the top loading beam to the entire length of the wall and the failure pattern is entirely diagonal shear. This could also be why most researchers found that

vertical reinforcement does not have any significant contribution to shear strength and consequently the splice also had no effect. Comparison of some of the wall sets did show significance according to the t-test, in particular, in the case of strength for constant vertical load (wall set 7). The t-test also showed that the reduction in energy for sets 2, 3, 4, 5, and 6 can be considered statistically significant compared to the appropriate control set. Similarly, there is a significant difference in the ductility for wall sets 5 and 7 compared to the control set according to the t-test.

5.9 Tensile Strength While Cracking

The initiation of diagonal shear cracks requires the presence of tensile forces as known from the concept of cohesive strength. However, the tensile stress that starts the first crack in masonry is an issue that needs more study. In this section, the force or stress causing first cracking, as reported by various researchers, and according to the test results of this study, are examined and an attempt is made to determine the tensile stresses of masonry using the concept of cylindrical and spheroidal cracks in masonry. This required the computation of the principal stresses applying the procedure described in Chapter 2. The cracking tensile strength is actually dependent on the vertical stress as well. Since the actual vertical stress distribution cannot be found accurately for all the walls without the use of FEM, here the vertical stress is considered as uniformly distributed for simplicity.

5.9.1 Analysis of Database Results

For the purposes of this analysis, some of the data discussed in Chapter 3 (where first cracking loads or stresses were reported) were grouped into partially grouted (Schultz (Schultz, 1996) and Yancey (Yancey & Scribner, 1989)) and fully grouted walls (Sveinsson, et al., 1985). All the data that were used in the analysis were tested under fixed-fixed support conditions. The tensile strengths computed are plotted in Figure 5.46. As shown in the figure and in Appendix 3, in all cases the spheroidal equation gives a lower estimation of tensile stress at cracking than the cylindrical assumption, irrespective of the type of grouting and for the partially grouted walls the calculated cracking stresses were much lower than for the fully grouted walls. The data were also analyzed to identify

a relationship between compressive strength of masonry and the tensile strength at first crack as shown in Table 5.22.

Fully grouted walls showed greater coefficient of variation than partially grouted walls. Although a spheroidal assumption of the initiating flaw gives lower values than for a cylindrical flaw type, it also gives slightly higher coefficient of variation. Although the COVs are quite high, this could be due to the high COV of the masonry compressive strength itself. The walls that are tested under high vertical stresses give high cracking stress which in turn gives high principal stress and as a result, high fracture tensile stress. For this reason some high peaks can be observed in Figure 5.46.

It is does not appear that any particular ratio of masonry compressive strength to tensile cracking strength can be identified for masonry unlike the value obtained for concrete which varies between 5 and 10. However, it may be that with further research, a range could be proposed for masonry as well.

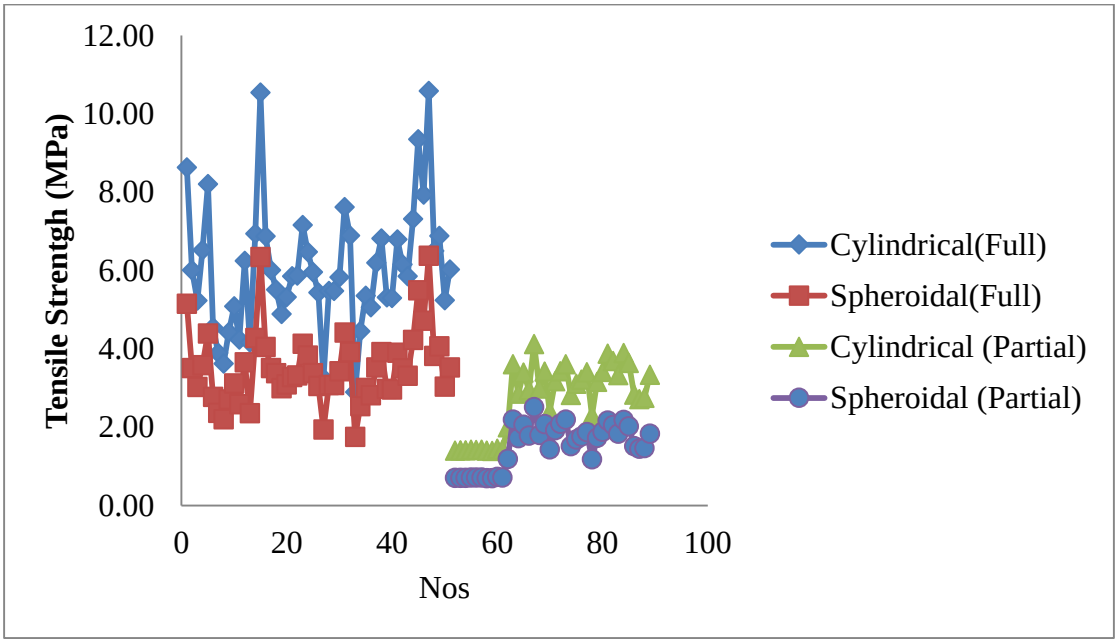

Figure 5.46 Plot of Tensile Stress for Different Types of Flaw and for Different Grout Conditions

Table 5.22 Compressive Strength to Tensile Strength Ratio for Full and Partial Grouting

Grouting type	Flaw type	Ratio of Masonry Compressive strength to tensile	Standard Deviation	COV	COV of Masonry Compressive Strength (%)
Partial	Cylindrical	5.6	1.0	18.5	28.9
	Spheroidal	10.2	2.1	20.3	
Full	Cylindrical	3.6	1.3	36.9	20.9
	Spheroidal	6.2	2.2	35.3	

5.9.2 Analysis of Test Results

For analysis of the results presented in this chapter, the first cracking force was considered as the maximum load in the cycle where the first diagonal crack was observed. Based on that assumption an attempt was made to find out the tensile strength that initiated the first diagonal cracks in each wall using the concept of cohesive strength. The shear stress at the time of cracking was determined by dividing the load (the maximum load of the cycle in which first diagonal crack was seen) by the net effective area of the masonry (considering 3 grouted cores and the rest as hollow blocks). The principal stresses were then computed by applying Mohr's stress formula. The tensile stress for cracking was then determined assuming either cylindrical or spheroidal voids. Table 5.22 shows the computed values.

The tensile strength of the masonry used in this study was not determined, however, some results for masonry tensile strength are reported in the literature. Hamid and Drysdale (1988) reported that the tensile strength for 190 mm hollow blocks with nominal compressive strength of 17 MPa was 1.7 MPa. The tensile strength of normal strength grout was reported to be 2.05 MPa. They found the tested tensile strength of prisms without grout to be 0.25 MPa and those with grout to be 1.57 MPa. According to Table 5.22 the tensile strength using the cylindrical assumption is much higher than the prediction of tensile strength using the spheroidal void assumption which has an average tensile strength of 1.76 MPa with a standard deviation of 0.28 and a COV of 15.9%. This

value is much higher than the values reported by Hamid and Drysdale (1988) except when compared to the unit tensile strength. The reason may be due to the fact that the force used for computing the cracking stress was the *maximum* value in the displacement cycle for which the first visible crack appeared, although the cracks did not actually appear at the peak of the cycle. Keeping in mind this limitation, the assumption of a spheroidal void to calculate tension failure seems more appropriate, however further study is needed to confirm that. The COV of the non-normalized principal tensile stresses in columns 7 and 8 are 14.0 and 15.9%. In the last two columns of Table 5.22 the tensile strength was normalized using the masonry compressive strength in order to eliminate the effect of masonry compressive strength. The coefficients of variation of the data in the last two columns are 20.7 and 22.5% respectively for the cylindrical and spheroidal assumptions. The normalization of the tensile stresses with respect to the masonry compressive strength deteriorates the COV. The concept of cohesive strength may be an effective approach for determining the cracking stress, however, masonry compressive strength depends on the conditions in the compressive strength test (specimen size, capping, etc.) therefore normalizing with compressive strength may not be the best approach to estimating cracking strength. The increase in variability when using the cohesive strength concept for the stresses at a flaw could be due to several factors – alone or in combination. For example, the compressive strength is determined on a specimen that is confined between steel platens and involves not just crack initiation, but also crack propagation before failure. Thus the "strength" reflects the boundary conditions on the specimen, the amount of confinement, the material used at the specimen steel interface etc. as well as crack initiation. Another factor might be that the specimens cracked along the mortar unit interface and the strength of masonry in compression may not be a good indicator of the strength of this interface. This should be examined further.

5.10 Summary

In this chapter, the test results were presented and discussed in detail. The results were analyzed and several aspects of behaviour including the energy dissipation, ductility, strength, stiffness degradation and tensile strength were compared. Although the change in parameters such as bond beam reinforcement anchorage and boundary conditions appeared to result in differences in behaviour, statistical analysis showed that in most cases, the effect was not significant.

Table 5.23 Tensile Stress in Walls at First Cracking

Wall ID	Masonry compressive strength (MPa)	Cracking Load (kN)	Shear Stress at Cracking load (MPa)	Principal Compression (MPa)	Principal Tension (MPa)	Cracking tensile stress (MPa) (according to cylindrical formula)	Cracking tensile stress (MPa) (according to spheroidal formula)	Normalized Tensile Stress For Cylindrical Assumption	Normalized Tensile Stress For Spheroidal Assumption
1-A	12.7	133.8	0.7	2.2	-0.2	2.8	1.5	0.2	0.1
1-B	12.7	157.3	0.8	2.3	-0.3	3.1	1.7	0.3	0.1
2-A	12.7	180.7	0.9	2.4	-0.4	3.4	1.9	0.3	0.2
2-B	12.7	213.1	1.1	2.5	-0.5	3.9	2.2	0.3	0.2
3-A	13.6	200.2	1.0	2.4	-0.4	3.7	2.1	0.3	0.2
3-B	12.7	174.7	0.9	2.3	-0.3	3.3	1.8	0.3	0.2
4-A	13.6	214.3	1.1	2.5	-0.5	3.9	2.2	0.3	0.1
4-B	12.7	196.7	1.0	2.4	-0.4	3.6	2.1	0.3	0.2

Wall ID	Masonry compressive strength (MPa)	Cracking Load (kN)	Shear Stress at Cracking load (MPa)	Principal Compression (MPa)	Principal Tension (MPa)	Cracking tensile stress (MPa) (according to cylindrical formula)	Cracking tensile stress (MPa) (according to spheroidal formula)	Normalized Tensile Stress For Cylindrical Assumption	Normalized Tensile Stress For Spheroidal Assumption
5-A	12.7	165.6	0.8	2.3	-0.3	3.2	1.8	0.3	0.1
5-B	12.7	179.6	0.9	2.4	-0.4	3.4	1.9	0.3	0.2
6-A	15.5	77.0	0.4	2.1	-0.1	2.3	1.2	0.2	0.1
6-B	15.5	161.6	0.8	2.3	-0.3	3.2	1.7	0.2	0.1
7-A	15.7	134.2	0.7	2.2	-0.2	2.8	1.5	0.2	0.1
7-B	15.7	124.1	0.6	2.2	-0.2	2.7	1.5	0.2	0.1
8-A	15.7	127.0	0.6	2.2	-0.2	2.8	1.5	0.2	0.1
8-B	15.7	175.1	0.9	2.3	-0.3	3.3	1.8	0.2	0.1

Chapter 6: Conclusions and Recommendations

6.1 Summary

The first chapter of the thesis contained some objectives that were addressed throughout the thesis. The fulfilled objectives are discussed below:

- A comprehensive literature review was presented in Chapter 2 that provided an overview of shear failure mechanisms, different test methods, the various factors affecting in-plane shear, and a look at the results from previous research. The literature review also resulted in development of a comprehensive database that was used in subsequent analysis presented in this thesis.
- The database generated from the literature review was used to analyze the effectiveness of different in-plane shear prediction models. The results of this analysis are discussed in detail in Chapter 3. This analysis lead to the proposal of a modified equation for predicting in-plane shear strength.
- An experimental investigation was carried out on full scale masonry walls to examine the effect of different types of horizontal reinforcement end anchorage conditions, various boundary conditions and different loading protocols. The detailed findings of these tests were discussed in the thesis and the conclusions are presented below.

6.2 Conclusions

The performance of reinforced concrete masonry shear wall under cyclic loading was studied. The walls were all reinforced with the same amount of vertical reinforcement but with different type and configuration of horizontal reinforcement. In some cases the boundary conditions and the loading protocol were also varied.

From the analysis of results the major findings are as follows:

- There was no significant difference observed in terms of shear capacity despite the changes made in the various parameters. However, observation of the crack patterns showed that the proportion of post-peak cracks increased for walls that had bond beams compared to the walls with joint reinforcement. In addition, in the walls with

bond beams, the crack patterns were more scattered; distributed throughout the wall, as compared to the walls with joint reinforcement where the final crack pattern took the typical form of a large X.

- When the ductility of the walls was compared, similar levels of ductility were seen for all walls with a bit of variation. In all cases the ductility decreased compared to the control walls. Amongst the walls with bond beams, the lowest ductility was observed for the walls where the bond beams were relocated to the 3rd and 6th courses, increasing the wall's resistance in the potential crack path. When the loading protocol was changed to apply constant vertical load, this also reduced ductility.
- Another important parameter of comparison was stiffness. The study showed higher initial stiffness for walls with bond beams than for walls with joint reinforcement. There were no significant changes observed for walls tested under a monotonic loading protocol rather than cyclic. Application of constant vertical load reduced the initial stiffness of the walls. The same level of stiffness degradation was observed for almost all wall sets except for the walls where the bond beams were relocated and also for the walls where the bond beam reinforcement had 180 degree hooks.
- Generally speaking, the total energy absorbed is less than 50% of the energy input and the energy absorption capacity increases with increased deformation. There was no noteworthy change in the total energy absorption capacity for any of the walls.
- The tensile cracking stress was computed for all walls by applying basic fracture mechanics theory for two types of flaws revealing that the spheroidal assumption produced results closer to the actual calculated results obtained from literature.

6.3 Recommendations

The following are recommendations for future research work:

- The tests showed no significant difference in strength due to changes in the bond beam anchorage type from straight to 180 degree hooks. This is most likely due to insufficient stress in the bar, stresses that do not exceed the bond strength between the grout and the reinforcement. Unless the stress in the bar exceeds the bond stress, the end anchorage is irrelevant. Future research must be carried out such that the full bond stress develops. One of the solutions may be to use a smaller

size of reinforcement in the bond beams than used in this research. Another reason behind the fact that the full capacity of reinforcement with 180 degree did not develop may be due to the large bend diameter of the reinforcement required by the code. If it is possible to provide a smaller bend diameter without breaking the reinforcement while bending it, it would wrap around the vertical reinforcement more closely, theoretically providing better anchorage. The size of walls tested here are similar to the piers between openings where diagonal cracks in walls are typically visible as shown in Figure 2.1. It may simply be the case that in practice, for cases like this, the effect of the anchorage of the reinforcement is not at all an issue to be taken into account. Further study is required.

- The shear stud used in this research had a stud size as described for reinforced concrete. So the effect of studs of different sizes could be another direction of research for future researchers to find the optimum size to be used.
- No significant changes in behaviour or strength were observed with the change in boundary conditions. As was observed during construction of the walls, some of the changes in boundary conditions, e.g. providing splices at the top, complicated the construction and testing quite significantly while resulting in no significant difference in the results. Therefore, it is not recommended to use top splices in testing or actual construction practice. This may also give researchers more confidence in analyzing data from different researchers where different boundary conditions are used.

Bibliography

Alcocer, S. & Meli, R., 1995. "Test Program on Seismic Behaviour of Confined Masonry Structures". TMS JOURNAL, 13(2), pp. 68-76.

Anderson, D. & Brzev, S., 2009. " Seismic Design Guide for Masonry Buildings". Toronto: Canadian Concrete Masonry Producers Association.

Anderson, D. & Priestley, M., 1992. "In Plane Shear Strength of Masonry Walls". Saskatchewan, Canada, 6th Canadian Masonry Symposium, pp. 223-234.

Brock-White, 2013. White Brock. [Online]
Available at:
http://ca.brockwhite.com/pages/item_image_popup.cfm?ITEM_ID=899&FILE_ID=1466

Chen, S., Hidalogo, P., Clough, R. & Mcniven, H., 1978. " Cyclic Loading Test of Masonry Single Piers, Volume 2 Height to Width Ratio of 1", Berkeley: Earthquake Engineering Research Center, University of California, Report No UCB/ EERC-78/28.

CSA-Concrete-Standard-A23.3-04, 2004. "Design of Concrete Structures". Toronto: Canadian Portland Cement Association.

CSA-Masonry-Standard, 2004. "Design of Masonry Structures-S304.1-04". Mississauga: Canadian Standards Association.

Davis, C., 2008. "Evaluation of Design Provisions for In-plane Shear in Masonry Walls". Washington: MS Thesis Department of Civil Engineering, Washington State University.

Dickie, J. & Lissel, S., 2010. "In-plane Shear Test Method for Reinforced Concrete Masonry and Preliminary Test Results". Dresden, 8th International Masonry Conference.

Dickie, J. & Lissel, S., 2011. "In-plane Shear Test Method for Reinforced Concrete Masonry and Comparison of Test Results". Queenstown, New Zealand, 9th Australian Masonry Conference.

Drysdale, R. & Hamid, A. A., 2005. "Masonry Structures: Behaviour and Design". Canadian ed. Mississauga, Ontario: Canada Masonry Design Centre.

Eikanas, I. K., 2003. "Behaviour of Concrete Masonry Shear Walls with Various Aspect Ratio and Flexural Reinforcement". Pullman, WA.: MS Thesis Department of Civil and Environmental Engineering Washington State University.

ESECMaSE, 1995. "Deliverable D6.2: Development of Test Methods for The Determination of Masonry Properties Under Lateral Loads in WP7, incl. Test Methods for European Standardisation", Munich: Institute of Concrete and Masonry Research, Technical University of Munich, Germany.

Expocrete-Concrete, 2013. http://www.expocrete.com/.

Fehling, E. & Schermer, E., 2008. "ESECMASE Shear Test Methods for Masonry Walls with Real Boundary Conditions". Toronto, Proceedings of 11th Canadian Masonry Symposium.

FEMA461, 2007. "Interim Testing Protocols for Determining the Seismic Performance Characteristics of Structural and Non structural Component", Washington D.C.: Federal Emergency Management Agency (FEMA) and National Earthquake Hazards Reduction Program.

Feng, J. & Xia, J., 1986. “Experimental Study of Shear Strength of Reinforced Masonry Walls Under Cyclic Loading”. New Brunswick, 4th Canadian Masonry Symposium, pp. 581-608.

Fujisawa, M., Kawashima, T. & Yamaguchi, Y., 1986. "Seismic Capacity of Reinforced Masonry Walls: Effects of Shear Span Ratio". Fredericton, Proceedings of 4th Canadian Masonry Symposium, University of New Brunswick.

Haider, W., 2007. “In-Plane Response of Widespread Reinforced Masonry Walls”, Queensland: Phd Thesis, Central Queensland University , Australia.

Haider, W. & Dhanasekar, M., 2011. "Effect of Spacing of Reinforcement on the Behaviour of Partially Grouted Masonry Shear Walls". Advances in Structural Engineering, pp. 281-294.

Hamid, A. & Drysdale, R., 1988. "Flexural Tensile Strength of Concrete Block Masonry". Journal of Structural Engineering, Volume 114, pp. 50-66.

Hatzinikolas, M. & Korany, M., 2005. “Masonry Design for Engineers and Architects”. Edmonton,: Canadian Masonry Publications,Alberta.

Hidalgo, P. A., Mayes, R. L., McNiven, H. D. & Clough, R. W., 1978. “Cyclic Loading Test of Masonry Single Piers- Volume 1 Height to Width Ratio of 2”, Berkeley: University of California, Report No. UCB-EERC 78/27.

Hiraishi, H., 1985. "Flexural Behaviour of Masonry Shear Walls". Tokyo, The First Joint Technical Coordinating Committee On Masonry Research: US Japan Cooperative Research Program.

Ingham, J., Davidson, B., Brammer, D. & Voon, K., 2001. "Testing And Codification of Partially Grout Filled Nominally Reinforced Concrete Masonry Subjected To In-Plane Cyclic Loads". The Masonry Society, Issue September, pp. 83-95.

Kaminsono, T. et al., 1988. “Experimental Study on Seismic Performance of Reinforced Masonry Walls”. Tokyo, Proceedings of Ninth World Conference of Earthquake Engineering., pp. 109-114.

Kasperik, T., 2009. "Behaviour of Partially Grouted Nominally Reinforced Masonry Shear Walls Under Dynamic Loading". Hamilton: University of McMaster.

Khattab, M. & Drysdale, R., 1993. "The Effect of Reinforcement on the Shear Response of Grouted Concrete Masonry". Philadelphia, The Sixth North American Masonry Conference, Pennsylvania.

Matsumura, A., 1987. "Shear Strength of Reinforced Hollow Unit Masonry Walls". Los Angeles, Proceedings of Ninth World Conference On Earthquake Engineering., pp. 50-1-50-16.

Mayes, R., Omote, Y. & Clough, R., 1976. “Cyclic Loading Test of Masonry Single Piers- Volume 1: Analysis of Test Results”, Berkeley: University of California, Berkeley, Report No. UCB-EERC 76/16.

Minaie, E., Hamid, A. & Moon, F., 2009. "Summary of the Research on Behaviour of Fully Grouted Reinforced Concrete and Clay Masonry Shear Walls", Skokie, Illinois: Portland Cement Association.

Minaie, E., Mota, M., Moon, F. & Hamid, A., 2010. "In-Plane Behaviour Of Partially Grouted Reinforced Concrete Masonry Shear Walls". Journal of Structural Engineering, Issue September, pp. 1089-1097.

Moroni, O., Gomez, C. & Astroza, M., 2002. World Housing Encyclopedia. [Online] Available at: http://www.world-housing.net/category/masonry/reinforced-masonry [Accessed 2012].

NBCC, 2005. National Building Code of Canada, Ontario: Canadian Commission on Building and Fire Codes, National Research Council of Canada.

NEHRP, 1997. "National Earthquake Hazards Reduction Program:Recommended Provisions for Seismic Regulations for New Buildings and Other Structures, Part-1 Provisions", Washington D.C.: Building Seismic Safety Councils.

Okamoto, S., Yamazaki, Y. T., Kaminosono, M. & Hirashi, H., 1987. "Seismic Capacity of Reinforced Masonry Walls and Beams in Wind and Seismic Effects", Raufaste, New Jersey.: NBSIR 87-3540, National Institute of Standards and Technology, Proceedings of the 18th Joint Meeting, U.S.-Japan Panel on Wind and Seismic Effects.

Paulay, T. & Priestley, M., 1993. "Stability of Ductile Structural Walls". ACI Structural Journal, Vol -90, No-4, pp. 385-392.

Priestley, M. J. N., 1976. "Cyclic Test of Heavily Reinforced Masonry Walls", Christchurch: Department of Civil Engineering , University of Canterbury, New Zealand, Research Report 76-12.October.

Priestley, M., Verma, R. & Xiao, Y., 1994. "Seismic Shear Strength of Reinforced Concrete Columns". Journal of Structural Engineering, 120(8), pp. 2310-2329.

Saiedi, H., 2011. "In-plane shake Table Testing of Heavily Reinforced Concrete Masonry Shear Walls". Calgary: MS Thesis, Department of Civil Engineering, University of Calgary.

Schneider, R., 1959. "Lateral Load Test on Reinforced Masonry Grouted Shear Walls", Los-Angeles: University of Southern California Engineering Center : report No 70-101.

Schultz, A. E., 1996. "Seismic Resistance of Partially Grouted Masonry Shear Walls". Acapulco, Proceedings of the 11th World Conference on Earthquake Engineering, Acapulco, Mexico, pp. 246-256.

Schultz, A., Hutchinson, R. & Cheok, G., 1998. "Seismic Performance of Masonry Walls with Bed Joint Reinforcement". Elsevier Science Limited.

Scrivener, J., 1967. "Static Racking Test on Concrete Masonry Walls". Texas, Proceedings of International Conference on Masonry Structural Systems., pp. 185-191.

Shedid, M., Drysdale, R. & El- Dakhakhni, W., 2008. "Behaviour of Fully Grouted Reinforced Concrete Masonry Shear Walls Failing In Flexure: Experimental Results". Journal of Structural Engineering, Issue November, pp. 1754-1767.

Shedid, M., El-Dakhakhni, W. & Drysdale, R., 2010. "Alternative Stratagies to Enhance the Seismic Performance of Reinforced Concrete Block Shear Wall Systems". Journal of Structural Engineering , Issue June, pp. 676-689.

Shing, P. B., Schuller, M. & Hoskere, V. S., 1990. "In-Plane Resistance of Reinforced Masonry Shear Walls,". Journal of Structural Engineering, 116(3), pp. 619-640.

Shrive, N., 1983. "Compression Testing and Cracking of Plain Concrete". Magazine of Concrete Research, March, 35(20), pp. 27-39.

Spec-Mix, 2009. "Corefill Masonry Grout". [Online]
Available at: www.specmix.com/pdf/product_datasheet_pclsand.pdf
[Accessed March 2012].

Spec-Mix, 2009. "Portland Lime & Sand Masonry (M,S,N)". [Online]
Available at: www.specmix.com/pdf/product_datasheet/datasheet_pclsand.pdf>>
[Accessed March 2012].

Subramanian, N., 2005. "Evaluation and Enhancing the Punching Shear Resistance of Flat Slabs Using HSC". The Indian Concrete Journal, pp. 31-37.

Sveinsson, B. I., Mayes, R. L. & McNiven, H. D., 1985. "Cyclic Loading of Masonry Single Piers", Berkeley: University of California, Berkeley, Volume 4 report no UCB/EERC-85/15,.

Timoshenko, S. & Goodier, J., 1951. "Theory of Elasticity". 2nd ed. York: Mc-GRAW HILL BOOK Company Inc. York, Pennsylvania.

Tomazevic, M., 1999. "Earthquake-Resistant Design of Masonry Buildings". London: Impress College Press, London.

Tomazevic, M. & Lutman, M., 1988. "Seismic Resistance of Reinforced Masonry Walls". Tokyo-kyoto,Japan, Proceedings of Ninth World Conference on Earthquake Engineering., pp. 97-102.

Tomazevic, M., Lutman, M. & Petcovic, L., 1996. "Seismic Behaviour of Masonry Walls: Experimental Simulation". Journal of Structural Engineering, Issue September, pp. 1040-1047.

Vliet, M. V., 2004. "Shear Test on Masonry Panels Literature Survey and Proposed for Experiments", Delft: TNO Building and Construction Reserach, Delft, Netherland.

Voon, K. C., 2007. "In-plane Seismic Design of Concrete Masonry Structures", Auckland: PhD thesis, Department of Civil and Environmental Engineering,University of Auckland.

Voon, K. & Ingham, J., 2007. "Design Expression for the In-plane Shear Strength of Reinforced Concrete Masonry". Journal of Structural Engineering, pp. 706-713.

Woodward, K. & Rankine, F., 1985. "Influence of Aspect Ratio on Shear Strength of Concrete Block Masonry Walls", Gaithersburg: NBSIR-84-299, US Department of Commerce, National Bureau of Standards, National Engineering Laboratory, Center for Building Technology, Gaithersburg, Maryland.

Xiao, X., 2009. "Fracture Mechanics of Masonry", Calgary: PhD Thesis, Department of Civil Engineering, University of Calgary.

Yancey, C. & Scribner, C., 1989. "Influence of Horizontal Reinforcmeent on Shear Resistance of Concrete Masonry Walls". Gaithersburg, US Department of Commerce, Gaithersburg, Maryland.

Appendix 1

Specimen Construction and Prism Tests:







Wall 1-A

Wall 1-B

Wall 2-A(180 hook)

Wall 2-B (180 hook)

Wall 3-A

Wall 3-B

Wall 4-A

Wall 4-B(While Testing)

Wall 4-B (At the end of testing)

Wall 5-A Wall 5-B

Wall 6-A Wall 6-B

Wall 7-A Wall 7-B

Wall 8-A

Wall 8-B

Wall 2A(180 hook)

Wall 2-B (1800 hook)

Wall 3-B(shear stud

Wall 4-A

Wall 4-B

Wall 6-B (top splice)

Wall 6-B

Wall 6-A (top splice)

Wall 5-A (w/o bottom splice)

Wall 7-A

Wall 7-B

Wall 8-A

Wall 8-B

South **North**

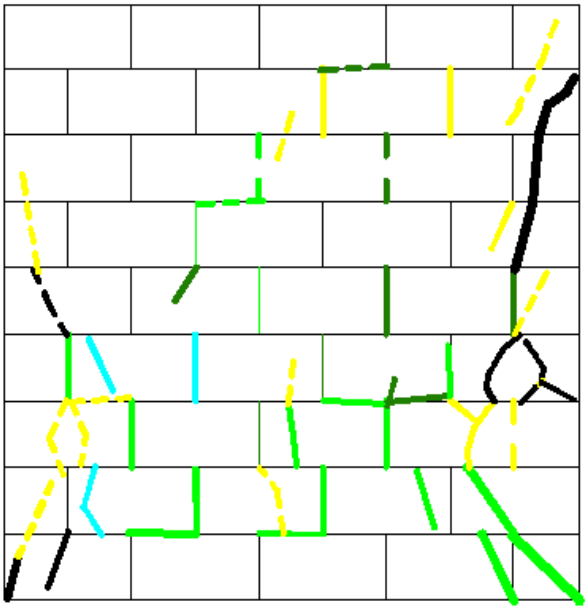

Wall 3-C

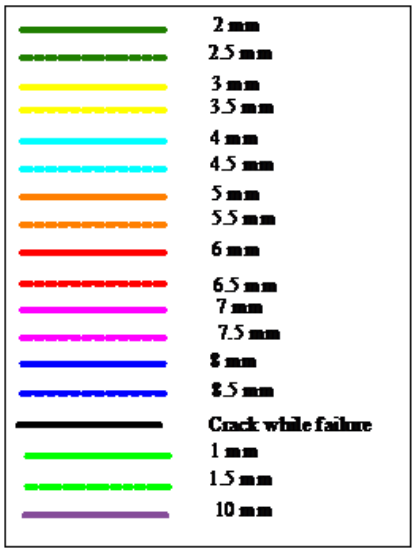

Appendix 2

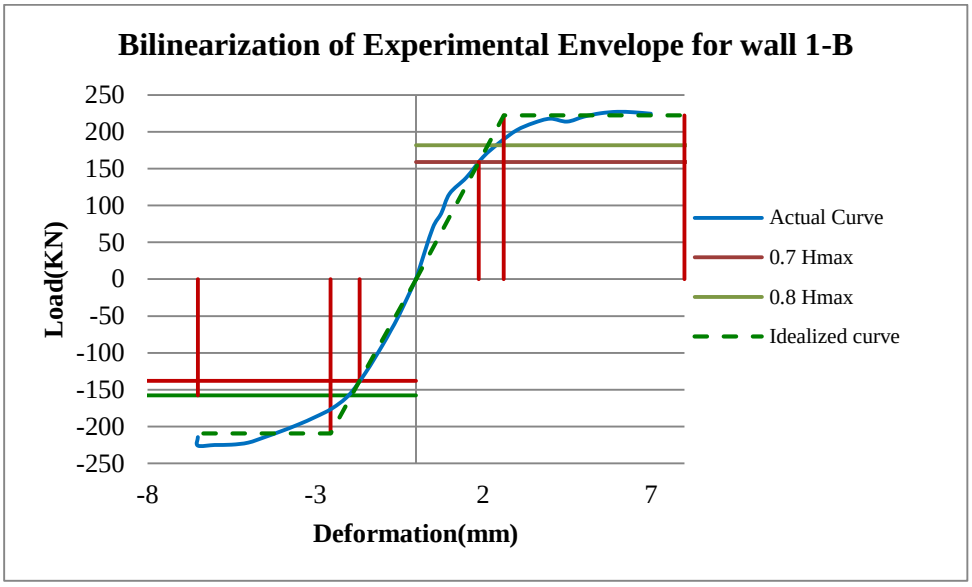
Bilinearization of Experimental Envelope for wall 1-B
250
200
150
100
50
0
-50
-100
-150
-200
-250
Load(KN)
-8
-3
2
7
Deformation(mm)
Actual Curve
0.7 Hmax
0.8 Hmax
Idealized curve

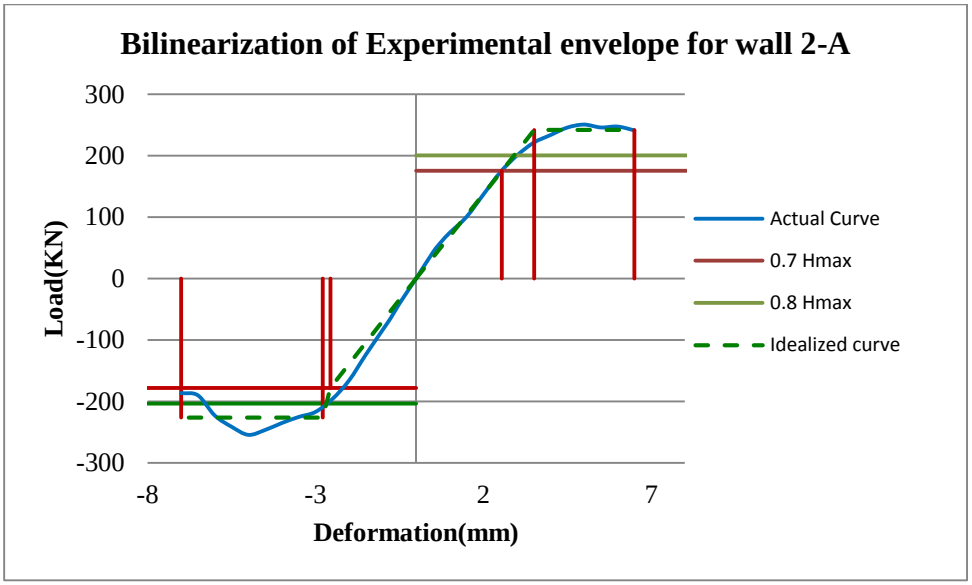
Bilinearization of Experimental envelope for wall 2-A
300
200
100
0
-100
-200
-300
Load(KN)
-8
-3
2
7
Deformation(mm)
Actual Curve
0.7 Hmax
0.8 Hmax
Idealized curve

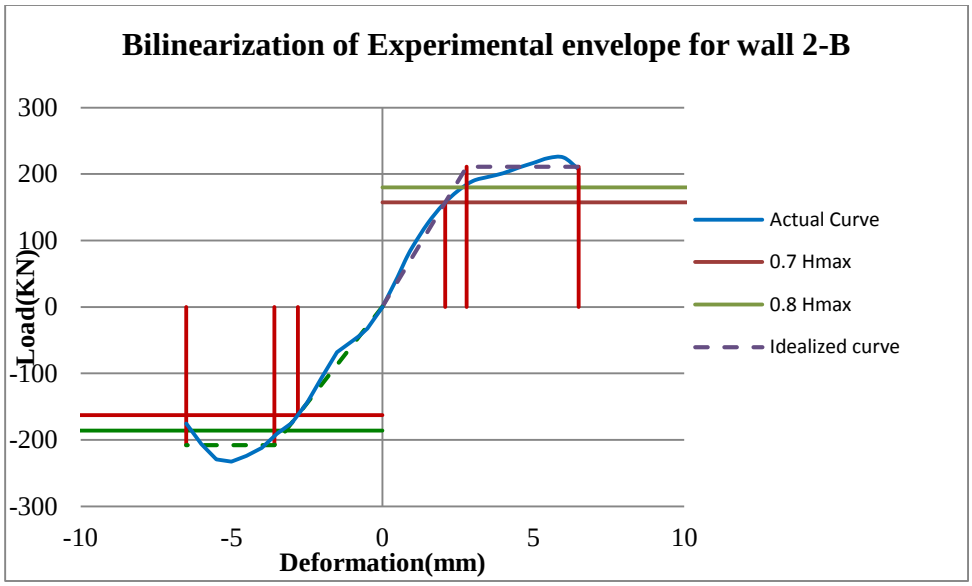
Bilinearization of Experimental envelope for wall 2-B
300
200
100
0
-100
-200
-300
-10
-5
0
5
10
Load(KN)
Deformation(mm)
Actual Curve
0.7 Hmax
0.8 Hmax
Idealized curve

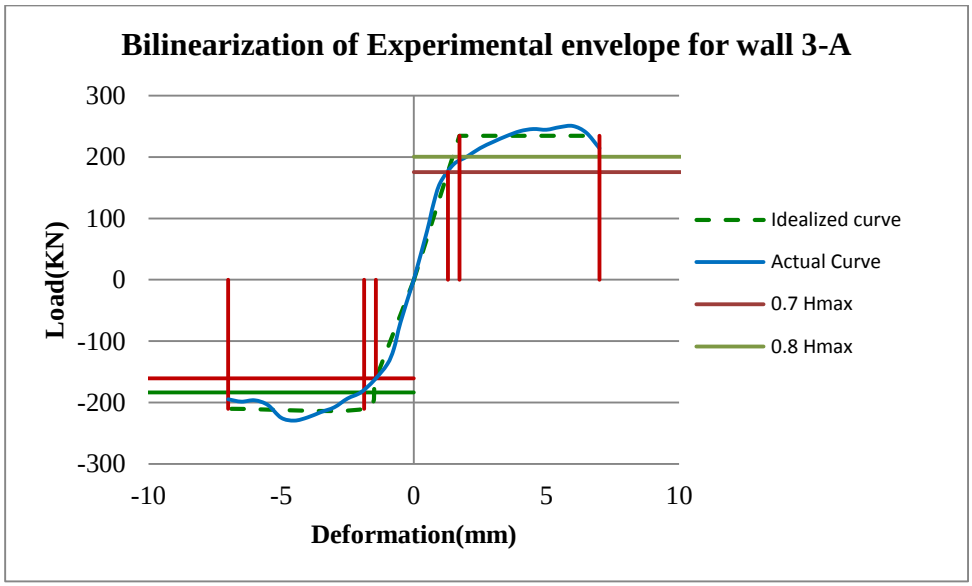
Bilinearization of Experimental envelope for wall 3-A
300
200
100
0
-100
-200
-300
-10
-5
0
5
10
Load(KN)
Deformation(mm)
Idealized curve
Actual Curve
0.7 Hmax
0.8 Hmax

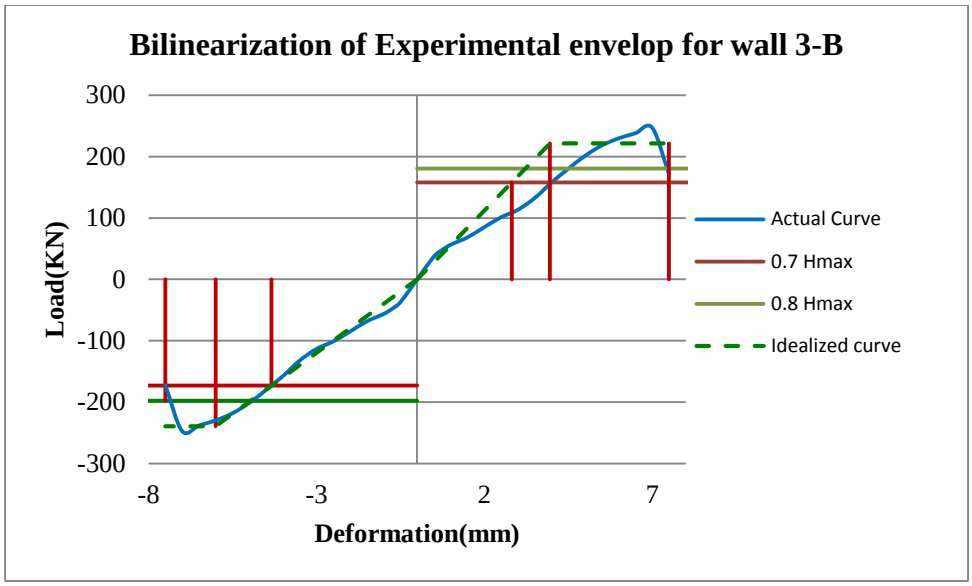
Bilinearization of Experimental envelop for wall 3-B
300
200
100
0
-100
-200
-300
-8
-3
2
7
Load(KN)
Deformation(mm)
Actual Curve
0.7 Hmax
0.8 Hmax
Idealized curve

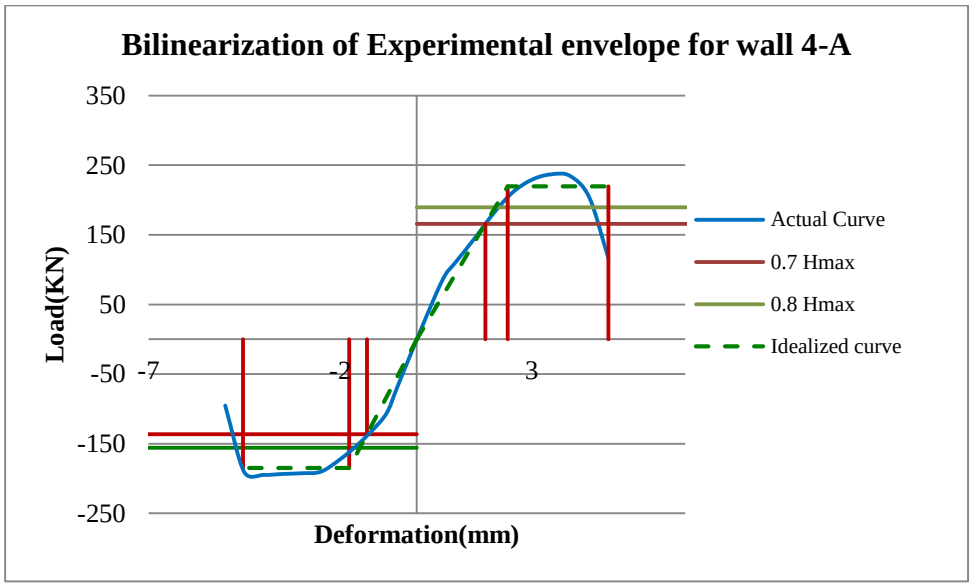
Bilinearization of Experimental envelope for wall 4-A
350
250
150
50
-50
-150
-250
-7
-2
3
Load(KN)
Deformation(mm)
Actual Curve
0.7 Hmax
0.8 Hmax
Idealized curve

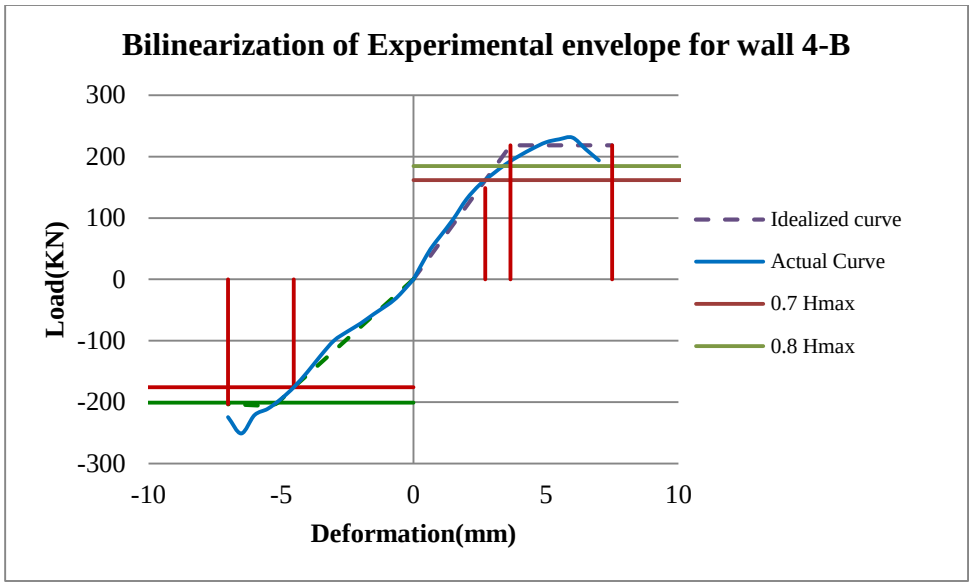
Bilinearization of Experimental envelope for wall 4-B
300
200
100
0
-100
-200
-300
-10
-5
0
5
10
Load(KN)
Deformation(mm)
Idealized curve
Actual Curve
0.7 Hmax
0.8 Hmax

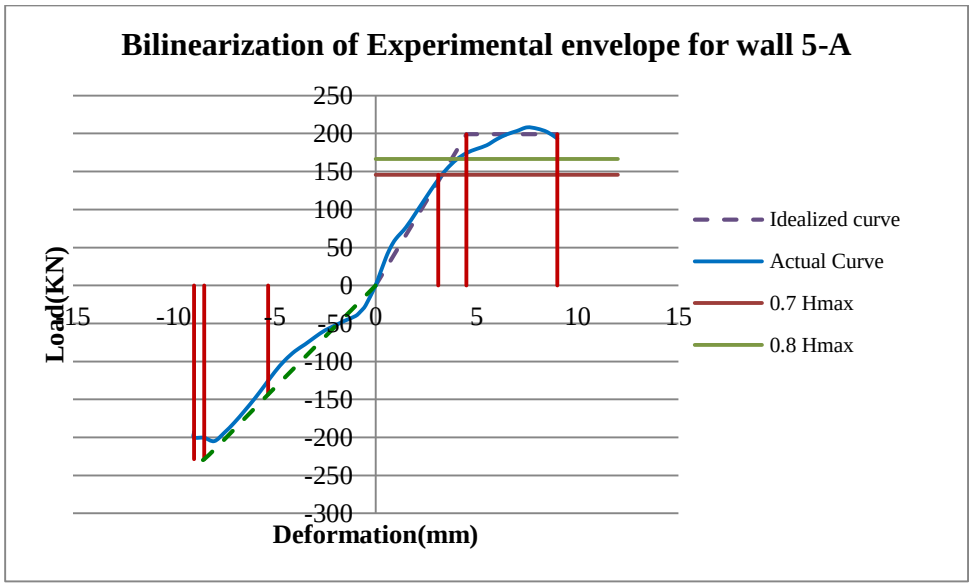
Bilinearization of Experimental envelope for wall 5-A
250
200
150
100
50
0
-50
-100
-150
-200
-250
-300
-15
-10
-5
0
5
10
15
Load(KN)
Deformation(mm)
Idealized curve
Actual Curve
0.7 Hmax
0.8 Hmax

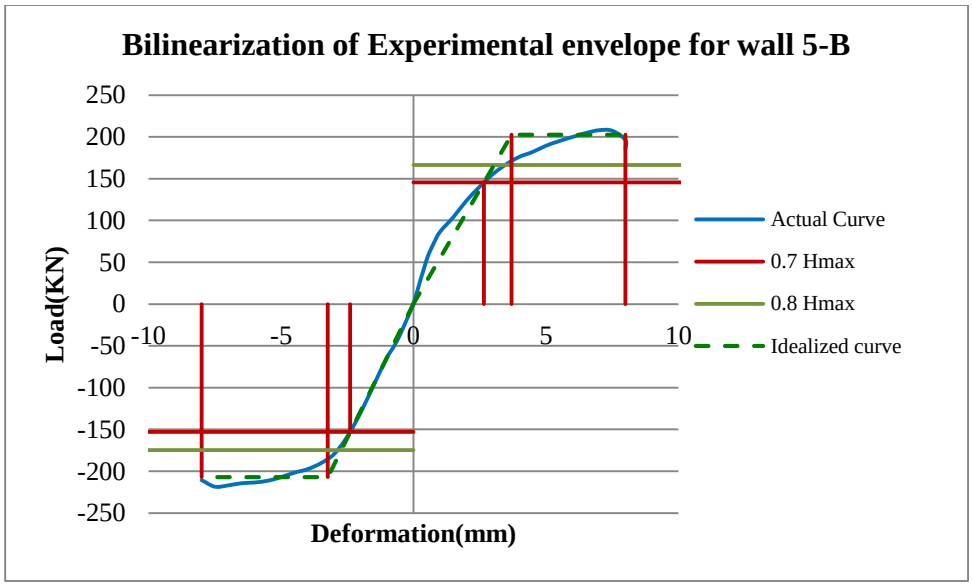
Bilinearization of Experimental envelope for wall 5-B
250
200
150
100
50
0
-50
-100
-150
-200
-250
-10
-5
0
5
10
Load(KN)
Deformation(mm)
Actual Curve
0.7 Hmax
0.8 Hmax
Idealized curve

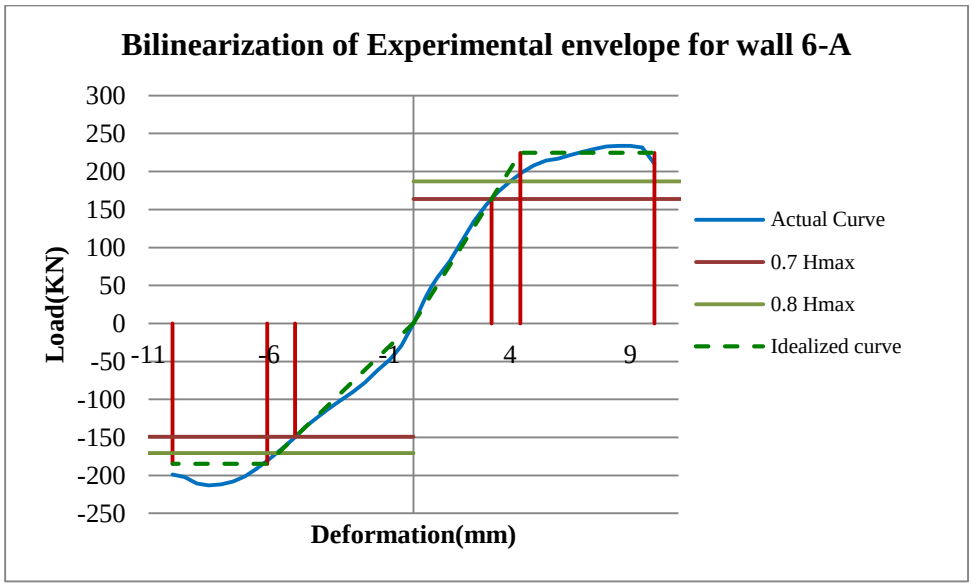
Bilinearization of Experimental envelope for wall 6-A
300
250
200
150
100
50
0
-50
-100
-150
-200
-250
-11
-6
-1
4
9
Load(KN)
Deformation(mm)
Actual Curve
0.7 Hmax
0.8 Hmax
Idealized curve

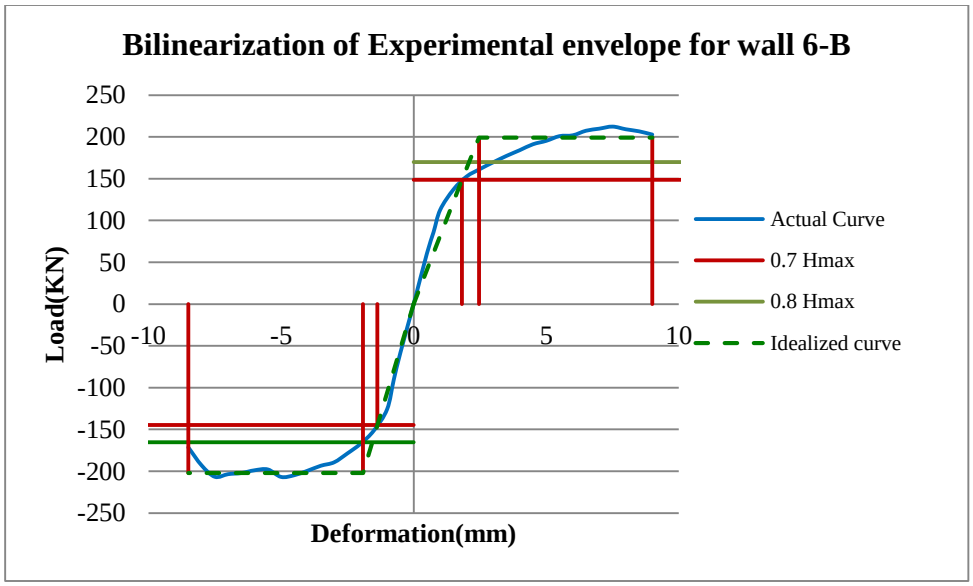
Bilinearization of Experimental envelope for wall 6-B
250
200
150
100
50
0
-50
-100
-150
-200
-250
-10
-5
0
5
10
Load(KN)
Deformation(mm)
Actual Curve
0.7 Hmax
0.8 Hmax
Idealized curve

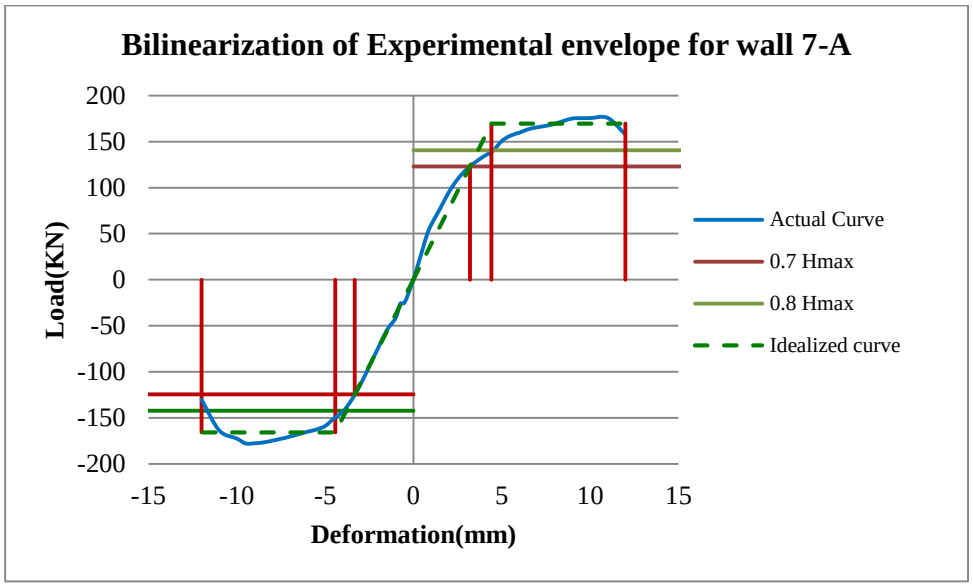
Bilinearization of Experimental envelope for wall 7-A
200
150
100
50
0
-50
-100
-150
-200
-15
-10
-5
0
5
10
15
Load(KN)
Deformation(mm)
Actual Curve
0.7 Hmax
0.8 Hmax
Idealized curve

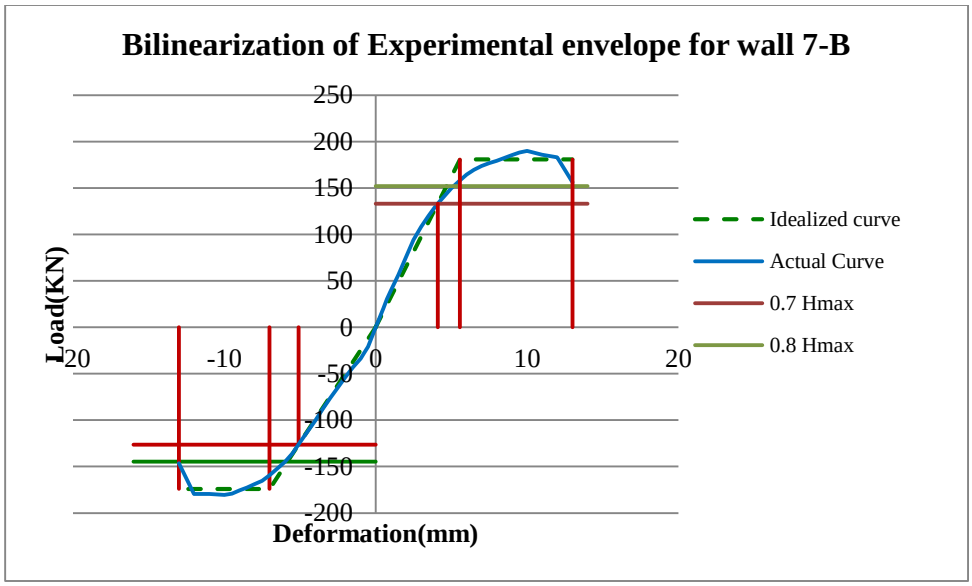
Bilinearization of Experimental envelope for wall 7-B
250
200
150
100
50
0
-50
-100
-150
-200
-20
-10
0
10
20
Load(KN)
Deformation(mm)
Idealized curve
Actual Curve
0.7 Hmax
0.8 Hmax

Appendix 3

Calculation of Wall Compressive Strength from prism strength for Wall 1-A:

Tested at 42 days.

Prism strength for ungrouted prism at 42 days: 18.2 MPa.

Prism strength for grouted prism at 42 days: 8.45 MPa.

Area of ungrouted Core of 190 mm Block=72400 mm^2/m

Area of Grouted Core of 190 mm Block=190000 mm^2/m

Among nine cores in the walls six were ungrouted and the rest 3 were grouted. If expressed in percentages then it becomes 67% and 33%.

So $f_m' = \frac{0.667*72.4\times10^3*18.2+0.33*190\times10^3*8.5}{0.667*72400+0.334*190000} = 12.7\ MPa$

Sample Calculation of Shear prediction:

For wall 1 A:

Calculation of In-plane shear according to CSA S304.1-04

$f_m' = 12.64\ MPa \quad L = 1800; \quad d = 0.8 * 1800 = 1440 \quad h = 1800; \quad P = 409\ kN$

$f_y = 450\ Mpa \quad A_v = 200\ mm^2 \quad s = 800mm$

$t = 190\ mm \quad \gamma_g = \frac{A_e}{A_g} \quad 0.33 \quad \frac{M}{VL} = \frac{Vh}{VL} = 1 \quad v_m = 0.16\left(2 - \frac{M}{VL}\right)\sqrt{f_m'}$

$= 0.638$

$V_r = 0.6(v_m * d * t + 0.25 * P) * \gamma_g + (0.6 * 0.85 * A_v f_y \frac{d_v}{s})$=193.5 kN.

Calculation of Sliding Shear:

$$P_{top\ max} = 410.94\ kN \quad \mu = 1(masonry\ to\ masonry)$$

$$P_{sliding} = \left(0.9\ P_{topmax} + A_y f_y\right)\mu = 639.85\ kN$$

Calculation of Flexure Shear:

$P = 409 = C_m + C_{si} - T_{si} = (1)(0.85 * 12.64)190 * 0.8 * c - 200 * 450 * 2$

Solving of this equation gives c=360.7 mm

Which means that assumption that two reinforcements will be under tension is correct.

$M_u = 0.85 * 12.64 * 0.8 * 360.7 * 190 * \left(\frac{1800}{2} - \frac{360.7}{2}\right) + 200 * 450 * (1600 - \frac{1800}{2})$

=486.9 kN-m-

F_{Flex}=Mu/h=270.5 kN.

Matlab Program for determination of area under curve

```
function Area=Area Under Curve(x,y)
close all
xpp=abs(max(x)-min(x));
ypp=abs(max(y)-min(y));
Tarea=(xpp*ypp);
figure(1)
h=fill(x,y,'r*');
axis([min(x) max(x) min(y) max(y)])
saveas(h,'xy','png');
xy=imread('xy.png');
xy1=im2bw(xy);
xy2=imcrop(xy1,[157 69 930 733]);
tareapixels=931*734;
Tframepixels=931*2+734*2;
Tgridpixels=120;
Tcurvepixels=bwarea(xy2)+Tframepixels+Tgridpixels;
Area=Tarea*(1-Tcurvepixels/tareapixels);
title(['Area=',num2str(Area),'Unit Area'])
end
```

Tables of critical F values for α=0.1

ndf	1	2	3	4	5	6	7	8	9	10	11	12	13	14	15	16	17	18
ddf	α=0.1																	
1	39.8610	49.5046	53.5963	55.8334	57.2348	58.2081	58.9118	59.4367	59.8576	60.1986	60.4712	60.7027	60.9067	61.0680	61.2153	61.3484	61.4673	61.571
2	8.5265	9.0000	9.1616	9.2434	9.2925	9.3257	9.3490	9.3670	9.3805	9.3916	9.4007	9.4081	9.4143	9.4201	9.4247	9.4288	9.4326	9.4359
3	5.5383	5.4624	5.3907	5.3426	5.3092	5.2847	5.2662	5.2517	5.2400	5.2305	5.2223	5.2156	5.2098	5.2047	5.2003	5.1965	5.1929	5.1899
4	4.5448	4.3245	4.1908	4.1073	4.0506	4.0098	3.9790	3.9550	3.9356	3.9199	3.9067	3.8955	3.8860	3.8776	3.8704	3.8639	3.8583	3.8531
5	4.0605	3.7797	3.6195	3.5202	3.4530	3.4045	3.3679	3.3393	3.3163	3.2974	3.2816	3.2682	3.2567	3.2468	3.2380	3.2303	3.2234	3.2172
6	3.7759	3.4633	3.2888	3.1808	3.1075	3.0545	3.0145	2.9830	2.9578	2.9370	2.9195	2.9047	2.8920	2.8809	2.8712	2.8626	2.8550	2.8481
7	3.5894	3.2574	3.0741	2.9605	2.8834	2.8274	2.7850	2.7516	2.7247	2.7025	2.6839	2.6681	2.6545	2.6426	2.6322	2.6230	2.6148	2.6074
8	3.4579	3.1131	2.9238	2.8064	2.7265	2.6683	2.6242	2.5894	2.5612	2.5380	2.5186	2.5020	2.4877	2.4752	2.4642	2.4545	2.4458	2.4381
9	3.3603	3.0065	2.8129	2.6927	2.6106	2.5509	2.5053	2.4694	2.4403	2.4163	2.3961	2.3789	2.3640	2.3511	2.3396	2.3295	2.3204	2.3124
10	3.2850	2.9245	2.7277	2.6054	2.5216	2.4606	2.4140	2.3772	2.3473	2.3226	2.3018	2.2841	2.2687	2.2553	2.2435	2.2331	2.2237	2.2153
11	3.2252	2.8595	2.6602	2.5362	2.4512	2.3891	2.3416	2.3040	2.2735	2.2482	2.2269	2.2087	2.1930	2.1792	2.1671	2.1563	2.1467	2.1380

Tables of critical F values for α=0.05

ndf	1	2	3	4	5	6	7	8	9	10	11	12	13	14	15	16	17	18
ddf	α=0.05																	
1	161.469	199.493	215.737	224.500	230.066	234.001	236.772	238.949	240.496	241.838	242.968	243.880	244.798	245.260	245.956	246.422	246.890	247.36
2	18.5128	18.9995	19.1642	19.2467	19.2969	19.3299	19.3536	19.3710	19.3852	19.3963	19.4043	19.4122	19.4186	19.4250	19.4297	19.4329	19.4377	19.440
3	10.1278	9.5522	9.2767	9.1173	9.0133	8.9408	8.8868	8.8452	8.8124	8.7857	8.7635	8.7446	8.7287	8.7150	8.7028	8.6923	8.6830	8.6745
4	7.7087	6.9444	6.5915	6.3882	6.2561	6.1631	6.0943	6.0411	5.9988	5.9644	5.9359	5.9117	5.8912	5.8733	5.8578	5.8440	5.8319	5.8211
5	6.6080	5.7861	5.4095	5.1922	5.0503	4.9503	4.8759	4.8184	4.7725	4.7350	4.7039	4.6777	4.6552	4.6358	4.6187	4.6038	4.5904	4.5785
6	5.9874	5.1433	4.7570	4.5337	4.3874	4.2838	4.2067	4.1468	4.0990	4.0600	4.0275	3.9999	3.9764	3.9560	3.9381	3.9223	3.9083	3.8957
7	5.5914	4.7374	4.3469	4.1204	3.9715	3.8660	3.7870	3.7257	3.6767	3.6366	3.6030	3.5747	3.5504	3.5292	3.5107	3.4944	3.4799	3.4669
8	5.3177	4.4590	4.0662	3.8378	3.6875	3.5806	3.5004	3.4381	3.3881	3.3472	3.3130	3.2839	3.2590	3.2374	3.2184	3.2017	3.1867	3.1733
9	5.1174	4.2565	3.8626	3.6331	3.4817	3.3738	3.2928	3.2296	3.1789	3.1373	3.1025	3.0729	3.0475	3.0255	3.0061	2.9890	2.9737	2.9600
10	4.9647	4.1028	3.7083	3.4781	3.3258	3.2171	3.1355	3.0717	3.0204	2.9782	2.9429	2.9130	2.8872	2.8648	2.8450	2.8276	2.8120	2.7981
11	4.8443	3.9823	3.5875	3.3567	3.2039	3.0946	3.0123	2.9480	2.8962	2.8536	2.8179	2.7876	2.7614	2.7386	2.7186	2.7009	2.6851	2.6709

3

Chi square Test Tables

df	0.1	0.05	0.02	0.01	0.005	0.002	0.001
1	2.7056	3.8415	5.4120	6.6350	7.8795	9.5497	10.8277
2	4.6051	5.9915	7.8242	9.2103	10.5965	12.4292	13.8158
3	6.2515	7.8147	9.8375	11.3452	12.8382	14.7961	16.2673
4	7.7795	9.4876	11.6679	13.2768	14.8601	16.9238	18.4678
5	9.2362	11.0706	13.3881	15.0859	16.7502	18.9084	20.5163
6	10.6449	12.5914	15.0328	16.8117	18.5477	20.7918	22.4591
7	12.0171	14.0670	16.6225	18.4751	20.2771	22.6006	24.3218
8	13.3613	15.5073	18.1689	20.0905	21.9558	24.3512	26.1244
9	14.6836	16.9189	19.6795	21.6660	23.5902	26.0572	27.8784
10	15.9876	18.3072	21.1602	23.2087	25.1895	27.7234	29.5903

Computation of Cracking Stress from Fracture Perspective

Name of Researcher	Shear stress While First Cracking (MPa)	Vertical Stress (MPa)	Principal Stress		Tensile Stress using Cylindrical Crack(MPa)	Tensile Stress using Spheroidal Crack(MPa)
			PC (MPa)	PT*[1] (MPa)		
Schultz	0.57	0.481	0.86	-0.38	2.00	1.19
Schultz	0.99	0.482	1.26	-0.78	3.61	2.20
Schultz	0.80	0.480	1.07	-0.59	2.86	1.73
Schultz	0.94	0.479	1.21	-0.73	3.40	2.06
Schultz	0.82	0.447	1.07	-0.63	2.96	1.79
Schultz	1.13	0.476	1.39	-0.91	4.13	2.52
Schultz	0.83	0.478	1.11	-0.63	2.99	1.81
Schultz	0.94	0.468	1.21	-0.74	3.42	2.08
Schultz	0.68	0.470	0.95	-0.48	2.40	1.44
Schultz	0.88	0.479	1.15	-0.68	3.18	1.93
Schultz	0.95	0.473	1.21	-0.74	3.43	2.09
Schultz	0.99	0.480	1.26	-0.78	3.61	2.20
Yancey	0.11	1.37	1.38	-0.01	1.41	0.707
Yancey	0.12	1.37	1.38	-0.01	1.41	0.713
Yancey	0.12	1.37	1.38	-0.01	1.41	0.712
Yancey	0.14	1.37	1.38	-0.01	1.43	0.721
Yancey	0.13	1.37	1.38	-0.01	1.42	0.715
Yancey	0.14	1.37	1.38	-0.01	1.43	0.722
Yancey	0.11	1.37	1.38	-0.01	1.40	0.706
Yancey	0.10	1.37	1.38	-0.01	1.40	0.704
Yancey	0.17	1.37	1.39	-0.02	1.45	0.737
Yancey	0.14	1.37	1.38	-0.01	1.43	0.720
Hiraishi	2.46	2.0	3.63	-1.67	8.63	5.15
Hiraishi	1.74	2.0	2.97	-1.01	6.01	3.51
Hiraishi	1.51	2.0	2.78	-0.82	5.24	3.03
Hiraishi	1.73	3.9	4.57	-0.65	6.53	3.59
Hiraishi	1.94	5.9	6.46	-0.58	8.21	4.40
Hiraishi	1.24	0.5	1.50	-1.01	4.55	2.78
Hiraishi	1.07	0.5	1.34	-0.85	3.90	2.37

Hiraishi	1.00	0.5	1.27	-0.78	3.63	2.21
Hiraishi	1.21	0.5	1.48	-0.99	4.43	2.71
Hiraishi	1.37	0.5	1.64	-1.15	5.09	3.12
Hiraishi	1.16	0.5	1.43	-0.94	4.24	2.59
Hiraishi	1.80	2.0	3.03	-1.07	6.25	3.66
Hiraishi	1.18	2.0	2.51	-0.55	4.16	2.36
Hiraishi	1.84	0.5	2.10	-1.61	6.95	4.28
Hiraishi	2.97	2.0	4.11	-2.15	10.55	6.35
Hiraishi	1.98	2.0	3.19	-1.23	6.88	4.05
Hiraishi	1.74	2.0	2.97	-1.01	6.01	3.51
Hiraishi	1.48	0.5	1.75	-1.26	5.51	3.38
Hiraishi	1.32	0.5	1.59	-1.10	4.89	3.00
Sveinsson	1.88	1.54	2.74	-0.86	5.33	3.09
Sveinsson	3.01	1.63	3.72	-0.71	5.85	3.28
Sveinsson	2.76	1.66	3.54	-0.78	5.88	3.33
Sveinsson	2.76	2.06	3.86	-1.10	7.16	4.13
Sveinsson	1.74	1.86	2.92	-1.18	6.48	3.83
Sveinsson	2.76	1.69	3.56	-0.80	5.96	3.38
Sveinsson	2.76	1.52	3.43	-0.67	5.44	3.06
Sveinsson	0.7	0.92	1.34	-0.64	3.25	1.94
Sveinsson	2.76	1.53	3.44	-0.68	5.48	3.08
Sveinsson	2.76	1.53	3.44	-0.68	5.48	3.08
Sveinsson	1.74	1.68	2.76	-1.02	5.83	3.43
Sveinsson	2.76	2.20	3.98	-1.22	7.62	4.42
Sveinsson	3.12	1.96	4.06	-0.94	6.89	3.92
Sveinsson	0.4	0.80	1.02	-0.62	2.90	1.76
Sveinsson	1.95	1.27	2.57	-0.62	4.45	2.54
Sveinsson	2.76	1.49	3.41	-0.65	5.36	3.01
Sveinsson	2.76	1.39	3.34	-0.58	5.06	2.82
Sveinsson	2.76	1.76	3.62	-0.86	6.20	3.53
Sveinsson	2.76	1.96	3.78	-1.02	6.82	3.92
Sveinsson	2.76	1.48	3.40	-0.64	5.32	2.98
Sveinsson	2.76	1.47	3.39	-0.63	5.30	2.97

Sveinsson	2.76	1.95	3.77	-1.01	6.80	3.90
Sveinsson	2.76	1.75	3.61	-0.85	6.16	3.50
Sveinsson	2.76	1.65	3.53	-0.77	5.86	3.32
Sveinsson	2.76	2.11	3.90	-1.14	7.32	4.23
Sveinsson	2.76	2.70	4.41	-1.65	9.35	5.50

*[1] Negative sign refers to tension in this column